Final Report

NSF Research Grant RG/2018/EA&ICT/01

Development of a Novel Predictive Based Smart Distribution Management System (S-DMS) to Maximize the Rooftop PV Absorption Capacity of Last Mile Networks

08th March 2019 to 09th November 2022

Principal Investigator: Dr. M. P. B. Ekanayake
Co-Investigators: Dr. G. M. R. I. Godaliyadda and Prof. J. B. Ekanayake

Schedule F

Guidelines / Format For Preparation of Final Report

- **Two bound** copies (One original and two photocopies) of the Final Report should be submitted to the NSF through the **Head of the Institution** within **three months** of the completion of the project period
- The Final Report should be printed on A4 paper using single space and font 12.
- An **electronic version** prepared in MS Word should also be submitted
- Copies of published papers should be submitted, provided the published material is relevant to the research project and is a direct outcome of the project.

Final Report should provide the following information

Section 1

Information regarding Project/Project Personnel:

i. Grant Number
ii. Title of the Project
iii. Principal Investigator
iv. Co-investigators
v. Institute(s) where research was carried out
vi. Date of award
vii. Date of completion of Project
viii. Total allocation of funds (Rs)
ix. Total spent (Rs)
x. Number of Research Students employed
xi. Postgraduate degree completed with dates
xii. Number of Technical Assistants and/or labourers employed and period of service
xiii. Publications/Communications arising from the project during the reporting period

Section 2

Executive Summary of the Project:
This should be limited to 200-250 words and include the scientific background and objectives, methodology and major findings

Section 3

Report in detail: should contain the following (not less than 2000 words excluding Tables and Figures)

i. Introduction/background
ii. Scientific scope of the project (overall and specific objectives)
iii. Materials and methods (including statistical methods)
iv. Results/outputs (Results should be given in detail)
v. Discussion
vi. Conclusions and recommendations
vii. References
viii. Problems if any, encountered during the course of the project

ix. Major findings
x. Follow-up in terms of technology development/start-up business (this information will be forwarded to the Technology Division of the NSF)

Section 4

Impact of Research results:

i. Relevance of results achieved to scientific advancement
ii Dissemination/application of research output – please give the tentative plan

(b) i Relevance of results achieved to national/socio-economic development - please give recommendations clearly as this write – up may be forwarded to the potential users who will benefit from the research

Section 5

Miscellaneous

i. List of major equipment acquired during the project period, their value and their functionality
ii. List of publications/communications arising from the project and/or presentations made at seminars, workshops etc. (Please attach copies)

Section 6

Summary Statement of Expenditure (indicate under Personnel, Equipment, Consumables, Lab services & sample analysis, Statistical analysis, Calibration of instruments, PG registration fee, Travel and Subsistence and Miscellaneous)

Section 7

i. Signatures of Investigators (PI as well as Co-Is)

ii. Comments of the Head of the Department/signature

iii. Head of the Institution's signature

Section 1: Information regarding Project/Project Personnel

(1) Grant Number

RG/2018/EA&ICT/01

(2) Title of the Project

Development of a novel predictive based Smart Distribution Management System (S-DMS) to maximize the rooftop PV absorption capacity of last mile networks.

(3) Principal Investigator

Dr. M. P. B. Ekanayake

(4) Co-investigators

Dr. G. M. R. I. Godaliyadda and Prof. J. B. Ekanayake

(5) Institute where research was carried out

Department of Electrical and Electronic Engineering, Faculty of Engineering, University of Peradeniya

(6) Date of award

Date of Award: 28th December 2018
Funds Granted: 24th April 2019
Commencement of the Project: 08th March 2019

(7) Date of completion of Project

Original Anticipated Date of Completion: 09th March 2021
First Extension Until: 09th June 2021
Second (and Final) Extension Until: 09th November 20221

(8) Total allocation of funds (Rs)

Total Funds Received: LKR 1,843,289.00

(9) Total spent (Rs)

Total Funds Received: LKR 1,038,300.00

(10) Number of Research Students employed

One (1) Research Student
Research student: Mr. W. G. C. Bandara (09th March 2019 – 31st December 2020)
Registered for postgraduate degree: No

(11) Postgraduate degree completed with dates

None

(12) Number of Technical Assistants and/or labourers employed and period of service

None

(13) Publications/Communications arising from the project during the reporting period

Journal Papers: Three (03)

(1) W.G. Chaminda Bandara, G.M.R.I. Godaliyadda, M.P.B. Ekanayake, J.B. Ekanayake, "Coordinated *Photovoltaic Re-Phasing:* A Novel Method to Maximize Renewable Energy Integration in Low Voltage Networks by Mitigating Network Unbalances", Applied Energy, Volume 280, 2020, 116022, Elesevier
SCIE Journal Impact Factor: 9.746

(2) Wele Gedara Chaminda Bandara, Dilini Almeida, Roshan Indika Godaliyadda, Mervyn Parakrama Ekanayake, Janaka Ekanayake, "A Complete State Estimation Algorithm for a Three-Phase Four-Wire Low Voltage Distribution System with High Penetration of Solar PV", Electrical Power and Energy Systems, Volume 124, 2021, 106332, Elesevier
SCIE Journal Impact Factor: 4.630

(3) A. S. Jameel Hassan, Umar Marikkar, G. W. Kasun Prabhath, Aranee Balachandran, W. G. Chaminda Bandara, Parakrama B. Ekanayake, Roshan I. Godaliyadda, Janaka Ekanayake, "A Sensitivity Matrix Approach Using Two-Stage Optimization for Voltage Regulation of LV Networks with High PV Penetration", Energies, Volume 14(20), 2021, 103390, MDPI
SCIE Journal Impact Factor: 3.004

Conference Papers: One (01)

(1) Aranee Balachandran, G. W. K. Prabhath, W. G. Chaminda Bandara, G. M. R. I. Godaliyadda, M. P. B. Ekanayake, J. B. Ekanayake, "Reactive Power Compensation for Voltage Violations in Distribution Network", 14th IEEE International Conference on Industrial and Information Systems (ICIIS), Kandy, Sri Lanka, 18-20 December, 2019

Patent Applications: One (01)

(1) Sri Lankan Patent Application Number 21543 (Submitted on 12th January, 2021; Under Review) Title: Single Phase Re-Phasing Solar Inverters for a Re-Configurable LV Network that has Accepted Voltage Profiles and Unbalances

Section 2: Executive Summary

The Sri Lankan Government promotes solar power through '*Suriya Bala Sangrahamaya*' and is hoping to develop 1000 MW of PV systems by 2024. Currently solar PV power systems in excess of 100 MW are in operation with roof-top solar modules making a small but significant contribution. However, in some areas, CEB is not allowing to connect roof-top PV modules due to the fears of possible over voltages in lines, overloading of lines and losing the supply security. Even though rooftop PV modules can be looked at as a burden to the last mile networks, if they are properly controlled and supervised they will bring many technical and economic advantages for the last mile networks.

Therefore, in this research network management strategies executed through a Smart Distribution Management System (S-DMS) that integrates different controllable entities within the last mile network is considered to support these networks thus increasing the absorbability of rooftop PV. The management of the following controllable entities through a S-DSM in a coordinated manner will be investigated:

- Smart inverters of rooftop PV systems that can provide grid support through active and reactive power control.
- Smart meters connected to the consumer premises that can make the load flexible by controlling, shifting or switching off some smart and non-critical loads and charging and discharging plug in electric vehicles.
- Smart transformer at the origin of the last mile network that can change its secondary side voltage continuously to manage the network voltages.

The aim of the research is to develop different building blocks of a S-DMS that include the load and solar PV prediction algorithms based on the smart meter measurements; state estimation algorithms to predict the network status ahead of the real time; algorithms to control and manage the smart inverters, smart transformer and demand side; and coordinated control algorithms to minimize network constraints and maximize rooftop PV penetration.

Section 3: Report in Detail

Literature Review

The demand for energy is increasing day by day. In order to meet this demand, different types of energy sources are widely used (e.g. coal, oil, natural gas, nuclear power, etc.). The consumption of fossil fuels to generate energy is increasing the emission of greenhouse gases and can lead to serious environmental problems. Recent advances in the technology associated with renewable energy sources (RES) such as solar and wind have significantly increased the integration of renewable energy into the power system. Among these RESs, photovoltaic (PV) solar energy is one of the fastest-growing renewable energy sources with an annual growth rate of $30\% - 40\%$ [1]. Over the past decade, the installation of single-phase grid-connected rooftop photovoltaic systems at consumer premises in the Low Voltage (LV) distribution networks have been increasing worldwide. The two main reasons for this increase are the better efficiency of PV systems and inverters, and the low cost due to government benefits such as rebates, subsidies for the initial cost of the system, feed-in tariff, etc. [1].

Due to the associated uncertainty, asynchronous nature and high variability of grid-connected PV systems, LV distribution networks face various power quality problems, such as voltage regulation, sustained interruptions, harmonics, and voltage drops [1]. These power quality problems are further exacerbated by the imbalance caused by the uneven distribution of single-phase loads, PV solar systems, and the integration of unconventional loads (e.g. EV charging units [2]). The impact of such an imbalance is profound and widely discussed in the literature [3]–[6]. The imbalance in the phase voltages and the consequent flow of large unbalanced currents can increase distribution and transformer losses due to overheating. Since most LV distribution systems are generally made with a three-phase four-wire circuit configuration, the presence of zero sequence current can cause a neutral conductor overload. High neutral currents generate higher neutral to ground voltages than the standard ratings [3]. When LV distribution networks are equipped with synchronous generators (e.g. wind turbines, micro-hydro, biodiesel-powered generators), the imbalance load can cause excessive mechanical stress (vibrations), noise, and malfunctions of the protection relays due to harmonic flow in the neutral. These neutral harmonics and high-frequency noise have also been found to severely interfere with Power Line Communications (PLC) [3]. The aforementioned impacts of distribution networks ultimately increase the overall costs of operation and maintenance of the power system. Therefore, it is highly desirable to reduce the unbalance in LV distribution networks to ensure power quality. How to effectively reduce the unbalance is a long-standing question, and much effort has been devoted to answering this question in the past decade.

In the literature, many techniques have been proposed to minimize the imbalance. These techniques can be divided mainly into two categories (see Figure 1). The first category mitigates the network imbalance by using neutral current compensation devices such as passive harmonic filters and specially designed transformers (e.g. synchronous machines as filters [7], T-connected transformer [8], star-hexagon transformer [9], zigzag transformer with single-phase series/shunt active power filter [10], and star-delta transformer with single-phase half-bridge PWM [11]), and specially designed *active power filters* (e.g. H-bridge shunt APF [12], three-phase four-wire capacitor midpoint APF [13] and 3P4W four-leg APF topology [14]). The second category is based on distribution network reconfiguration techniques and can be divided into two types: distribution feeder reconfiguration (DFR) and phase balancing. The DFR technique alters the topological structure of the network by closing tie switches or opening sectionalizing switches to achieve the desired objective function subject to network and

operational constraints. The phase balancing technique alters the phase combination between the three-phases to mitigate the network imbalance. It is important to note that both DFR and phase balancing techniques use non-linear, non-differentiable, highly combinatorial, and constrained optimization algorithms to find the optimal solution [15].

Due to the advent of smart grid technology and the availability of reliable network information in real-time, it is possible to operate DFR and phase balancing techniques remotely from a central control system. Additionally, phase balancing and DFR techniques can reduce total power loss, voltage, or current imbalance without purchasing new equipment when compared with the first category. Due to these reasons, DFR and phase balancing techniques are widely utilized to mitigate the impact of voltage imbalance in smart grids. In the subsequent sections, the state-of-the-art DFR and phase balancing techniques are discussed in detail.

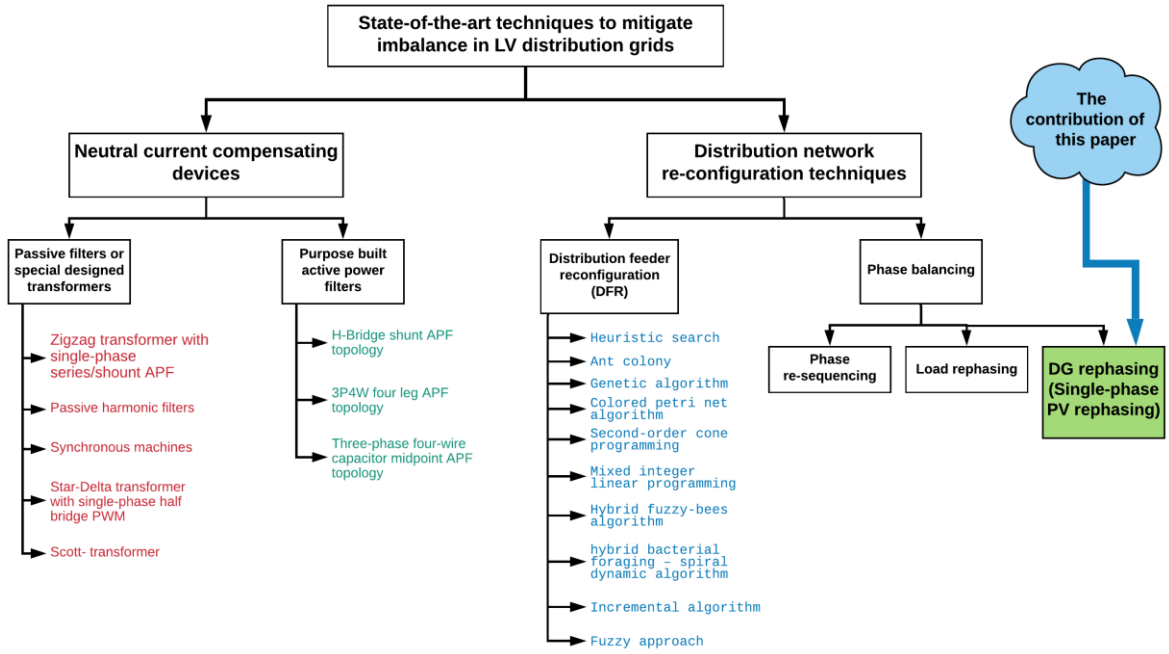

Figure 1: Available practical techniques to mitigate imbalance in the LV distribution networks

DFR techniques

The DFR technique optimizes the open or closed state of sectionalizing switches and tie switches to transfer the loads from overloaded feeders to the lightly loaded feeders to minimize desired objective functions (e.g., voltage imbalance, load imbalance, power loss, etc.) while preserving the radial configuration of the LV distribution systems [16].

Many researchers have used different optimization techniques such as heuristic search [17], ant colony optimization [18], [19], genetic algorithm [17], [20]–[22], incremental algorithm [23], fuzzy approach [24], [25], colored petri net algorithm [26], [27], second-order cone programming [28], mixed-integer linear programming [29], hybrid bacterial foraging - spiral dynamic [30] algorithms to mitigate load imbalance and power loss using DFR techniques. The time-varying nature of loads and distributed generators, and their uneven distribution in the network cause LV feeders to often become unbalanced. Although the DFR techniques can only mitigate imbalance at the system level it cannot mitigate phase imbalance at the feeder level [3]. Hence, phase balance techniques have been proposed to mitigate feeder level imbalance.

Phase Balancing Techniques

The phase balancing technique can be implemented in two ways: (1) load re-sequencing [4], [31]–[39] and (2) load re-phasing [40]–[42]. In the load re-sequencing technique, the phase sequence at each busbar is re-sequenced to their optimal combination. To avoid the reverse operation of inductive loads, the positive and negative phase sequences are only taken into account [43], [44]. In the load re-phasing technique, the loads from the overloaded phases are transferred to the lightly loaded phases by analyzing the current or power difference between the phases. To identify the optimum phase sequence for the three-phase loads and optimum phase combination for the single-phase loads, different optimization techniques have been proposed. Examples of these include, heuristic search [31], [33], [41], mixed integer programming [32], fuzzy logic and combinatorial optimization [40], particle swarm optimization [43], bacterial foraging – particle swarm optimization [43], simulated annealing [35], [45] and genetic algorithm [36]–[38], [42]. However, these techniques were tested on the small LV networks with a few loads and have not been considered for large LV networks due to the high computational time they take to identify the optimum solution. Finally, these phase balancing techniques based on single-phase and three-phase loads and feeders raise many concerns, such as:

- The fact that load switches must be installed between the phases, at each end of the client. As a result, these phase balancing techniques are not suitable for large LV networks, due to the high initial cost for the installation of load switches [3].
- In addition to the high initial cost, these load re-phasing techniques are subject to several indirect costs such as the cost of customer interruption, the cost of customer reliability, etc. [46].
- The fact that sequencing or re-phasing loads can adversely affect the operation of customer devices.

  In order to avoid the aforementioned practical problems in load re-sequencing and load re-phasing methods, this paper proposes a novel re-phasing technique based on grid-connected single-phase PV systems.

Hardware Emulation and Inverter Design

Many researchers focus on mitigation techniques and use either hardware or simulation-based environments to validate their solutions. Any of this method should be accurate, reproducible and at the same time be economical and easy to implement. Alternatively, the test environment should be kept at minimal risk. Authors of [10] shows that most of these techniques are tested in a simulation-based manner. Reference [11] presents a study on the effect of line impedance and loading on the voltage profile in distribution network with distributed solar photovoltaic system using MATLAB/SIMULINK platform. Reference [12] has used OpenDSS along with Python and MATLAB to investigate the effects of distributed generation on power system. In reference [13] the complete power system is implemented in MATLAB/Simulink and, LabVIEW has been used to enable fast and reliable measurement functions.

However, all above kinds of simulations have a gap with the real scenario as they do not consider most of the real time effects on distribution networks such as temperature variations, load changes etc. Only a limited number of research have been done considering this aspect [14,15,16]. To address this issue, our focus was on developing an emulator of a distribution

network with high PV penetration. This emulator mainly attempts to mimic the behavior of a real distribution line and is a compromise of smart metering infrastructure, energy storage system, solar PV setup with open-source inverters and a SCADA system.

PV re-phasing arrangement

In this section, the structure of the re-phasing switch and the operating mechanism of automatic PV re-phasing in LV distribution grids are explained.

Structure of the PV re-phasing switch

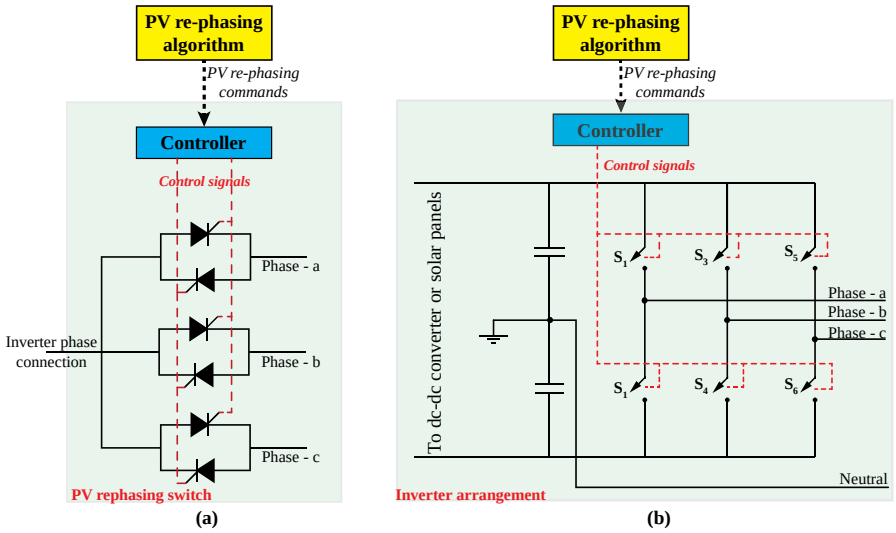

Figure 2: (a)-Thyristor switch, (b)-Inverter arrangement

Figure 2-(a) shows a schematic of a PV rephasing switch that can be connected to the output of the single-phase inverter. As can be seen, switching between phases can be achieved by blocking the already conducting pair of thyristors (or triac) and turning the pair of thyristors that are connected to the phase to which output should be connected. In order to avoid any circulating current between phases, a dead band should be introduced between the blocking signal and the turning on signal. However, this will eventually course the PV inverter to take the start-up mode, thus, introducing an interruption of a few minutes (less than 3 min). The inverter shown in Figure 2-(b) can be used to prevent such a transient. In this arrangement, a half-bridge inverter is used to convert dc into ac. If the output needs to be connected to Phase - a then switches S_1 and S_2 are operated in a complementary manner using a PWM switching pattern and all the other switches are blocked. If the output needs to be connected to Phase - b then S_1 and S_2 will be blocked and S_3 and S_4 will be turned on. As these switching transients take nanosecond level times, it can be used as a rapid rephasing arrangement but with extra cost for the two switching arms. The same arrangement can be introduced for full-bridge single-phase inverters.

The architecture of the automatic PV re-phasing arrangement

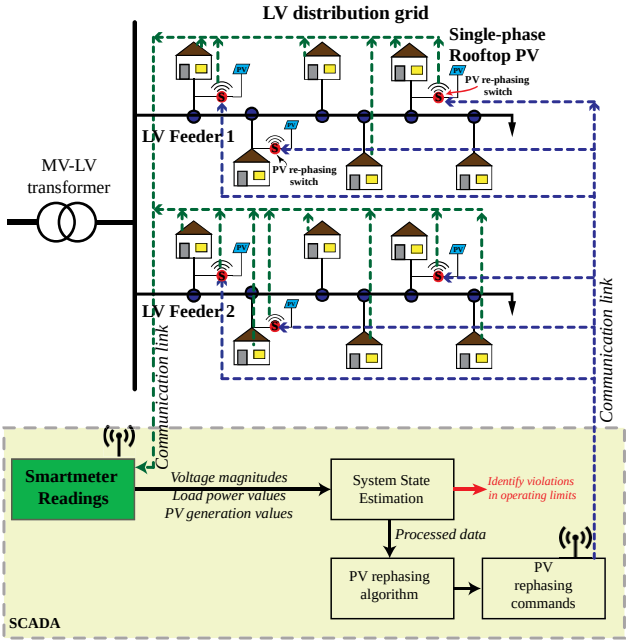

Figure 3: Schematic of the automatic PV re-phasing arrangement

Figure 3 shows the operating mechanism of the proposed PV re-phasing strategy. The necessary data such as PV generations and load demands are measured from smart meters and transmit to the supervisory control and data acquisition unit (SCADA). Typically, these smart meter measurements are subjected to different types of systematic, random, and communication errors. Therefore, in the next step, state estimation is performed to detect the presence of bad data. These preprocessed smart meter data are sent to the PV re-phasing algorithm to determine the optimal phase combination of grid-connected PV systems such that the overall voltage unbalance of the network is minimized. Finally, the re-phasing program transmits the required phase changes of PV systems to the SCADA system. Then, SCADA sends required re-phasing commands to the installed PV re-phasing switches and re-phasing operation is carried out.

Problem formulation

The aim of this work is to develop a strategy to minimize the overall voltage unbalance of the network such that the power quality and the reliability of the distribution system can be improved. The objective of this optimization problem can be expressed as the minimization of the mean voltage unbalance factor ($\overline{VUF}$) of the network as in,

$$\overline{VUF} = \frac{1}{N}\sum_{n=1}^{N} VUF_n \qquad (1)$$

where, VUF_n is the voltage unbalance factor at n-th busbar and N is the total number of busbars in the network.

Subjected to the constraints:

1. Voltage unbalance at each busbar (VUF_n) must be strictly below the specified maximum unbalance level (VUF_{max}):
$$VUF_n \leq VUF_{max} \quad (\mathbf{2})$$
for $n = 1,2,3,\dots,N$.
2. Phase voltage magnitudes ($V_n^a, V_n^b,$ and V_n^c) must strictly between the upper (V_{max}) and lower (V_{min}) limits:
$$V_{min} \leq V_n^a, V_n^b, V_n^c \leq V_{max} \quad (\mathbf{3})$$
for $n = 1,2,3,\dots,N$, where, V_n^a, V_n^b and V_n^c are the voltage magnitudes of a, b, and c phases at n-th busbar, respectively.

Equation **(1)** corresponds to the objective function to be minimized and represents the overall voltage unbalance ($\overline{VUF}$) of the distribution network. The inequality in **(2)** considers a constraint for voltage unbalance factor and ensures individual voltage unbalance factors (VUF_n for $n = 1,2,..,N$) are below the specified maximum value, VUF_{max}. The inequality in **(3)** deals with the constraints for voltage magnitudes. It ensures the phase voltages ($V_n^a, V_n^b,$ and V_n^c) fall within the acceptable voltage limits (lower limit V_{min} and upper limit V_{max}). In this study, V_{min} was considered as 0.94 pu and V_{max} was considered as 1.06 pu. In other words, **(2)** and **(3)** define the feasible regions for voltage unbalance (VUF_n) and phase voltage magnitudes (V_n^a, V_n^b, V_n^c), respectively.

In order to minimize **(1)** while simultaneously satisfying the constraints **(2)** and **(3)**, penalty functions were introduced. The main idea of these penalty functions is that an optimal PV configuration (i.e. the optimal solution) requires that constraints be active so that this optimal solution lies in the feasible regions for voltage unbalance and phase voltage magnitudes. To ensure this, a penalty is applied to possible solutions when constraints are not satisfied. Therefore, the aforementioned optimization problem was reformulated as the minimization of the penalized objective function, $J(\boldsymbol{x})$, given by,

$$J(\boldsymbol{x}) = \overline{VUF} + k_1 \sum_{n=1}^{n=N} \mu_{VUF_n} + k_2 \left(\sum_{n=1}^{n=N} \mu_{V_n^a} + \sum_{n=1}^{n=N} \mu_{V_n^b} + \sum_{n=1}^{n=N} \mu_{V_n^c} \right) \quad (\mathbf{4})$$

where,

the penalty function for voltage unbalance (μ_{VUF_n}) is given by:

$$\mu_{VUF_n} = \begin{cases} VUF_n - VUF_{max} & ; \text{ when } VUF_n > VUF_{max} \\ 0 & ; \text{ when } VUF_n \leq VUF_{max} \end{cases} \quad \text{for } n = 1, \dots, N,$$

the penalty function for voltage magnitudes of phase A ($\mu_{V_n^a}$) is given by:

$$\mu_{V_n^a} = \begin{cases} |V_n^a - V_{min}| & ; \text{when } V_n^a < V_{min} \\ 0 & ; \text{when } V_{min} \leq V_n^a \leq V_{max} \\ V_n^a - V_{max} & ; \text{when } V_n^a > V_{max} \end{cases} \quad \text{for } n = 1, \dots, N,$$

the penalty function for voltage magnitudes of phase B ($\mu_{V_n^b}$) is given by:

$$\mu_{V_n^b} = \begin{cases} |V_n^b - V_{min}| \text{ ; when } V_n^b < V_{min} \\ 0 \text{ ; when } V_{min} \leq V_n^b \leq V_{max} \\ V_n^b - V_{max} \text{ ; when } V_n^b > V_{max} \end{cases} \quad \text{for } n = 1, \dots, N,$$

the penalty function for voltage magnitudes of phase C ($\mu_{V_n^c}$) is given by:

$$\mu_{V_n^c} = \begin{cases} |V_n^c - V_{min}| \text{ ; when } V_n^c < V_{min} \\ 0 \text{ ; when } V_{min} \leq V_n^c \leq V_{max} \\ V_n^c - V_{max} \text{ ; when } V_n^c > V_{max} \end{cases} \quad \text{for } n = 1, \dots, N,$$

$\boldsymbol{x}$ is the PV configuration vector, and $k_1$and k_2 are the constant imposed on the penalty functions. The graphical illustrations of these penalty functions are shown in Figure 4.

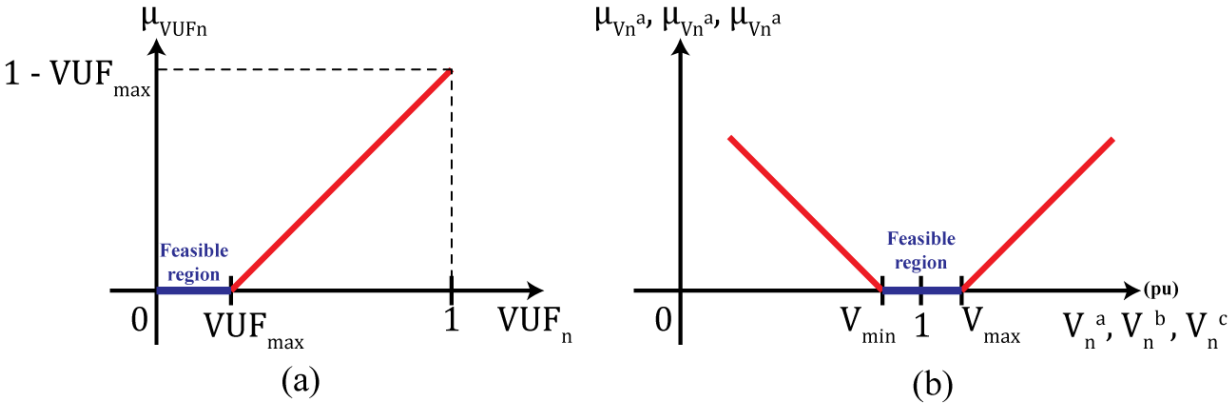

Figure 4: Penalty functions for (a) voltage unbalance and (b) phase voltage magnitudes.

The phase combination of grid-connected PV systems at a given time is represented by the *PV configuration vector*, $\boldsymbol{x}$. Therefore, for a network having N_{pv} number of grid-connected PV systems, the PV configuration vector $\boldsymbol{x}$ consists of N_{pv} number of phase entries where each phase entry corresponds to the phase of a grid-connected PV system in the network. Hence, each element (x_m) in the PV configuration vector, $\boldsymbol{x}$ can take one of the three phases ($i.e. \boldsymbol{x}_m \in \mathbb{P}, \mathbb{P} = \{a, b, c\}$). The format of the PV configuration vector is illustrated in Figure 5 with an example PV combination.

Format of the PV configuration vector $\boldsymbol{x} \in \mathbb{P}^{N_{pv}}$

Phase of PV_1	Phase of PV_2	Phase of PV_3	…	…	Phase of PV_m	…	…	…	Phase of $PV_{N_{pv}}$

Example PV configuration vector $\boldsymbol{x}^i$

Phase a	Phase b	Phase c	…	…	$x_m \in \mathbb{P}$	…	…	…	Phase a

Figure 5: The format of the PV configuration vector $\boldsymbol{x}$

It is important to note that there are different definitions available for the voltage unbalance factor; in this paper, the IEC definition [47] was used. In the IEC definition (IEC TR 61000-3-14:2011), the voltage unbalance factor is calculated as the ratio of negative sequence voltage component to the positive sequence voltage component and can be expressed as follows [47]:

$$VUF_n = \frac{V_n^-}{V_n^+} = \frac{\text{Negative sequence voltage component at } n^{\text{th}} \text{ busbar}}{\text{Positive sequence voltage component at } n^{\text{th}} \text{ busbar}} \quad (\mathbf{5})$$

The three-phase sequence voltage components were obtained by the symmetrical transformation. The steps for the computation of three-phase sequence voltage components from three-phase voltages can be found in [4].

Bacterial Foraging Optimization

Bacterial foraging optimization algorithm (BFOA) is a smart optimization technique that has proven to be very effective in search domains having several dimensions. BFOA is inspired by the social foraging behavior of *E. coli* bacteria. The underlying biology behind the foraging strategy of *E. coli* is emulated and used as a simple optimization algorithm [48], [49]. In this paper, a discrete and adaptive version of BFOA is introduced to solve the PV re-phasing problem.

Concept of BFOA

During the foraging period, real bacteria achieve their motion with the help of their tensile flagella. Using these tensile flagella, bacteria can perform two basic motion types called tumble and swim. In the classical BFOA, the bacteria undergo *chemotaxis*, where they like to move towards nutrient gradient while avoiding the noxious environments. When they get a sufficient amount of food, they increase their length and under suitable temperature, they break in the middle to form an exact replica of itself. This phenomenon is called the event of *reproduction* in BFOA. However, due to the occurrence of sudden environmental changes or attacks, the chemotaxis progress may be destroyed and a group of bacteria may move to some other place or some other mutation may be introduced to the bacteria population. This phenomenon is called the *elimination dispersal event* in BFOA, where all the bacteria in the region are killed or a group is dispersed into a new part of the environment. References [30], [48]–[52] provide a comprehensive analysis of the classical BFOA in different optimization problems.

Primary steps of the proposed DBFOA

The proposed DBFOA improves upon the classical BFOA by modifying the principal mechanisms to specifically handle the PV re-phasing problem. The modified versions of the principal mechanisms of the algorithm were named as *D-Chemotaxis***,** *D-Reproduction***,** and *D-Elimination dispersal*. The following subsections discuss these three principal mechanisms which drive the proposed DBFOA. The mapping of the terms in the PV re-phasing problem and the classical BFOA problem are shown in Table 1.

Table 1: Related terminology

Variable	Definition in PV rephrasing problem	Definition in classical BFOA
N_{pv}	The number of grid-connected PV systems in the network	The dimension of the search space
S	The number of PV configuration initializers	Total population of the bacterium
N_c	The number of D-chemotactic steps	The number of chemotactic steps
N_r	The maximum number of random phase changing steps performed	The swimming length
N_{re}	The number of D-Reproduction steps	The number of reproduction steps
P_{ed}	D-elimination dispersal probability	Elimination dispersal probability
i	i-th PV configuration vector	The i-th bacterium in the population
j	Incremental counter (index) for D-chemotaxis step	Index for the chemotaxis step
k	Incremental counter (index) for D-reproduction step	Index for the reproduction step
l	Incremental counter (index) for D-elimination dispersal step	Index of the elimination-dispersal event
r	Incremental counter (index) for the random phase changing step	Index for swimming step
$J(i,k,k,l)$	The cost of i-th PV configuration vector $\boldsymbol{x^i}(j,k,l)$	The cost at the location of the i-th bacterium $\boldsymbol{x^i}(j,k,l)$

Discrete Chemotaxis (D-Chemotaxis):

The D-Chemotaxis step updates the phase combination in a PV configuration vector such that the new phase combination has a lower cost value compared to its previous phase combination. In other words, the D-Chemotaxis step updates the phase combination in a direction corresponding to a gradient of decreasing cost value.

Here, the present phase combination in i-th PV configuration vector is given by $\boldsymbol{x}^i(j,k,l)$ and it's updated version is denoted by $\boldsymbol{x}^i(j+1,k,l)$ where, j, k, and l are the index for D-Chemotaxis, D-Reproduction, and D-Elimination dispersal, respectively.

The proposed D-Chemotaxis step first identifies the highest unbalance region (${\mathbb{H}_{VU}}^i$) in the network corresponding to the phase combination in the i-th PV configuration vector, $x^i(j,k,l)$. Here, the highest unbalance region is referred to the busbars within $\mathrm{k_n}$ number of busbars from the busbar with highest unbalance ($\mathrm{n_{VUF_{max}}}$). Once the highest unbalance region ${\mathbb{H}_{VU}}^i$ is identified, only the phase combinations of grid-connected PV systems in the highest unbalance region, ${\mathbb{H}_{VU}}^i$, are randomly changed to generate the updated phase combination, $x^i(j+1,k,l)$. This reduces the number of possible phase configurations greatly, while mitigating the impact of re-phasing on the overall network. However, the random change in the phases of PV systems in the highest unbalance region ${\mathbb{H}_{VU}}^i$ does not guarantee that it finds a phase combination with a lower cost value compared to its present phase combination $x^i(j,k,l)$ at once. Therefore, in such a situation, the random phase changing is repeated until it finds a suitable phase combination with lower-cost value, within a maximum of N_r iterations. If D-Chemotaxis is unable to find a phase combination with lesser cost value within the maximum N_r cycles, then the present phase combination $x^i(j,k,l)$ is retained as its updated phase combination $x^i(j+1,k,l)$ as it is reasonable to assume that we have reached a low-cost point through random changes.

The pseudocode of the D-chemotaxis procedure is given in Algorithm 1 and the main steps are depicted in Figure 6.

Algorithm 1: D-Chemotaxis

Step 1: Perform a load flow analysis for the phase combination in i-th *PV configuration vector*, $\boldsymbol{x^i}(j,k,l)$.

Step 2: Evaluate the cost function-$J(i,j,k,l)$ based on the load flow results, and set $J_{last} = J(i,j,k,l)$.

Step 3: Identify the busbar with the highest voltage unbalance $n_{VUF_{max}}$ and, then identify the busbars within the radius of k_n busbars from the busbar with highest unbalance $n_{VUF_{max}}$ to form the highest unbalance region, $\mathbb{H}_{VU}$.

Step 4: Randomly change the phase combination of PV systems in the highest unbalance region $\mathbb{H}_{VU}$ to find a phase combination with lower-cost value compared to J_{last}.

Step 5: If a suitable phase combination is identified within N_r steps, then use that phase combination as the updated phase combination, $\boldsymbol{x}^i(j+1,k,l)$.

Step 6: Else, $\boldsymbol{x^i}(j+1,k,l) = \boldsymbol{x}^i(j,k,l)$.

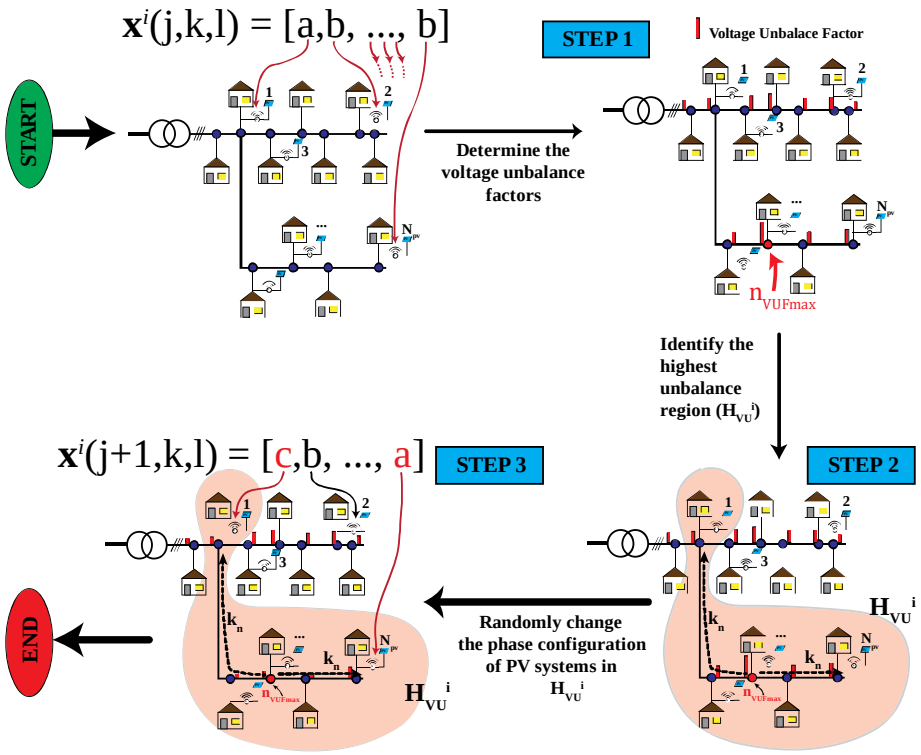

Figure 6: Proposed D-Chemotaxis procedure

Discrete Reproduction (D-Reproduction)

In *D-Reproduction*, the PV configuration vector having the highest cumulative cost (i.e. worst PV configuration) is eventually replaced by the PV configuration vector with the least cumulative cost (i.e. best PV configuration). The cumulative cost of the i-th PV configuration vector (J_C^i) for a given k and l was calculated from,

$$J_C^i = \sum_{j=1}^{N_C+1} J(i,j,k,l) \qquad (6)$$

The pseudocode of the D-Reproduction step is given in Algorithm 2.

Algorithm 2: D-Reproduction

Step 1: Determine the cumulative cost J_C of all the *PV configuration vector*s for given k and l from Equation **(6)**.

Step 2: Replace the phase combination of the PV configuration vector having the highest cumulative cost by the phase combination of the *PV configuration vector* having the least cumulative cost.

Discrete Elimination Dispersal (D-Elimination Dispersal)

In *D-Elimination Dispers*al, some PV configuration vectors are randomly liquidated (eliminated) with a very small probability P_{ed} while the new replacements are randomly initialized over the search space. The D-Elimination Dispersal operator helps PV combinations that are trapped in local minima to escape.

The pseudocode of the D-Elimination Dispersal step is given in Algorithm 3.

Algorithm 3: D-Elimination Dispersal

Step 1: For all PV configuration vectors (i.e. for $i = 1,2,3, \dots, S$) repeat the following steps to perform D-Elimination dispersal.

Step 2: Generate a Random Number between 0 and 1: $RN^i = rand(0,1)$.

Step 3: If $RN^i \leq P_{ed}$, Replace the phase combination in i-th PV configuration vector by a random phase combination.

Step 4: Else, proceed to **Step 2** for the next PV configuration vector ($i = i + 1$).

Initialization of PV configuration vectors

The BFOA is a population-based optimization algorithm. Hence, the quality of the optimal solution and the time to convergence heavily depend on the initial population (in this paper the initial population is also referred to as the set of PV configuration initializers to add more contextual flavor). In most of the situations, the initial population is randomly selected from the solution space. However, it has been noted that random initialization is not an effective way to initialize the PV configuration initializers, especially when more contextual information is available to better optimize the selection of the initial points. Therefore, a novel initialization method was introduced to identify the suitable phase combinations for PV configuration initializers. A performance comparison is added in the results and discussion to highlight the effectiveness of the proposed initialization technique.

The proposed initialization method determines the initial phase combinations for the PV configuration initializers in such a way that those initial phase combinations have a small active power mismatch (see algorithm 4, step 4) at the secondary side of the MV-LV transformer. The suitable phase combinations with minimum active power mismatch were selected from the brute force checking strategy where the active power mismatch for the whole solution space is computed to identify the phase combinations that have, smaller active power mismatch. However, for a network that has a large number of grid-connected PV systems, the brute force searching will take a long time to find a set of suitable phase combinations with smaller active power mismatch. Therefore, in order to improve the speed of the initialization, such large networks are partitioned into smaller regions ($R_1, R_2, R_3, \dots$) and the active power balancing was considered separately for each region (see Figure 9). In other words, a regional minimization is performed to facilitate the global optimization. The proposed initialization process is graphically illustrated in Figure 7 and the pseudocode is given in Algorithm 4.

Algorithm 4: Initialization of PV configuration initializers

Step 1: Collect the active power consumption of loads and the active power generation through smart meters.

Step 2: Partition the large network into smaller regions ($R_1, R_2, R_3, \dots, R_r$).

Step 3: Identify the solution space (i.e. all possible phase combinations) for each region. Note: For a region having w number of grid-connected PV systems, there are 3^w possible phase combinations in the solution space.

Step 4: ***Execute in parallel for*** $R_1, R_2, R_3, \ldots, R_r$**:**
1) Calculate the active power mismatch for each phase combination in the solution space. The active power mismatch is quantified by the standard deviation of the three-phase active power in that region.
2) Identify $k_R(=4)$ phase combinations having a smallest active power mismatch among the all possible phase combinations.

Step 5: Randomly combine the identified phase combinations for each region to form the initial phase combinations for PV configuration initializers.

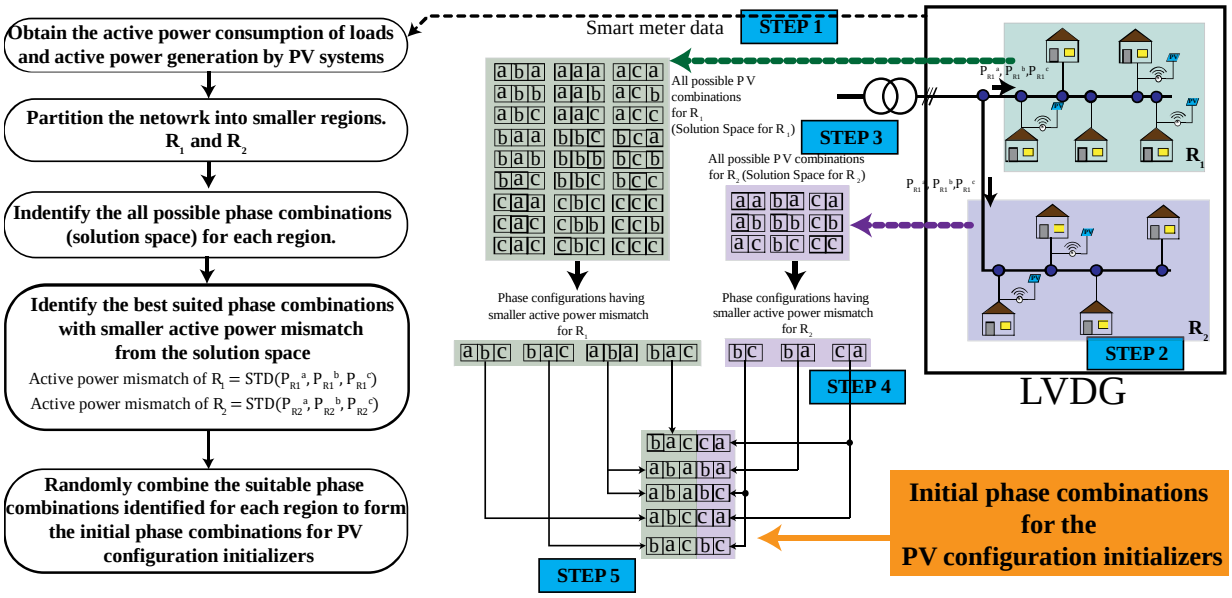

Figure 7: Generation of initial phase combinations for PV configuration initializers based on active power balancing technique for a large distribution network.

Implementation of DBFOA

The complete structure of the proposed DBFOA

The complete structure of the proposed DBFOA is shown in Figure 8.

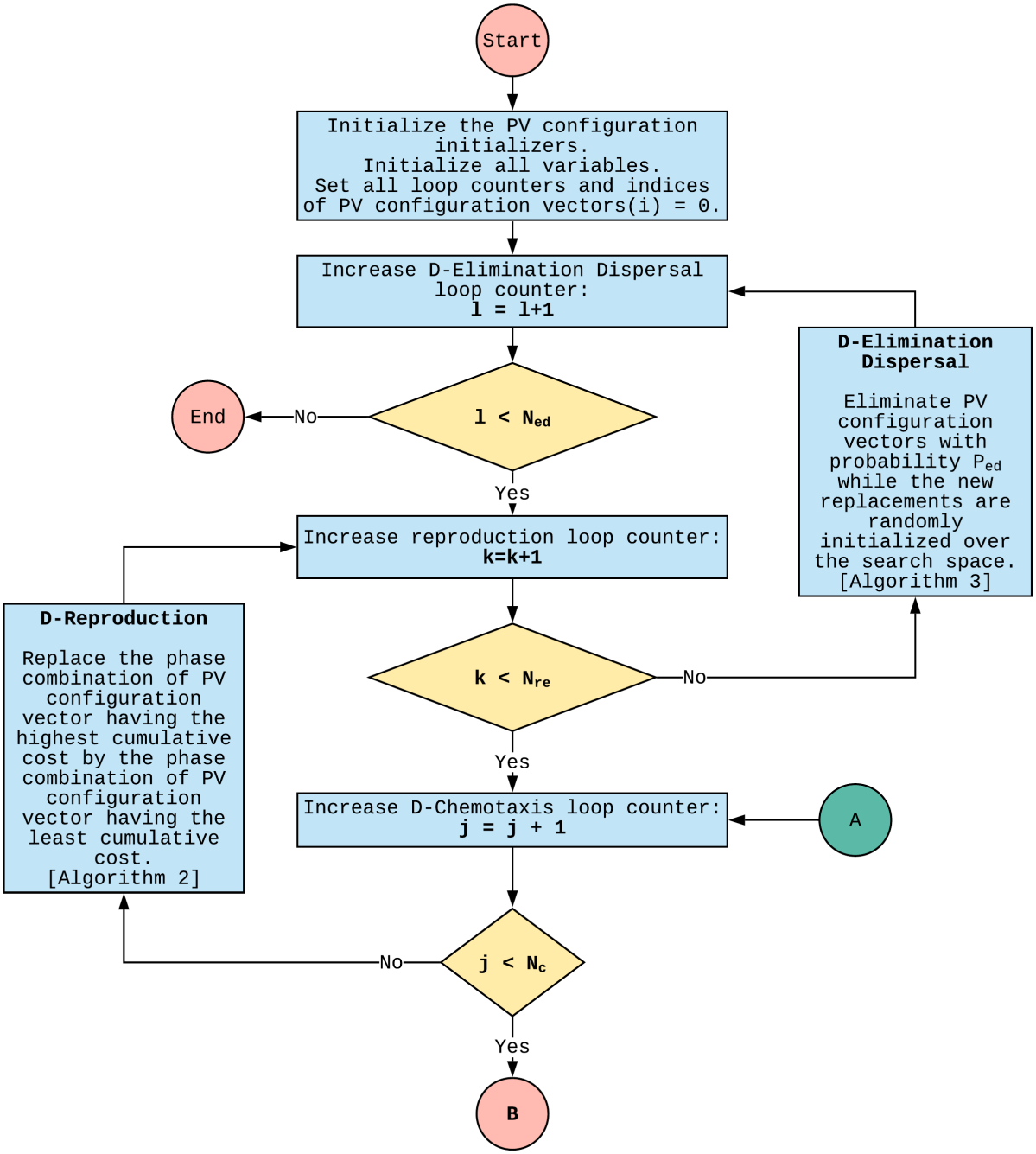

Figure 8: Continued.

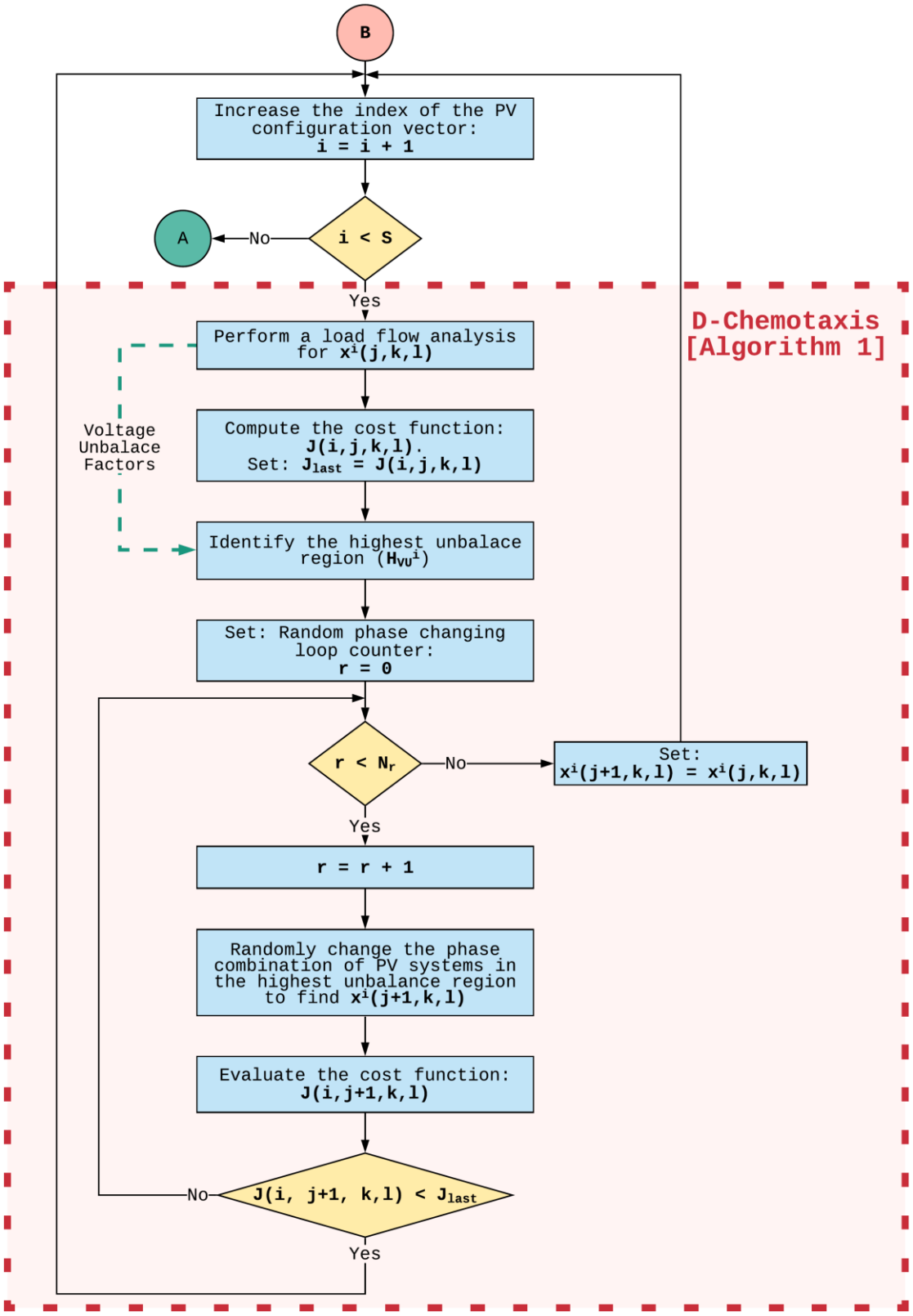

Figure 8: The complete structure of the proposed DBFOA

]

Pseudocode of DBFOA

The pseudocode of the proposed DBFOA applied to reduce the overall unbalance of a network is given in Algorithm 5.

Algorithm 5: The proposed DBFOA

Step 1: **Initialize all the PV configuration initializers - $\boldsymbol{x^i}$ (use Algorithm 4). Initialize of the following parameters:**

- S: The number of PV configuration initializers.
- N_c: The maximum number of D-Chemotaxis is performed.
- N_s: The Maximum number of times random phase changing is performed.
- N_{re}: The maximum number of times D-Reproduction is performed.
- P_{ed}: The probability that each *PV configuration vector*s are eliminated.

Set all loop counters to zero.

- Incremental counter for D-Elimination dispersal step $(l) = 0$.
- Incremental counter for D-Reproduction step $(k) = 0$.
- Incremental counter for D-Chemotaxis step $(j) = 0$.
- Index of the *PV configuration vector*s $(i) = 0$.

Step 2: D-Elimination Dispersal loop: $l = l + 1$.

Step 3: D-Reproduction loop: $k = k + 1$.

Step 4: **D-Chemotaxis loop**, $j = j + 1$. **[Algorithm 1]**

A. **For** $i = 1,2, \dots, S$, execute a D-Chemotaxis step for i-th *PV configuration vector* as follows.

B. Perform a load flow analysis for the phase combination in i-th *PV configuration vector* - $\boldsymbol{x}^i(j,k,l)$ to obtain three-phase voltages and voltage unbalance factors.

C. Evaluate the cost function $J(i,j,k,l)$.

D. Let $J_{last} = J(i,j,k,l)$ so that the *PV configuration vector* having a lower cost could be identified.

E. Identify the highest voltage unbalance region $\mathbb{H}_{VU}^{i}$ corresponding to phase combination $\boldsymbol{x}^i(j,k,l)$ from the voltage unbalance factors obtained in **Step 4 B**.

F. Set: random phase changing loop counter to zero, $r = 0$.

G. While $r < N_r$,

i. Increment the random phase changing loop counter: $r = r + 1$.

ii. Randomly change the phase combination of the PV systems in the highest unbalance region to determine the new phase combination of i-th *PV configuration vector* $\boldsymbol{x}^i(j+1,k,l)$.

iii. Evaluate the cost function $J(i,j+1,k,l)$ corresponding to the phase combination $\boldsymbol{x}^i(j+1,k,l)$.

iv. **If:** $J(i,j+1,k,l) < J_{last}$,
Go to the next *PV configuration vector* $(i = i+1)$ (i.e. Go to **Step 4 B.** to process the next *PV configuration vector*).

v. **Else:**
Go to **Step 4 G.**

H. End of while.
Couldn't find a phase combination better than $\boldsymbol{x}^i(j,k,l)$.
Set $\boldsymbol{x}^i(j+1,k,l) = \boldsymbol{x}^i(j,k,l)$.
Go to the next *PV configuration vector* $(i = i+1)$ (i.e. Go to **Step 4 B.** to process the next *PV configuration vector*).

Step 5: **If,** $j < N_c$ go to **Step 4** $(j = j+1)$. In this case, continue D-Chemotaxis.

Else, go to **Step 6**.

Step 6: **D-Reproduction** [Algorithm 2]:

A. For the given k and l, and for each $i = 1,2,\ldots,S$ evaluate the cumulative cost of i-th *PV configuration vector* as follows:

$$J_C^i = \sum_{j=1}^{N_c+1} J(i,j,k,l)$$

B. Replace the phase combination of the *PV configuration vector* having the highest cumulative cost by the phase combination of the *PV configuration vector* having the least cumulative cost.

Step 7: **If** $k < N_{re}$, go to **Step 3** $(k = k+1)$. We have not reached the number of specified D-reproduction steps, so we start the next generation of the D-Chemotaxis loop.

Else, go to **Step 8**.

Step 8: **D-Elimination Dispersal** [Algorithm 3]:

- **For** $i = 1,2, \ldots, S$, eliminate *PV configuration vectors* with probability P_{ed} while the new replacements are randomly initialized over the search space.

Step 9: **If**, $l < N_{ed}$, go to *Step 2* ($l = l + 1$);
Else, End.

Parameters of DBFOA

The parameter values used in the proposed DBFOA are given in Table 2. The number of PV configuration initializers (S), and the values for N_c, N_r, N_{re}, and N_{ed} were selected by considering the convergence speed of the DBFOA and the values used in the previous studies [30], [48], [50]. The elimination-dispersal probability - P_{ed} and the radius of the highest unbalance region - k_n were selected to maximize the convergence speed of DBFOA by executing the algorithm for a possible range of values for P_{ed} and k_n.

Table 2: Parameter values used for the proposed DBFOA

Parameter	Value
Number of PV configuration initializers (S)	10
Maximum number of D-Chemotaxis steps (N_c)	5
Maximum number of random phase changing steps (N_r)	5
Maximum number of D-Reproduction steps (N_{re})	5
Maximum number of D-Elimination steps (N_{ed})	5
Elimination & dispersal probability (P_{ed})	0.2
The radius of the highest voltage unbalance region - $\mathbb{H}_{VU}$ (k_n)	3
The maximum limit for phase voltage magnitudes (V_{max})	1.06 pu
The minimum limit for phase voltage magnitudes (V_{min})	0.94 pu
The maximum limit for voltage unbalance factors (VUF_{max})	0.3 %
Number of grid-connected PV systems in the network (N_{pv})	26
Number of busbars in the network (N)	63

Test network

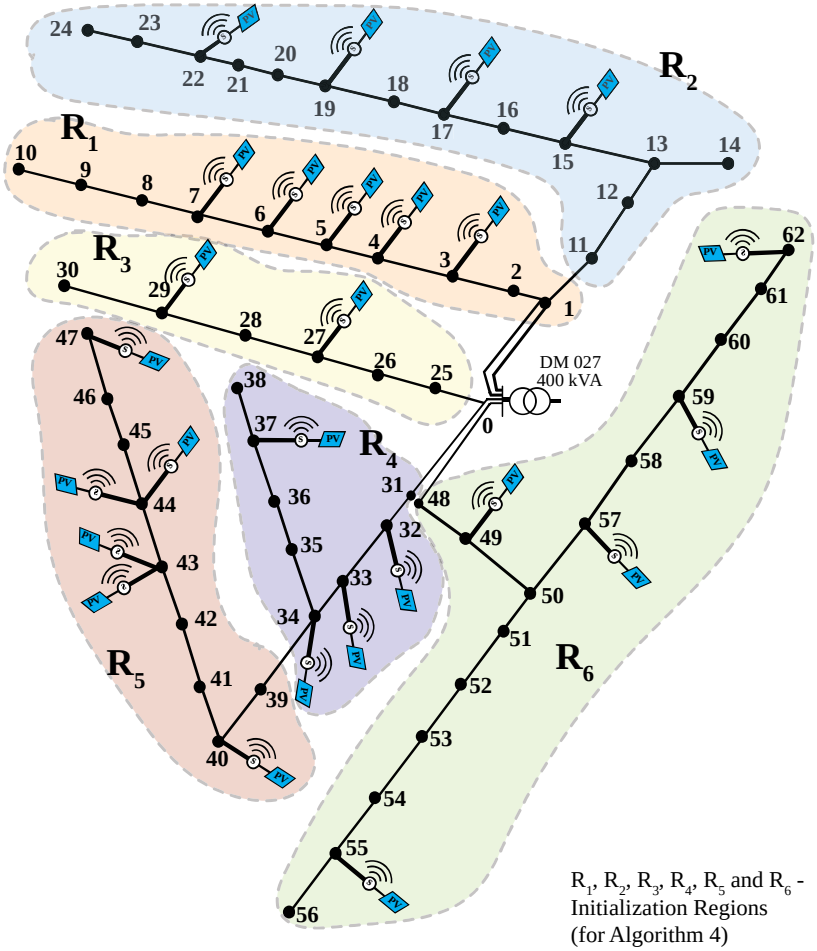

Figure 9: Single line diagram of the test LVDG network (Lotus Grove, Sri Lanka) used for the simulations.

The network topology with 63 busbars as shown in Figure 9 was used for the simulations. The number 0 node is the root node and connected to the secondary side of the MV-LV transformer. The rated capacity of the transformer is 400 kVA and the input/output voltage rating is 11 kV/415 V. The solid lines in Figure 9 represent the three-phase feeders with three-phase or single-phase loads and PV systems connected. The per length impedance matrix of the feeder line is given in Table 3.

Table 3: Impedance matrix (Z^{abcn}) per km for the overhead cable (ABC 70) in the network.

	Phase a	Phase b	Phase c	neutral
Phase a	$0.4918 + 0.7888i$	$0.0486 + 0.6292i$	$0.0487 + 0.6701i$	$0.0486 + 0.7000i$
Phase b	$0.0486 + 0.6292i$	$0.4918 + 0.7888i$	$0.0487 + 0.6405i$	$0.0486 + 0.6490i$
Phase c	$0.0487 + 0.6701i$	$0.0487 + 0.6405i$	$0.4918 + 0.7888i$	$0.0487 + 0.7080i$
Neutral	$0.0486 + 0.7000i$	$0.0486 + 0.6490i$	$0.0487 + 0.7080i$	$0.6790 + 0.7910i$

There are 26 grid-connected single-phase PV systems and 92 single-phase or three-phase loads. The capacity of PV systems, their locations, and their default phase configuration

are given in Table 4 and the daily operation curve (hourly generation profile) of PV systems is shown in Figure 10-(a).

Table 4: The details of the grid-connected single-phase PV systems connected to the network

PV No.	Connected busbar	Initial phase configuration (Fixed phase)	Capacity (P_{max})/ kW
PV1	**3**	a	3.60
PV2	**4**	b	10.80
PV3	**5**	a	7.20
PV4	**6**	c	3.60
PV5	**7**	a	9.00
PV6	**15**	a	7.56
PV7	**17**	b	7.56
PV8	**19**	a	3.60
PV9	**22**	c	18.00
PV10	**27**	a	7.20
PV11	**29**	c	9.72
PV12	**32**	a	9.00
PV13	**33**	b	5.94
PV14	**34**	a	9.00
PV15	**37**	b	4.68
PV16	**40**	c	6.30
PV17	**43**	c	12.60
PV18	**43**	b	12.60
PV19	**44**	c	12.60
PV20	**44**	b	12.60
PV21	**47**	a	14.40
PV22	**49**	a	18.00
PV23	**55**	c	9.54
PV23	**57**	b	8.64
PV25	**59**	a	12.42
PV26	**61**	c	7.74

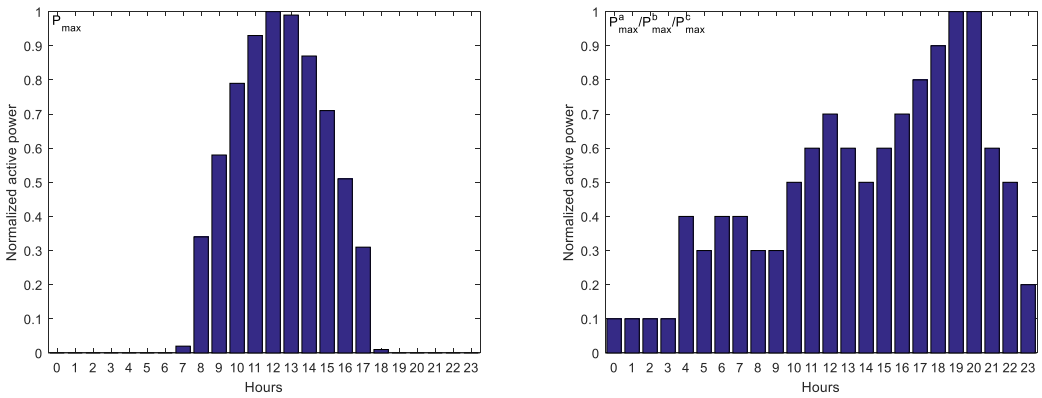

Figure 10: (a) Hourly generation profile of PV systems (b) hourly load profile for single-phase/ three-phase loads.

Moreover, the network shown in Figure 9 consists of 92 single-phase and three-phase loads. The maximum capacity of loads and their power factor values at each busbar are given in Table 5, and the hourly load profile of loads is shown in Figure 10-(b).

Table 5: The capacity of loads and power factor values at each busbar

Busbar	Active power/ (kW)			pf	Busbar	Active power/ (kW)			pf
	P^a_{max} (kW)	P^b_{max} (kW)	P^{ac}_{max} (kW)			P^a_{max} (kW)	P^b_{max} (kW)	P^c_{max} (kW)	
1	2.19	0.55	1.85	0.981	**35**	0.85	0.88	0.75	0.949
1	1.28	0.46	0.55	0.991	**36**	0.67	1.45	1.27	0.945
1	2.43	0.28	1.88	0.913	**37**	0.79	0.66	1.24	0.965
2	2.33	0.26	1.50	0.991	**37**	1.91	1.14	1.63	0.971
3	0.19	0.45	0.34	0.963	**38**	1.97	1.55	1.27	0.975
3	0.12	0.69	0.68	0.910	**41**	1.72	1.05	2.01	0.928
4	0.33	0.58	0.17	0.928	**41**	1.35	1.15	1.39	0.968
4	0.48	0.52	1.08	0.955	**42**	0.47	0.60	0.32	0.966
5	0.54	1.36	0.69	0.996	**42**	1.27	1.50	1.11	0.916
5	1.43	1.43	1.33	0.996	**43**	1.97	0.30	2.12	0.912
6	1.53	2.22	0.64	0.916	**43**	1.27	1.04	0.87	0.950
6	1.04	0.78	0.27	0.997	**44**	0.98	0.25	1.86	0.996
7	0.24	0.25	0.29	0.996	**44**	1.72	0.65	0.41	0.934
7	0.56	1.24	0.79	0.949	**45**	1.06	1.71	1.81	0.959
8	0.54	1.09	2.46	0.980	**45**	0.70	0.76	1.02	0.922
8	1.76	0.42	0.90	0.914	**45**	0.41	2.49	1.99	0.975
9	1.03	2.79	0.86	0.942	**45**	0.69	1.43	1.07	0.926
9	1.18	0.51	0.99	0.992	**46**	0.46	0.15	0.18	0.951
10	0.91	4.05	0.06	0.979	**46**	2.11	1.02	1.85	0.970
13	1.39	1.45	0.74	0.996	**46**	1.01	1.88	1.50	0.989
14	0.16	0.38	0.15	0.966	**47**	1.22	1.05	1.22	0.996
15	4.93	1.57	0.14	0.904	**47**	2.59	1.19	1.10	0.955
15	1.39	2.17	0.32	0.985	**47**	1.39	2.61	0.29	0.914
16	0.96	0.90	0.53	0.993	**50**	2.03	0.89	1.17	0.915
16	1.44	2.95	0.50	0.968	**51**	2.05	0.87	1.86	0.926
17	0.77	0.69	0.72	0.976	**51**	0.48	0.17	0.54	0.984
17	0.92	1.05	0.82	0.974	**52**	0.42	0.43	0.24	0.925
18	0.21	0.74	1.13	0.939	**52**	1.20	1.57	1.52	0.981
18	1.03	1.18	1.88	0.966	**53**	0.59	0.29	0.81	0.924
19	0.34	2.01	1.63	0.917	**53**	1.76	2.61	0.42	0.993
19	1.51	1.04	1.44	0.971	**54**	0.78	1.12	0.89	0.935
20	1.14	1.03	0.21	0.903	**54**	3.42	1.45	0.18	0.920
21	0.73	0.58	0.97	0.928	**55**	0.16	0.04	0.19	0.925
22	1.37	1.89	0.52	0.905	**55**	0.13	0.09	0.06	0.962
22	1.32	1.94	1.02	0.910	**56**	2.36	1.45	0.97	0.947
23	1.28	1.45	1.56	0.982	**57**	0.76	1.03	1.79	0.935
23	0.40	0.27	0.21	0.969	**57**	1.56	0.83	0.99	0.983
24	0.26	0.07	0.26	0.932	**58**	1.69	0.33	1.56	0.959
25	0.90	1.99	0.69	0.995	**58**	1.32	1.37	1.60	0.955
26	2.04	1.80	0.84	0.903	**59**	0.98	1.85	3.82	0.992
27	4.62	0.12	0.30	0.944	**59**	0.95	0.68	0.75	0.929
28	0.52	2.18	1.98	0.938	**60**	0.99	1.35	1.45	0.976
29	0.27	0.59	0.42	0.977	**60**	0.74	1.04	0.81	0.975
30	1.35	2.42	0.72	0.980	**61**	0.98	1.85	3.82	0.938
35	2.25	0.92	0.82	0.919	**62**	0.95	0.68	0.75	0.957

Convergence characteristics of the proposed DBFOA

The effect of D-Chemotaxis

This section demonstrates the effectiveness of the D-Chemotaxis procedure utilized in DBFOA. The proposed D-Chemotaxis is specially designed for the PV re-phasing

problem as opposed to merely directly adopting it from classical chemotaxis. The proposed D-Chemotaxis identifies the region around the busbar with the highest unbalance ($\mathbb{H}_{VU}$) and then, only the phase combination of grid-connected PV systems in that region are randomly changed to find the optimal solution iteratively. However, in classical chemotaxis, a fixed number of PV systems are randomly selected from the network and then, the phase configurations of those PV systems are randomly changed. This random selection of PV systems in classical chemotaxis may result in the formation of much higher unbalance levels in the network, thus, ultimately resulting in slower convergence.

Since the increase in voltage unbalance levels of a particular region of a network is mainly due to the mismatch of active and reactive power levels in the same region, the proposed D-chemotaxis step randomly changes the phase configuration of PV systems in the highest unbalance region iteratively. This could lead to a dramatic increase in the convergence speed of the DBFOA as shown in Figure 10. According to the results, the proposed D-chemotaxis step in the DBFOA resulted in faster convergence of the algorithm when compared to the classical chemotaxis under the same conditions (same initial population, same values for parameters, etc.). Also, the proposed chemotaxis step causes the optimal solution to settle in a place with lower cost value as opposed to classical chemotaxis where final settling cost is much higher as Figure 10 depicts.

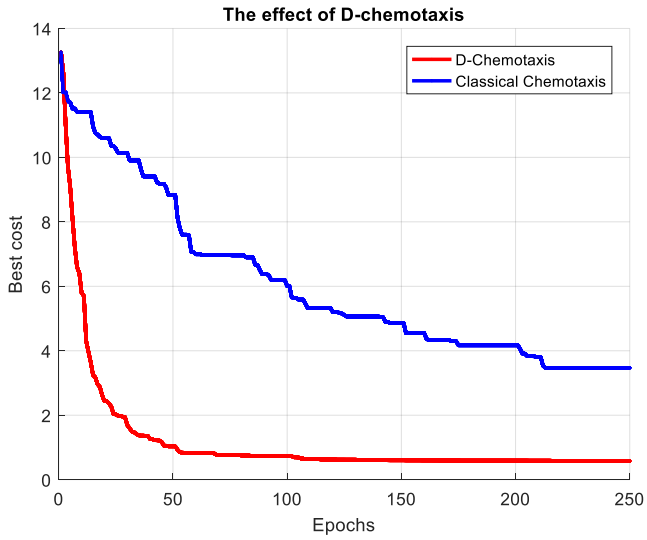

Figure 10: The effect of D-chemotaxis on the convergence of DBFOA.

Effect of the initialization of the PV configuration initializers

As described in section 4.3, an active power balancing approach was introduced to find initial phase combinations for the PV configuration initializers as opposed to the random initialization of the classical technique. Figure 11 depicts the convergence properties of the DBFOA under two cases: (1). The PV configuration initializers were initialized based on the active power balancing technique and (2). The PV configuration initializers were randomly initialized. According to the results, the starting cost of DBFOA under the proposed power balancing initialization is approximately 83% lower than the random initialization. This implies that the active power balancing technique was able to generate phase combinations that are closer to the optimal phase

combination. Ultimately, the DBFOA with the proposed initialization technique converged to the optimal solution with fewer iterations compared to the random initialization.

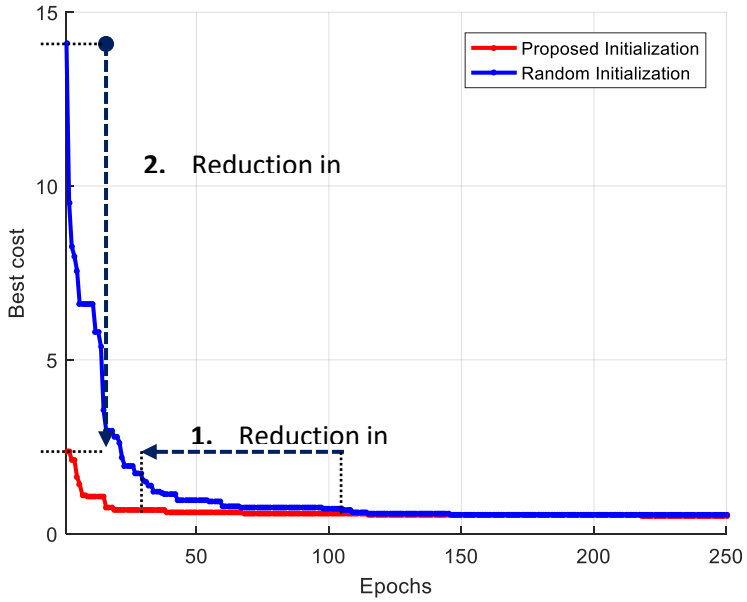

Figure 11: Convergence of the DBFOA for proposed and random initialization methods.

Effects of PV re-phasing

This section demonstrates the effect of PV re-phasing on voltage unbalance and phase voltage magnitudes of residential distribution grid with high penetration of solar power. The proposed PV re-phasing algorithm was implemented on the real distribution network shown in Figure 8. The variations of loads and PV power generation throughout the day were considered in the simulations by utilizing hourly load and PV generation profiles shown in Figure 9.

The goal of PV re-phasing is to reduce overall voltage unbalance ($\overline{\mathrm{VUF}}$) of the network by dynamically changing the phase configuration of rooftop solar systems in the network. Figure 12 and 13 clearly illustrate the effect of PV re-phasing on the overall voltage unbalance and phase voltages, respectively. According to Figure 12, significantly high voltage unbalances are observed during the daytime when PV systems have a fixed phase configuration. Whereas the dynamic PV re-phasing significantly reduces the overall voltage unbalance of the network (mean unbalance is below 1 %) especially during the period from 8 am to 5 pm, where high PV penetration is present. In addition, Table 7 provides the optimal phase configuration of PV systems that are determined from the proposed DBFOA from 6 am to 7 pm. The colored cells in Table 7 belong to the phases of PV systems that are not changed in the subsequent hour. Since not each rooftop PV system is subjected to PV re-phasing at each hour, SCADA needs to send the PV re-phasing commands only for the rooftop solar systems that are required to re-phase in the next PV-rephasing operation. Moreover, the proposed algorithm can be improved to minimize the number of PV re-phasing

operations that each rooftop PV system undergoes throughout the day by modifying the cost function of the optimization algorithm. Finally, these results confirm that the proposed re-phasing strategy is successful in reducing the voltage unbalance levels of domestic distribution grids that have many grid-connected rooftop PV systems, while simultaneously maintaining the phase voltages within their acceptable limits.

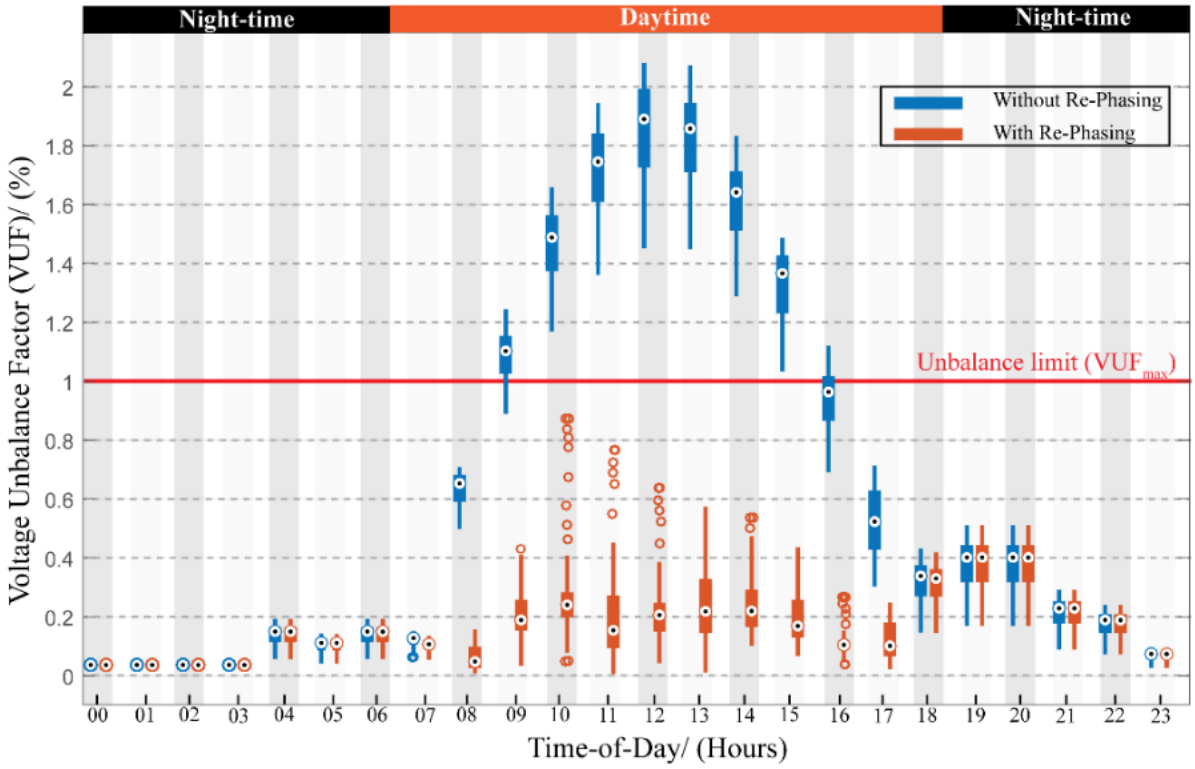

Figure 12: Distribution of voltage unbalance values of the network throughout the day for ‘with’ and ‘without’ PV re-phasing.

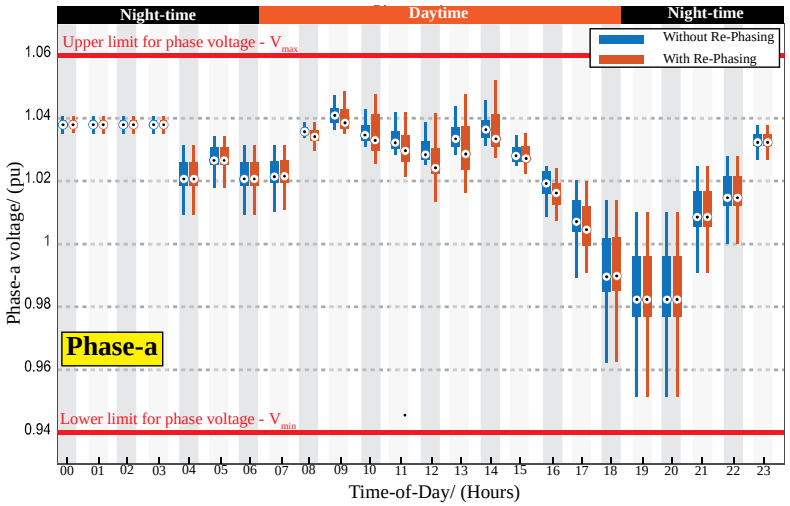

(a)

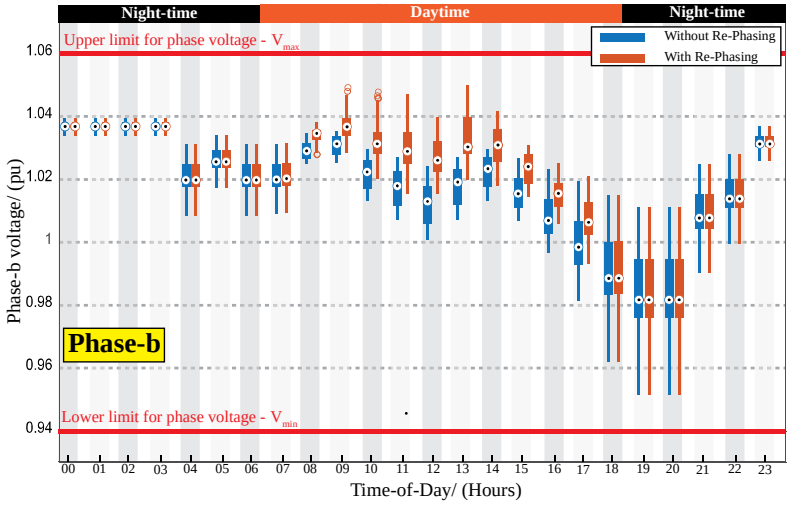

(b)

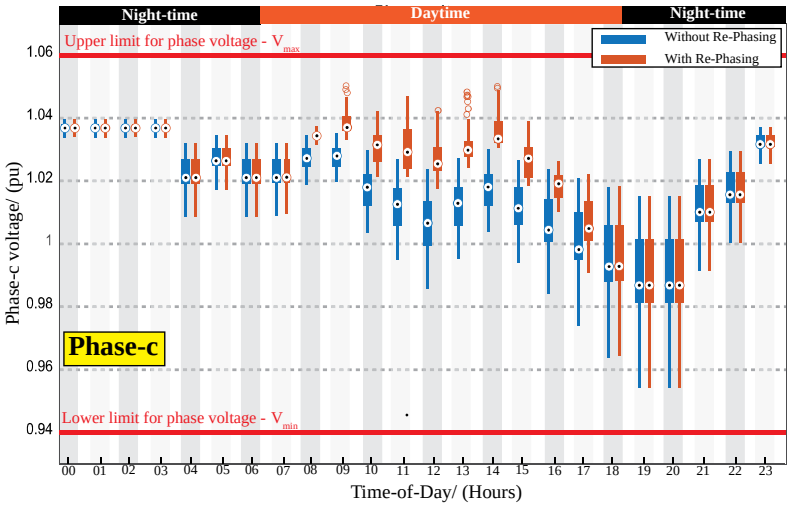

(c)

Figure 13: Evolution of (a) phase-a, (b) phase-b, and (c) phase-c voltage of the network throughout the day for ‘with’ and ‘without’ PV re-phasing.

Table 7: Hourly phase configurations of rooftop PV systems determined by the proposed DBFOA. The colored cells in the table represent the phase configuration of rooftop solar systems that are not changed in the subsequent hour.

Time	Hourly phase configuration of rooftop PV systems (a = Phase a, b = Phase b, and c= Phase c)																									
	1	2	3	4	5	6	7	8	9	10	11	12	13	14	15	16	17	18	19	20	21	22	23	24	25	26
6 - 7 am	b ↓	b ↓	a ↓	a ↓	c ↓	b ↓	c ↓	c ↓	b ↓	b ↓	a ↓	b ↓	c ↓	a ↓	a ↓	a ↓	a ↓	a ↓	a ↓	a ↓	a ↓	b ↓	a ↓	b ↓	b ↓	a ↓
7 - 8 am	a ↓	a ↓	a ↓	b ↓	a ↓	a ↓	b ↓	a ↓	a ↓	c ↓	a ↓	c ↓	a ↓	a ↓	c ↓	b ↓	a ↓	a ↓	a ↓	a ↓	a ↓	a ↓	b ↓	b ↓	a ↓	a ↓
8 - 9 am	a ↓	a ↓	a ↓	a ↓	a ↓	a ↓	a ↓	b ↓	b ↓	a ↓	a ↓	a ↓	b ↓	b ↓	a ↓	a ↓	a ↓	a ↓	a ↓	a ↓	b ↓	b ↓	b ↓	a ↓	a ↓	a ↓
9 - 10 am	a ↓	c ↓	a ↓	b ↓	b ↓	a ↓	a ↓	c ↓	b ↓	c ↓	c ↓	b ↓	b ↓	a ↓	b ↓	c ↓	a ↓	a ↓	a ↓	a ↓	a ↓	a ↓	a ↓	a ↓	b ↓	a ↓
10 - 11 am	c ↓	a ↓	c ↓	a ↓	a ↓	c ↓	a ↓	a ↓	b ↓	a ↓	b ↓	c ↓	a ↓	a ↓	c ↓	b ↓	b ↓	a ↓	b ↓	c ↓	b ↓	a ↓	a ↓	a ↓	a ↓	b ↓
11 - 12 am	a ↓	a ↓	a ↓	a ↓	b ↓	a ↓	a ↓	a ↓	a ↓	c ↓	c ↓	b ↓	c ↓	b ↓	b ↓	c ↓	a ↓	b ↓	a ↓	a ↓	a ↓	a ↓	a ↓	a ↓	a ↓	a ↓
12 - 1 pm	b ↓	a ↓	a ↓	a ↓	a ↓	a ↓	a ↓	c ↓	c ↓	a ↓	b ↓	a ↓	a ↓	a ↓	b ↓	a ↓	a ↓	a ↓	a ↓	b ↓	a ↓	b ↓	a ↓	a ↓	b ↓	b ↓
1 - 2 pm	a ↓	b ↓	a ↓	a ↓	a ↓	a ↓	a ↓	a ↓	b ↓	b ↓	c ↓	b ↓	b ↓	b ↓	a ↓	b ↓	a ↓	a ↓	b ↓	a ↓	c ↓	b ↓	a ↓	a ↓	a ↓	a ↓
2 - 3 pm	a ↓	a ↓	b ↓	a ↓	a ↓	a ↓	a ↓	a ↓	a ↓	c ↓	a ↓	c ↓	a ↓	a ↓	c ↓	a ↓	a ↓	a ↓	a ↓	a ↓	b ↓	a ↓	c ↓	b ↓	a ↓	a ↓
3 - 4 pm	a ↓	a ↓	a ↓	a ↓	a ↓	a ↓	a ↓	b ↓	b ↓	b ↓	a ↓	b ↓	b ↓	b ↓	b ↓	b ↓	a ↓	a ↓	a ↓	a ↓	b ↓	b ↓	a ↓	a ↓	a ↓	a ↓
4 - 5 pm	a ↓	a ↓	a ↓	a ↓	a ↓	a ↓	a ↓	c ↓	b ↓	b ↓	c ↓	b ↓	b ↓	b ↓	a ↓	c ↓	a ↓	a ↓	a ↓	a ↓	b ↓	b ↓	a ↓	a ↓	a ↓	a ↓
5 - 6 pm	a ↓	a ↓	a ↓	a ↓	b ↓	b ↓	a ↓	a ↓	a ↓	b ↓	a ↓	a ↓	c ↓	c ↓	b ↓	b ↓	a ↓	b ↓	a ↓	a ↓	b ↓	a ↓	a ↓	a ↓	a ↓	a ↓
6 - 7 pm	a ↓	a ↓	a ↓	a ↓	a ↓	a ↓	a ↓	a ↓	b ↓	a ↓	b ↓	b ↓	a ↓	b ↓	a ↓	a ↓	a ↓	a ↓	a ↓	a ↓	a ↓	b ↓	a ↓	a ↓	a ↓	a ↓
7 - 8 pm	a ↓	b ↓	a ↓	b ↓	a ↓	a ↓	b ↓	b ↓	c ↓	b ↓	b ↓	b ↓	c ↓	c ↓	c ↓	c ↓	a ↓	a ↓	b ↓	a ↓	c ↓	c ↓	a ↓	a ↓	b ↓	b ↓

Since the proposed PV re-phasing technique can maintain the voltage imbalances of the network well below the 1% threshold during the daytime while keeping the phase voltages within their acceptable voltage range, utility providers can allow additional rooftop solar systems into the network. In order to get a clear idea about the amount of

additional renewable energy capacity facilitated by the PV re-phasing operation, simulations were performed by adding new rooftop solar systems (on top of existing 140.4 kW of solar PV as specified by Table 5) to the existing network. For each addition of a new rooftop solar system, 20 Monte-Carlo simulations were performed by randomly changing its connection point in the LV network to ensure an unbiased and fair simulation. For this study, the capacity of each new rooftop solar system to be connected to the existing LV network is considered to be 5.4 kW that corresponds to the average capacity of a rooftop PV system in the existing network. The maximum voltage unbalances and maximum phase voltage values of the network recorded for "with" and "without" re-phasing are depicted in Figure 14.

According to Figure 14-(c), the maximum voltage unbalance of the network is well below the 1% threshold for the proposed PV re-phasing technique even under the integration of new rooftop solar systems up to a total capacity of 302.4 kW. In contrast, as can be seen from Figure 14-(a), the maximum voltage unbalance values of the network exceed the 1% threshold line for the fixed phase configuration. However, as depicted in Figure 14 – (b) and (d), the maximum voltage of the network gradually increases with the addition of new rooftop solar systems to the network. Due to this reason, rooftop solar systems with a total capacity of 248.4 kW can be safely integrated into the LV network without violating the statutory limits of both voltage unbalance and phase voltage magnitudes. This is about a 77% increase in the rooftop solar capacity of the network compared to the originally installed solar capacity (140.4 kW). Therefore, it is apparent that the proposed PV re-phasing strategy can completely overcome the voltage unbalance issue due to the installation of distributed energy sources in the LV and facilitate to install additional rooftop solar systems into the network.

In addition, it should be pointed out that the above conclusions are made under the assumption that the voltage unbalance should be kept below 1%, and the phase voltage can vary between $0.94\,pu$ and $1.06\,pu$ ($\pm 6\%$ tolerance level). However, some countries/regions allow the phase voltage to vary within a larger range, such as $0.9\,pu$ to $1.1\,pu$ (that is, a $\pm 10\%$ tolerance level). Under this new voltage limit, the proposed PV re-phasing approach can increase the usable PV capacity of the network to more than $the\ capacity$ obtained with a voltage tolerance of $\pm 6\%$. It can be seen from Figure 14-(d) that if the maximum allowable voltage level is $1.1\,pu$, solar PV totaling more than $302.4\,kW$ can be safely integrated into the original network. That is approximately a 115% increase compared to the originally installed solar capacity ($140.4\,kW$) of the network.

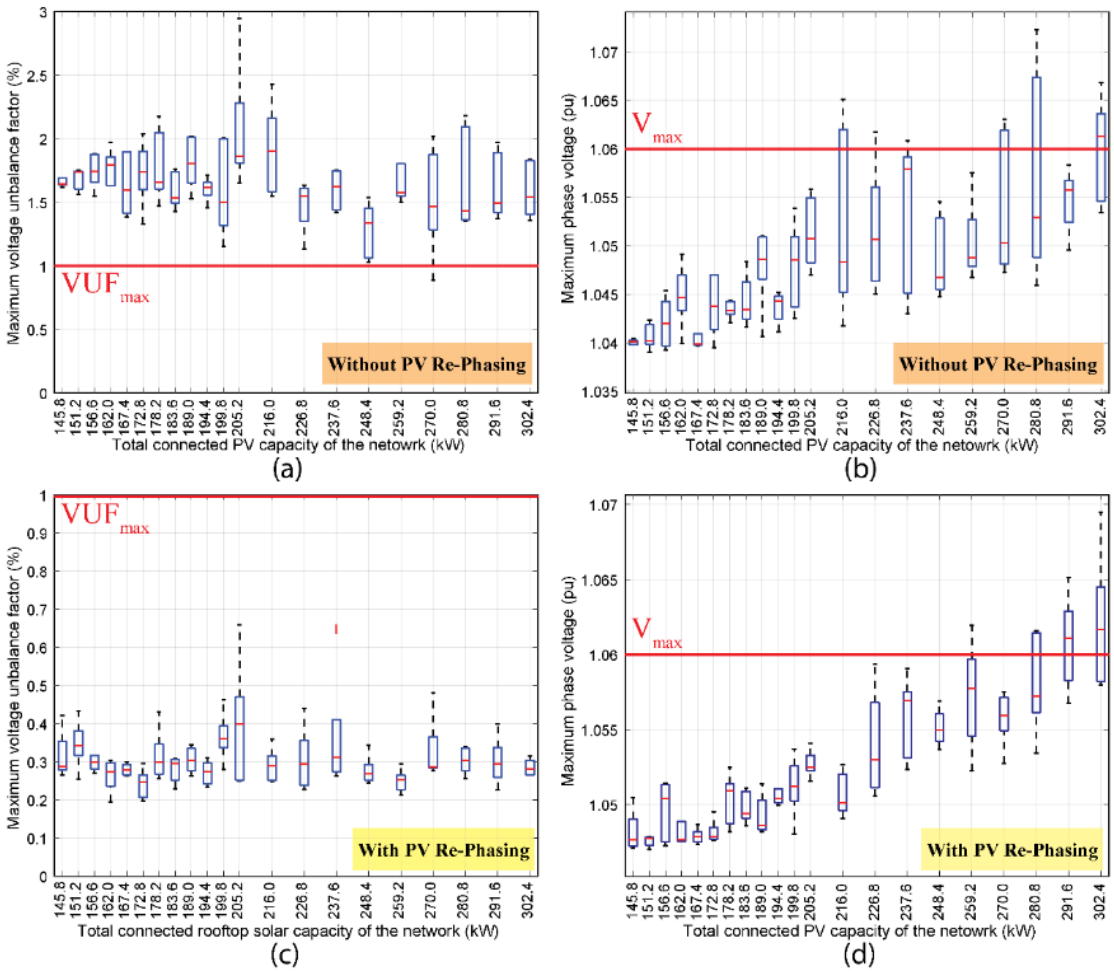

Figure 14: Variation of (a) maximum voltage unbalance and (b) maximum voltage unbalance with the total connected PV capacity of the LVDG network for "without" re-phasing. Variation of (c) maximum voltage unbalance and (d) phase voltage magnitude with the total connected rooftop solar capacity for "with" re-phasing.

Comparison of different optimization techniques

In order to predict the superiority of the proposed DBFOA, the convergence characteristics of the proposed DBFOA for the test system is compared with three other widely used optimization algorithms in power systems, namely, Discrete Genetic Algorithm (DGA), Shuffled Frog-Leaping Algorithm (SFLA) and Heuristic Search (HS), and the results are shown in Figure 15. The algorithms were written on Matlab® (version: R2016a) - Open DSS (version: 8.4.1.1) co-simulation environment and executed on a processor with Intel Core i7-7700HQ with 32 GB RAM running at 3.4 GHz. From the figure, it is clear that the DBFOA only takes 38 iterations to converge to the best solution. In addition to that, DBFOA shows a stable and quick convergence with a global searching capability to find the optimal phase configuration. Thereby, ensuring that the LVDG maintains strict power quality standards, even under heavy PV penetration in a near-real-time fashion.

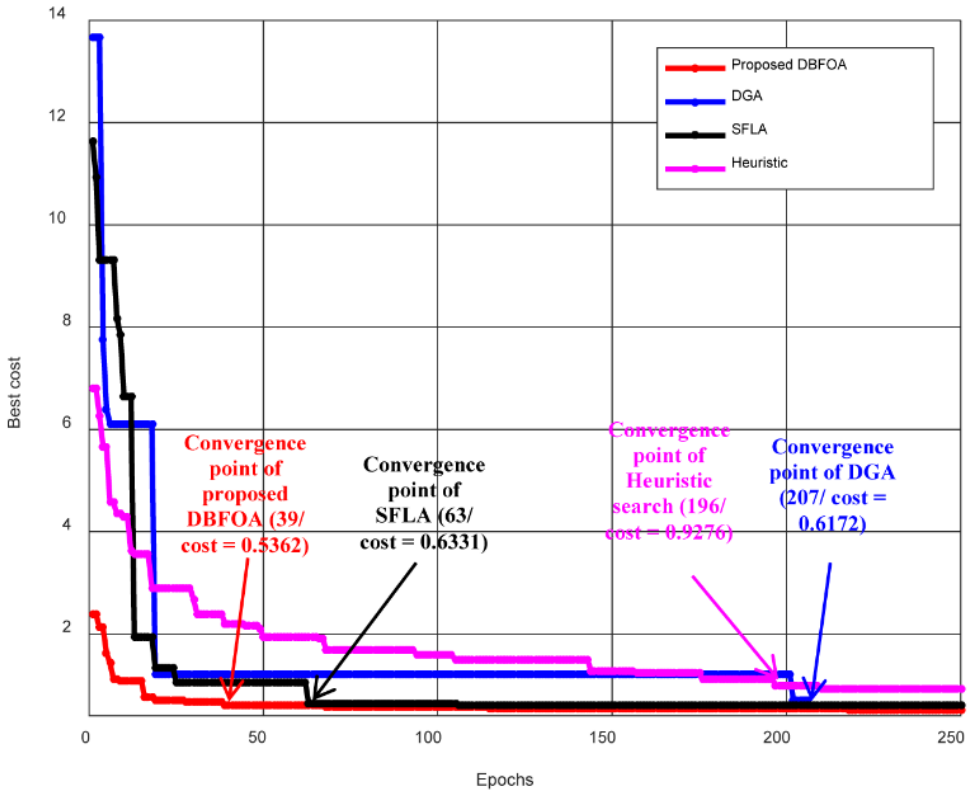

Figure 15: Performance comparison of proposed DBFOA with DGA, SFLA, and Heuristic search.

Table 8 shows the computational performance of the four algorithms. The average execution time of a single epoch for the three algorithms is almost the same. However, the proposed DBFOA converges to the optimal solution very fast compared to DGA, SFLA, and Heuristic Search.

Table 8: Computational efficiency of DBFOA, DGA, SFLA, and Heuristic search in terms of CPU time

Algorithm	Execution time/Epoch (s)	Time to convergence/ (s)	Cost after 250 epochs
Proposed DBFOA	0.888	**33.744**	**0.5362**
DGA	0.846	175.122	0.6172
SFLA	0.897	56.511	0.6331
Heuristic search	0.622	121.912	0.9276

Line Model

400 V three-phase four-wire distribution system with the total length of 540 m is modeled using resistors and inductors. All aluminum bare conductor (AAC/ Fly) parameters are used to develop the model. This model can be used to create voltage violations for testing purposes and techniques for mitigating voltage violations can be also tested.

Calculations for the Line Model

Parameter values of a Fly conductor
DC resistance of the line conductors = 0.451 Ω/km
Inductance = 0.291 mH/km
Current carrying capacity = 199 A

Base values are selected as shown in Table 01.

Table 01: Base Values for the Calculation

	For the real line	For three-phase model
V_{base}	400 V	400 V
I_{base}	150 A	5 A
S_{base}	$\sqrt{3}\times400\times150$ = 103.9 kW Taken as 100 kW	$\sqrt{3}\times400\times5$ = 3.46 kW Taken as 3.5 kW
Z_{base}	$400^2/100x10^3$ = 1.6 Ω	$400^2/3.50x10^3$ = 45.7 Ω

Considering 1km Fly conductor, calculations in Table 02 can be done.

Table 02: Parameters for 1 km Fly Conductor

	Ohm	p.u.
Resistance of a conductor	0.451	0.29293
Reactance of a conductor	0.291	0.18901

Considering 180m long Fly line segment and calculations in Table 03 can be done.

Table 03: Parameters for 180 m Fly Conductor

	Real Line		Model	
	Ohm	p.u.	Ohm	p.u.
Resistance of a conductor	0.08118	0.05074	2.6	0.05074
Reactance of a conductor	0.05238	0.03274	1.5	0.03274

Using the reactance value of 1.5 Ω, corresponding inductance value can be obtained as 5 mH.

Line model consists of three 180 m long Fly conductor equivalent segments. Therefore, the total length is 540 m. 1 Ω resistors with 2kW power and 5 mH inductors are used to hardware implementation. Single 180 m long segment is shown in Figure 1.

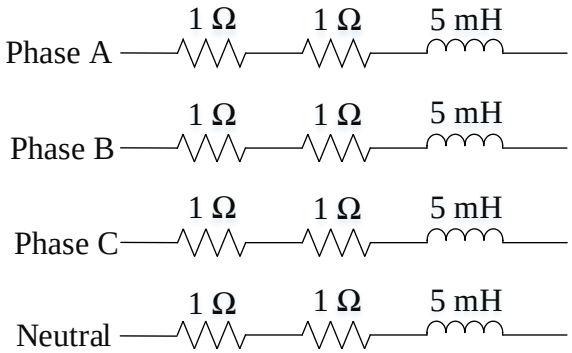

Figure 01: 180 m Fly Conductor Model

Two 1 Ω resistors are connected in series to get the total of 2 Ω resistance which corresponds to the resistance of 180 m long Fly conductor. 5 mH inductors are connected in series with the resistors to get the reactance corresponds to 180 m long Fly conductor. 6 resistors and 4 inductors are required for single 180 m long Fly line segment. Total of 24 resistors and 12 inductors are required to develop the complete line model of 540 m as shown in Figure 02.

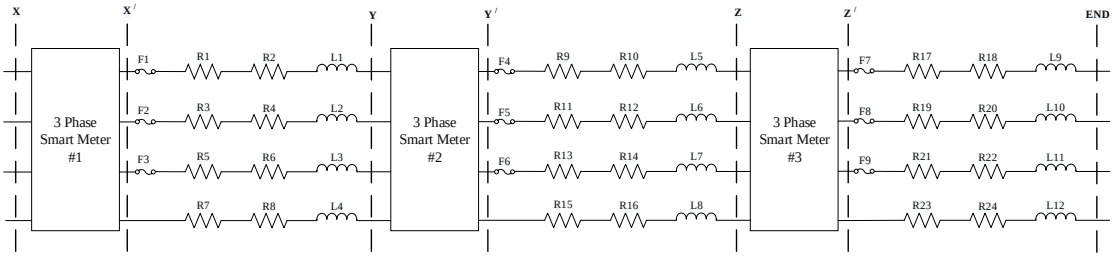

Figure 02: Complete Line Model Circuit Diagram

X/ - Y, Y/ - Z and Z/ - END are the three 180 m long segments of the line model. X/ - Y segment can be named as line segment 1, Y/ - Z segment can be named as line segment 2 and Z/ -END segment can be named as line segment 3. R1 to R24 represent 1 Ω resistors and L1 to L12 represent the 5 mH inductors. F1 to F9 represent the 5 A fuses used in the phase conductors. Three 3-phase smart meters are used at the beginning of the line segment 1, beginning of line segment 2 and at the beginning of line segment 3 as shown in Figure 02.

Figure 03 shows a sketch of the front panel of the line model. Figure 04 shows the front panel of the hardware implemented model.

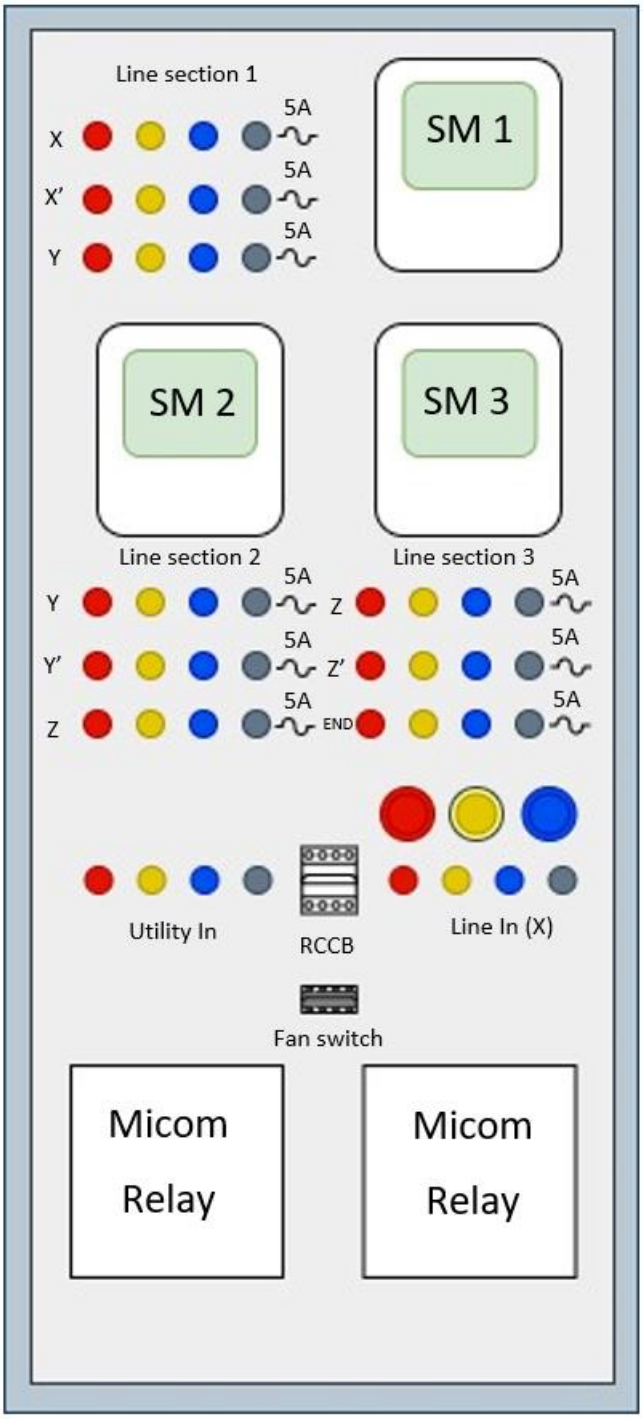

Figure 03: Sketch of the front panel of the line model

Figure 04: Front panel of the line model

Figure 02 and Figure 03 can be compared for more clarity. In Figure 03, it can be observed that there are two X terminal sets, two Y terminal sets and two Z terminal sets. The purpose of using two terminal sets is to operate the line segments separately.

As an example, if we want to operate only the line segment 1 i.e., only 180m, then no need to short circuit Y-Y point and Z-Z points. Connecting X-X is sufficient. For operation of full 540 m model, Y-Y and Z-Z points has to be short circuited.

Figure 05 and 06 show the front and rear views of the internal of the line model. Figure 07 is the labeled circuit diagram. Cables, resistors and inductors are labeled in the hardware model according to the Figure 07.

Figure 05: Front view of the inside of the line model

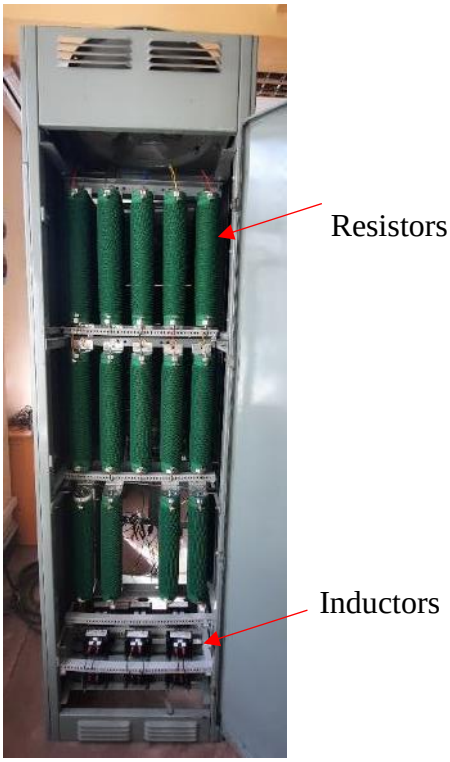

Figure 06: Rear view of the inside of the line model

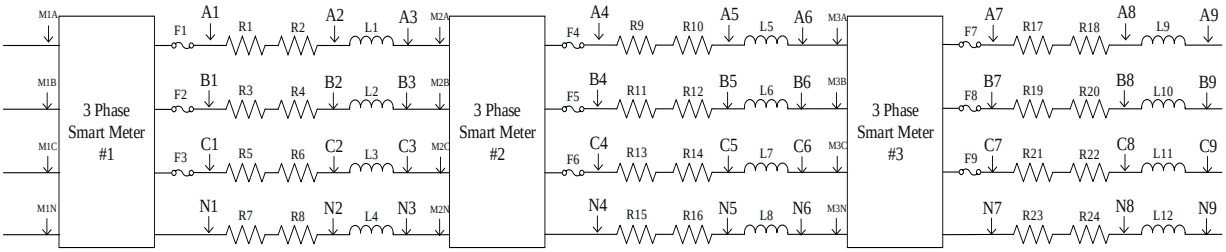

Figure 07: Labeled circuit diagram of the complete line model

Refer Figure 07 to identify the components in the hardware setup. Two extreme corners of the cables are labeled in the hardware setup along with the resistor and inductor labels according to the Figure 07.

Inverter Design

This project is based on two drawbacks in PV systems. One is the low energy extraction problem and the other one is the phase unbalance due to the random installation of small size rooftop PV systems in LV network. A single-phase three-limb inverter is designed to test the solutions. The ultimate proposed solution for efficiency problem and phase unbalance problem in distribution network is to design and test a three-limb single-phase inverter which can do re-phrasing while running at its maximum power point. The intention is to introduce an MPPT unit to the designed inverter in the laboratory and make it to do re-phasing according to the optimized data obtained using DBFOA from LV network. Block diagram of the system is shown in Figure 08.

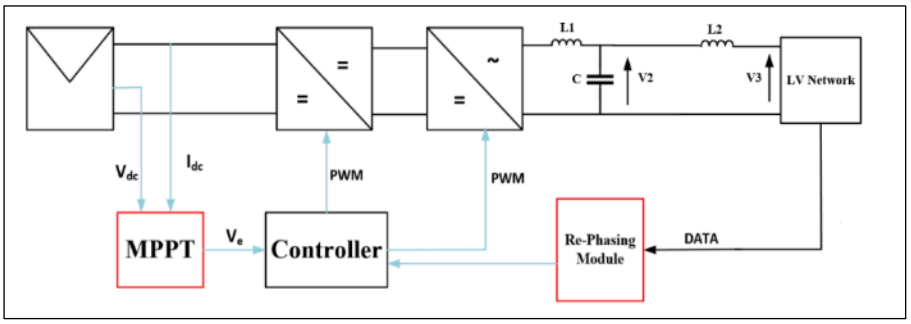

Figure 08: Introducing Units for the Available Three-Phase Inverter to Mitigate Efficiency Problem and Phase Unbalance Problem

Hardware Design and Implementation

Initially the algorithms were tested in simulation platform. They were expected to test in hardware setup. For that, three-limb inverter and the filter were designed in the laboratory. The output of the designed inverter and capability of working long hours by withstanding temperature were verified in the laboratory environment under open loop running condition.

The Printed Circuit Board (PCB) was soldered as shown in Figure 09. Intelligent Power Module (IPM) FSBB20CH60F was used to facilitate the requirement of six IGBTs of the inverter. When soldering, minimum amount of wire lengths were used to minimize the capacitive effect of wires.

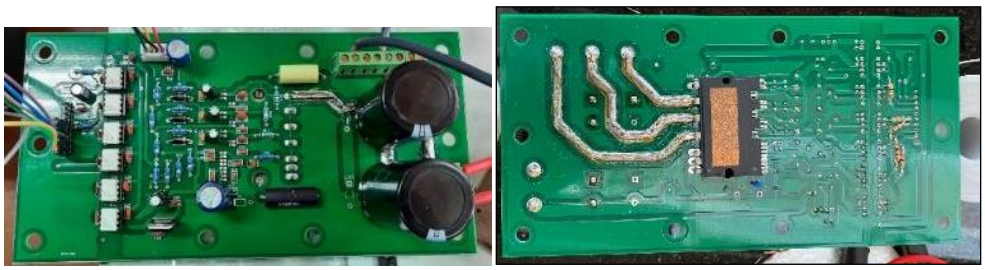

Figure 09: Top and Bottom View of Soldered Inverter Setup

Results and Outputs of the Inverter Design

Open Loop Output Voltage and Current Testing

There are three-limbs in the inverter. They are for phase A, phase B and phase C. Two phases were considered at a time and checked the output waveform. A rheostat was connected instead of the LV network shown in Fig.2. since the setup was executed in open loop condition. Then the output voltage V3 was observed using the oscilloscope.

The PWM signal was given using the model created in Simulink through a TI C2000 control board. Modulation index can be changed using the model in Simulink. According to the switching frequency of the PWM signal, filter characteristics were changed. As shown in Fig.2, an LCL filter was used for the setup. For 10 kHz switching frequency, L1=0.7 mH, L2=0.7 mH, C=5 uF while for 5 kHz switching frequency, L1=1.25 mH, L2=1.25 mH, C=8 uF were used.

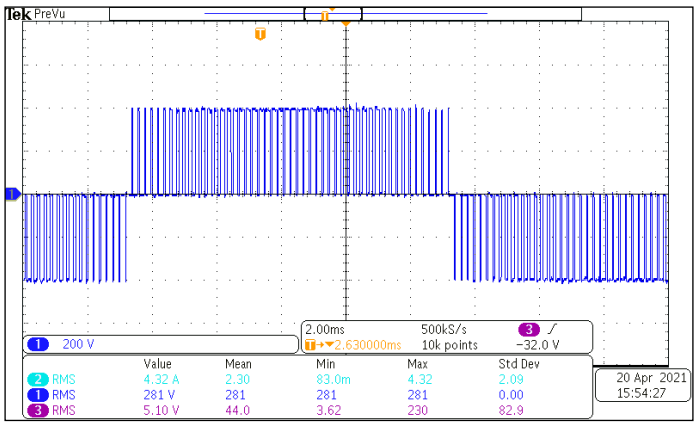

Figure 10. Output Voltage Waveform before Filtering

The switching frequency of the PWM signal was set to 10 kHz. Input DC voltage of 400V with modulation index of 0.8 was given to the inverter using a solar emulator. Rheostat of 160Ω was used as the output load. Output voltage waveform of the inverter before filtering is shown in figure 10. Filtered output voltage and current are shown in figure 11 and figure 12.

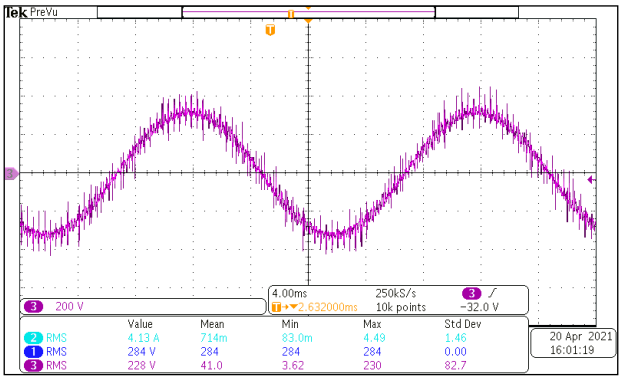

Figure 11: Filtered Output Voltage Waveform

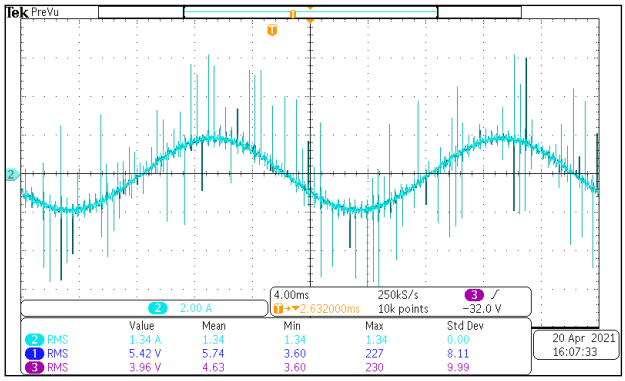

Figure 12: Filtered Output Current Waveform

As shown in figure 10, the width of square pulses was altered according to the PWM signal. The desired amplitude of 400V was obtained. Figure 11 shows that, after filtering, the sinusoidal output voltage waveform with 320 V amplitude was obtained. Since the modulation index was 0.8 and input DC voltage was 400V, this result can be accepted. The capacitive effect of wires may have caused the noise presented in both current and voltage waveforms.

Temperature Testing

The inverter has to be capable of working long hours without any interruption. When working continuously, temperature in the hardware setup will increase. Therefore, the designed inverter was checked for temperature withstanding capability. As a safety measure, setup was mounted on a heat sink. The input voltage of 300V was given with 0.8 modulation index. Rheostat of 160Ω was connected through the output phases. Temperature on capacitor, inductors, heat sink and near IPM were taken in 30 minutes intervals under natural cooling condition.

Temperature on capacitor, inductors, heat sink and near IPM were taken in 30 minutes intervals under natural cooling condition. Table 4 summarizes the results obtained.

Table 4: Temperature Variation

Time	Inductor 1 /^{0}C	Inductor 2 /^{0}C	Capacitor /^{0}C	IPM /^{0}C	Heat Sink /^{0}C
9.30 a.m	30.8	27.8	27.8	32.9	30.4
10.00 a.m.	63.3	28.5	29.7	37.8	33.8
10.30 a.m.	77.0	29.2	29.7	38.6	31.0
11.00 a.m.	91.3	29.2	30.5	42.5	32.0

Temperature of inductor 1 was increased rapidly under natural cooling. The reason may have been the large harmonic currents flowing through it. Forced cooling is suggested for more reliable operation.

Noise Analysis

The distortion visible in the output waveforms were analyzed for both 10 kHz and 5 kHz switching frequencies. 10 kHz design was executed for both 10 kHz and 5 kHz while the 5 kHz design was also executed for both 5 kHz and 10 kHz. Then the output voltage waveform V3 and voltage across the capacitor V2 (as shown in figure 08.) were extracted. Then the simulation model constructed in Simulink was used to get the desired V2 and V3 waveforms. Simulation waveforms were compared with hardware executed V2 and V3 waveforms to get the error signal. Then the noise Probability Density Functions (PDFs) for V2 and V3 waveforms were constructed. Kurtosis values for each case were noted.

The PWM switching frequency plays a major role in inverter. For more precise filtering typically 5 kHz or 10 kHz PWM switching frequency is used. To investigate the effect of changing PWM frequency, noise analysis is done for four cases mentioned in here. Figure 13 shows the noise PDF for filtered output voltage (V3) while figure 14 shows the noise PDF for voltage across the capacitor (V2). Kurtosis values for each case are also shown beside the figures.

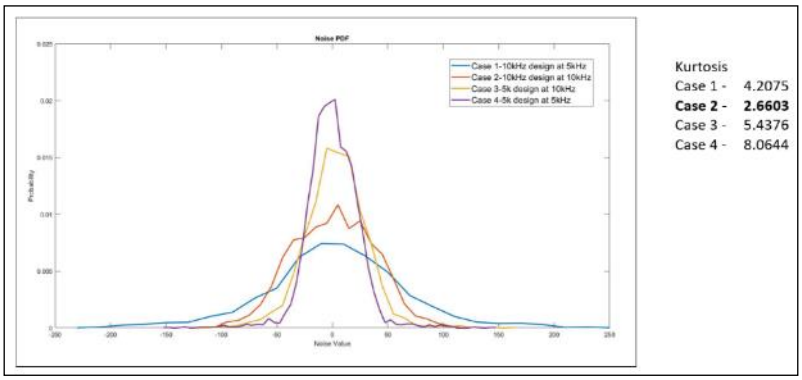

Figure 13. Noise PDFs and Kurtosis Values for Filtered Output

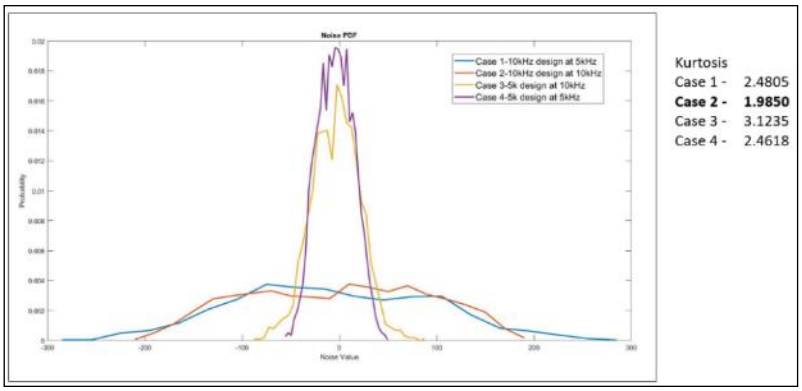

Figure 14: Noise PDFs and Kurtosis Values for Voltage across the Capacitor

When observing figure 13 and 14, it can be observed that the noise PDFs are Gaussian bell shaped. When considering Kurtosis, the kurtosis value of 3 implies the Gaussian noise. Therefore, it can be concluded that case 1 and case 2 (i.e., 10 kHz design results) noises are more Gaussian while case 3 and case 4 (i.e. 5 kHz design results) are closer to super Gaussian noise. The reason for super Gaussian noise may have been an external

effect on the 5 kHz system. Therefore, it can be concluded that 10 kHz design is better since 5 kHz design showing super Gaussian noise distribution.

Conclusion

In this paper, a novel method was introduced to mitigate the voltage unbalance in LV distribution grids through coordinated re-phasing of grid-connected rooftop PV systems. The optimum phase combination of grid-connected rooftop PV systems is determined from the modified discrete bacterial foraging optimization algorithm (DBFOA) at fixed time intervals. The DBFOA takes smart meter measurements such as load demands and PV generations as the inputs to determine the optimum phase configuration such that the resulting phase combination minimizes the overall voltage unbalance in the network, subject to various operating and network parameters. In order to perform automatic PV re-phasing, a PV re-phasing switch is introduced. This can connect to the output of the single-phase PV inverters to enable the PV re-phasing. To nullify the transient time associated with the automatic re-phasing switch, a half-bridge inverter arrangement is also proposed.

In order to demonstrate the effectiveness of the proposed re-phasing strategy, the PV re-phasing algorithm was simulated on a real LV distribution network. The time-varying nature of loads and solar PV was considered using the hourly load and PV generation profiles. The results show that the proposed re-phasing strategy can significantly reduce the voltage unbalance well below the 1% threshold line as compared to the fixed phase configuration during the daytime where PV penetration is high. Thereby the proposed PV re-phasing strategy facilitates utility providers to allow more rooftop solar systems into LV networks. The proposed case studies demonstrate that PV re-phasing technique can increase the renewable energy penetration into the considered LV network by 77%.

The main advantage of the proposed PV re-phasing technique compared to existing load and feeder reconfiguration techniques is that this method only deals with single-phase PV systems. Hence, it will not create any impact on supply reliability. Furthermore, the initial cost for installation of PV re-phasing switches, and other indirect costs such as customer interruption cost and reliability cost are significantly minimal, as compared to existing state-of-the-art DFR and phase balancing techniques. The initial cost for installing PV re-phasing switches can be recovered by the long-term economic benefits due to the improvement in usable PV capacity and due to the possibility of operating the system in a near balanced condition. Further, compared to the rephasing arrangements reported in the literature, i.e. introducing rephasing switches to all loads, the cost incurred due to the introduction of re-phasing switches, only to PV plants, makes the proposed method more cost-effective.

The main limitation of this work is that the proposed PV re-phasing method is only effective during the daytime and cannot make a significant reduction to the unbalance factor at night. However, the Volt-Var (Q-control) control can be used to reduce voltage unbalance and improve power quality during night-time, because PV inverters can supply reactive power (Q) to the grid up to their rated capacity at night. Therefore, combining the PV re-phasing technique with Volt-Var control would be an ideal

solution and is considered as future research work. In addition, it should be noted that the unbalance reduction capability of the proposed PV re-phasing technique greatly depends on the number of grid-connected rooftop solar systems in the distribution network. Therefore, for distribution systems with a smaller number of grid-connected rooftop solar systems, the number of possible configurations is limited, thus, optimization via fine-tuning through re-phasing is not possible as the number of configurations to adjust is limited. Further, a communication protocol needs to be developed to ensure that the PV re-phasing command issued by the algorithm is actually performed by the switches, because if one/several re-phasing switch commands are not executed due to communication errors or other technical issues, the system can be at a worse state than before. Therefore, improvements should be made to address these, before implementing the proposed PV re-phasing technique in an actual network.

Even though the proposed re-phasing algorithm concentrates on mitigation of voltage unbalance, it is also possible to modify the objective function to minimize the number of PV re-phasings required for each PV re-phasing operation as well. Furthermore, additional research is required to determine the optimal timing for PV re-phasing operations and the effectiveness of a hybrid algorithm based on PV and load re-phasing techniques.

Based on the hardware implemented inverter results, it can be stated that the designed inverter can be used to get accurate outputs. Forced cooling system has to be used to obtain a more reliable operation. According to the noise analysis, 10 kHz PWM switching frequency is better with corresponding filter inductors and capacitor values.

The hardware implemented line model can be used to create voltage violations for testing purposes and techniques for mitigating voltage violations can be also tested.

References

[1] K. Jadeja, “Major Technical issues with increased PV penetration on the existing electrical grid.,” Murdoch University, 2012.

[2] J. García-Villalobos, I. Zamora, K. Knezović, and M. Marinelli, “Multi-objective optimization control of plug-in electric vehicles in low voltage distribution networks,” *Appl. Energy*, vol. 180, pp. 155–168, Oct. 2016.

[3] M. R. Islam, H. Lu, M. J. Hossain, and L. Li, “Mitigating unbalance using distributed network reconfiguration techniques in distributed power generation grids with services for electric vehicles: A review,” *J. Clean. Prod.*, vol. 239, p. 117932, Dec. 2019.

[4] S. H. Soltani, M. Rashidinejad, and A. Abdollahi, “Dynamic phase balancing in the smart distribution networks,” *Int. J. Electr. Power Energy Syst.*, vol. 93, pp. 374–383, Dec. 2017.

[5] V. Behravesh, R. Keypour, and A. Akbari Foroud, “Control strategy for improving voltage quality in residential power distribution network consisting of roof-top photovoltaic-wind hybrid systems, battery storage and electric vehicles,” *Sol. Energy*, vol. 182, no. February, pp. 80–95, 2019.

[6] G. Carpinelli, F. Mottola, D. Proto, and P. Varilone, “Minimizing unbalances in low-voltage microgrids: Optimal scheduling of distributed resources,” *Appl. Energy*, vol. 191, pp. 170–182, 2017.

[7] T. Fukami, T. Onchi, N. Naoe, and R. Hanaoka, “Compensation for neutral current harmonics in a three-phase four-wire system by a synchronous machine,” in *IEMDC 2001. IEEE International Electric Machines and Drives Conference (Cat. No.01EX485)*, pp. 466–470.

[8] B. Singh, P. Jayaprakash, and D. P. Kothari, “A T-Connected Transformer and Three-leg VSC Based DSTATCOM for Power Quality Improvement,” *IEEE Trans. Power Electron.*, vol. 23, no. 6, pp. 2710–2718, Nov. 2008.

[9] P. Jayaprakash, B. Singh, and D. P. Kothari, “Three-Phase 4-Wire DSTATCOM Based on H-Bridge VSC with a Star/Hexagon Transformer for Power Quality Improvement,” in *2008 IEEE Region 10 and the Third international Conference on Industrial and Information Systems*, 2008, pp. 1–6.

[10] H.-L. Jou, J.-C. Wu, K.-D. Wu, W.-J. Chiang, and Y.-H. Chen, “Analysis of Zig-Zag Transformer Applying in the Three-Phase Four-Wire Distribution Power System,” *IEEE Trans. Power Deliv.*, vol. 20, no. 2, pp. 1168–1173, Apr. 2005.

[11] P. Enjeti, W. Shireen, P. Packebush, and I. Pitel, “Analysis and design of a new active power filter to cancel neutral current harmonics in three phase four wire electric distribution systems,” in *Conference Record of the 1993 IEEE Industry Applications Conference Twenty-Eighth IAS Annual Meeting*, pp. 939–946.

[12] C. A. Quinn and N. Mohan, “Active filtering of harmonic currents in three-phase, four-wire systems with three-phase and single-phase nonlinear loads,” in *[Proceedings] APEC ’92 Seventh Annual Applied Power Electronics Conference and Exposition*, pp. 829–836.

[13] H.-L. Jou, K.-D. Wu, J.-C. Wu, C.-H. Li, and M.-S. Huang, “Novel power converter topology for three-phase four-wire hybrid power filter,” *IET Power Electron.*, vol. 1, no. 1, p. 164, 2008.

[14] D. Sreenivasarao, P. Agarwal, and B. Das, “Neutral current compensation in three-phase, four-wire systems: A review,” *Electr. Power Syst. Res.*, vol. 86, pp. 170–180, May 2012.

[15] O. Ramos-figueroa, M. Quiroz-castellanos, and E. Mezura-montes, “Metaheuristics to solve grouping problems : A review and a case study,” *Swarm Evol. Comput.*, vol. 53, no. August 2019, p. 100643, 2020.

[16] M. A. Kashem, V. Ganapathy, and G. B. Jasmon, “Network reconfiguration for load balancing in distribution networks,” *IEE Proc. - Gener. Transm. Distrib.*, vol. 146, no. 6, p. 563, 1999.

[17] P. R. Babu, K. A. Kumar, and G. C. Teja, “New heuristic search approach to enhance the distribution system load balance,” in *2013 International Conference on Power, Energy and Control (ICPEC)*, 2013, pp. 159–164.

[18] P. R. Babu, R. Shenoy, N. Ramya, Soujanya, and S. Shetty, “Implementation of ACO technique for load balancing through reconfiguration in electrical distribution system,” in *2014 Annual International Conference on Emerging Research Areas: Magnetics, Machines and Drives (AICERA/iCMMD)*, 2014, pp. 1–5.

[19] Y. Yuehao, Z. Zhongqing, B. Wei, X. Jun, Q. Limin, and D. Yaoheng, “Optimal distribution network reconfiguration for load balancing,” in *2016 China International Conference on Electricity Distribution (CICED)*, 2016, vol. 2016-Septe, no. Ciced, pp. 1–4.

[20] Fu-Yuan Hsu and Men-Shen Tsai, “A Multi-Objective Evolution Programming Method for Feeder Reconfiguration of Power Distribution System,” in *Proceedings of the 13th International Conference on, Intelligent Systems Application to Power Systems*, 2005, vol. 2005, pp. 55–60.

[21] S. A. Taher and M. H. Karimi, “Optimal reconfiguration and DG allocation in

balanced and unbalanced distribution systems," *Ain Shams Eng. J.*, vol. 5, no. 3, pp. 735–749, Sep. 2014.
[22] T. S. Vitor and J. C. M. Vieira, "Optimal voltage regulation in distribution systems with unbalanced loads and distributed generation," in *2016 IEEE Innovative Smart Grid Technologies - Asia (ISGT-Asia)*, 2016, pp. 942–947.
[23] K. Nara, Y. Mishima, and T. Satoh, "Network reconfiguration for loss minimization and load balancing," in *2003 IEEE Power Engineering Society General Meeting (IEEE Cat. No.03CH37491)*, 2003, vol. 4, pp. 2413–2418.
[24] Qin Zhou, D. Shirmohammadi, and W.-H. E. Liu, "Distribution feeder reconfiguration for service restoration and load balancing," *IEEE Trans. Power Syst.*, vol. 12, no. 2, pp. 724–729, May 1997.
[25] H. B. Tolabi, M. H. Ali, Shahrin Bin Md Ayob, and M. Rizwan, "Novel hybrid fuzzy-Bees algorithm for optimal feeder multi-objective reconfiguration by considering multiple-distributed generation," *Energy*, vol. 71, pp. 507–515, Jul. 2014.
[26] Y.-L. Ke, C.-S. Chen, M.-S. Kang, J.-S. Wu, and T.-E. Lee, "Power Distribution System Switching Operation Scheduling for Load Balancing by Using Colored Petri Nets," *IEEE Trans. Power Syst.*, vol. 19, no. 1, pp. 629–635, Feb. 2004.
[27] C.-H. Lin, "Distribution network reconfiguration for load balancing with a coloured Petri net algorithm," *IEE Proc. - Gener. Transm. Distrib.*, vol. 150, no. 3, p. 317, 2003.
[28] H. Ji *et al.*, "An enhanced SOCP-based method for feeder load balancing using the multi-terminal soft open point in active distribution networks," *Appl. Energy*, vol. 208, pp. 986–995, Dec. 2017.
[29] H. F. Zhai, M. Yang, B. Chen, and N. Kang, "Dynamic reconfiguration of three-phase unbalanced distribution networks," *Int. J. Electr. Power Energy Syst.*, vol. 99, pp. 1–10, Jul. 2018.
[30] M. R. Kaveh, R. A. Hooshmand, and S. M. Madani, "Simultaneous optimization of re-phasing, reconfiguration and DG placement in distribution networks using BF-SD algorithm," *Appl. Soft Comput. J.*, vol. 62, pp. 1044–1055, 2018.
[31] C.-C. Kuo and Y.-T. Chao, "Energy management based on AM/FM/GIS for phase balancing application on distribution systems," *Energy Convers. Manag.*, vol. 51, no. 3, pp. 485–492, Mar. 2010.
[32] Jinxiang Zhu, Mo-Yuen Chow, and Fan Zhang, "Phase balancing using mixed-integer programming [distribution feeders]," *IEEE Trans. Power Syst.*, vol. 13, no. 4, pp. 1487–1492, 1998.
[33] M. Dilek, R. P. Broadwater, J. C. Thompson, and R. Seqiun, "Simultaneous phase balancing at substations and switches with time-varying load patterns," *IEEE Trans. Power Syst.*, vol. 16, no. 4, pp. 922–928, 2001.
[34] M. Sathiskumar, A. Nirmal kumar, L. Lakshminarasimman, and S. Thiruvenkadam, "A self adaptive hybrid differential evolution algorithm for phase balancing of unbalanced distribution system," *Int. J. Electr. Power Energy Syst.*, vol. 42, no. 1, pp. 91–97, Nov. 2012.
[35] J. Zhu, G. Bilbro, and Mo-Yuen Chow, "Phase balancing using simulated annealing," *IEEE Trans. Power Syst.*, vol. 14, no. 4, pp. 1508–1513, 1999.
[36] Tsai-Hsiang Chen and Jeng-Tyan Cherng, "Optimal phase arrangement of distribution transformers connected to a primary feeder for system unbalance improvement and loss reduction using a genetic algorithm," *IEEE Trans. Power Syst.*, vol. 15, no. 3, pp. 994–1000, 2000.
[37] A. B. Knolseisen, J. Coelho, S. F. Mayerle, F. J. S. Pimentel, and R. H. Guembarovski, "A model for the improvement of load balancing in secondary networks," in *2003 IEEE Bologna Power Tech Conference Proceedings*, vol. 3, pp. 822–828.

[38] Chia-Hung Lin, Chao-Shun Chen, Hui-Jen Chuang, Ming-Yang Huang, and Chia-Wen Huang, "An Expert System for Three-Phase Balancing of Distribution Feeders," *IEEE Trans. Power Syst.*, vol. 23, no. 3, pp. 1488–1496, Aug. 2008.
[39] M.-Y. Huang, C.-S. Chen, C.-H. Lin, M.-S. Kang, H.-J. Chuang, and C.-W. Huang, "Three-phase balancing of distribution feeders using immune algorithm," *IET Gener. Transm. Distrib.*, vol. 2, no. 3, p. 383, 2008.
[40] R. Chitra and R. Neelaveni, "A realistic approach for reduction of energy losses in low voltage distribution network," *Int. J. Electr. Power Energy Syst.*, vol. 33, no. 3, pp. 377–384, Mar. 2011.
[41] D. V. Nicolae and J. A. Jordaan, "Control algorithm of a smart grid device for optimal radial feeder load reconfiguration," in *2013 9th Asian Control Conference (ASCC)*, 2013, pp. 1–5.
[42] F. Shahnia, A. Ghosh, G. Ledwich, and F. Zare, "Voltage unbalance improvement in low voltage residential feeders with rooftop PVs using custom power devices," *Int. J. Electr. Power Energy Syst.*, vol. 55, pp. 362–377, 2014.
[43] R. A. Hooshmand and S. Soltani, "Fuzzy Optimal Phase Balancing of Radial and Meshed Distribution Networks Using BF-PSO Algorithm," *IEEE Trans. Power Syst.*, vol. 27, no. 1, pp. 47–57, Feb. 2012.
[44] S. H. Soltani, M. Rashidinejad, and A. Abdollahi, "Dynamic phase balancing in the smart distribution networks," *Int. J. Electr. Power Energy Syst.*, vol. 93, pp. 374–383, 2017.
[45] M. A. Kashem, V. Ganapathy, and G. B. Jasmon, "A novel approach for network reconfiguration based load balancing in distribution networks," *Electr. Power Components Syst.*, vol. 28, no. 5, pp. 415–431, 2000.
[46] M. K. Gray and W. G. Morsi, "Economic assessment of phase reconfiguration to mitigate the unbalance due to plug-in electric vehicles charging," *Electr. Power Syst. Res.*, vol. 140, pp. 329–336, Nov. 2016.
[47] H. Wen, D. Cheng, Z. Teng, S. Guo, and F. Li, "Approximate Algorithm for Fast Calculating Voltage Unbalance Factor of Three-Phase Power System," *IEEE Trans. Ind. Informatics*, vol. 10, no. 3, pp. 1799–1805, Aug. 2014.
[48] K.M. Passino, "Biomimicry of bacterial foraging for distributed optimization and control," *IEEE Control Syst.*, vol. 22, no. 3, pp. 52–67, Jun. 2002.
[49] S. Das, A. Biswas, S. Dasgupta, and A. Abraham, "Bacterial Foraging Optimization Algorithm: Theoretical Foundations, Analysis, and Applications," in *Foundations of Computational Intelligence Volume 3. Studies in Computational Intelligence*, Berlin, Heidelberg: Springer-Verlag, 2009, pp. 23–55.
[50] S. Devi and M. Geethanjali, "Application of Modified Bacterial Foraging Optimization algorithm for optimal placement and sizing of Distributed Generation," *Expert Syst. Appl.*, vol. 41, no. 6, pp. 2772–2781, May 2014.
[51] K. R. Devabalaji, K. Ravi, and D. P. Kothari, "Optimal location and sizing of capacitor placement in radial distribution system using Bacterial Foraging Optimization Algorithm," *Int. J. Electr. Power Energy Syst.*, vol. 71, pp. 383–390, Oct. 2015.
[52] K. Sathish Kumar and T. Jayabarathi, "Power system reconfiguration and loss minimization for an distribution systems using bacterial foraging optimization algorithm," *Int. J. Electr. Power Energy Syst.*, vol. 36, no. 1, pp. 13–17, Mar. 2012.

Problems if any, Encountered During the Course of the Project

The world, the country as well as the university was marred with all sorts of problems, difficulties and challenges over the span of this project. Inevitably, all of those issues had some adverse effects on the progress and flow of this project.

The component of the projects, which is heavily dependent on computational developments (albeit, using real data from a segment of the low-voltage grid of Sri Lanka) progressed rapidly, converting all these external hindrances to a blessing. As the "regular" work was stopped several times (including the Easter Attack, some Union Actions, then ultimately lockdowns due to COVID), it gave extra time to spend on the components which only require computational and intellectual commitment.

One immediate consequence of all these hindrances was the fact that the Research Student was unable to register for a research degree (viz. MPhil). As he was scheduled to apply for his doctoral studies, this delay resulted in an impossible timeline, should he register for an MPhil.

The most severe adverse effect of all these stoppages of work was the hindrances on completing the procurement of equipment and consumables. The investigators sought two extensions to complete the procurement process. However, due to delays resulted form all these issues and the reluctance by vendors to respond to the calls for quotations (due to the rather negative perception of the economic factors caused by the pandemic), the procurement processes could not be completed even at the lapse of the two extensions.

Nevertheless, being resourceful, the investigators were able to implement the prototypes of the hardware setups utilizing some equipment on a shared basis. Therefore, the downside is, though the concepts have been validated and proved in hardware, the so developed hardware setups do not belong to the grant.

Subjected to these alterations and workarounds, the entire work framework envisioned and proposed under this grant was completed, albeit, *with more publications than anticipated*.

The investigators would like to refer to the Gantt Chart proposed in the research proposal as well as the extension request letters (which provide justification for the delays) at this point. These documents are provided as appendices at the end of this report.

Major Findings

The major findings of this work can be summarized as follows:

- The renewable energy penetration can be maximized through coordinated re-phasing of solar photovoltaic (PV) generators in the low-voltage grid
- An automatic photovoltaic re-phasing switch that can be connect to single-phase photovoltaic inverters to realize this switching action effectively
- A modified discrete bacterial foraging optimization to determine the optimum phase combination of photovoltaic systems, this sets the stage for possible other such compatible techniques for optimization of the PV absorption

For detailed discussion of the research contributions, please refer the publications resulted from this grant.

Follow-Up In Terms of Technology Development/Start-up Business

The first and foremost follow-up action prior to commercialization (i.e. commercial technology development and/or start-up) is to secure the intellectual property rights. Once they are secured, the developed prototypes may be developed in industrial standards, and then subjected to field testing. Therefore, though the outcomes of this work are promising, still a significant amount of rigorous work remains to be completed in order to serve as a commercial technology. Nevertheless, the work is quite promising and deployable.

Section 4: Impact of Research Results

Part A:

(1) Relevance of results achieved to scientific advancement

The work done under this grant was accepted for publication in three high impact journals, which are also highly reputed as journals at the cutting edge of engineering development and research. Therefore, it is evident that the results achieved under this grant are at a pristine level and that they contribute naturally to scientific advancement as well as technological development.

(2) Dissemination/application of research output – please give the tentative plan

Maximizing the absorption of solar PV generated in the LV grid has major consequences towards achieving energy sustainability. Higher influx of renewable sources have the tendency to intrinsically impair the electric grid due to its variability. The principal impairment is the grid instability and voltage violations. As outcomes of this research, we provide the analysis of these issues, a remedial course of action, a viable hardware tool and an appropriate optimization tool to achieve the desired performance.

There lies a significant requirement for the improvement of the inverter and the inverter control strategy based on this premise. Therefore, these tools and techniques have to be further developed and advanced. The next is to scale-up the design, This is mostly a technological development, and therefore, will be heavily in need of extensive testing. Next, the setup must be tested upon a "model house" and then tested in a "controlled network" and then, test with some pilot cases.

Part B:

Relevance of results achieved to national/socio-economic development - please give recommendations clearly as this write – up may be forwarded to the potential users who will benefit from the research

Energy security is by far the most important factor for achieving economic success. The work carried under the banner of this grant provides several key steps in making energy security a reality by providing a viable, sustainable and economical solution.

Section 5: Miscellaneous

(1) List of major equipment acquired during the project period, their value and their functionality

None

(2) List of publications/communications arising from the project and/or presentations made at seminars, workshops etc. (Please attach copies)

Journal Papers: Three (03)

(1) W.G. Chaminda Bandara, G.M.R.I. Godaliyadda, M.P.B. Ekanayake, J.B. Ekanayake, "Coordinated *Photovoltaic Re-Phasing:* A Novel Method to Maximize Renewable Energy Integration in Low Voltage Networks by Mitigating Network Unbalances", Applied Energy, Volume 280, 2020, 116022, Elesevier
SCIE Journal Impact Factor: 9.746

(2) Wele Gedara Chaminda Bandara, Dilini Almeida, Roshan Indika Godaliyadda, Mervyn Parakrama Ekanayake, Janaka Ekanayake, "A Complete State Estimation Algorithm for a Three-Phase Four-Wire Low Voltage Distribution System with High Penetration of Solar PV", Electrical Power and Energy Systems, Volume 124, 2021, 106332, Elesevier
SCIE Journal Impact Factor: 4.630

(3) A. S. Jameel Hassan, Umar Marikkar, G. W. Kasun Prabhath, Aranee Balachandran, W. G. Chaminda Bandara, Parakrama B. Ekanayake, Roshan I. Godaliyadda, Janaka Ekanayake, "A Sensitivity Matrix Approach Using Two-Stage Optimization for Voltage Regulation of LV Networks with High PV Penetration", Energies, Volume 14(20), 2021, 103390, MDPI
SCIE Journal Impact Factor: 3.004

Conference Papers: One (01)

(1) Aranee Balachandran, G. W. K. Prabhath, W. G. Chaminda Bandara, G. M. R. I. Godaliyadda, M. P. B. Ekanayake, J. B. Ekanayake, "Reactive Power Compensation for Voltage Violations in Distribution Network", 14th IEEE International Conference on Industrial and Information Systems (ICIIS), Kandy, Sri Lanka, 18-20 December, 2019

Patent Applications: One (01)

Sri Lankan Paten Application Number 21543 (Submitted on 12th January, 2021; Under Review)
Title: Single Phase Re-Phasing Solar Inverters for a Re-Configurable LV Network that has Accepted Voltage Profiles and Unbalances

Section 6: Summary Statement of Expenditure

Vote	Total Received (Rs.)	Total Amount Spent To Date (Rs.)	Percentage Spent out of total Allocation	Comments
Personnel	**1,200,000.00**	**1,038,300.00**	**87%**	Research Student was employed for less than 22 months
Equipment	**54,300.00**	**0.00**.	**0%**	Unable to complete procurement process due to COID*
Consumables	**568,989.00**	**0.00**.	**0%**	Unable to complete procurement process due to COID*
Lab Services & Sample Analysis				
Travel and subsistence	-	-	-	
Postgraduate registration fees	-	-	-	
Statistical analysis	-	-	-	
Calibration of instruments	-	-	-	
Miscellaneous	**20,000.00**	-	**0%**	Unable to complete procurement process due to COID*
Total	***1,843,289.00***	***1,038,300.00***		***Balance Rs. 804,989.00***

* Two extensions were sought from the NSF and were granted. However, due to the calamity amidst the COVID-19 pandemic and the frequent cessation of work due to lockdowns etc., the procurement process was severely hampered. In addition, the vendors were reluctant to respond further delaying the procurement process. Eventually, the procurement process was not completed before the expiration of the grant.

Section 7: Signatures and Approval

(1) Signatures of the Investigators

Principal Investigator
Dr. M. P. B. Ekanayake

Co-Investigator
Dr. G. M. R. I. Godaliyadda

Co-Investigator
Prof. J. B. Ekanayake

(2) Comments of the Head of Department / Signature

Comments:

Signature:

(3) Head of the Institution's Signature

Signature:

Publications

Electrical Power and Energy Systems 124 (2021) 106332

Contents lists available at ScienceDirect

Electrical Power and Energy Systems

journal homepage: www.elsevier.com/locate/ijepes

A complete state estimation algorithm for a three-phase four-wire low voltage distribution system with high penetration of solar PV☆

Wele Gedara Chaminda Bandara[a,*], Dilini Almeida[a], Roshan Indika Godaliyadda[a], Mervyn Parakrama Ekanayake[a], Janaka Ekanayake[a,b]

[a] Department of Electrical and Electronic Engineering, Faculty of Engineering, University of Peradeniya, Peradeniya 20400, Sri Lanka
[b] School of Engineering, Cardiff University, The Parade, Cardiff CF24 3AA, United Kingdom

ARTICLE INFO

Keywords:
State estimation
Admittance matrix
Solar PV
Energy management system
Low voltage distribution grids

ABSTRACT

Low Voltage Distribution Grids (LVDGs) become highly unbalanced due to the advent of single-phase solar PV plants. As a result, the voltage and current levels of the neutral conductor show a significant increase. Therefore, monitoring of the entire state of the network is essential. However, the existing state estimation algorithms estimate voltage states of the phase conductors while ignoring the state of the neutral conductor. This paper presents a novel approach to estimate the complete state of the LVDGs. A novel state reduction method was introduced to model the three-phase four-wire feeder line using a 3×3 admittance matrix, which incorporates the neutral coupling effect on phase conductors. Next, the reduced admittance matrix together with the linear approximations of active and reactive power functions were combined to formulate the Low Voltage-Linear State Estimation (LV-LSE) algorithm. Finally, the performance of LV-LSE algorithm was analyzed for different measurement uncertainties, scales of line lengths of the network, and data-loss conditions. Results show that, for all the cases, LV-LSE algorithm together with the proposed reduction method can estimate voltage states with an average maximum voltage magnitude error of less than 4.32×10^{-3} pu and current states with an average maximum current magnitude error of less than 1.81×10^{-3} pu.

1. Introduction

It is now recognized that one of the main contributors to climate change is the higher percentage of emissions from conventional power generating sources. This has encouraged the governments around the world to constitute several targets for the integration of Renewable Energy Sources (RESs) into the grid. Out of different RESs, the capital cost of solar photovoltaic (PV) continues to fall at a considerably higher rate. According to a recent report by the regulator of Australia, AEMO, it has been forecasted that solar PV would be the main contributor to electricity generation by 2050 [1].

During the last decade, the number of PV plants connected to LVDGs have shown a rapid increase. However, the integration of scattered PV plants instigates additional challenges to the existing LVDGs and those challenges become aggravated with the increasing level of PV penetration.

Traditionally, power systems have been designed to operate on unidirectional power flows. However, due to the high proliferation of PV systems, bidirectional power flows can be seen on the LVDGs, thus causing adverse consequences. Some of the possible impacts are voltage rise, voltage fluctuations and unbalances, thermal overloads, higher levels of harmonics etc. The severity of these impacts depends on the configuration of the distribution network, penetration level, and the location of the PV node in the distribution network.

1.1. Impact of high intake of solar PV

A study on investigating the impact of high intake of solar PV was reported in [2]. A Monte Carlo based methodology was developed and applied for a typical unbalanced residential network (Fig. 1) in Sri Lanka using a three-phase, four wire LV network model.

Under the Monte Carlo implementation, pre-defined number of PV panels having randomly generated PV capacity between 2 and 7 kW was connected to randomly generated nodes and phases of the distribution system. One hundred power flow simulations were performed by varying the PV capacity and location, and several critical parameters

☆ This research was supported by the National Science Foundation (NSF), Sri Lanka (grant number: RG/2018/EA & ICT/01).
* Corresponding author.
E-mail addresses: chaminda.bandara@eng.pdn.ac.lk (W.G. Chaminda Bandara), dilinialmeida2@gmail.com (D. Almeida), roshangodd@ee.pdn.ac.lk (R.I. Godaliyadda), mpb.ekanayake@ee.pdn.ac.lk (M.P. Ekanayake), ekanayakej@cardiff.ac.uk (J. Ekanayake).

https://doi.org/10.1016/j.ijepes.2020.106332
Received 9 November 2019; Received in revised form 27 May 2020; Accepted 27 June 2020

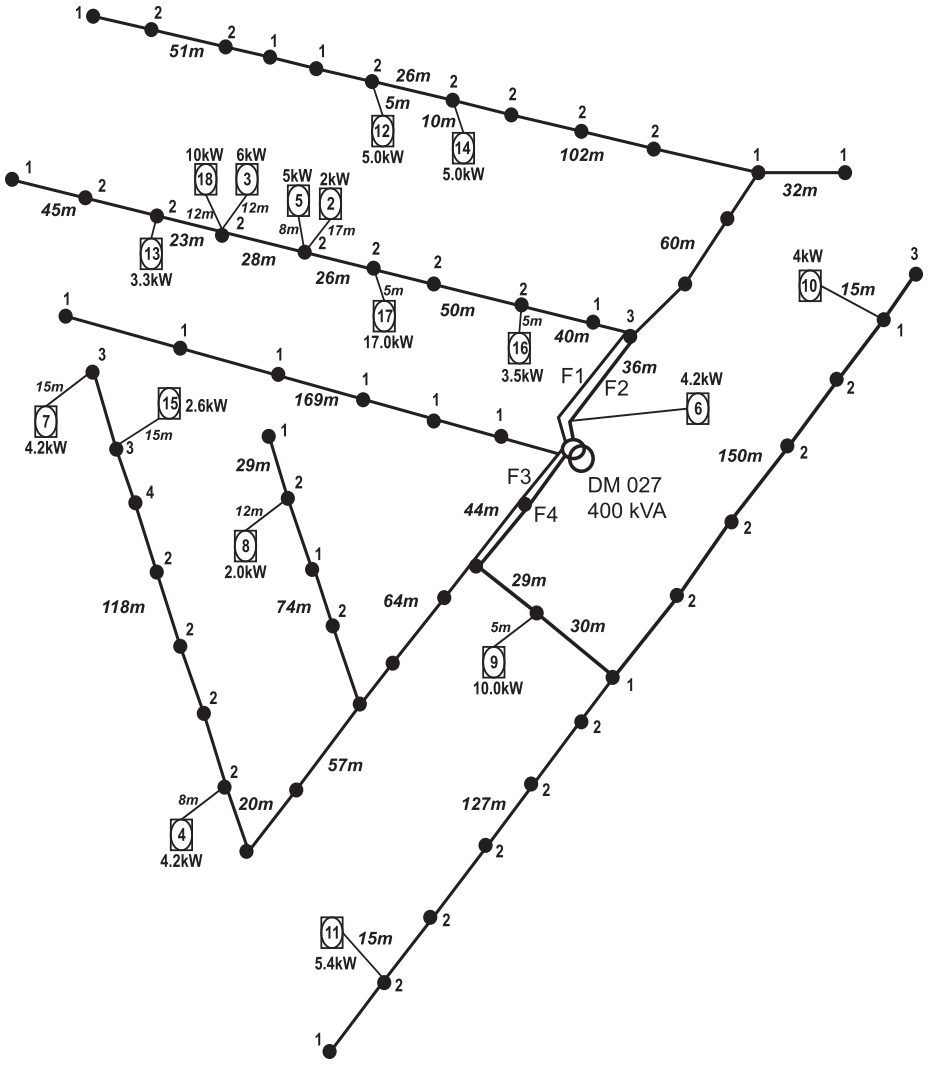

Fig. 1. Single line diagram of the residential network. More details about the network can be obtained from [2] and Appendix A.

were extracted from the load flow results. Then the impacts were analyzed using voltage unbalances, neutral currents, voltage and thermal limits. A more comprehensive study on this is accepted for publication [3] and only some preliminary results are shown here to highlight the importance of determining the state of the neutral conductor.

Fig. 2 illustrates the maximum value of the variation throughout the one hundred simulations (arranged in ascending order) for neutral current and voltage unbalance factor for the worst-case scenario, i.e. minimum loading and maximum PV generation. The variation of maximum voltage with the total installed PV capacity is shown in Fig. 3 for the same case.

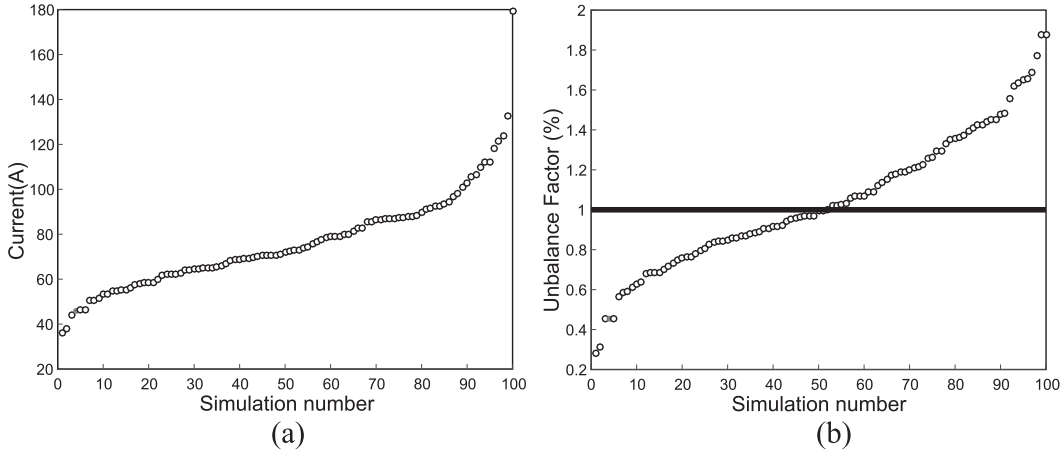

Fig. 2. Variation of (a) maximum neutral current and (b) maximum voltage unbalance factor for hundred simulations.

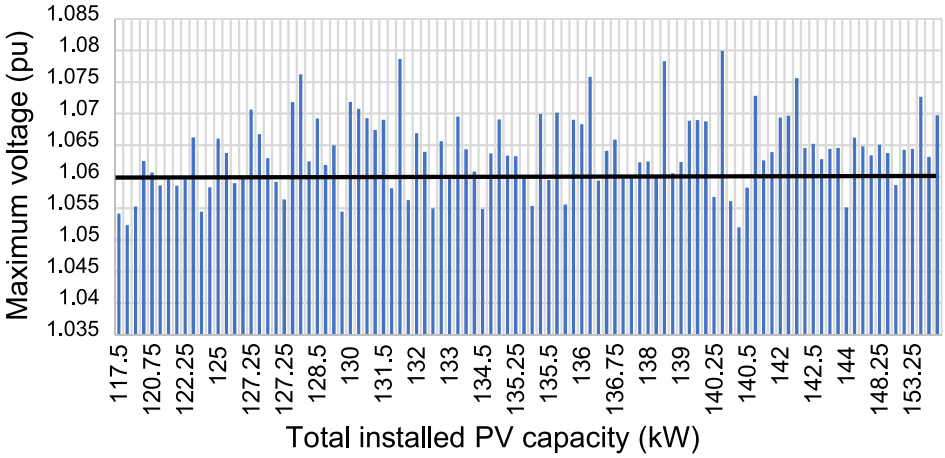

Fig. 3. Variation of maximum voltage with total installed PV capacity.

Results from the impact assessment revealed that under high penetration of solar PV, depending on their location and phase, some of the critical parameters such as voltage and voltage unbalance factor violated the statutory limits. Also, it was observed that the highly unbalanced allocation of single-phase PV units can create significantly large neutral currents.

In order to mitigate the aforementioned impacts of solar PV and thereafter to ensure optimal, secure, reliable and coordinated operation of LVDGs, an Energy Management System (EMS) is crucial. State Estimation (SE) is considered as an essential element of the EMS as it is not possible to perform real-time monitoring and control without knowing the state of the entire LVDG [4].

1.2. Distribution System State Estimation (DSSE)

Distribution System State Estimation (DSSE) algorithms process raw measurements (including voltage and current magnitudes, active and reactive power measurements) and additional pseudo values to estimate the actual state of a power system. DSSE enables real-time distribution grid monitoring and provides the initial condition of the power system for a variety of applications including voltage control, feeder reconfiguration and Demand Side Management (DSM).

Algorithms developed for DSSE were widely adapted from estimation techniques developed for Transmission System State Estimation (TSSE) that have been developed for over six decades [5]. When considering TSSE, the Weighted Least Squares (WLS) approach is the most popular SE algorithm among the many alternatives proposed [6–11]. The common choices for state variables are node voltage or branch current [12,13]. There is always an assumption of a “balanced system” at transmission-level. This allows for the decoupling of the three-phase system, making in per-phase positive sequence network data being sufficient for analysis [14–18].

In contrast, distribution grids under radial and weakly-meshed operations have highly unbalanced three-phase branches due to numerous combinations of unequal single-phase, two-phase, three-phase loads and small-scale distributed generators. In distribution networks, real-time measurements are limited and network observability is not achieved unless pseudo values and network reduction techniques are used. These distinct features of distribution systems prohibit the direct application of mature state estimation methods developed for TSSE [19,5].

In addition to the state estimators proposed for transmission systems, three-phase DSSE that accommodates unsymmetrical characteristics of distribution systems are reported in the literature. In [20], a multi-phase DSSE that calculates system states by utilizing a constrained WLS method while including standard three-phase state estimation capabilities is presented. In [21], a two-step procedure has been introduced for multi-area state estimation in distribution systems. Here, the first step local estimations are refined through a WLS based second step which integrates the information available from neighboring zones. In [22], a three-phase admittance matrix-based DSSE model has been proposed. The proposed DSSE model tackles issues related to consistency, zero-injections, and inclusion of voltage measurements. The real and imaginary parts of the bus voltages are utilized as state variables while power and voltage measurements are converted into equivalent currents and voltages. Reference [23] proposed a DSSE model using particle swarm optimization to estimate on-load tap changing for voltage control. The proposed method utilized both discrete and continuous variables to estimate transformer tap positions.

However, due to the different grounding configurations, the asymmetrical nature of loads, distributed energy sources, and the number of available measurements, will limit the universal applicability of the aforementioned DSSE models proposed in the existing literature. References [20–23] can be utilized for LVDGs with a multi-grounded neutral configuration where neutral voltages are zero and can be naturally excluded. Successively, an original admittance matrix can be reduced to 3×3 using the Kron’s reduction. However, rather than multi-grounded neutral, in some countries, the neutral conductor is only grounded at the secondary side of the MV-LV transformer, which renders non-zero potential across the neutral conductor. Furthermore, the recent deployment of proliferated distributed energy sources resulted in high levels of neutral currents and voltages as studied in this paper. This warrants increased interest in three-phase DSSE models that incorporates the neural conductor states. However, incorporating the neutral conductor states in a DSSE model increases the number of states to be estimated and increases the size of the Jacobian matrix, thus introducing a significant computational burden. Nevertheless [19] considered a three-phase DSSE algorithm with explicit neutral configuration. In this reference, a multi-phase DSSE model has been proposed for distribution systems with a three-phase four-wire configuration. The proposed DSSE model utilized two types of state reduction strategies to improve its computational performance. The first is the use of the KCL theorem at neutral to represent neutral voltage as a linear combination of non-neutral phases. The second is the elimination of voltages at zero injection phases by linearly combining voltages of non-zero neutral and non-zero injection phases. Consequently, only voltages of non-neutral and non-zero injection phases are used as state variables to reduce the scale of the DSSE model. Moreover, different types of measurements such as phase-to-ground voltages, phase-to-neutral voltages, neutral currents, and non-neutral currents are utilized to achieve full network observability. However, the aforementioned DSSE model has not been generalized as an admittance matrix reduction technique that can be

used for any three-phase four-wire DSSE model or any load flow algorithm to eliminate neutral conductor states. Also, it does not estimate the voltage states of neutral and zero-injection phases. It should be stressed that, the estimation of complete state estimation is essential for the Distribution System Operators (DSOs) for highly unbalanced distribution systems. In this paper, solutions to all these above issues are addressed.

With the recent deployment of smart meters and distribution system measuring infrastructure, the visibility of LVDGs was enhanced. smart meters are installed at the connection points of some customers' that are capable of monitoring the real-time active and reactive power flows and additional information required by the DSOs such as voltage and current [24–26]. Different types of DSSE techniques that utilized such smart meter data have been proposed in recent literature. In [25] the technical feasibility of using smart meters and their measurements for LV network observability and controllability through SE techniques have been analyzed. In [26,27], LV SE through real-time measurements of smart meters have been proposed. In [28], the impact of different uncertainty sources such as smart meters, non-synchronized measurements and synchronized measurements provided by Phasor Measurement Units (PMSs) on three-phase SE has been analyzed. In [29], a smart control system for LVDGs has been designed using an automatic evaluation of critical voltage nodes based on power snapshot data collected from smart meters. A three-phase SE algorithm which utilized customers' energy bills to calculate average demands and a three-phase load flow algorithm to generate pseudo-measurements of voltage magnitudes, active and reactive power injections which ensures complete observability and a low investment cost for application in a typical distribution system has been proposed in [30]. In [31], a three-phase four-wire state estimation algorithm has been proposed by utilizing (4×4) admittance matrix. However, to avoid numerical instabilities in this method, the sum of currents are assumed to be zero at all nodes of the LV network, even at the non-injection nodes. This is not a realistic assumption when LVDGs are highly unbalanced.

Smart meters can provide real-time measurements unless there are no communication errors [32]. Ideally, an LVDG with 100% smart meter coverage, where all smart meters can upload their measurements in real-time, can directly estimate the total load of the LVDG. However, in reality, due to the fact that a large number of smart meters are sparsely distributed in an LVDG, only a small fraction of smart meters can report their voltage and power values at the same time. In addition, the information collection procedure of smart meters is subjected to data loss because smart meters use wireless signals to transmit data from smart meters to an Access Point (AP) [33]. Due to these practical problems with smart meters, the amount of measurements in an LVDG is far from enough to guarantee observability. Thus, the DSSE model based on linearized active and reactive power functions proposed in this paper, which provides complete state estimation of the network, even under 60% availability of smart meters tackles the limited measurement availability problem more effectively compared to existing SE techniques. Further, the performance of the proposed LV-LSE algorithm was analyzed under different levels of smart meter data loss to demonstrate its robustness under such adverse conditions.

1.3. Objective and contribution of the paper

The contributions of this paper are summarized as follows:

- ***An accurate reduction technique to model three-phase four-wire system*** by incorporating the neutral coupling effect on phase conductors. The use of Kron's reduction to simplify LV feeder lines leads to inaccurate results in the monitoring of LVDGs, especially when the system is highly unbalanced. Therefore, the proposed reduction method is a more generalized approach to simplify the three-phase four-wire system and significantly improves the accuracy of the LV-LSE algorithm.
- ***An efficient sequential LV-LSE algorithm:*** The existing WLS based SE algorithms require a larger amount of measurements compared to the number of state variables that are required to be estimated by a factor of 1.7 to 2.2. In most of the practical situations, available measurements are limited due to the limited number of smart meters installed, unavailability of smart meters, communication errors at a given time, and possibility of data loss during transmission. The linearized active and reactive power functions, the assignment of pseudo values for loads, voltage magnitudes and angles, and the sequential nature of estimating voltage states allow the proposed LV-LSE algorithm to operate effectively, even with 60% availability of smart meter data.

2. Materials and methods

2.1. LV feeder model

2.1.1. Representation of three-phase feeder lines as a 4×4 admittance matrix

Most of the distribution lines in LVDGs consist of four conductors (thee phase conductors and one neutral conductor). The mutual coupling between each conductor is significant since the conductors are arranged in geometrically close distances and carry significant amount of current through them. Fig. 4 shows the series and mutual impedances of a three-phase distribution line. The method developed by Carson [34] can be used to accurately compute series and mutual impedances for both overhead and underground distribution lines. The application of Carsons's equation has become the standard for computation of line impedances. Because Carson's equation has resulted in an infinite series, a modified version of Carson's equations have been proposed in [35]. The modified Carson's equations compute series and mutual impedance values with an error less than 0.3% compared with the values obtained using the original Carson's equations. Therefore, the modified Carson's equations were used to calculate series and mutual impedance values. The modified Carson's equations for a overhead cable assuming a frequency of 50 Hz and a ground resistivity of 100 Ωm are:

$$z_{ii} = 0.0493 + r_i + j0.0628\left(ln\left(\frac{0.3048}{GMR_i}\right) + 8.0251\right)\Omega/\text{km} \tag{1}$$

$$z_{ij} = 0.0493 + j0.0628\left(ln\left(\frac{0.3048}{D_{ij}}\right) + 8.0251\right)\Omega/\text{km} \tag{2}$$

where, z_{ii} is the self impedance of the i-th conductor (Ω/km), z_{ij} is the mutual impedance between i-th conductor and j-th conductor (Ω/km), r_i is the ac resistance of the i-th conductor (Ω), GMR_i is the geometric mean radius of the i-th conductor (m) and D_{ij} is the distance between i-th conductor and j-th conductor (m). Therefore, the impedance matrix of the unbalanced three-phase four wire system was formulated as,

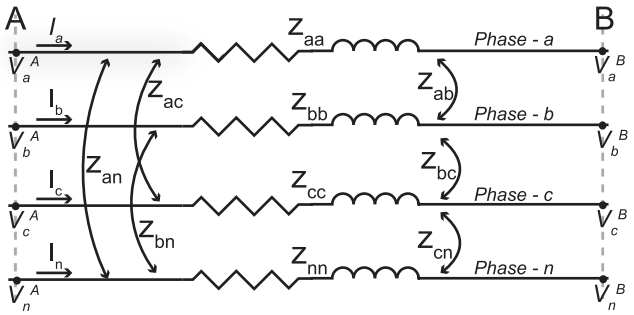

Fig. 4. Impedance of LV three-phase feeder section [17,36].

$$Z^{abcn} = \begin{bmatrix} z_{aa} & z_{ab} & z_{ac} & z_{an} \\ z_{ba} & z_{bb} & z_{bc} & z_{bn} \\ z_{ca} & z_{cb} & z_{cc} & z_{cn} \\ z_{na} & z_{nb} & z_{nc} & z_{nn} \end{bmatrix} \tag{3}$$

where, the diagonal elements in Z^{abcn} represents the self-impedance (z_{ii}) of each conductor and the off-diagonal elements represents the mutual-impedance (z_{ij}) between the two conductors. Z^{abcn} matrix relates the voltage drop between each conductor and the phase currents. From the Z^{abcn}, Y^{abcn} was computed by taking the matrix inverse of Z^{abcn}.

2.1.2. Representation of three-phase feeder line as a 3 × 3 admittance matrix

Most of the SE algorithms then reduce 4 × 4 admittance matrix to a simpler form of 3 × 3 under several assumptions. The most common reduction method is to use Kron's reduction. Kron's reduction [37] can be used to simplify 4 × 4 admittance matrix to a 3 × 3 admittance matrix by decoupling the neutral conductor from phase conductors. Kron's reduction achieves this by assuming the potential of the neutral conductor is zero. However, this assumption is not valid in most of the LVDGs. The primary objective of this section is to develop an accurate reduction method to simplify 4 × 4 admittance matrix into a 3 × 3 admittance matrix by accounting for the possible non-zero potential of the neutral conductor.

The 4 × 4 admittance matrix relates the phase currents and voltage drop of the line section as,

$$\begin{bmatrix} I_a^{AB} \\ I_b^{AB} \\ I_c^{AB} \\ I_n^{AB} \end{bmatrix} = \begin{bmatrix} y_{aa} & y_{ab} & y_{ac} & y_{an} \\ y_{ba} & y_{bb} & y_{bc} & y_{bn} \\ y_{ca} & y_{cb} & y_{cc} & y_{cn} \\ y_{na} & y_{nb} & y_{nc} & y_{nn} \end{bmatrix} \begin{bmatrix} \Delta V_a^{AB} \\ \Delta V_b^{AB} \\ \Delta V_c^{AB} \\ \Delta V_n^{AB} \end{bmatrix} \tag{4}$$

where, I_a^{AB}, I_b^{AB}, I_c^{AB} and I_n^{AB} denote the phase currents and ΔV_a^{AB}, ΔV_b^{AB}, ΔV_c^{AB} and ΔV_n^{AB} denote the voltage drop across each phase between A and B points (see Fig. 4). Therefore, current through the phase-$m \in \{a, b, c, n\}$ was written as,

$$I_m^{AB} = \sum_{k=a,b,c,n} y_{mk} \cdot \Delta V_k^{AB} \tag{5}$$

where, (5) generates a set of four equations for phases-a, b, c, and n. The neutral current (I_n^{AB}) was approximated as,

$$I_n^{AB} \approx - \sum_{\ell=a,b,c} I_\ell^{AB} \tag{6}$$

The negative sign in the (6) indicates that the direction of neutral current flow is opposite to the current flow of phase conductors. By equating (5) when $m = n$ and (6),

$$I_n^{AB} \approx - \sum_{\ell=a,b,c} I_\ell^{AB} = \sum_{k=a,b,c,n} y_{nk} \cdot \Delta V_k^{AB} \tag{7}$$

Therefore,

$$\Delta V_n^{AB} = \frac{- \sum_{\ell=a,b,c} I_\ell^{AB} - \sum_{k=a,b,c} y_{nk} \cdot \Delta V_k^{AB}}{y_{nn}} \tag{8}$$

By substituting to ΔV_n^{AB} in (5) from (8) and after simplification for $m \in \{a, b, c\}$, generate three set of equations as,

$$\left(1 + \frac{y_{mn}}{y_{nn}}\right) I_m^{AB} + \sum_{p=m_1,m_2} \frac{y_{mn}}{y_{nn}} I_p^{AB} = \sum_{q=a,b,c} \left(y_{mq} - \frac{y_{mn} y_{nq}}{y_{nn}}\right) \Delta V_q^{AB} \tag{9}$$

where, in the equation for phase– m, variables m_1 and m_2 denotes the other two phases. For example, if $m = b$ then m_1, $m_2 = a$, c. Thereafter, by rearranging the set of three equations generated in (9) for $m \in \{a, b, c\}$ in matrix form,

$$\begin{bmatrix} \left(1 + \frac{y_{an}}{y_{nn}}\right) & \frac{y_{an}}{y_{nn}} & \frac{y_{an}}{y_{nn}} \\ \frac{y_{bn}}{y_{nn}} & \left(1 + \frac{y_{bn}}{y_{nn}}\right) & \frac{y_{bn}}{y_{nn}} \\ \frac{y_{cn}}{y_{nn}} & \frac{y_{cn}}{y_{nn}} & \left(1 + \frac{y_{cn}}{y_{nn}}\right) \end{bmatrix} \begin{bmatrix} I_a^{AB} \\ I_b^{AB} \\ I_c^{AB} \end{bmatrix}$$
$$= \begin{bmatrix} \left(y_{aa} - \frac{y_{an}y_{na}}{y_{nn}}\right) & \left(y_{ab} - \frac{y_{an}y_{nb}}{y_{nn}}\right) & \left(y_{ac} - \frac{y_{an}y_{nc}}{y_{nn}}\right) \\ \left(y_{ba} - \frac{y_{bn}y_{na}}{y_{nn}}\right) & \left(y_{bb} - \frac{y_{bn}y_{nb}}{y_{nn}}\right) & \left(y_{bc} - \frac{y_{bn}y_{nc}}{y_{nn}}\right) \\ \left(y_{ca} - \frac{y_{cn}y_{na}}{y_{nn}}\right) & \left(y_{cb} - \frac{y_{cn}y_{nb}}{y_{nn}}\right) & \left(y_{cc} - \frac{y_{cn}y_{nc}}{y_{nn}}\right) \end{bmatrix} \begin{bmatrix} \Delta V_a^{AB} \\ \Delta V_b^{AB} \\ \Delta V_c^{AB} \end{bmatrix} \tag{10}$$

Let's denote Eq. (10) as,

$$L \cdot I_{abc}^{AB} = Y^{abc} \cdot \Delta V_{abc}^{AB} \tag{11}$$

where, $I_{abc}^{AB} = [I_a^{AB}\ I_b^{AB}\ I_c^{AB}]^T$, $\Delta V_{abc}^{AB} = [\Delta V_a^{AB}\ \Delta V_b^{AB}\ \Delta V_c^{AB}]^T$, L is a complex valued scalar matrix and Y^{abc} is exactly the same as in the Kron's reduction ($I_{abc}^{AB} = Y^{abc} \Delta V_{abc}^{AB}$). As can be noted, the introduction of the L matrix is the innovation of the proposed method and it incorporates the neutral conductor coupling effects on the phase conductors. In addition, it can be clearly seen that the matrix L has a full rank, hence the inverse of L always exists. Therefore, the proposed reduction method was written as,

$$I_{abc}^{AB} = (L^{-1} Y^{abc}) \cdot \Delta V_{abc}^{AB} = \overline{Y}^{abc} \cdot \Delta V_{abc}^{AB} \tag{12}$$

The matrix: $\overline{Y}^{abc} = L^{-1} Y^{abc}$ defined in (12) is the reduced version of the Y^{abcn} in (4), while including the effects of the neutral conductor on phase conductors. Let's denote the elements of the $\overline{Y}^{abc}$ as,

$$\overline{Y}^{abc} = \begin{bmatrix} \bar{y}_{aa} & \bar{y}_{ab} & \bar{y}_{ac} \\ \bar{y}_{ba} & \bar{y}_{bb} & \bar{y}_{bc} \\ \bar{y}_{ca} & \bar{y}_{cb} & \bar{y}_{cc} \end{bmatrix} \tag{13}$$

2.1.3. Kron's reduction

Kron's reduction assumes there is no significant current through the neutral conductor (i.e. a balanced three-phase system). Hence, voltage drop across the neutral conductor can be approximated as zero. For this reason, the conventional SE algorithms assume that the neutral conductor is grounded at both ends of the distribution line (see Fig. 5) and that is represented as a zero potential across the neutral conductor of the whole system. This assumption allows the Kron's reduction to eliminate the neutral conductor and reduce 4 × 4 admittance matrix (Y^{abcn}) to a simpler form of 3 × 3 (Y^{abc}) [37–39],

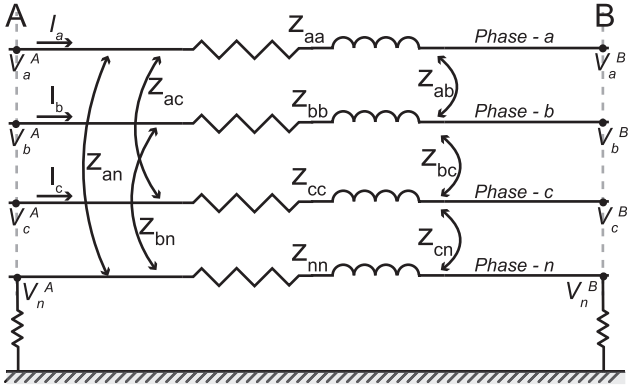

Fig. 5. A four-wire multi-grounded distribution line.

$$Y^{abc} = \begin{bmatrix} \left(y_{aa} - \frac{y_{an}y_{na}}{y_{nn}}\right) & \left(y_{ab} - \frac{y_{an}y_{nb}}{y_{nn}}\right) & \left(y_{ac} - \frac{y_{an}y_{nc}}{y_{nn}}\right) \\ \left(y_{ba} - \frac{y_{bn}y_{na}}{y_{nn}}\right) & \left(y_{bb} - \frac{y_{bn}y_{nb}}{y_{nn}}\right) & \left(y_{bc} - \frac{y_{bn}y_{nc}}{y_{nn}}\right) \\ \left(y_{ca} - \frac{y_{cn}y_{na}}{y_{nn}}\right) & \left(y_{cb} - \frac{y_{cn}y_{nb}}{y_{nn}}\right) & \left(y_{cc} - \frac{y_{cn}y_{nc}}{y_{nn}}\right) \end{bmatrix} \tag{14}$$

where the symbols have the same meanings as defined previously. Due to the "balanced" assumption made in the Kron's reduction, the accuracy of the SE results significantly decreases specially when the system is highly unbalanced. In contrast, the proposed reduction technique ($\overline{Y}^{abc}$) incorporates the neutral coupling effects on phase conductors and thereby allows SE algorithms to perform well under severely unbalance situations.

2.2. State estimation algorithm

2.2.1. The SE problem

The objective of the SE is to calculate consistent values for state variables, based on a set of real-time measurements available at the EMS from the smart meters and other LV measuring infrastructure. The WLS SE problem was formulated as a minimization of objective function ($J(x)$) as in [40,41],

$$J(x) = \sum_{i=1}^{m} w_i e_i^2 \tag{15}$$

subjected to the constraint,

$$z = h(x) + e \tag{16}$$

where, w_i is the weighting factor for respective measurement, e is the m dimensional measurement error vector, z is the m dimensional measurement vector, consists of active and reactive power flows and bus voltage magnitudes, x is the n dimensional state vector, which consists of all the bus voltage magnitudes and angles and $h(\cdot)$ is the measurement function which relates x to z.

2.2.2. Measurement redundancy (η)

A necessary condition for the application of WLS based SE is a positive measurement redundancy ($\eta > 0$) [42–44]. In other words, the number of available measurements (m) must be greater than the number of state variables (n). The above definition of the measurement redundancy can be expressed in a mathematical form as [44],

$$\eta = \frac{m}{n} - 1,\ n = N_{phases}\cdot\left(2N - 1\right) \tag{17}$$

where, N_{phases} is the number of phases considered in the SE algorithm and N is the total number of nodes in a network. For example: $N_{phases} = 1$ for per-phase SE in transmission networks, $N_{phases} = 3$ for three-phase SE in distribution networks and $N_{phases} = 4$ for SE in LVDGs including the neutral conductor.

In most of the practical cases η is in the range of 0.7 to 1.2 [42]. As mentioned in the introduction, achieving a positive measurement redundancy is difficult in LVDGs because not each and every household is equipped with smart meters - even the available smart meters are not highly reliable and only measures voltage magnitudes and complex power flows. Therefore, in this research it was assumed that about 60% of households are equipped with smart meters which measure voltage magnitudes and complex power flows at the location where they are installed. As can be noted from Eq. (17), the inclusion of the neutral conductor states in the SE algorithm also reduces the measurement redundancy in LVDGs. Hence, these practical limitations present in the LVDGs prohibit the use of WLS based SE algorithms to effectively determine the complete states of network. Therefore, a sequential LV-LSE was developed by utilizing the novel reduction technique as outlined in section 2.1.2 to achieve a positive measurement redundancy. The proposed sequential LV-LSE algorithm is described in the following sections.

2.2.3. Linearization of the measurement function

Generally, the measurement function ($h(\cdot)$) is nonlinear for all measurements (active and reactive power flows, current magnitudes, etc.) except for voltage magnitudes. In this section, the nonlinear active and reactive power functions were linearized using the Taylor series approximations of $\sin(\cdot)$ and $\cos(\cdot)$ terms.

In Section 2.1.2, three-phase, four-wire line was modeled using a 4×4 admittance matrix and then reduced to a 3×3 admittance matrix ($\overline{Y}$) while accounting for the effects of the neutral conductor. Moreover, $\overline{Y}$ matrix relates the phase currents and voltage drop across the line segment AB using the relationship,

$$I_{abc}^{AB} = \overline{Y}^{abc}.\Delta V_{abc}^{AB} \tag{18}$$

The complex power flow (S_m^{AB}) through phase-m is given by the equation for $m \in \{a, b, c\}$, as,

$$S_m^{AB} = V_m^A \times (I_m^{AB})^* = V_m^A\left(\sum_{\ell=a,b,c} \bar{y}_{m\ell}\Delta V_\ell^{AB}\right)^* \tag{19}$$

where, * denotes the complex conjugation.

Let's denote, ψ_m^A is the voltage angle for node-A and phase-m, $|V_m^A|$ is the voltage magnitude for node-A and phase-m, $\bar{g}_{m\ell}$ and $\bar{b}_{m\ell}$ are the conductance and the susceptance of admittance element $\bar{y}_{m\ell}$ of the admittance matrix $\overline{Y}$. Therefore, (19) was expanded as,

$$S_m^{AB} = |V_m^A|\ \angle\psi_m^A\left(\sum_{\ell=a,b,c} [(\bar{g}_{m\ell} + j\bar{b}_{m\ell})(|V_\ell^A|\ \angle\psi_\ell^A - |V_\ell^B|\ \angle\psi_\ell^B)]\right)^* \tag{20}$$

Let's denote,

$$\begin{aligned} &\Delta\psi_{m\ell}^{AB} = \psi_m^A - \psi_\ell^B \text{ for } m, \ell \in \{a, b, c\} \\ &\cos_{m\ell}^{AB}{=}\cos(\Delta\psi_{m\ell}^{AB}) \text{ and } \sin_{m\ell}^{AB}{=}\sin(\Delta\psi_{m\ell}^{AB}) \end{aligned} \tag{21}$$

using the above notations in (21) the active power (P_m^{AB}) and reactive power (Q_m^{AB}) flows for phase-m can be expressed as (see Appendix C for the derivation),

$$\begin{aligned} P_m^{AB} &= |V_m^A| \sum_{\ell=a,b,c} \{|V_\ell^A|[\bar{g}_{m\ell}\cdot\cos_{m\ell}^{AA} + \bar{b}_{m\ell}\cdot\sin_{m\ell}^{AA}] \\ &\quad - |V_\ell^B|\cdot[\bar{g}_{m\ell}\cdot\cos_{m\ell}^{AB} + \bar{b}_{m\ell}\cdot\sin_{m\ell}^{AB}]\} \end{aligned} \tag{22}$$

$$\begin{aligned} Q_m^{AB} &= |V_m^A| \sum_{\ell=a,b,c} \{|V_\ell^A|[\bar{g}_{m\ell}\cdot\sin_{m\ell}^{AA} - \bar{b}_{m\ell}\cdot\cos_{m\ell}^{AA}] \\ &\quad - |V_\ell^B|\cdot[\bar{g}_{m\ell}\cdot\sin_{m\ell}^{AB} - \bar{b}_{m\ell}\cdot\cos_{m\ell}^{AB}]\} \end{aligned} \tag{23}$$

The Taylor series approximations of $\sin(\cdot)$ and $\cos(\cdot)$ were defined as (only linear terms were considered),

$$\begin{aligned} \sin_{ml}^{AA}{=}\sin(\Delta\psi_{ml}^{AA}) &\approx \sin(\Delta\psi_{ml,r}^{AA}) + \cos(\Delta\psi_{ml,r}^{AA})\cdot\Delta\psi_{ml}^{AA} \\ \cos_{ml}^{AA}{=}\cos(\Delta\psi_{ml}^{AA}) &\approx \cos(\Delta\psi_{ml,r}^{AA}) - \sin(\Delta\psi_{ml,r}^{AA})\cdot\Delta\psi_{ml}^{AA} \\ \sin_{ml}^{AB}{=}\sin(\Delta\psi_{ml}^{AB}) &\approx \sin(\Delta\psi_{ml,r}^{AB}) + \cos(\Delta\psi_{ml,r}^{AB})\cdot\Delta\psi_{ml}^{AB} \\ \cos_{ml}^{AB}{=}\cos(\Delta\psi_{ml}^{AB}) &\approx \cos(\Delta\psi_{ml,r}^{AB}) - \sin(\Delta\psi_{ml,r}^{AB})\cdot\Delta\psi_{ml}^{AB} \end{aligned} \tag{24}$$

The assignment of operating points (points where the functions are linearized) for the voltage angles were conducted as,

$$\Delta\psi_{m\ell,r}^{AA} \approx \Delta\psi_{m\ell,r}^{AB} = \begin{cases} 0, & \text{if } (m - \ell) = 0 \\ \frac{2\pi}{3}, & \text{if } (m - \ell) = -1 \vee 2 \\ \frac{-2\pi}{3}, & \text{if } (m - \ell) = -2 \vee 1 \end{cases} \tag{25}$$

under the assignment of phase $a = 1$, phase $b = 2$ and phase $c = 3$.

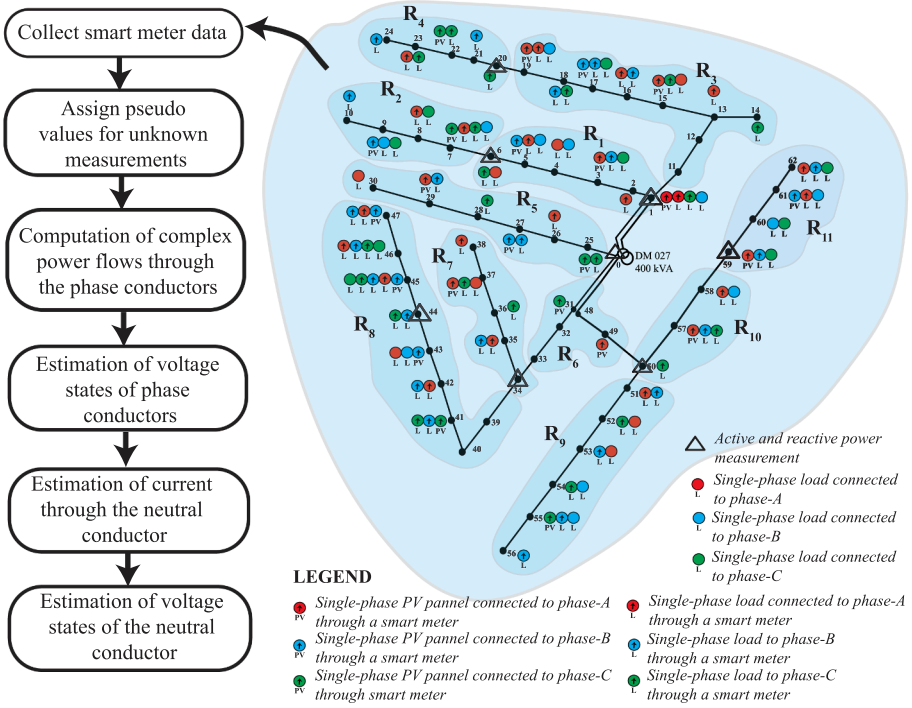

Fig. 6. Flow chart of the proposed sequential LV-LSE algorithm.

The operating points (points where the functions are linearized) for voltage magnitudes were calculated locally for each line segment by utilizing the available smart meter data to improve SE accuracy. Let's assume q number of smart meter voltage measurements ($|V_i|$) were received for line segment AB. Then the local operating point for voltage magnitude $|V_r|$ was calculated as,

$$|V_r| \approx \frac{1}{q}\sum_{i=1}^{q} |V_i| \tag{26}$$

Assuming the operating points for voltage angles as given by (25) and voltage magnitudes as given by (26), and applying Taylor series approximations on (22) and (23), the linearized approximations for the active ($\overline{P}_m^{AB}$) and reactive ($\overline{Q}_m^{AB}$) power functions for phase-m were expressed after simplifications as (see Appendix D for the derivation),

$$\overline{P}_m^{AB} = \sum_{\ell=a,b,c} |V_r|\cdot\Phi_P\cdot(|V_\ell^A| - |V_\ell^B|) - \sum_{\ell=a,b,c} |V_r|^2\cdot\Psi_P\cdot(\phi_\ell^A - \phi_\ell^B) \tag{27}$$

$$\overline{Q}_m^{AB} = \sum_{\ell=a,b,c} |V_r|\cdot\Phi_Q\cdot(|V_\ell^A| - |V_\ell^B|) - \sum_{\ell=a,b,c} |V_r|^2\cdot\Psi_Q\cdot(\phi_\ell^A - \phi_\ell^B) \tag{28}$$

where,

$$\Phi_P = \bar{g}_{m,\ell}\cos(\Delta_{m\ell,r}^{AB}) + \bar{b}_{m,\ell}\sin(\Delta_{m\ell,r}^{AB})$$
$$\Psi_P = -\bar{g}_{m,\ell}\sin(\Delta_{m\ell,r}^{AB}) + \bar{b}_{m,\ell}\cos(\Delta_{m\ell,r}^{AB})$$
$$\Phi_Q = -\Psi_P = \bar{g}_{m,\ell}\sin(\Delta_{m\ell,r}^{AB}) - \bar{b}_{m,\ell}\cos(\Delta_{m\ell,r}^{AB})$$
$$\Psi_Q = \Phi_P = \bar{g}_{m,\ell}\cos(\Delta_{m\ell,r}^{AB}) + \bar{b}_{m,\ell}\sin(\Delta_{m\ell,r}^{AB})$$

After linearizing the active and reactive power flow functions through phase conductors, the measurement function ($h(\cdot)$) given in (16) was represented as a linear equation for feeder section AB as,

$$z = H\cdot x + e \tag{29}$$

where, z and e have the same meanings as previously described in (16) and H is the linearized measurement matrix. With the application of WLS, the estimated state vector $\hat{x}$ was calculated with the equation given by,

$$\hat{x} = [(H^T U^{-1} H)^{-1} H^T U^{-1}]\cdot z \tag{30}$$

where, U is the diagonal matrix with respective measurement variances of measuring instruments given by,

$$U = diag(\sigma_1^2,\ \sigma_2^2,\ \sigma_3^2,\ ...,\sigma_m^2) \tag{31}$$

2.3. Overall procedure of LV-LSE algorithm

The proposed sequential LV-LSE algorithm consists of five steps, which is shown in Fig. 6. It also shows the location of the smart meters and the type of measurements available to the LV-LSE algorithm for a selected Monte-Carlo simulation.

STEP: 1 Collect smart meter data and assign pseudo values for unknown measurements: An LVDG network having single-phase PV plants and single-phase households were considered for this study. As mentioned previously, it was assumed that all the PV plants and about 60% of single-phase customers are connected to the LVDG through smart meters. The location, phase, and availability of smart meters of single-phase customers and PV plants are shown in Fig. 6 and summarized in Table 1. In addition to the smart meters, three-phase power meters were distributed among the LVDG as shown in Fig. 6 (denoted by the triangles).

For the unknown single-phase loads, load pseudo values were generated by utilizing available active and reactive power measurements collected from households, PV-plants, and three-phase power meters. As shown in Fig. 6, the considered LVDG network was divided into eleven regions (denoted by R_r where $r = 1, \cdots, 11$) for the generation of load pseudo values. The net power consumption ($P_{R_r,m}^{Net}$) in a particular region-(R_r) for phase-$m \in a, b, c$ was calculated from three-phase power meter measurements by applying the power balance equation (i.e. $P_{R_r,m}^{Net}$ = Power coming into the R_r - Power going out from the R_r - Power loss in R_r). Then, the load pseudo values for unknown loads in the region-R_r were randomly generated subjected to the constraints,

Table 1
Detailed description of single-phase loads and PV panels connected to the LVDG network, and the availability of smart meters at the connection points.

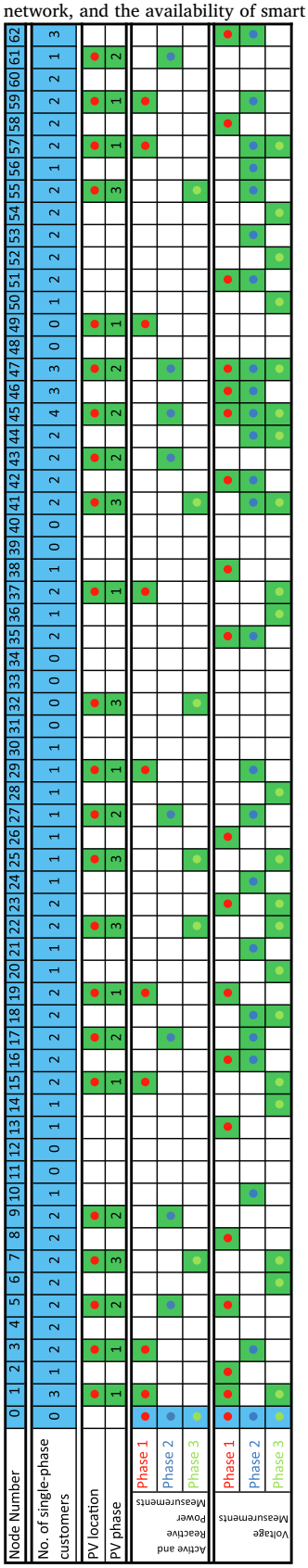

$$\sum_{\forall i \in R_r} P_{m,i}^{pseudo} = P_{R_r,m}^{Net} + \sum_{\forall j \in R_r} P_{m,j}^{pv} - \sum_{\forall k \in R_r} P_{m,k}^{load} \tag{32}$$

and,

$$P_{min}^{load} \leqslant P_{m,i}^{pseudo} \leqslant P_{max}^{load} \tag{33}$$

where, $\sum_{\forall i \in R_r} P_{m,i}^{pseudo}$ is the sum of load pseudo values of phase-m in region-R_r, $P_{R_r,m}^{Net}$ is the net power consumption of phase-m in region-R_r, $\sum_{\forall j \in R_r} P_{m,j}^{pv}$ is the total power generated by the PV plants connected to phase-m in the region-R_r, $\sum_{\forall k \in R_r} P_{m,k}^{load}$ is the total power consumption of households with a smart meters connected to phase-m in the region-R_r and, P_{max}^{load} and P_{min}^{load} are the maximum and minimum active power consumption values of a household, respectively. The maximum and minimum possible values of single-phase loads were obtained from prior knowledge about the LVDG. In addition, the power factor values of single-phase households for the considered network are generally around 0.90. Hence, the power factor values of known loads were randomly generated between 0.85 and 0.95.

STEP: 2 ***Backward step: Computation of complex power flows through the phase conductors:*** Once the active and reactive power values of each household and PV plant were known, the complex power flow (S_m^{AB}) through each branch was computed in the backward direction starting from the last branch and proceeding backwards towards the root node at each step (see the direction of blue arrows in Fig. 7).

STEP: 3 ***Forward step: Estimation of voltage states of phase conductors:*** In this step, the voltage states of all the nodes were evaluated in sequential manner starting from the secondary side of the MV-LV transformer and then proceeding towards the end of network at each step (see the direction of red arrows in Fig. 7). The sequential nature of the SE algorithm allows to achieve the requirement of positive measurement redundancy ($\eta > 0$) despite the low availability of smart meter data. Consider the first branch of the MV-LV transformer. Let it be the line segment AB as shown in Fig. 4. Therefore, the node-A is equivalent to the secondary side of the transformer. The active and reactive power flows through phase conductors (P_a, Q_a, P_b, Q_b, P_c, and Q_c) are available from step 2. In addition, the phase voltage magnitudes of node A ($|V_a^A|$, $|V_b^A|$, and $|V_c^A|$) are known to the SE algorithm from the measuring instrument placed at the secondary side of the transformer. The pseudo values for voltage angles for three-phases at node-A (ϕ_a^A, ϕ_b^A, and ϕ_c^A) were assumed to be 0^o, -120^o and -240^o. Thus, the measurement vector z was formulated as,

$$z = [|V_a^A|, |V_b^A|, |V_c^A|, \phi_a^A, \phi_b^A, \phi_c^A, P_a, Q_a, P_b, Q_b, P_c, Q_c]^T \tag{34}$$

by assuming, no measurements were available from node-B. If any measurement is taken from the node-B, it should be included in (34) to enrich the accuracy and the measurement redundancy (η) of LV-LSE algorithm. Then, the state vector ($x = [|V_a^A|, \phi_a^A, |V_b^A|, \phi_b^A, |V_c^A|, \phi_c^A, |V_a^B|, \phi_a^B, |V_b^B|, \phi_b^B, |V_c^B|, \phi_c^B]^T$) for distribution line-AB was calculated by utilizing Eq. (30). It is important to note that Eq. (30) can always provide the optimal solution under the linearized condition when the length of the measurement vector (z) is equal to or greater than the length of the state vector (x) at any given time. To ensure the above condition, the estimated voltage states of the previous branch will be utilized as pseudo values when formulating the measurement vector for the current branch. For example, when calculating the state vector for distribution line BC, the voltage states determined in the previous step of node B ($|V_a^B|$, $|V_b^B|$, $|V_c^B|$, ϕ_a^B, ϕ_b^B, ϕ_c^B) were used as the pseudo-values for unknown voltage magnitudes and angles in this step, so

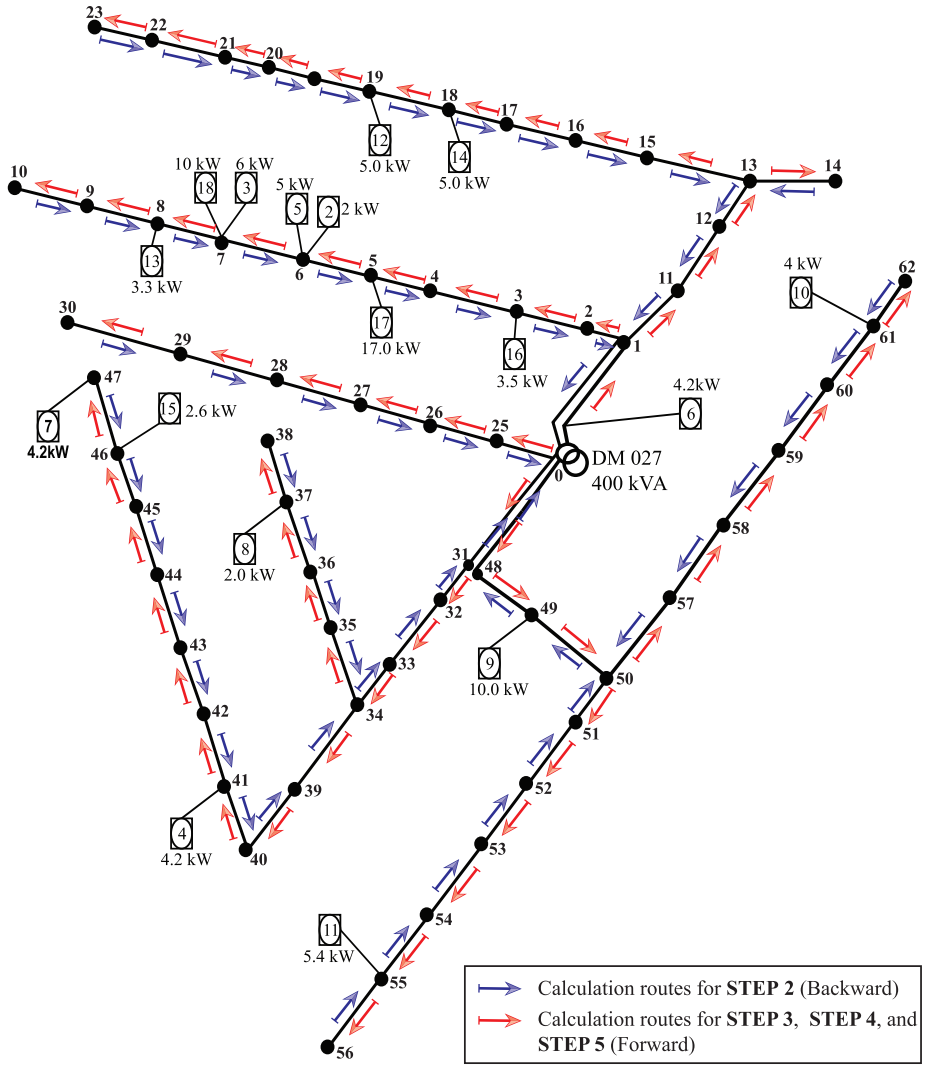

Fig. 7. Calculation routes for the proposed LV-LSE algorithm.

Table 2
Maximum measurement uncertainties of smart meters.

	Voltage		Active and Reactive Power	
	Full-Scale	Uncertainty	Full-Scale	Uncertainty
Case I	300 V	0.5%	7 kW	1.0%
Case II	300 V	0.5%	7 kW	1.5%
Case III	300 V	1.0%	7 kW	1.5%
Case IV	300 V	1.0%	7 kW	2.0%

that a positive measurement redundancy can be guaranteed. By repeating the process for each proceeding line segment in the forward direction as shown in Fig. 7 - red arrows, voltage states of all phase conductors at all nodes were evaluated.

STEP: 4 Forward step: Estimation of current through the neutral conductor: Next, the complex current flow of each branch for phase-$m \in \{a, b, c\}$ was calculated using,

$$I_m^{AB} = \left(\frac{S_m^{AB}}{V_m^A}\right)^* = \left(\frac{P_m^{AB} + jQ_m^{AB}}{V_m^A}\right)^* \tag{35}$$

where, I_m^{AB} is the current flow of phase-m from node-A to node-B, $S_m^{AB} = P_m^{AB} + jQ_m^{AB}$ is the complex power flow of phase-m from node-A to node-B and V_m^A is the phase voltage at node A for phase m. Then, the neutral current flow from node-A to node-B (I_n^{AB}) was calculated by the relationship,

$$I_n^{AB} = -\sum_{\ell=a,b,c} I_\ell^{AB} \tag{36}$$

STEP: 5 Forward step: Estimation of voltage states of the neutral conductor

In most of the LVDGs, the neutral connection is firmly grounded on the secondary side of the MV-LV transformer. Therefore, the potential of the neutral conductor is approximately zero on the secondary side of the MV-LV transformer. Thus the voltage states of the neutral conductor was determined for each node using the relation given by,

$$V_n^B = V_n^A - \sum_{\ell=a,b,c,n} z_{n\ell} \cdot I_\ell^{AB} \tag{37}$$

For optimum performance, it is important to follow the calculation routes defined in Fig. 7 and the steps described above.

2.4. Application of proposed LV-LSE algorithm for three-phase three-wire systems

The proposed analysis on the assumption that, the neutral conductor

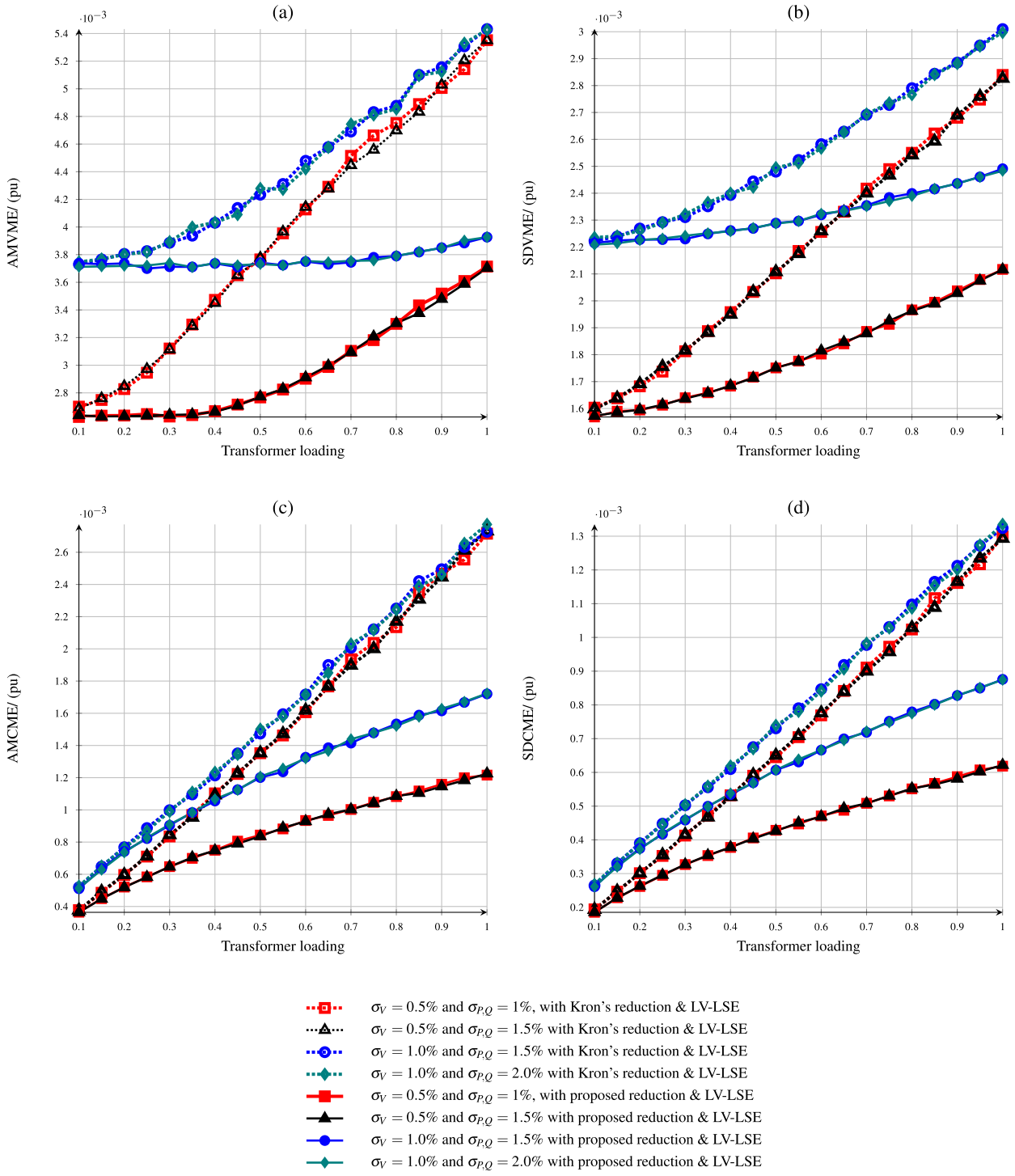

Fig. 8. Performance of LV-LSE algorithm with Kron's reduction - Y^{abc} (represented by dotted lines and unfilled markers) and with proposed reduction - $\overline{Y}^{abc}$ (represented by solid lines and filled markers) for different measurement uncertainties of smart meters (for the four cases given in Table 2) with transformer loading (a) AMVME (pu) (b) SDVME (pu) (c) AMCME (pu) and (d) SDCME (pu).

and its associated state variables are present in all distribution lines. However, the proposed LV-LSE algorithm can be easily adapted for the state estimation of three-wire systems with a simple modification.

Three-wire distribution lines can be represented using 3×3 admittance matrices considering self-impedances of phases a, b, and c as the diagonal elements and the mutual coupling among them as off-diagonal elements. Following this model, the admittance matrix ($Y^{abc}_{3-ph,3-wire}$) of a three-wire distribution line was written as,

$$Y^{abc}_{3-ph,3-wire} = \begin{bmatrix} y_{aa} & y_{ab} & y_{ac} \\ y_{ba} & y_{bb} & y_{bc} \\ y_{ca} & y_{cb} & y_{cc} \end{bmatrix} \tag{38}$$

where the symbols have the same meanings as defined previously. Since there is no neutral coupling effect on phase conductors, these admittance values can be directly utilized in the LV-LSE algorithm without any further modification. Also, STEP 5 in the LV-LSE algorithm described in Section 2.3 can be discarded as there were no neutral voltage

Table 3
Comparison of performance metrics of the proposed LV-LSE algorithm with Kron's reduction and proposed reduction under different voltage, active and reactive power measurement uncertainties of smart meters (refer Table 2) for *full transformer loading condition.*

Case No.	Error Metric	Error of LV-LSE algorithm with		Percentage reductionof error
		Kron's reduction - Y^{abc}	Proposed reduction - $\overline{Y}^{abc}$	
Case I	AMVME (pu)	5.35×10^{-3}	3.71×10^{-3}	30.60%
	SDVME (pu)	2.84×10^{-3}	2.12×10^{-3}	25.45%
	AMCME (pu)	2.72×10^{-3}	1.22×10^{-3}	55.21%
	SDCME (pu)	1.30×10^{-3}	0.62×10^{-3}	52.40%
Case II	AMVME (pu)	5.35×10^{-3}	3.70×10^{-3}	30.78%
	SDVME (pu)	2.83×10^{-3}	2.12×10^{-3}	25.12%
	AMCME (pu)	2.73×10^{-3}	1.23×10^{-3}	55.13%
	SDCME (pu)	1.29×10^{-3}	0.62×10^{-3}	51.92%
Case III	AMVME (pu)	5.43×10^{-3}	3.93×10^{-3}	27.71%
	SDVME (pu)	3.01×10^{-3}	2.49×10^{-3}	17.24%
	AMCME (pu)	2.73×10^{-3}	1.72×10^{-3}	36.90%
	SDCME (pu)	1.32×10^{-3}	0.88×10^{-3}	33.85%
Case IV	AMVME (pu)	5.43×10^{-3}	3.93×10^{-3}	27.63%
	SDVME (pu)	3.00×10^{-3}	2.48×10^{-3}	17.15%
	AMCME (pu)	2.77×10^{-3}	1.72×10^{-3}	37.87%
	SDCME (pu)	1.33×10^{-3}	0.87×10^{-3}	34.61%

states to be estimated in the three-wire system.

2.5. Ground truth generation and performance metrics

2.5.1. Ground truth generation

A Monte Carlo based simulation scheme for the proposed LV-LSE was implemented on the Matlab-OpenDSS hybrid environment. Under the Monte Carlo implementation, load power values, load power factor values, capacities of PV plants and the location of smart meters were randomly assigned for each simulation run. Next, a load flow analysis was performed on the LV network shown in Fig. 1, and the corresponding voltage and current values (magnitudes and angles) were used as the ground truth for the SE algorithm.

2.5.2. Performance metrics

The following performance metrics were used to analyze the performance of the proposed LV-LSE algorithm.

1. Average Maximum Voltage Magnitude Error - AMVME (pu)

$$AMVME = ||\Delta V||_{\infty}^{avg} = \frac{1}{MC}\sum_{i=1}^{MC}\max_{1\leqslant j\leqslant N_{|V|}}\left|\widehat{V}_j^i - V_j^i\right| \text{ pu} \tag{39}$$

2. Standard Deviation of Voltage Magnitude Error - SDVME (pu)

$$SDVME = \left\|\Delta V\right\|_2^{avg} = \frac{1}{MC}\sum_{i=1}^{MC}\frac{\sqrt{\sum_{j=1}^{N_{|V|}}\left\|\widehat{V}_j^i - V_j^i\right\|^2}}{\sqrt{N_{|V|}}} \text{ pu} \tag{40}$$

3. Average Maximum Current Magnitude Error - AMCME (pu)

$$AMCME = \left\|\Delta I\right\|_{\infty}^{avg} = \frac{1}{MC}\sum_{i=1}^{MC}\max_{1\leqslant j\leqslant N_{|I|}}\left|\widehat{I}_j^i - I_j^i\right| \text{ pu} \tag{41}$$

4. Standard Deviation of Current Magnitude Error - SDCME (pu)

$$SDCME = \left\|\Delta I\right\|_2^{avg} = \frac{1}{MC}\sum_{i=1}^{MC}\frac{\sqrt{\sum_{j=1}^{N_{|I|}}\left\|\widehat{I}_j^i - I_j^i\right\|^2}}{\sqrt{N_{|I|}}} \text{ pu} \tag{42}$$

where, MC is the number of Monte Carlo simulation performed for each case (MC = 500), $N_{|V|}$ is the total number of voltage states in the network ($N_{|V|}$= 63 nodes × 4 [voltage states/node] = 252 voltage states), $\widehat{V}_j^i$ is the estimated voltage magnitude (pu) of j-th state variable at the i-th Monte Carlo simulation, V_j^i is the true voltage magnitude of the j-th state variable at the i-th Monte Carlo simulation (obtained from the load flow analysis), $\widehat{I}_j^i$ is the estimated current magnitude (pu) of j-th branch current at the i-th Monte Carlo simulation, I_j^i is the true current magnitude (pu) of the j-th branch current at the i-th Monte Carlo simulation (obtained from the load flow analysis), and $N_{|I|}$ is the total number of branch currents (including the neutral current flows) in the network ($N_{|I|}$ = 62 feeder sections × 4 [current states/feeder section] = 248 current states).

3. Results and discussion

The network shown in Fig. 1 was used to implement the proposed LV-LSE algorithm. The network consists of 92 households and 19 rooftop PV plants, with a total installed PV capacity of approximately 60 kW. The capacity of loads and rooftop PV plants for each simulation were randomly assigned. For the simulations, about 60% of households and all the rooftop PV plants were assumed to be connected to the LVDG through smart meters. In addition, there is a measuring device at the secondary side of the MV-LV transformer to measure aggregated power flows into the LVDG and node voltages. For this network, it was assumed that P_{min}^{load} = 0.2 kW and P_{max}^{load} = 7 kW.

The performance of the proposed LV-LSE algorithm was analyzed under three scenarios: (A) for different measurement uncertainties of smart meters (B) for different scales of the original network and (C) for different data loss conditions of smart meter data.

3.1. Performance under different measurement uncertainties of smart meters

Smart meters with various precision levels are currently available in the market to measure voltage, current, active and reactive power flows. High-performance smart meters measure these voltages, currents, and power levels with great accuracy and do not require advanced SE algorithms to determine the true states of the network. However, high-accuracy smart meters are expensive and are not economical for large-scale deployment. In contrast, low-accuracy smart meters are cheaper to use in LVDGs, however they add some uncertainty to the original measurement. This allows more burden on SE algorithms to accurately estimate the actual states of the network. In this case study, the influence of smart meter measurement uncertainty on the accuracy of the proposed LV-LSE algorithm was explored. The measured voltage magnitudes, active and reactive power values (z_{meas}) for the LV-LSE algorithm were calculated using,

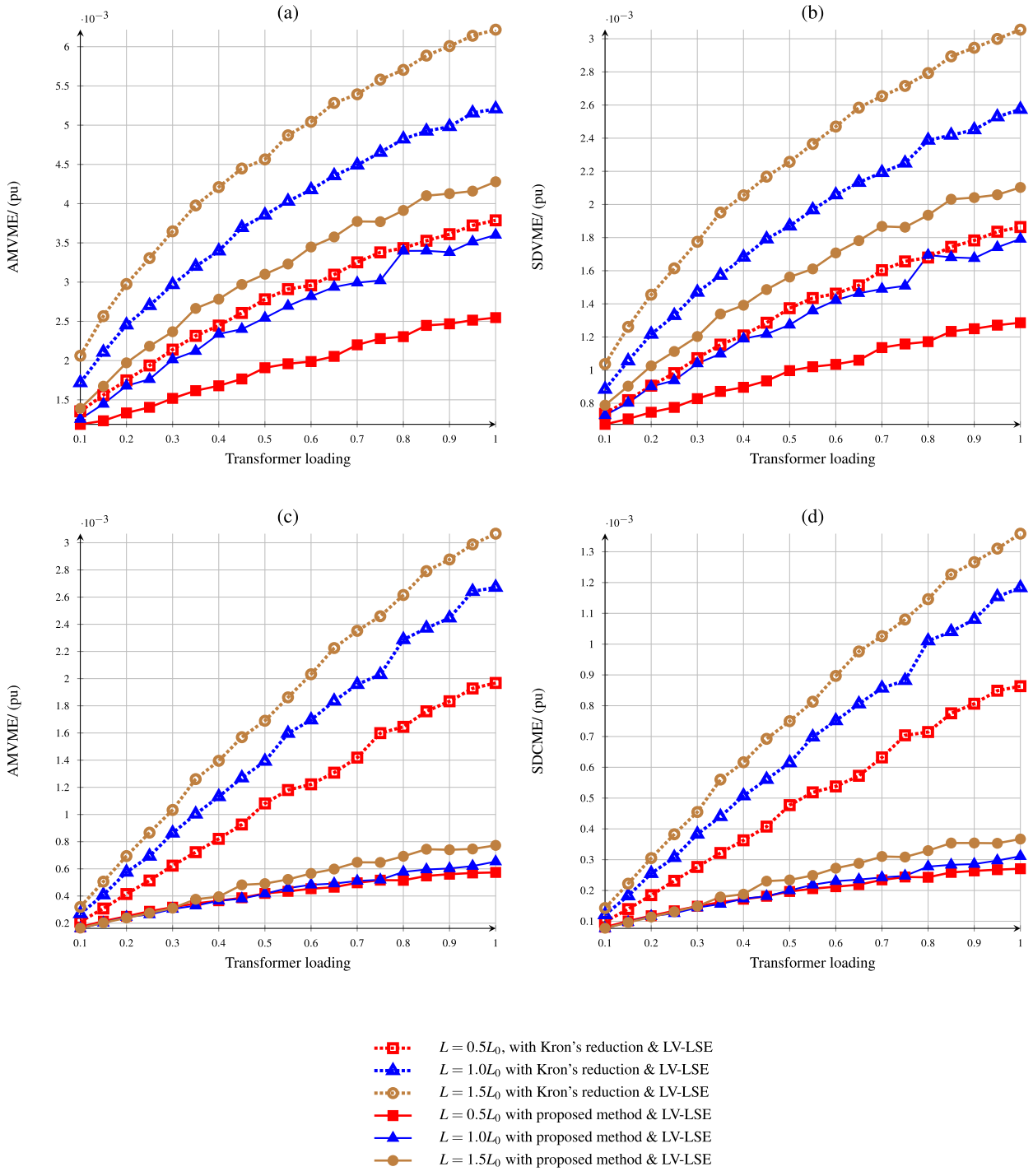

Fig. 9. Performance of LV-LSE algorithm with Kron's reduction - Y^{abc} (represented by dotted lines and unfilled markers) and with proposed reduction - $\overline{Y}^{abc}$ (represented by solid lines and filled markers) for different scales of the original network ($L = 0.5 \times L_0$, $L = 1.0 \times L_0$, and $L = 1.5 \times L_0$) with transformer loading. (a) AMVME (b) SDVME (c) AMCME (d) SDCME.

$$z_{meas} = z_{true} + FS{\cdot}N(0, \sigma_{P,Q,|V|}) \tag{43}$$

where, z_{true} is the true value of the measurement which was obtained from the load-flow analysis, FS is the full-scale meter reading related to each type of measurement, and $\sigma_{P,Q,|V|}$ is the standard measurement uncertainty related to the each type of measurement, which was determined from dividing the maximum measurement error values given in Table 2 by 1.96 to ensure 95% of confidence level, and $N(0, \sigma_{P,Q,|V|})$ is the normally distributed random variable with zero mean and $\sigma^2_{P,Q,|V|}$ variance.

The performance of the proposed LV-LSE algorithm was analyzed for both Kron's reduction and the proposed reduction method under different measurement uncertainties of smart meters (as listed in Table 2) with transformer loading from 10% to 100% as shown in

Table 4
Comparison of performance metrics of the proposed LV-LSE algorithm with Kron's reduction and proposed reduction under different scales of line lengths of the network ($L = 0.5 \times L_0$, $L = 1.0 \times L_0$ and $L = 1.5 \times L_0$) shown in Fig. 1 for *full transformer loading condition*

Case	Error Metric	Error of LV-LSE algorithm with		Percentage reductionof error
		Kron's reduction - Y^{abc}	Proposed reduction - $\overline{Y}^{abc}$	
$L = 0.5 \times L_0$	AMVME (pu)	3.79×10^{-3}	2.55×10^{-3}	32.73%
	SDVME (pu)	1.86×10^{-3}	1.29×10^{-3}	30.99%
	AMCME (pu)	1.97×10^{-3}	0.57×10^{-3}	77.66%
	SDCME (pu)	0.86×10^{-3}	0.27×10^{-3}	68.66%
$L = 1.0 \times L_0$	AMVME (pu)	5.21×10^{-3}	3.60×10^{-3}	30.85%
	SDVME (pu)	2.57×10^{-3}	1.79×10^{-3}	30.28%
	AMCME (pu)	2.67×10^{-3}	0.65×10^{-3}	75.56%
	SDCME (pu)	1.18×10^{-3}	0.31×10^{-3}	73.71%
$L = 1.5 \times L_0$	AMVME (pu)	6.22×10^{-3}	4.28×10^{-3}	31.17%
	SDVME (pu)	3.05×10^{-3}	2.10×10^{-3}	31.16%
	AMCME (pu)	3.07×10^{-3}	0.77×10^{-3}	74.80%
	SDCME (pu)	1.36×10^{-3}	0.37×10^{-3}	72.98%

Fig. 8. For each of the cases, the performance metrics given in Section 2.5.2 were calculated by performing Monte Carlo simulations.

From the results shown in Fig. 8, the proposed LV-LSE algorithm with the proposed reduction method outperforms the proposed LV-LSE algorithm with Kron's reduction for all of the uncertainty cases. For example, let us consider the case I where voltage uncertainty of 0.5% and active and reactive power uncertainty of 1.0%. The variation of the performance metrics of the LV-LSE algorithm with Kron's reduction and proposed reduction method against the transformer loading is shown using dotted red lines with unfilled markers and continuous red lines with filled markers, respectively. As can be noted from Fig. 8 - (a), (b), (c) and (d), all the error metrics (AMVME, SDVME, AMCME, and SDCME) gradually increase with transformer loading; however the error values of the proposed LV-LSE algorithm with the proposed reduction method is always considerably small as compared to LV-LSE algorithm with Kron's reduction.

It can also be observed that, the accuracy of the SE algorithm is more sensitive to the uncertainties in voltage measurements than to uncertainties in active and reactive power measurements. This phenomenon can be distinguished by comparing the variation of the error metrics for the cases I and II with cases III and IV. In cases I (Fig. 8 - red lines) and II (Fig. 8 - black lines), when only the uncertainty of active and reactive power measurements are different; however, the variation of the error metrics almost coincide with each other throughout all the transformer loading conditions. In contrast, when considering cases II (Fig. 8 - black lines) and III (Fig. 8- blue lines), when only the uncertainty of voltage measurements is different (voltage uncertainty of case III is higher than the voltage uncertainty of case II), leading to a significant increase in error metrics in case III compared to case II.

A comparison of the error metrics (AMVME, SDVME, AMCME, and SDCME) under full transformer loading conditions for each of the uncertainty cases are listed in Table 3 for LV-LSE algorithm with proposed reduction and LV-LSE algorithm with Kron's reduction.

3.2. Performance under different line lengths

In this case study, the performance metrics of the proposed LV-LSE algorithm were analyzed for different scales of line lengths of the original LVDG shown in Fig. 1, assuming all smart meters have voltage uncertainty of 0.5% and power uncertainty of 1% (case I in the previous case study).

In general, most LVDGs have a total length of about 2 km. The total length of the network shown in Fig. 1 is about 1.3 km. Therefore, there is a possibility of expanding the original network by a factor of 2 km/1.3 km = 1.5 in maximum. Thus, the performance metrics for LV-LSE were calculated for two different scales of original line lengths (i.e., 0.5 and 1.5) for Kron's reduction and proposed reduction methods, as shown in Fig. 9. The results shown in Fig. 9 revealed that the performance metrics are sensitive to the variation of line length of the network.

From the results shown in Fig. 9, the proposed LV-LSE algorithm with the proposed reduction method performs better as compared to the proposed LV-LSE algorithm with Kron's reduction for all of the uncertainty cases. Besides, as we observed in the previous case study, the use of the proposed reduction method in the LV-LSE algorithm (represented by continuous lines with filled markers) resulted in the degradation of all error metrics as compared to the use of Kron's reduction (represented by dotted lines with unfilled markers). In order to highlight this observation, a comparison of the error metrics (AMVME, SDVME, AMCME, and SDCME) under full transformer loading conditions for different scales of the original network is listed in Table 4 for LV-LSE algorithm with proposed reduction and LV-LSE algorithm with Kron's reduction.

3.3. Performance under different data loss conditions

As discussed earlier, it was assumed that about 60% of households in the network shown in Fig. 1 are equipped with smart meters. Moreover, pseudo values for unknown measurements were assigned as give by the Eq. (32) and (33) to obtain a positive measurement redundancy.

Various communication technologies have been developed to transmit smart meter data to EMS (or DSOs). The most common technique is to use the Wide Area Network (WAN). However, not all of these communication techniques are 100% reliable and are subject to data loss. Therefore, this section analyzed and presented the performance of LV-LSE under data loss conditions.

It is essential to mention the underlying meaning behind the communication/transmission data loss. For example, "5% data loss" implies that 5% of the voltage, active, and reactive power measurements, which are previously known to the SE algorithm (from the installed smart meters), are now unknown due to losses in the communication network. Therefore, for the vacated measurements, pseudo values were assigned in the same manner as described in Section 2.3.

Fig. 10 depicts the variation of error metrics with transformer loading for different data loss conditions from 0% to 25% in steps of 5% for the LV-LSE algorithm with Kron's reduction and with the proposed reduction. According to the figures, voltage and current magnitude errors of the LV-LSE algorithm gradually increase with the data loss, as expected. Also, it is clear that the values of error metrics are considerably low for the LV-LSE algorithm with the proposed reduction method (illustrated in continuous lines filled markers in Fig. 10) as compared to the LV-LSE with Kron's reduction (illustrated in dotted lines an unfilled markers in Fig. 10). Moreover, the comparison of error metrics under the full transformer loading condition for the LV-LSE algorithm with Kron's reduction and LV-LSE algorithm with the proposed reduction method is given in Table 5.

3.4. Computational performance of the LV-LSE algorithm

The proposed LV-LSE algorithm was written on Matlab® (version: R2016a) - Open DSS (version: 8.4.1.1) hybrid environment. When this algorithm was executed on a processor with Intel Core i7-7700HQ with

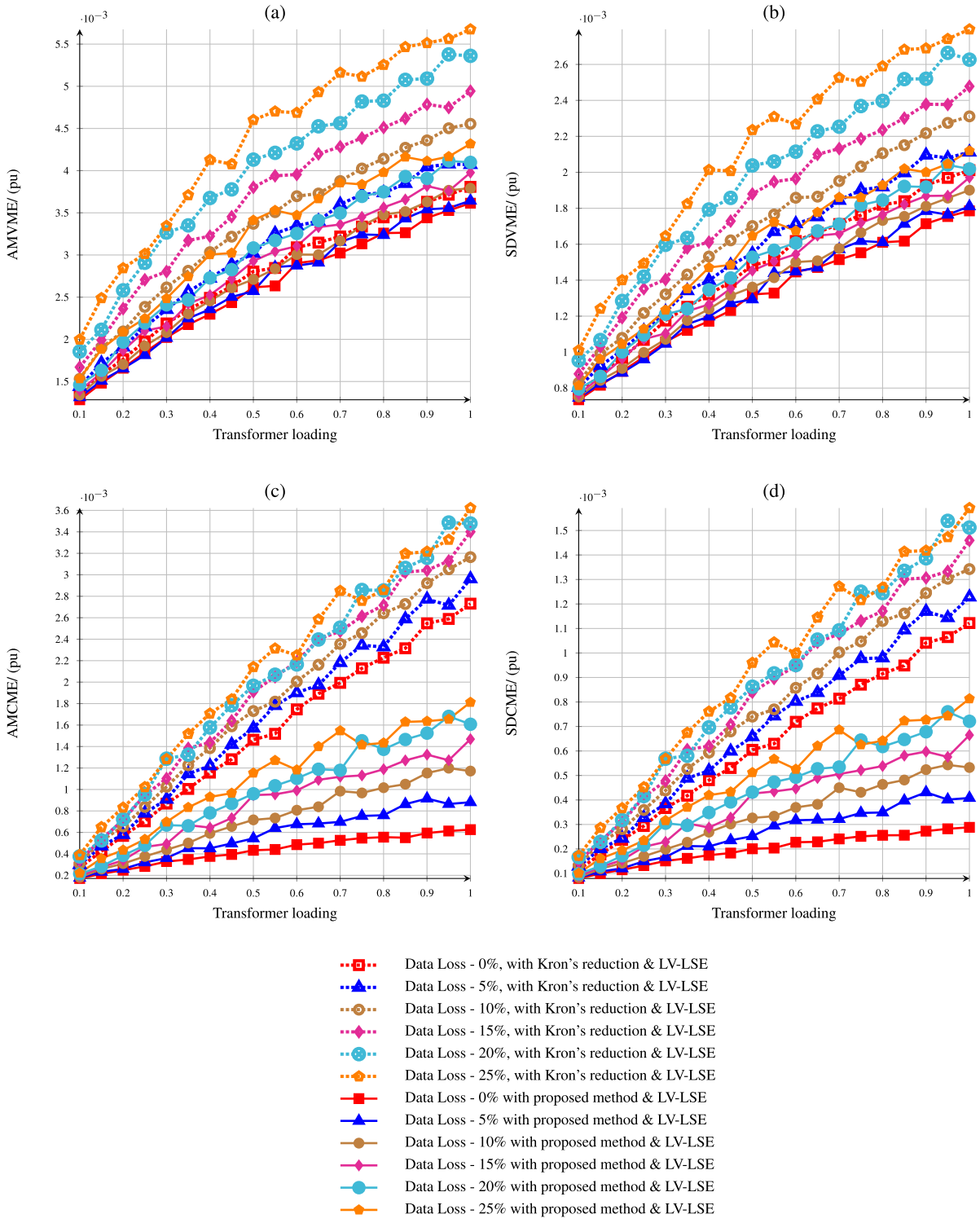

Fig. 10. Performance of LV-LSE algorithm with Kron's reduction - Y^{abc} (represented by dotted lines and unfilled markers) and with proposed method - $\overline{Y}^{abc}$ (represented by solid lines and filled markers) under different data loss conditions (0 %, 5 %, 10%, 15%, 20%, and 25%) with transformer loading. (a) AMVME (b) SDVME (c) AMCME (d) SDCME.

32 GB RAM running at 2.8 GHz, the average value of time to process the LV-LSE was 0.0928 s. When implemented on a regular low-cost processor unit with Intel Core i5-8250U and an 8 GB RAM running at 2.53 GHz, the average execution time was 0.1022 s. Moreover, the number of Floating-Point Operations (FLOPS) of the proposed LV-LSE algorithm was calculated to be 16368, using a Matlab® program developed by Hang Qian [45]. The average execution time of the iterative WLS SE was recorded as 1.0340 s (on the processor with Intel Core i7-7700HQ) which exceeds the average execution time of the proposed LV-LSE algorithm (0.0928 s). Hence, the proposed LV-LSE algorithm is computationally efficient when compared to the iterative WLS SE algorithm.

Table 5
Comparison of performance metrics of the proposed LV-LSE algorithm with Kron's reduction and proposed reduction under different data loss conditions of the network (0%, 5%, 10%, 15%, 20%, and 25%) shown in Fig. 1 for *full transformer loading condition*

Percentage DataLoss	Error Metric	Error of LV-LSE algorithm with		Percentage reduction of error
		Kron's reduction	Proposed reduction	
0%	AMVME (pu)	3.81×10^{-3}	3.61×10^{-3}	05.09%
	SDVME (pu)	2.01×10^{-3}	1.79×10^{-3}	11.24%
	AMCME (pu)	2.73×10^{-3}	0.63×10^{-3}	77.08%
	SDCME (pu)	1.12×10^{-3}	0.29×10^{-3}	74.31%
5%	AMVME (pu)	4.07×10^{-3}	3.64×10^{-3}	10.49%
	SDVME (pu)	2.11×10^{-3}	1.81×10^{-3}	14.27%
	AMCME (pu)	2.96×10^{-3}	0.88×10^{-3}	70.25%
	SDCME (pu)	1.23×10^{-3}	0.41×10^{-3}	66.76%
10%	AMVME (pu)	4.55×10^{-3}	3.79×10^{-3}	16.75%
	SDVME (pu)	2.31×10^{-3}	1.90×10^{-3}	11.75%
	AMCME (pu)	3.16×10^{-3}	1.17×10^{-3}	62.97%
	SDCME (pu)	1.34×10^{-3}	0.53×10^{-3}	60.33%
15%	AMVME (pu)	4.94×10^{-3}	3.98×10^{-3}	19.54%
	SDVME (pu)	2.48×10^{-3}	1.97×10^{-3}	20.45%
	AMCME (pu)	3.40×10^{-3}	1.47×10^{-3}	56.81%
	SDCME (pu)	1.46×10^{-3}	0.66×10^{-3}	54.45%
20%	AMVME (pu)	5.36×10^{-3}	4.10×10^{-3}	23.56%
	SDVME (pu)	2.63×10^{-3}	2.02×10^{-3}	23.14%
	AMCME (pu)	3.48×10^{-3}	1.61×10^{-3}	53.78%
	SDCME (pu)	1.51×10^{-3}	0.72×10^{-3}	52.30%
25%	AMVME (pu)	5.68×10^{-3}	4.32×10^{-3}	23.91%
	SDVME (pu)	2.80×10^{-3}	2.12×10^{-3}	24.17%
	AMCME (pu)	3.48×10^{-3}	1.81×10^{-3}	49.96%
	SDCME (pu)	1.59×10^{-3}	0.81×10^{-3}	48.90%

4. Conclusion

This work outlines a complete state estimation algorithm, developed to estimate and monitor the overall states of the low voltage distribution network under high PV penetration. The proposed algorithm performs accurately, even under severely unbalanced conditions. The proposed LV-LSE algorithm has been simulated on a typical unbalanced residential network that consists of 92 single-phase and three-phase loads, and 19 rooftop PV plants.

The proposed LV-LSE algorithm uses a novel method for simplifying the 4×4 admittance matrix of the three-phase four-wire feeder line into a 3×3 admittance matrix, while incorporating the effect of the neutral states on phase conductor states. The LV-LSE algorithm developed based on this simplified feeder model and the Taylor series approximations of active and reactive power functions, was able to provide accurate and fast results even under low availability of smart meter data on the network.

Above all, the proposed LV-LSE algorithm has been validated on an OpenDSS-Matlab hybrid simulation environment for three different practical scenarios, namely for different measurement uncertainties of smart meters, different scales of feeder lengths and different measurement data loss conditions. Results of these case studies reveal that the proposed state estimation algorithm has been able to estimate voltage states with the average maximum voltage error of 4.48×10^{-3} pu and average voltage error of about 2.54×10^{-3} pu, under 1% measurement uncertainty for voltage measurements and 0.5% measurement uncertainty for power measurements at 100% transformer loading and 60% availability of smart meters. As the average value of time to process the LV-LSE is approximately 0.1 s, a commonly available smart meter with accuracy type 1% and sampling rate 1 s is adequate to implement the proposed LV-LSE.

Moreover, it has been observed that the accuracy of the state estimation algorithm can be improved by increasing the number of measuring nodes in the distribution system's infrastructure. The estimation of the optimum number of instruments required and optimal placement of measuring nodes will be explored as future work.

Declaration of Competing Interest

The authors declare that they have no known competing financial interests or personal relationships that could have appeared to influence the work reported in this paper.

Acknowledgment

We would like to acknowledge the financial support provided by the National Science Foundation (NSF), Sri Lanka (Research Grant No: RG/2018/EA & ICT/01).

Appendix A. Details of the residential network

Details of the residential network used for the analysis is given in Table A.6.

Table A.6
Details of the LVDG network shown in Fig. 1

Property	Description
Distribution transformer specifications	11 kV/415 V, 400 kVA
Distribution transformer vector group	Dy11
Transformer earthing type	Solid-earthed neutral
No. of distribution feeders	4
Number of customers	94 (single phase)
Number of rooftop PV systems	18 (single phase)
Total installed PV capacity	93.4 kW
Total length of the network	1.3 km
Medium of electricity distribution	Overhead cable, type ABC-70

Appendix B. Technical information of the overhead line in the residential network

The technical information of the overhead cables used in the LVDG network is given in Table B.7.

Table B.7
Technical information of the overhead line (ABC-70) used in LVDG network shown in Fig. 1

Property	Value/ (units)
Nominal area of the phase conductors	70 mm^2
Nominal area of the neutral conductor 1	54.6 mm^2
Insulation material	XLPE
Conductor shape	Circular
DC resistance of phase conductors	0.443 Ω/km
DC resistance of neutral conductor	0.630 Ω/km
Insulation thickness of phase conductors	1.8 mm
Insulation thickness of neutral conductor	1.6 mm

Appendix C. Derivation of non-linear active (P_m^{AB}) and reactive power (Q_m^{AB}) flow functions

$$S_m^{AB} = |V_m^A| \angle\psi_m^A \left(\sum_{\ell=a,b,c} [(\bar{g}_{m\ell} + j\bar{b}_{m\ell})(|V_\ell^A| \angle\psi_\ell^A - |V_\ell^B| \angle\psi_\ell^B)] \right)^* \tag{C.1}$$

$$S_m^{AB} = |V_m^A| \angle\psi_m^A \sum_{\ell=a,b,c} [\bar{g}_{m\ell} |V_\ell^A| \angle\psi_\ell^A - \bar{g}_{m\ell} |V_\ell^B| \angle\psi_\ell^B + j\bar{b}_{m\ell} |V_\ell^A| \angle\psi_\ell^A - j\bar{b}_{m\ell} |V_\ell^B| \angle\psi_\ell^B]^* \tag{C.2}$$

$$S_m^{AB} = |V_m^A| \angle\psi_m^A \sum_{\ell=a,b,c} [\bar{g}_{m\ell} |V_\ell^A| \angle -\psi_\ell^A - \bar{g}_{m\ell} |V_\ell^B| \angle -\psi_\ell^B - j\bar{b}_{m\ell} |V_\ell^A| \angle -\psi_\ell^B + j\bar{b}_{m\ell} |V_\ell^B| \angle -\psi_\ell^B] \tag{C.3}$$

Using the notations given in (21), the above equation was simplified as,

$$S_m^{AB} = |V_m^A| \sum_{\ell=a,b,c} [\bar{g}_{m\ell} |V_\ell^A| \angle\Delta\psi_{ml}^{AA} - \bar{g}_{m\ell} |V_\ell^B| \angle\Delta\psi_{ml}^{AB} - j\bar{b}_{m\ell} |V_\ell^A| \angle\Delta\psi_{ml}^{AA} + j\bar{b}_{m\ell} |V_\ell^B| \angle\Delta\psi_{ml}^{AB}] \tag{C.4}$$

Let us separate the above equation to it's real and imaginary components as,

$$\begin{aligned} S_m^{AB} &= |V_m^A| \sum_{\ell=a,b,c} \{|V_\ell^A|[\bar{g}_{m\ell}\cdot\cos_{m\ell}^{AA} + \bar{b}_{m\ell}\cdot\sin_{m\ell}^{AA}] - |V_\ell^B|[\bar{g}_{m\ell}\cdot\cos_{m\ell}^{AB} + \bar{b}_{m\ell}\cdot\sin_{m\ell}^{AB}]\} \\ &+ j\ |V_m^A| \sum_{\ell=a,b,c} \{|V_\ell^A|[\bar{g}_{m\ell}\cdot\sin_{m\ell}^{AA} - \bar{b}_{m\ell}\cdot\cos_{m\ell}^{AA}] - |V_\ell^B|[\bar{g}_{m\ell}\cdot\sin_{m\ell}^{AB} + \bar{b}_{m\ell}\cdot\cos_{m\ell}^{AB}]\} \end{aligned} \tag{C.5}$$

The real part of (C.5) gives the active power flow through phase-$m \in \{a, b, c, \}$ between busbars A and B (P_m^{AB}) as,

$$P_m^{AB} = |V_m^A| \sum_{\ell=a,b,c} \{|V_\ell^A|[\bar{g}_{m\ell}\cdot\cos_{m\ell}^{AA} + \bar{b}_{m\ell}\cdot\sin_{m\ell}^{AA}] - |V_\ell^B|[\bar{g}_{m\ell}\cdot\cos_{m\ell}^{AB} + \bar{b}_{m\ell}\cdot\sin_{m\ell}^{AB}]\} \tag{C.6}$$

The imaginary part of (C.5) gives the reactive power flow through phase-$m \in \{a, b, c, \}$ between bus-bars A and B (Q_m^{AB}) as,

$$Q_m^{AB} = |V_m^A| \sum_{\ell=a,b,c} \{|V_\ell^A|[\bar{g}_{m\ell}\cdot\sin_{m\ell}^{AA} - \bar{b}_{m\ell}\cdot\cos_{m\ell}^{AA}] - |V_\ell^B|[\bar{g}_{m\ell}\cdot\sin_{m\ell}^{AB} + \bar{b}_{m\ell}\cdot\cos_{m\ell}^{AB}]\} \tag{C.7}$$

Appendix D. Derivation of linearized active ($\overline{P}_m^{AB}$) and reactive power ($\overline{Q}_m^{AB}$) flow functions

Let us consider the non-linear active power function ($\overline{P}_m^{AB}$) for phase-m$\in \{a, b, c\}$ given by,

$$P_m^{AB} = |V_m^A| \sum_{\ell=a,b,c} \{|V_\ell^A|[\bar{g}_{m\ell}\cdot\cos_{m\ell}^{AA} + \bar{b}_{m\ell}\cdot\sin_{m\ell}^{AA}] - |V_\ell^B|\cdot[\bar{g}_{m\ell}\cdot\cos_{m\ell}^{AB} + \bar{b}_{m\ell}\cdot\sin_{m\ell}^{AB}]\} \tag{D.1}$$

The nonlinear $\sin(\cdot)$ and $\cos(\cdot)$ functions were substituted with their Taylor series approximations (24) as,

$$\begin{aligned} \overline{P}_m^{AB} &= |V_m^A| \sum_{\ell=a,b,c} \{|V_\ell^A|[\bar{g}_{m\ell}\cdot(\cos(\Delta\psi_{ml,r}^{AA}) - \sin(\Delta\psi_{ml,r}^{AA})\cdot\Delta\psi_{ml}^{AA}) \\ &+ \bar{b}_{m\ell}\cdot(\sin(\Delta\psi_{ml,r}^{AA}) + \cos(\Delta\psi_{ml,r}^{AA})\cdot\Delta\psi_{ml}^{AA})] \\ &- |V_\ell^B|[\bar{g}_{m\ell}\cdot(\cos(\Delta\psi_{ml,r}^{AB}) - \sin(\Delta\psi_{ml,r}^{AB})\cdot\Delta\psi_{ml}^{AB}) \\ &+ \bar{b}_{m\ell}\cdot(\sin(\Delta\psi_{ml,r}^{AB}) + \cos(\Delta\psi_{ml,r}^{AB})\cdot\Delta\psi_{ml}^{AB})]\} \end{aligned} \tag{D.2}$$

It was assumed that $\Delta\psi_{m\ell,r}^{AA} \approx \Delta\psi_{m\ell,r}^{AB}$ because the distance between two adjacent basbars in LVDGs are very small as compared to MVDGs (see Fig. 1). With this assumption, above equation was rewritten as,

$$\begin{aligned}\overline{P}_m^{AB} &= |V_m^A| \sum_{\ell=a,b,c} \{|V_\ell^A|[\bar{g}_{m\ell}\cdot(\cos(\Delta\psi_{ml,r}^{AB}) - \sin(\Delta\psi_{ml,r}^{AB})\cdot\Delta\psi_{ml}^{AA}) \\ &+ \bar{b}_{m\ell}\cdot(\sin(\Delta\psi_{ml,r}^{AB}) + \cos(\Delta\psi_{ml,r}^{AB})\cdot\Delta\psi_{ml}^{AA})] \\ &- |V_\ell^B|[\bar{g}_{m\ell}\cdot(\cos(\Delta\psi_{ml,r}^{AB}) - \sin(\Delta\psi_{ml,r}^{AB})\cdot\Delta\psi_{ml}^{AB}) \\ &+ \bar{b}_{m\ell}\cdot(\sin(\Delta\psi_{ml,r}^{AB}) + \cos(\Delta\psi_{ml,r}^{AB})\cdot\Delta\psi_{ml}^{AB})]\}\end{aligned} \tag{D.3}$$

Eq. (D.3) was rearranged as,

$$\begin{aligned}\overline{P}_m^{AB} &= |V_m^A| \sum_{\ell=a,b,c} \{(\bar{g}_{m\ell}\cos(\Delta\psi_{ml,r}^{AB}) + \bar{b}_{m\ell}\sin(\Delta\psi_{ml,r}^{AB}))\cdot(|V_\ell^A| - |V_\ell^B|) \\ &+ (-\bar{g}_{m\ell}\sin(\Delta\psi_{ml,r}^{AB}) + \bar{b}_{m\ell}\cos(\Delta\psi_{ml,r}^{AB}))\cdot(|V_\ell^A|\cdot\Delta\psi_{ml}^{AA} - |V_\ell^B|\cdot\Delta\psi_{ml}^{AB})\}\end{aligned} \tag{D.4}$$

The local operating points for the voltage magnitudes were assigned (as given in (26)) to (D.4) as,

$$\begin{aligned}\overline{P}_m^{AB} &= |V_r| \sum_{\ell=a,b,c} \{(\bar{g}_{m\ell}\cos(\Delta\psi_{ml,r}^{AB}) + \bar{b}_{m\ell}\sin(\Delta\psi_{ml,r}^{AB}))\cdot(|V_\ell^A| - |V_\ell^B|) \\ &+ (-\bar{g}_{m\ell}\sin(\Delta\psi_{ml,r}^{AB}) + \bar{b}_{m\ell}\cos(\Delta\psi_{ml,r}^{AB}))\cdot(|V_r|\cdot\Delta\psi_{ml}^{AA} - |V_r|\cdot\Delta\psi_{ml}^{AB})\}\end{aligned} \tag{D.5}$$

Eq. (D.5) was simplified as,

$$\begin{aligned}\overline{P}_m^{AB} &= \sum_{\ell=a,b,c} \{|V_r|(\bar{g}_{m\ell}\cos(\Delta\psi_{ml,r}^{AB}) + \bar{b}_{m\ell}\sin(\Delta\psi_{ml,r}^{AB}))\cdot(|V_\ell^A| - |V_\ell^B|) \\ &+ |V_r|^2\cdot(-\bar{g}_{m\ell}\sin(\Delta\psi_{ml,r}^{AB}) + \bar{b}_{m\ell}\cos(\Delta\psi_{ml,r}^{AB}))\cdot(\Delta\psi_{ml}^{AA} - \Delta\psi_{ml}^{AB})\}\end{aligned} \tag{D.6}$$

As previously defined in (21), it is known that $\Delta\psi_{m\ell}^{AA} = \psi_m^A - \psi_l^A$ and $\Delta\psi_{m\ell}^{AB} = \psi_m^A - \psi_l^B$. Therefore, $\Delta\psi_{ml}^{AA} - \Delta\psi_{ml}^{AB} = -(\psi_\ell^A - \psi_\ell^B)$. By substituting this to (C.5), the linearized active power function for phase-m ($\overline{P}_m^{AB}$)was obtained as,

$$\begin{aligned}\overline{P}_m^{AB} &= \sum_{\ell=a,b,c} \{|V_r|(\bar{g}_{m\ell}\cos(\Delta\psi_{ml,r}^{AB}) + \bar{b}_{m\ell}\sin(\Delta\psi_{ml,r}^{AB}))\cdot(|V_\ell^A| - |V_\ell^B|) \\ &- |V_r|^2\cdot(-\bar{g}_{m\ell}\sin(\Delta\psi_{ml,r}^{AB}) + \bar{b}_{m\ell}\cos(\Delta\psi_{ml,r}^{AB}))\cdot(\psi_\ell^A - \psi_\ell^B)\}\end{aligned} \tag{D.7}$$

Similarly, the linearized reactive power function for phase-m ($\overline{Q}_m^{AB}$)was obtained as,

$$\begin{aligned}\overline{Q}_m^{AB} &= \sum_{\ell=a,b,c} \{|V_r|(\bar{g}_{m\ell}\sin(\Delta\psi_{ml,r}^{AB}) - \bar{b}_{m\ell}\cos(\Delta\psi_{ml,r}^{AB}))\cdot(|V_\ell^A| - |V_\ell^B|) \\ &- |V_r|^2\cdot(\bar{g}_{m\ell}\cos(\Delta\psi_{ml,r}^{AB}) + \bar{b}_{m\ell}\sin(\Delta\psi_{ml,r}^{AB}))\cdot(\psi_\ell^A - \psi_\ell^B)\}\end{aligned} \tag{D.8}$$

Appendix E. Supplementary material

Supplementary data associated with this article can be found, in the online version, at https://doi.org/10.1016/j.ijepes.2020.106332.

References

[1] Graham PW, Hayward J, Foster J, Story O, Havas L. GenCost 2018 Updated projections of electricity generation technology costs. CSIRO 2018:1–63.

[2] Almeida DW, Abeysinghe AHMSMS, Ekanayake JB. Analysis of rooftop solar impacts on distribution networks. Ceylon J Sci 2020;48(2):103–12. https://doi.org/10.4038/cjs.v48i2.7614.

[3] Almeida D, Abeysinghe S, Ekanayake MP, Godaliyadda RI, Ekanayake J, Pasupuleti J. Generalized approach to assess and characterise the impact of solar pv on lv networks. Int J Electr Power Energy Syst 2020;121:106058. https://doi.org/10.1016/j.ijepes.2020.106058. http://www.sciencedirect.com/science/article/pii/S0142061519335173.

[4] Liacco TD. The role and implementation of state estimation in an energy management system. Int J Electr Power Energy Syst 1990;12(2):75–9. https://doi.org/10.1016/0142-0615(90)90002-S.

[5] Primadianto A, Lu C-N. A review on distribution system state estimation. IEEE Trans Power Syst 2016;32(5):3875–83.

[6] Alsac O, Vempati N, Stott B, Monticelli A. Generalized state estimation. IEEE Trans Power Syst 1998;13(3):1069–75. https://doi.org/10.1109/59.709101.

[7] Li Ke. State estimation for power distribution system and measurement impacts. IEEE Trans Power Syst 1996;11(2):911–6. https://doi.org/10.1109/59.496174.

[8] Alsac O, Vempati N, Stott B, Monticelli A. Generalized state estimation. IEEE Trans Power Syst 1998;13(3):1069–75. https://doi.org/10.1109/59.709101.

[9] Bose A, Clements KA. Real-time modeling of power networks. Proc IEEE 1987;75(12):1607–22. https://doi.org/10.1109/PROC.1987.13930.

[10] Schweppe FC, Wildes J. Power system static-state estimation, part i: Exact model. IEEE Trans Power Apparatus Syst 1970;PAS-89(1):120–5. https://doi.org/10.1109/TPAS.1970.292678.

[11] Brandalik R, Waeresch D, Wellssow WH, Tu J. Linear three-phase state estimation for lv grids using pseudo-measurements based on approximate power distributions. CIRED Open Access Proc J 2017;2017(1):1871–4. https://doi.org/10.1049/oap-cired.2017.0071.

[12] Primadianto A, Lu C. A review on distribution system state estimation. IEEE Trans Power Syst 2017;32(5):3875–83. https://doi.org/10.1109/TPWRS.2016.2632156.

[13] Geisler KI. Ampere magnitude line measurements for power systems state estimation. IEEE Trans Power Apparatus Syst 1984;PAS-103(8):1962–9. https://doi.org/10.1109/TPAS.1984.318500.

[14] Chen T, Chen M, Inoue T, Kotas P, Chebli EA. Three-phase cogenerator and transformer models for distribution system analysis. IEEE Trans. Power Delivery 1991;6(4):1671–81. https://doi.org/10.1109/61.97706.

[15] Sakis Meliopoulos AP, Zhang Fan. Multiphase power flow and state estimation for power distribution systems. IEEE Trans Power Syst 1996;11(2):939–46. https://doi.org/10.1109/59.496178.

[16] Vempati N, Shoults RR, Chen MS, Schwobel L. Simplified feeder modeling for loadflow calculations. IEEE Trans Power Syst 1987;2(1):168–74. https://doi.org/10.1109/TPWRS.1987.4335094.

[17] Chen T, Chen M, Hwang K, Kotas P, Chebli EA. Distribution system power flow analysis-a rigid approach. IEEE Trans Power Delivery 1991;6(3):1146–52. https://doi.org/10.1109/61.85860.

[18] Sun DIH, Abe S, Shoults RR, Chen MS, Eichenberger P, Farris D. Calculation of energy losses in a distribution system. IEEE Trans Power Apparatus Syst 1980;PAS-99(4):1347–56. https://doi.org/10.1109/TPAS.1980.319557.

[19] Liu Y, Li J, Wu L. State estimation of three-phase four-conductor distribution systems with real-time data from selective smart meters. IEEE Trans Power Syst 2019;34(4):2632–43. https://doi.org/10.1109/TPWRS.2019.2892726.

[20] Džafic I, Jabr RA, Huseinagic I, Pal BC. Multi-phase state estimation featuring industrial-grade distribution network models. IEEE Trans Smart Grid 2017;8(2):609–18.

[21] Pau M, Ponci F, Monti A, Sulis S, Muscas C, Pegoraro PA. An efficient and accurate solution for distribution system state estimation with multiarea architecture. IEEE Trans Instrum Meas 2017;66(5):910–9.

[22] de Almeida MC, Ochoa LF. An improved three-phase amb distribution system state estimator. IEEE Trans Power Syst 2017;32(2):1463–73.

[23] Nanchian S, Majumdar A, Pal BC. Three-phase state estimation using hybrid particle swarm optimization. IEEE Trans Smart Grid 2015;8(3):1035–45.

[24] Dedé A, Della Giustina D, Rinaldi S, Ferrari P, Flammini A, Vezzoli A. Smart meters as part of a sensor network for monitoring the low voltage grid. 2015 IEEE sensors applications symposium (SAS) 2015. p. 1–6. https://doi.org/10.1109/SAS.2015.7133616.
[25] Abdel-Majeed A, Braun M. Low voltage system state estimation using smart meters. In: 2012 47th international universities power engineering conference (UPEC); 2012. p. 1–6. doi:10.1109/UPEC.2012.6398598.
[26] Leite JB, Mantovani JRS. State estimation of distribution networks through the real-time measurements of the smart meters. 2013 IEEE grenoble conference 2013. p. 1–6. https://doi.org/10.1109/PTC.2013.6652170.
[27] Alimardani A, Therrien F, Atanackovic D, Jatskevich J, Vaahedi E. Distribution system state estimation based on nonsynchronized smart meters. IEEE Trans Smart Grid 2015;6(6):2919–28. https://doi.org/10.1109/TSG.2015.2429640.
[28] Muscas C, Sulis S, Angioni A, Ponci F, Monti A. Impact of different uncertainty sources on a three-phase state estimator for distribution networks. IEEE Trans Instrum Meas 2014;63(9):2200–9. https://doi.org/10.1109/TIM.2014.2308352.
[29] Dedé A, Giustina DD, Rinaldi S, Ferrari P, Flammini A, Vezzoli A. Smart Meters as Part of a Sensor Network for Monitoring the Low Voltage Grid 00416.
[30] Soares TM, Bezerra UH, Tostes MEdL. Full-observable three-phase state estimation algorithm applied to electric distribution grids. Energies 2019;12(7):1327.
[31] Alam MJE, Muttaqi KM, Sutanto D. A three-phase power flow approach for integrated 3-wire mv and 4-wire multigrounded lv networks with rooftop solar pv. IEEE Trans Power Syst 2013;28(2):1728–37.
[32] Li H, Mao R, Lai L, Qiu RC. Compressed meter reading for delay-sensitive and secure load report in smart grid. 2010 First IEEE international conference on smart grid communications. IEEE; 2010. p. 114–9.
[33] Chen Q, Kaleshi D, Armour S, Fan Z. Reconsidering the smart metering data collection frequency for distribution state estimation. 2014 IEEE international conference on smart grid communications (SmartGridComm). IEEE; 2014. p. 517–22.
[34] Carson JR. Wave propagation in overhead wires with ground return. Bell Syst Tech J 1926;5(4):539–54. https://doi.org/10.1002/j.1538-7305.1926.tb00122.x.
[35] Kersting WH, Green RK. The application of carson's equation to the steady-state analysis of distribution feeders. 2011 IEEE/PES power systems conference and exposition 2011. p. 1–6. https://doi.org/10.1109/PSCE.2011.5772579.
[36] Sun DIH, Abe S, Shoults RR, Chen MS, Eichenberger P, Farris D. Calculation of energy losses in a distribution system. IEEE Trans Power Apparatus Syst 1980;PAS-99(4):1347–56. https://doi.org/10.1109/TPAS.1980.319557.
[37] Dorfler F, Bullo F. Kron reduction of graphs with applications to electrical networks. IEEE Trans Circuits Syst I Regul Pap 2013;60(1):150–63. https://doi.org/10.1109/TCSI.2012.2215780.
[38] Kettner AM, Paolone M. Performance assessment of kron reduction in the numerical analysis of polyphase power systems. 2019 IEEE Milan PowerTech. 2019. p. 1–6.
[39] Lu CN, Teng JH, Liu WE. Distribution system state estimation. IEEE Trans Power Syst 1995;10(1):229–40. https://doi.org/10.1109/59.373946.
[40] Nanchian S, Majumdar A, Pal B. Three-phase state estimation using hybrid particle swarm optimization. 2016 IEEE power and energy society general meeting (PESGM) 2016. p. 1. https://doi.org/10.1109/PESGM.2016.7741159.
[41] Rousseaux P, Mallieu D, Cutsem TV, Ribbens-Pavella M. Dynamic state prediction and hierarchical filtering for power system state estimation. Automatica 1988;24(5):595–618. https://doi.org/10.1016/0005-1098(88)90108-2.
[42] Toyoshima D, Castillo MRC, Fantin CA, London JBA. Observability and measurement redundancy analysis on three-phase state estimation. 2012 IEEE power and energy society general meeting 2012. p. 1–8. https://doi.org/10.1109/PESGM.2012.6345507.
[43] Fantin CA, Massignan JAD, Castillo MR, London JBA. Observability, redundancy and gross error processing in state estimation using scada and synchronized phasor measurements. 2015 IEEE Eindhoven PowerTech 2015. p. 1–5. https://doi.org/10.1109/PTC.2015.7232434.
[44] Waeresch D, Brandalik R, Wellssow WH, Jordan J, Bischler R, Schneider N. Linear state estimation in low voltage grids based on smart meter data. 2015 IEEE Eindhoven PowerTech 2015. p. 1–6. https://doi.org/10.1109/PTC.2015.7232343.
[45] Qian H. Counting the floating point operations (flops), Matlab central file exchange 23. https://in.mathworks.com/matlabcentral/fileexchange/50608-counting-the-floating-point-operations-flops.

Applied Energy 280 (2020) 116022

Contents lists available at ScienceDirect

Applied Energy

journal homepage: www.elsevier.com/locate/apenergy

Coordinated *photovoltaic re-phasing*: A novel method to maximize renewable energy integration in low voltage networks by mitigating network unbalances☆

W.G. Chaminda Bandara [a], G.M.R.I. Godaliyadda [a], M.P.B. Ekanayake [a], J.B. Ekanayake [a,b,*]

[a] Department of Electrical and Electronic Engineering, University of Peradeniya, Peradeniya, 20400, Sri Lanka
[b] School of Engineering, Cardiff University, The Parade, Cardiff CF24 3AA, United Kingdom

HIGHLIGHTS

- Maximize renewable energy penetration through coordinated re-phasing of solar photovoltaic.
- An automatic photovoltaic re-phasing switch that can connect to single-phase photovoltaic inverters.
- A modified discrete bacterial foraging optimization to determine the optimum phase combination of photovoltaic systems.
- The key mechanisms of discrete bacterial foraging optimization are modified to cater to photovoltaic re-phasing problem.
- A contextually optimized initializer to improve the convergence speed of discrete bacterial foraging optimization.

ARTICLE INFO

Keywords:
Renewable energy integration
Rooftop solar PV
PV re-phasing
Network unbalance
LV distribution networks
Bacterial foraging optimization

ABSTRACT

As combating climate change has become a top priority and as many countries are taking steps to make their power generation sustainable, there is a marked increase in the use of renewable energy sources (RESs) for electricity generation. Among these RESs, solar photovoltaics (PV) is one of the most popular sources of energy connected to LV distribution networks. With the greater integration of solar PV into LV distribution networks, utility providers impose caps to solar penetration in order to operate their network safely and within acceptable norms. One parameter that restricts solar PV penetration is unbalances created by loads and single-phase rooftop schemes connected to LV distribution grids. In this paper, a novel method is proposed to mitigate voltage unbalance in LV distribution grids by optimally re-phasing grid-connected rooftop PV systems. A modified version of the discrete bacterial foraging optimization algorithm (DBFOA) is introduced as the optimization technique to minimize the overall voltage unbalance of the network as the objective function, subjected to various network and operating parameters. The impact of utilizing the proposed PV re-phasing technique as opposed to a fixed phase configuration are compared based on overall voltage unbalance, which was observed hourly throughout the day. The case studies show that the proposed approach can significantly mitigate the overall voltage unbalance during the daytime and can facilitate to increase the usable PV capacity of the considered network by 77%.

Abbreviations: ACO, Ant Colony Optimization; ADN, Active Distribution Network; APF, Active Power Filter; BFOA, Bacterial Foraging Optimization Algorithm; BF-SD, Bacterial Foraging-Spiral Dynamic; CPN, Colored Petri nets; CPU, Central Processing Unit; DBFOA, Discrete Bacterial Foraging Optimization; DG, Distributed Generators; DFR, Distribution Feeder Reconfiguration; DGA, Discrete Genetic Algorithm; DSS, Distribution System Simulator; DVR, Dynamic Voltage Restorer; FPV, Floating PV; GA, Genetic Algorithm; GPV, Ground-mounted PV; HS, Heuristic Search; IEC, International Electrotechnical Commission; LV, Low Voltage; LVDG, Low Voltage Distribution Grid; MV, Medium Voltage; PV, Photovoltaic; PWM, Pulse Width Modulation; RES, Renewable Energy Sources; RMS, Root Mean Square; SA, Simulated Annealing; SCADA, Supervisory Control and Data Acquisition; SFLA, Shuffled Frog Leaping Algorithm; SOP, Soft Open Points; SOCP, Second-Order Cone Programming; S-MILP, Stochastic Mixed-Integer Linear Programming; VUF, Voltage Unbalance Factor.

☆ This research was supported by the National Science Foundation (NSF), Sri Lanka (grant number: RG/2018/EA & ICT/01).

* Corresponding author at: Department of Electrical and Electronic Engineering, University of Peradeniya, Peradeniya, 20400, Sri Lanka and School of Engineering, Cardiff University, The Parade, Cardiff CF24 3AA, United Kingdom.
E-mail addresses: chaminda.bandara@eng.pdn.ac.lk (W.G. Chaminda Bandara), roshangodd@ee.pdn.ac.lk (G.M.R.I. Godaliyadda), mpb.ekanayake@ee.pdn.ac.lk (M.P.B. Ekanayake), jbe@ee.pdn.ac.lk, ekanayakej@cardiff.ac.uk (J.B. Ekanayake).

https://doi.org/10.1016/j.apenergy.2020.116022
Received 11 July 2020; Received in revised form 14 September 2020; Accepted 10 October 2020
Available online 6 November 2020

Nomenclature

$\mathbb{H}_{VU}{}^{i}$	Highest unbalance region in the network
i	Index of i-th PV configuration vector
j	Incremental counter (index) for D-Chemotaxis step
J_C^i	Cumulative cost of i-th PV configuration vector
J_{last}	Best cost recorded
$J(i,j,k,l)$	Cost of i-th PV configuration vector at j-th D-Chemotaxis step, k-th D-Reproduction step and l-th D-Elimination Dispersal step
$J(\boldsymbol{x})$	Penalized objective function
k	Incremental counter (index) for D-Reproduction step
k_n	Radius of the highest unbalance region
k_R	Number of phase combinations having smallest active power mismatch
l	Incremental counter (index) for D-Elimination Dispersal step
$n_{VUF_{max}}$	Busbar with the highest voltage unbalance
N	Total number of busbars in the network
N_c	Number of D-Chemotaxis steps
N_{pv}	Number of grid-connected PV systems in the network
N_r	Maximum number of random phase changing steps performed
N_{re}	Number of D-Reproduction steps
P_{ed}	D-Elimination Dispersal probability
r	Incremental counter (index) for the random phase changing step
RN^i	A random number between 0 and 1
S	Number of PV configuration initializers
$\overline{VUF}$	Mean voltage unbalance factor
VUF_{max}	Specified maximum unbalance level
VUF_n	Voltage unbalance factor at n-th busbar
V_{max}	Specified maximum phase voltage magnitude
V_{min}	Specified minimum phase voltage magnitude
V_n^-	Negative sequence voltage component at n-th busbar
V_n^+	Positive sequence voltage component at n-th busbar
V_n^a	Voltage magnitude of phase-a at n-th busbar
V_n^b	Voltage magnitude of phase-b at n-th busbar
V_n^c	Voltage magnitude of phase-c at n-th busbar
$\boldsymbol{x}$	PV configuration vector
x_m	m-th element of the PV configuration vector
$\boldsymbol{x}^i(j,k,l)$	i-th PV configuration vector at j-th D-Chemotaxis step, k-th D-Reproduction step and l-th D-Elimination Dispersal step
Z^{abcn}	Impedance matrix for the overhead cable
$\mu_{V_n^a}$	Penalty function for voltage magnitude of phase-a
$\mu_{V_n^b}$	Penalty function for voltage magnitude of phase-b
$\mu_{V_n^c}$	Penalty function for voltage magnitude of phase-c
μ_{VUF_n}	Penalty function for voltage unbalance

1. Introduction

With the de-carbonization agenda of many countries, the integration of renewable energy sources (RES) such as solar and wind energy into the power system has increased considerably. Among these RES, photovoltaic solar energy (PV) is one of the fastest-growing renewable energy sources with an annual growth rate of 35 to 40% [1]. At the end of 2019, the global cumulative solar energy capacity stood at 580 GW. These installations come in three forms: ground-mounted PV (GPV) [2,3], floating PV (FPV) [4,5], and rooftop PV [6,7]. As GPV and FPV use dedicated feeders for connection to the network, there is no local impact on the network, whereas the random installation of small-size rooftop PV systems in LV networks causes a voltage unbalance. The unbalance in the phase voltages and the resulting flow of large neutral currents can increase the distribution and transformer losses due to overheating and can overload the neutral conductor [8,9]. Due to these consequences of voltage unbalance, utility providers limit the usable PV capacity that they can accommodate for LV networks [10–12]. Therefore, an effective solution is needed to improve the future integration of solar PV sources into LV networks. How to effectively reduce the unbalance is a long-standing question, and much effort has been devoted to answering this question in the past decade.

Table 1 summarizes the various approaches proposed in the literature in order to minimize network unbalance along with their advantages and limitations. As can be seen from Table 1, these techniques can be mainly divided into two categories [13]. The first category mitigates the network unbalance by using neutral current compensation devices such as passive harmonic filters and specially designed active power filters. The second category is based on distribution network reconfiguration techniques and can be divided into two: distribution feeder reconfiguration (DFR) and phase balancing. It is important to note that both DFR and phase balancing techniques use non-linear, non-differentiable, highly combinatorial, and constrained optimization algorithms to find the optimal solution [14].

The neutral current compensation devices do not mitigate the network imbalance, but they filter excess neutral current flowing through the neutral conductor. In [15], a synchronous machine has been used to filter out all the zero-sequence harmonic currents of the neutral. Apart from the synchronous machines, different transformer topologies have also been analyzed by the researches to compensate neutral current. Commonly used topologies to reduce the neutral current are a zig-zag transformer [16], a star-delta transformer [17], T-connected transformer [18] and, star-hexagon transformer constructed from three single-phase three-winding transformers [19]. Nowadays, power-electronic-based compensators such as H-bridge shunt Active Power Filter (APF) [20], capacitor midpoint APF [21], and three-phase four-wire four-leg APF [22], and Dynamic Voltage Restorer (DVR) [23] have also been used to overcome neutral current and other power quality problems. However, all of the aforementioned methods reduce only the neutral current but cannot reduce total power loss, voltage, or current unbalance. Hence, many researchers have used DFR techniques to mitigate system-level unbalance and power losses.

The DFR technique optimizes the open or closed status of sectionalizing switches and tie switches to transfer the loads from overloaded feeders to the lightly loaded feeders in order to minimize desired objective functions (e.g., voltage unbalance, load unbalance, power loss, etc.) [24]. Many researchers have used different optimization techniques to identify the optimum states of the sectionalizing and/or tie switches. In [25], a heuristic search methodology has been utilized for the feeder reconfiguration problem. In [26], Ant Colony Optimization (ACO) along with Graph Theory has been used to determine the optimum status while maintaining the system radiality. In [27], a method to convert distribution network reconfiguration problem into a spanning tree of the graph is proposed, then an improved ACO algorithm is utilized to solve the reconfiguration problem. In [28], the genetic algorithm (GA) is utilized for the reconfiguration problem using a composite multi-objective function of power loss saving, voltage profile, voltage unbalance and current unbalance of the system. In [29], a multi-objective evolution programming method with adapted weight calculation is applied in order to overcome the weakness of the traditional GAs [30,31]. In [32], a combined optimization technique has been developed with heuristic rules and fuzzy logic for efficiency and robust performance. A hybrid optimization algorithm based on fuzzy logic and Bees algorithm is also used in reconfiguration and multiple DG

Table 1
Summary of available techniques to mitigate network unbalances from the literature.

Category	Technique	Examples	Advantages	Limitations
Neutral current compensating devices	*Passive filters and transformers*	Synchronous machines as filters [15]	• Not require any additional controller • Synchronous machine can be operated as a synchronous condenser (to reactive power control) and/or motor or generator.	• Compensation characteristic depends on the zeros sequence impedance of the synchronous machine • High initial and maintenance cost • Bulky
		T connected transformer [18]	• Neutral current can be compensated to a large extent	• Compensation characteristics are depending on the impedance of the transformer, location, and source voltage
		Star-hexagon transformer [19]	• Can reduce the zero-sequence harmonic current to a large extent	
		Star-Delta transformer [17]	• Neutral current can be reduced to a large extent	
		Zig-zag transformer [16]	• Neutral current can be reduced to a large extent	• Neutral voltage variations may lead to abnormal operation of the load side.
	Active power filters	H-bridge shunt APF [20]	• Control can be done either as a three-phase unit or three separate single-phase units	• Increased number of switching devices
		Three-phase four-wire capacitor midpoint APF [21]	• Ability to reduce power quality problems • Compensate not only the neutral current but also the harmonics from loads	• Voltage unbalance between the capacitors
		Three-phase, four-wire, four-leg APF [22]	• Most suitable for compensation of high neutral currents • Better controllability • Lower DC voltage requirement	• Difficulty in controlling the four-leg inverter
Distribution network reconfiguration techniques	*Distribution feeder reconfiguration*	[24,25,26,27,28,29,30,31,32,33,34,35,36,37,38,39,40]	• Minimize load imbalance • Loss reduction • Congestion management • Increased hosting capacity in normal conditions • Capability to isolate fault areas by maintaining continuity of power supply to non-faulted areas	• Only mitigate the system level unbalance and cannot mitigate the phase level unbalance
	Phase balancing (load re-sequencing and load re-phasing)	[41,42,43,44,45,46]	• Ability to minimize phase level unbalance	• A large number of re-phasing switches need to be installed • Require complex optimization techniques to find optimal phase combination for load switches

placement [33]. In addition, a Colored Petri nets (CPN) inference mechanism-based distribution feeder load balancing technique has been proposed in [34]. An improved version of an aforementioned CPN optimization algorithm is proposed in [35]. Recently, an enhanced second-order cone programming (SOCP)-based method for load balancing using multi-terminal soft open points (SOP) has been proposed in [36]. An improved version of the aforementioned algorithm has been proposed in [37] which allocates SOPs and DG units simultaneously with and without network reconfiguration. In [38], a dynamic distribution network reconfiguration approach is proposed in the context of the active distribution network (ADN) under high penetration of distributed generations. In [39], an optimal network reconfiguration technique is formulated as a multi-objective stochastic mixed-integer linear programming (S-MILP) model. In [40], a new technique based on Bacterial Foraging with Spiral Dynamic (BF-SD) is applied for simultaneous optimization of re-phasing, reconfiguration, and DG placement. Although the aforementioned DFR techniques can only mitigate unbalance at the system level it cannot mitigate phase unbalance at the feeder level [13]. Hence, phase balancing techniques have been proposed to mitigate feeder level unbalance.

The phase balancing technique can be implemented in two ways: (1) load re-sequencing and (2) load re-phasing. In the load re-sequencing technique, the phase sequence at each busbar is re-sequenced to their optimal combination. To avoid any reverse operation of inductive loads, the positive and negative phase sequences are only taken into account [41]. In the load re-phasing technique, the loads from the overloaded phases are transferred to the lightly loaded phases by analyzing the current or power difference between the phases. To identify the optimum phase sequence for the three-phase loads and optimum phase combination for the single-phase loads, different optimization techniques have been proposed. In [42], a mixed-integer programming formulation for phase balancing optimization has been proposed. In [43], Simulated Annealing (SA) has been introduced as an effective method to solve the phase balancing problem while paying attention to the non-linear effects such as voltage drops and energy losses. In [44], an application program is developed which contains a function of load flow and phase balancing of feeders with phase re-phasing. In [45], A fuzzy logic-based phase balancing approach along with an optimization oriented expert system has been proposed for LVDGs. An advanced version of the aforementioned algorithm has been proposed in [46] in which the algorithm is extended for both radial and meshed distribution networks in the presence of unbalanced loads. In [47,48], the economic feasibility of the phase balancing approach to mitigate network unbalance has been analyzed under the presence of plug-in battery electric vehicles changing and distributed energy storage systems. However, all of these phase balancing techniques have been tested on small LV networks with a few loads and have not been implemented in large LV networks due to the high computational time they use to identify the optimum solution.

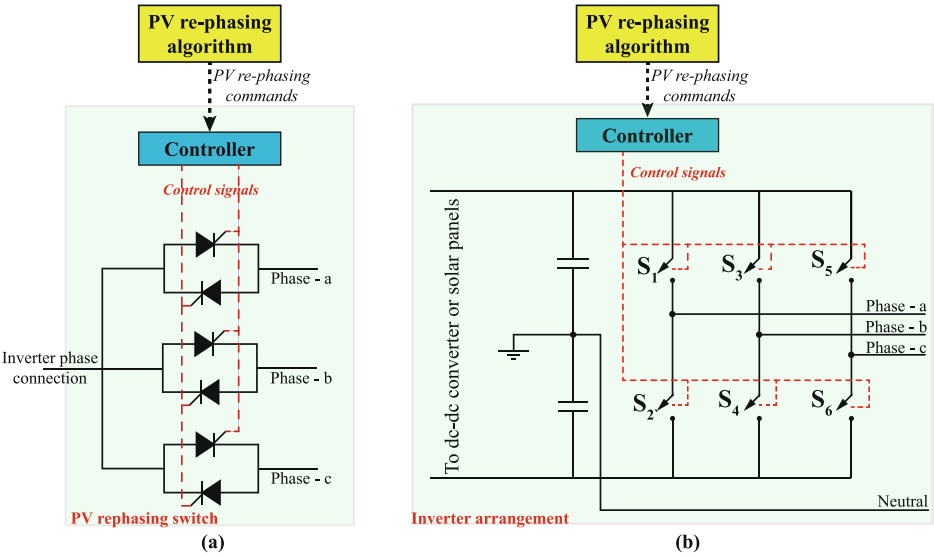

Fig. 1. (a) Thyristor switch, (b) Inverter arrangement.

Also, the aforementioned unbalance mitigation techniques raise many concerns when they implemented in practical networks such as:

- *high initial cost* due to the fact that load switches need to be installed between the phases, at each end of the client [13],
- *several other indirect costs* such as the cost of customer interruption, the cost of customer reliability, etc. [47], and
- *possible harm or damage* to the customer equipment at the time of re-phasing.

Considering the above limitations of load re-phasing, in this paper, a PV re-phasing technique is proposed that only relies on the rooftop solar systems to minimize the network unbalance. Therefore, the re-phasing switches need to be installed only at the connection point of each rooftop solar system and require much fewer re-phasing switches per network as compared to load/feeder re-phasing techniques. Due to this low capital requirement for the implementation of the proposed PV re-phasing technique, it is ideal for the large-scale deployment in LV networks to minimize the network unbalance. Also, the proposed PV re-phasing technique has no impact on supply reliability and requires minimum or no customer interruption. Therefore, the proposed PV re-phasing technique is a more economical and effective way to minimize the network unbalance, and thereby facilitate to improve the integration of clean and renewable solar energy into the LV networks. The main contributions of this paper are listed as follows:

- ***A novel strategy to minimize unbalance in LV networks based on automatic re-phasing of grid-connected rooftop PV systems.*** The grid-connected rooftop solar systems are periodically re-phased to their optimal phase combination at pre-selected time intervals to minimize the system unbalance. The proposed PV re-phasing technique can maintain the voltage unbalance well below the 1% threshold line while simultaneously maintaining the phase voltages within their acceptable limits. This will help utility providers to allow more rooftop solar systems into the network without bothering about network unbalance. The case studies demonstrate that the proposed PV re-phasing strategy can improve the usable PV capacity of the considered network by 77%.
- ***A PV rephasing switch is proposed to perform automatic rephasing of grid-connected single-phase PV systems.*** Since the re-phasing switch only re-phases rooftop PV systems, not the loads or the feeders, it will not have any impact on supply reliability. Additionally, no customer interruption is required at the time of PV re-phasing.
- ***A discrete bacterial foraging optimization algorithm (DBFOA) was introduced to determine the optimal phase combination of grid-connected single-phase PV systems.*** The proposed DBFOA improves upon the classical BFOA by modifying the principal mechanisms of the classical method to specifically catered to the PV re-phasing problem, thereby increasing both convergence speed and accuracy. The proposed bacterial foraging optimization algorithm determines the optimal phase combination for rooftop PV systems such that it will minimize the violations of voltage unbalance and phase voltage magnitudes.

The rest of the paper is organized as follows. Section 2 describes the structure of the proposed re-phasing switch and the overall operating mechanism of the PV re-phasing technique. Section 3 formulates the PV re-phasing problem. Section 4 describes the principal mechanisms of the proposed bacterial foraging optimization algorithm and the implementation details (i.e. the flow chart and the pseudo-code), as well as the simulation results, are given in Section 5. Finally, Section 6 presents our conclusions and future work.

2. PV re-phasing arrangement

In this section, the structure of the re-phasing switch and the operating mechanism of automatic PV re-phasing in LV distribution grids are explained.

2.1. Structure of the PV re-phasing switch

Fig. 1(a) shows a schematic of a PV rephasing switch that can be connected to the output of the single-phase inverter. As can be seen, switching between phases can be achieved by blocking the already conducting pair of thyristors (or trial) and turning the pair of thyristors that are connected to the phase to which output should be connected. In order to avoid any circulating current between phases, a dead band should be introduced between the blocking signal and the turning on signal. However, this will eventually course the PV inverter to take the start-up mode, thus, introducing an interruption of a few minutes (less than 3 min). This configuration is widely used for ac switching applications and its operation can be found in standard textbooks [49]. The thyristors used for this configuration should be able to continuously

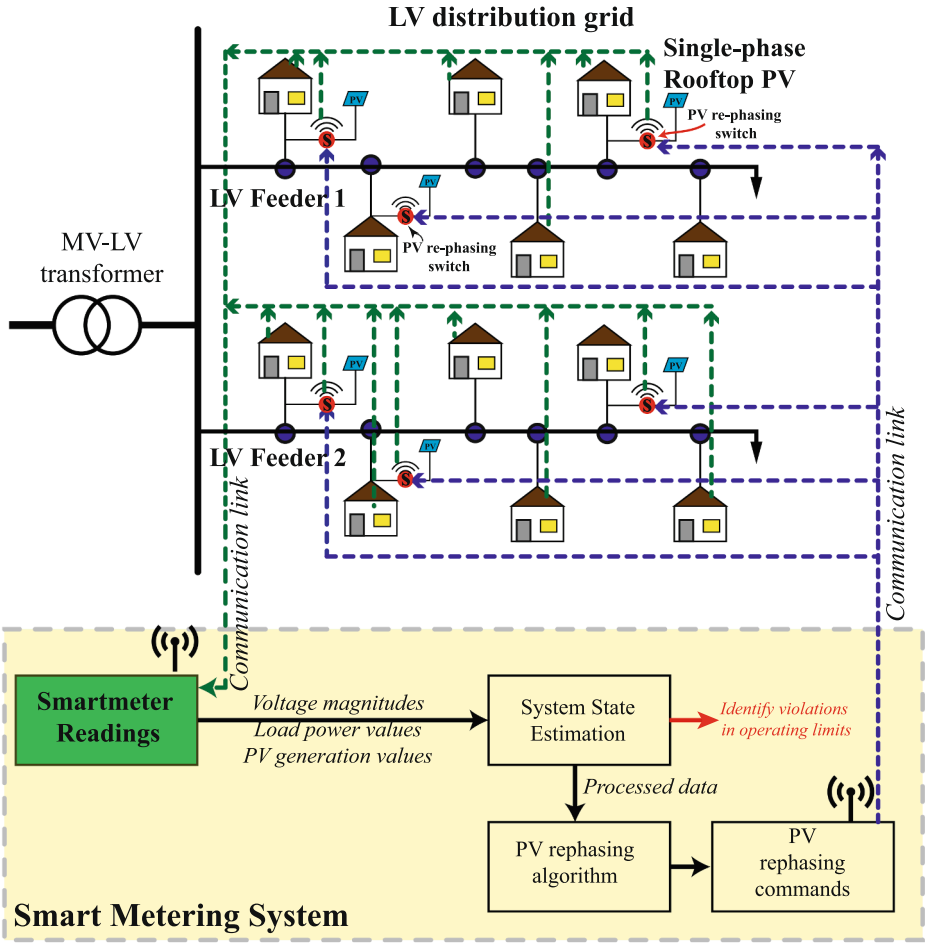

Fig. 2. Schematic of the automatic PV re-phasing arrangement.

carry the maximum current that the PV plant generates. The main drawbacks are the continuous on-state loss (equal to the square of the current times dynamic resistance of the thyristor) and the extra cost due to the introduction of three back-to-back thyristors and its control circuits.

The inverter in Fig. 1(b) shows an alternative rephasing arrangement that can be used for nanosecond level transients from one phase to another. In this arrangement, a half-bridge inverter is used to convert dc into ac. If the output needs to be connected to Phase - a then switches S_1 and S_2 are operated in a complementary manner using a PWM switching pattern and all the other switches are blocked. If the output needs to be connected to Phase - b then S_1 and S_2 will be blocked and S_3 and S_4 will be turned on. Therefore, the leg S_3 – S_4 is idling until the rephasing algorithm instructed to change the connection of the single-phase PV source from Phase – a to b. Even though the presence of two extra arms incurs an additional cost, there are no additional losses due to the introduction of two more arms. The same arrangement can be introduced for full-bridge single-phase inverters.

When the above arrangements are employed for PV rephasing, switching from one phase to another will take place throughout the day and power electronic switches will experience transient switching. Back-to-back thyristor switches are used in power factor correction arrangements that are used for power factor correction and harmonic filtering. In this arrangement, the back-to-back thyristor switches operate frequently depending on the power factor of the load, and they have proven to be robust under such frequent switching operations for many

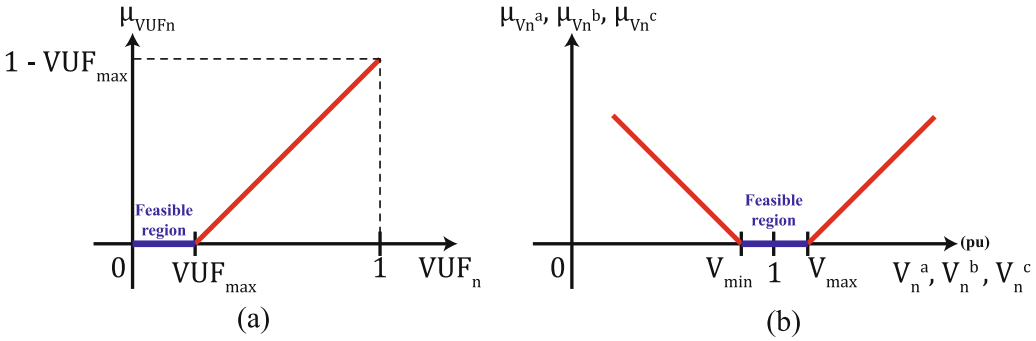

Fig. 3. Penalty functions for (a) voltage unbalance and (b) phase voltage magnitudes.

Format of the PV configuration vector $\boldsymbol{x} \in \mathbb{P}^{N_{pv}}$

Phase of PV_1	Phase of PV_2	Phase of PV_3	…	…	Phase of PV_m	…	…	…	Phase of $PV_{N_{pv}}$

Example PV configuration vector $\boldsymbol{x}^i$

Phase a	Phase b	Phase c	…	…	$x_m \in \mathbb{P}$	…	…	…	Phase a

Fig. 4. The format of the PV configuration vector.$\boldsymbol{x}$

Table 2
Related terminology.

Variable	Definition in PV rephrasing problem	Definition in classical BFOA
N_{pv}	The number of grid-connected PV systems in the network	The dimension of the search space
S	The number of PV configuration initializers	Total population of the bacterium
N_c	The number of D-chemotactic steps	The number of chemotactic steps
N_r	The maximum number of random phase changing steps performed	The swimming length
N_{re}	The number of D-Reproduction steps	The number of reproduction steps
P_{ed}	D-elimination dispersal probability	Elimination dispersal probability
i	i-th PV configuration vector	The i-th bacterium in the population
j	Incremental counter (index) for D-Chemotaxis step	Index for the chemotaxis step
k	Incremental counter (index) for D-Reproduction step	Index for the reproduction step
l	Incremental counter (index) for D-Elimination Dispersal step	Index of the elimination-dispersal event
r	Incremental counter (index) for the random phase changing step	Index for swimming step
$J(i,j,k,l)$	The cost of i-th PV configuration vector$\boldsymbol{x}^i(j,k,l)$	The cost at the location of the i-th bacterium$\boldsymbol{x}^i(j,k,l)$

decades. Therefore, the employment of back-to-back thyristor switches in the arrangement proposed in Fig. 1(a) should be robust under PV re-phasing operations. This additional switching transient that operates on switches in Fig. 1(b) will not have any impact on switches as they are anyway switched at 5–10 kHz frequency by PWM during normal operation.

2.2. The architecture of the automatic PV re-phasing arrangement

Fig. 2 shows the operating mechanism of the proposed PV re-phasing strategy. The necessary data such as PV generations and load demands are measured from smart meters and transmitted to the smart metering system. Typically, these smart meter measurements are subjected to different types of systematic, random, and communication errors

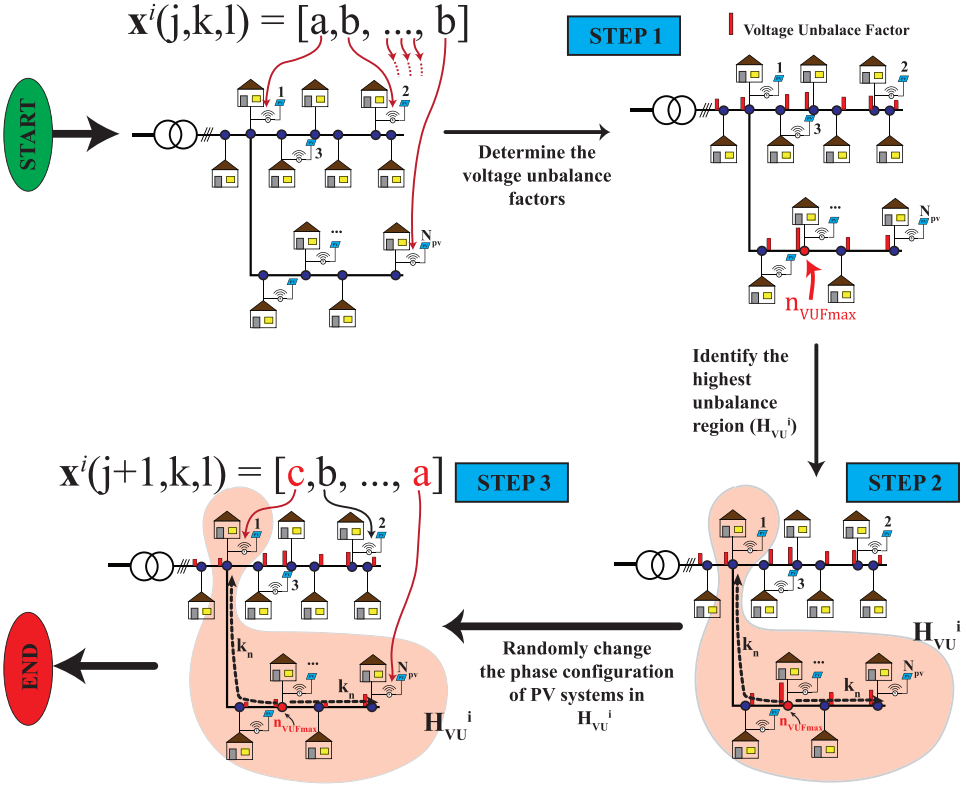

Fig. 5. Proposed D-Chemotaxis procedure.

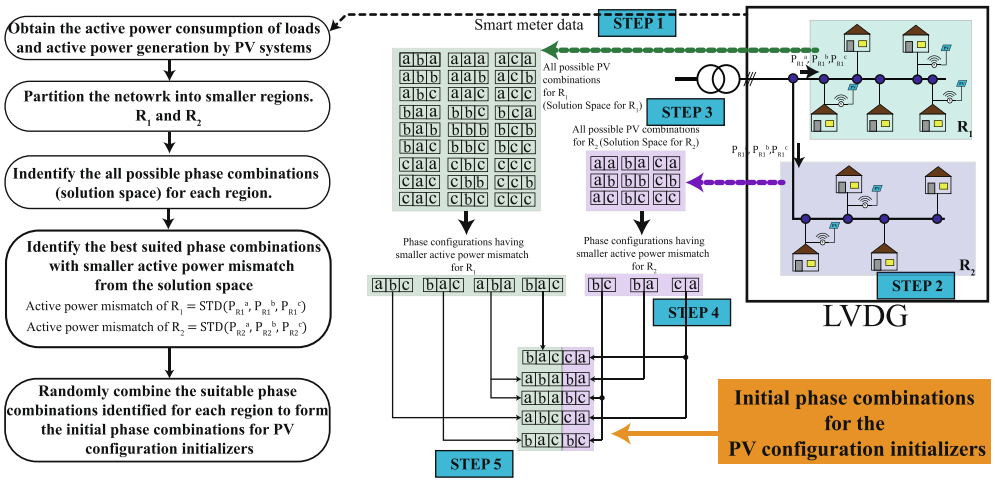

Fig. 6. Generation of initial phase combinations for PV configuration initializers based on active power balancing technique for a large distribution network.

[50,51]. Therefore, in the next step, state estimation is performed to detect the presence of bad data. These preprocessed smart meter data are sent to the PV re-phasing algorithm to determine the optimal phase combination of grid-connected PV systems, such that the overall voltage unbalance of the network is minimized. Finally, the re-phasing program transmits the required phase changes of PV systems through the smart metering system to the installed PV re-phasing switches and the re-phasing operation is carried out.

The time required for a PV re-phasing operation depends on the time it takes to transmit smart meter data from consumers and producers to the smart metering system (about 4.7 sec under 112 OFDM Symbol Data Frame [52]), the time required for system state estimation (about 0.10 sec [53]), the time required to execute the PV rephasing algorithm (about 33.7 sec – see Table 8), and the time it takes to transmit PV rephasing commands from smart metering system to PV rephasing switches (about 4.7 sec under 112 OFDM Symbol Data Frame [52]). Therefore, the need for a PV re-phasing operation can be detected and then successfully executed in approximately 43.2 s. As mentioned in Section 2.1, the actual operation of the PV rephasing switches could vary from 3 min for the topology shown in Fig. 1(a) to a few nanoseconds for the topology shown in Fig. 1(b).

3. Problem formulation

The aim of this work is to develop a strategy to minimize the overall voltage unbalance of the network such that the power quality and the reliability of the distribution system can be improved. The objective of this optimization problem can be expressed as the minimization of the mean voltage unbalance factor ($\overline{VUF}$) of the network as in,

$$\overline{VUF} = \frac{1}{N}\sum_{n=1}^{N} VUF_n \tag{1}$$

where VUF_n is the voltage unbalance factor at n-th busbar and N is the total number of busbars in the network.

Subjected to the constraints:

1. Voltage unbalance at each busbar (VUF_n) must be strictly below the specified maximum unbalance level (VUF_{max}):

$$VUF_n \le VUF_{max} \tag{2}$$

for $n = 1, 2, 3, \cdots, N$.

2. Phase voltage magnitudes $\left(V_n^a, V_n^b, \text{and} V_n^c\right)$ must strictly between the upper (V_{max}) and lower (V_{min}) limits:

$$V_{min} \le V_n^a, V_n^b, V_n^c \le V_{max} \tag{3}$$

for $n = 1, 2, 3, \cdots, N$, where, V_n^a, V_n^b and V_n^c are the voltage magnitudes of a, b, and c phases at n-th busbar, respectively.

Eq. (1) corresponds to the objective function to be minimized and represents the overall voltage unbalance $\left(\overline{VUF}\right)$ of the distribution network. The inequality in (2) considers a constraint for voltage unbalance factor and ensures individual voltage unbalance factors (VUF_n for $n = 1, 2, .., N$) are below the specified maximum value, VUF_{max}. The inequality in (3) deals with the constraints for voltage magnitudes. It ensures the phase voltages $\left(V_n^a, V_n^b, \text{and} V_n^c\right)$ fall within the acceptable voltage limits (lower limit V_{min} and upper limit V_{max}). In this study, V_{min} was considered as 0.94 pu and V_{max} was considered as 1.06 pu. In other words, (2) and (3) define the feasible regions for voltage unbalance (VUF_n) and phase voltage magnitudes (V_n^a, V_n^b, V_n^c), respectively.

In order to minimize (1) while simultaneously satisfying the constraints (2) and (3), penalty functions were introduced. The main idea of these penalty functions is that an optimal PV configuration (i.e. the optimal solution) requires that constraints be active so that this optimal solution lies in the feasible regions for voltage unbalance and phase voltage magnitudes. To ensure this, a penalty is applied to possible solutions when constraints are not satisfied. Therefore, the aforementioned optimization problem was reformulated as the minimization of the penalized objective function, $J(\boldsymbol{x})$, given by,

$$J(\boldsymbol{x}) = \overline{VUF} + k_1 \sum_{n=1}^{n=N} \mu_{VUF_n} + k_2 \left(\sum_{n=1}^{n=N} \mu_{V_n^a} + \sum_{n=1}^{n=N} \mu_{V_n^b} + \sum_{n=1}^{n=N} \mu_{V_n^c} \right) \tag{4}$$

where,

the penalty function for voltage unbalance (μ_{VUF_n}) is given by:

$$\mu_{VUF_n} = \begin{cases} VUF_n - VUF_{max};\ when\ VUF_n > VUF_{max} \\ 0;\ when\ VUF_n \le VUF_{max} \end{cases} \text{for } n = 1, \cdots, N \tag{5}$$

the penalty function for voltage magnitudes of phase-a ($\mu_{V_n^a}$) is given by:

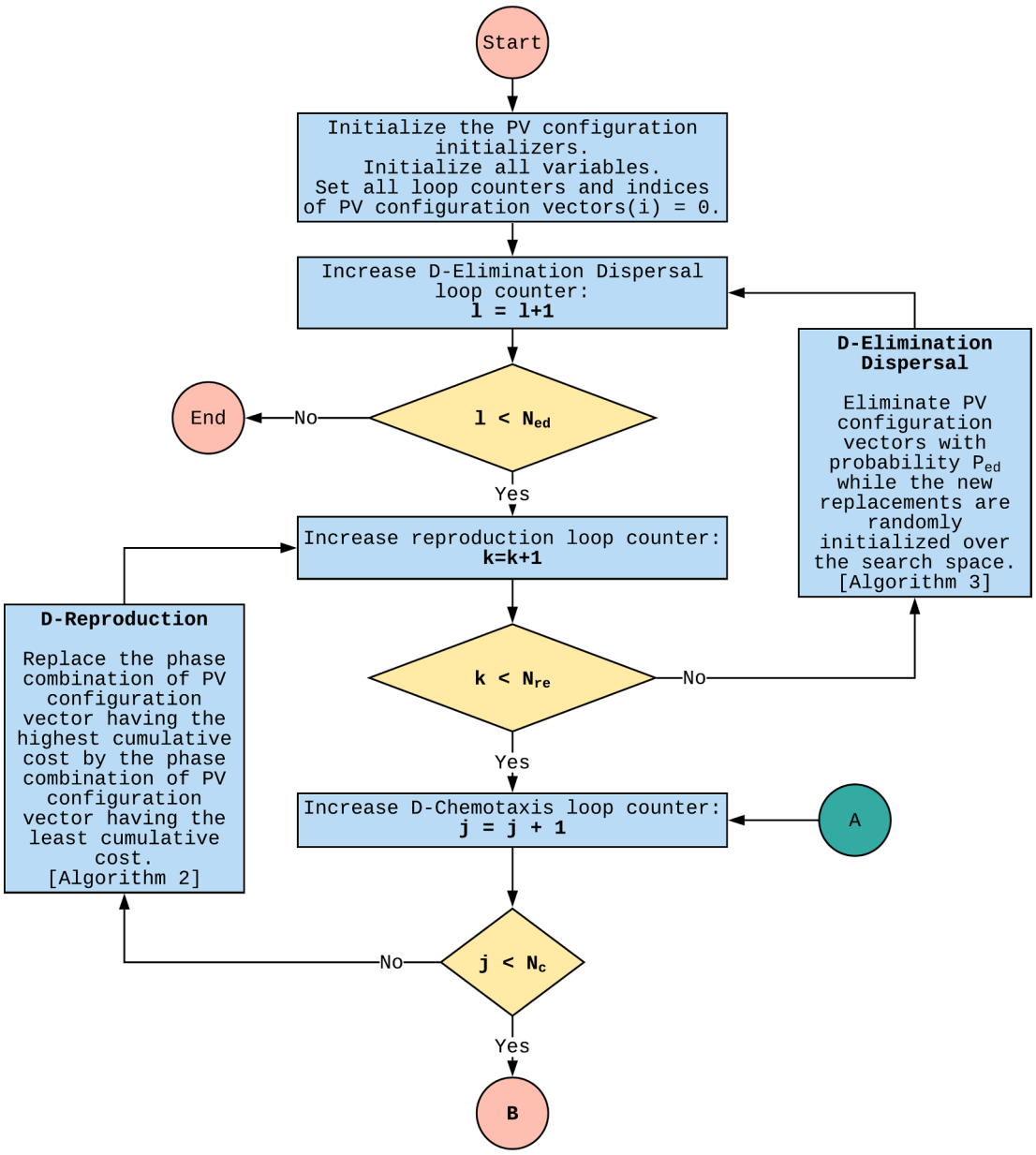

Fig. 7. The complete structure of the proposed DBFOA.

$$\mu_{V_n^a} = \begin{cases} |V_n^a - V_{min}|;\ when\ V_n^a < V_{min} \\ 0;\ when\ V_{min} \le V_n^a \le V_{max} \\ V_n^a - V_{max};\ when\ V_n^a > V_{max} \end{cases} \quad \text{for } n = 1, \cdots, N \tag{6}$$

the penalty function for voltage magnitudes of phase-b ($\mu_{V_n^b}$) is given by:

$$\mu_{V_n^b} = \begin{cases} |V_n^b - V_{min}|;\ when\ V_n^b < V_{min} \\ 0;\ when\ V_{min} \le V_n^b \le V_{max} \\ V_n^b - V_{max};\ when\ V_n^b > V_{max} \end{cases} \quad \text{for } n = 1, \cdots, N \tag{7}$$

the penalty function for voltage magnitudes of phase-c ($\mu_{V_n^c}$) is given by:

$$\mu_{V_n^c} = \begin{cases} |V_n^c - V_{min}|;\ when\ V_n^c < V_{min} \\ 0;\ when\ V_{min} \le V_n^c \le V_{max} \\ V_n^c - V_{max};\ when\ V_n^c > V_{max} \end{cases} \quad \text{for } n = 1, \cdots, N \tag{8}$$

$\boldsymbol{x}$ is the PV configuration vector, and k_1 and k_2 are the constant imposed on the penalty functions. The graphical illustrations of these penalty functions are shown in Fig. 3.

The phase combination of grid-connected PV systems at a given time is represented by the *PV configuration vector*, $\boldsymbol{x}$. Therefore, for a network having N_{pv} number of grid-connected PV systems, the PV configuration vector $\boldsymbol{x}$ consists of N_{pv} number of phase entries where each phase entry corresponds to the phase of a grid-connected PV system in the network. Hence, each element (x_m) in the PV configuration vector-$\boldsymbol{x}$ can take one of the three phases ($i.e. x_m \in \mathbb{P}, \mathbb{P} = \{a, b, c\}$). The format of the PV

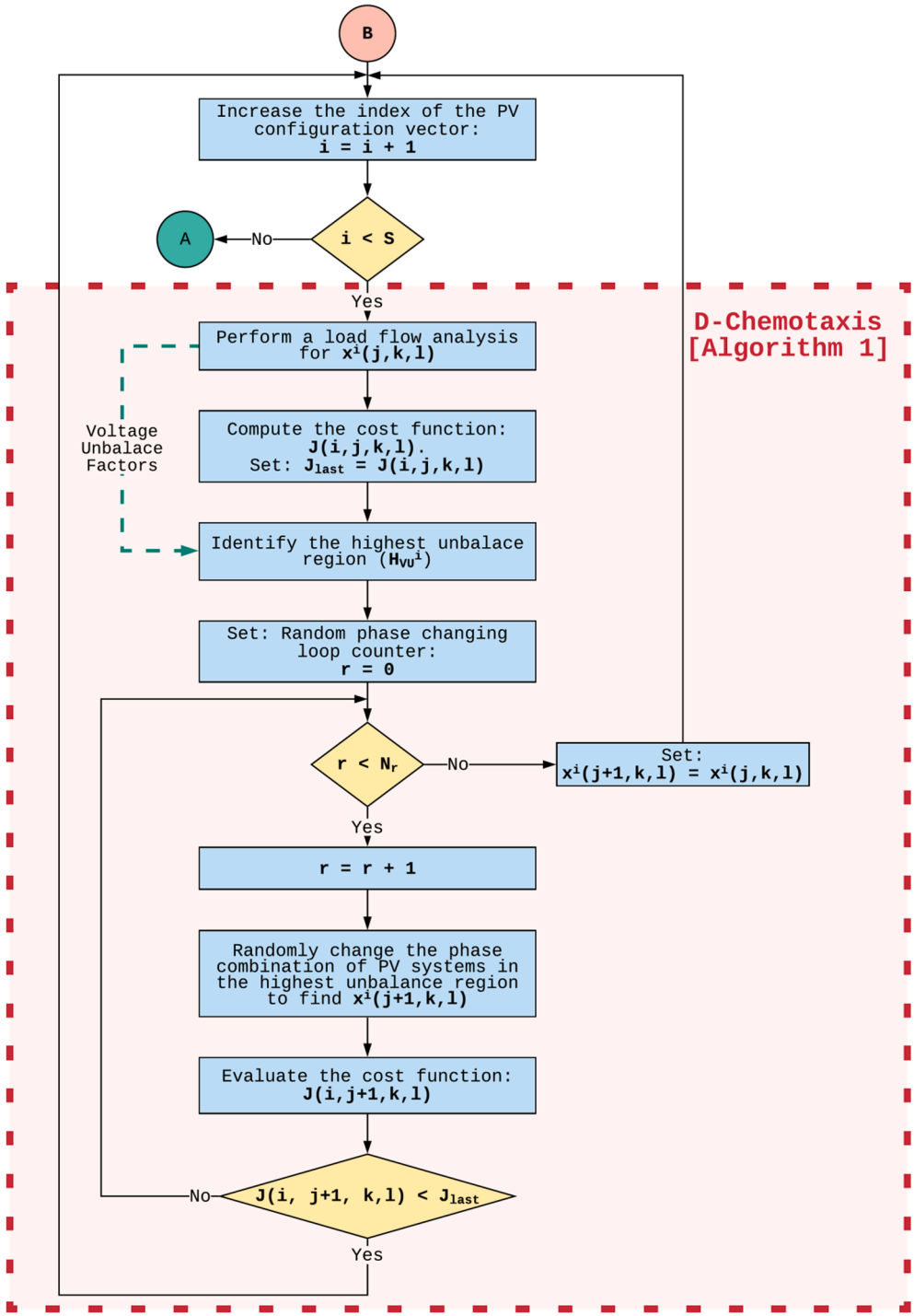

Fig. 7. (*continued*).

configuration vector is illustrated in Fig. 4 with an example PV combination.

It is important to note that there are different definitions available for the voltage unbalance factor; in this paper, the IEC definition [54] was used. In the IEC definition (IEC TR 61000–3-14:2011), the voltage unbalance factor is calculated as the ratio of negative sequence voltage component to the positive sequence voltage component and can be expressed as follows [54]:

$$VUF_n = \frac{V_n^-}{V_n^+} = \frac{\text{Negative sequence voltage component at } n^{\text{th}} \text{ busbar}}{\text{Positive sequence voltage component at } n^{\text{th}} \text{ busbar}} \times 100\% \quad (9)$$

The three-phase sequence voltage components were obtained by the symmetrical transformation. The steps for the computation of three-phase sequence voltage components from three-phase voltages can be found in [41].

4. Bacterial foraging optimization

Bacterial foraging optimization algorithm (BFOA) is a smart optimization technique that has proven to be very effective in search domains having several dimensions. BFOA is inspired by the social foraging behavior of *E. coli* bacteria. The underlying biology behind the foraging strategy of *E. coli* is emulated and used as a simple optimization

Table 3
Parameter values used for the proposed DBFOA.

Parameter	Value
Number of PV configuration initializers(S)	10
Maximum number of D-Chemotaxis steps(N_c)	5
Maximum number of random phase changing steps(N_r)	5
Maximum number of D-Reproduction steps(N_{re})	5
Maximum number of D-Elimination steps(N_{ed})	5
Elimination & dispersal probability(P_{ed})	0.2
The radius of the highest voltage unbalance region -$\mathbb{H}_{VU}(k_n)$	3
The maximum limit for phase voltage magnitudes(V_{max})	1.06 pu
The minimum limit for phase voltage magnitudes(V_{min})	0.94 pu
The maximum limit for voltage unbalance factors(VUF_{max})	1%
Number of grid-connected PV systems in the network(N_{pv})	26
Number of busbars in the network(N)	63

algorithm [55,56]. In this paper, a discrete and adaptive version of BFOA is introduced to solve the PV re-phasing problem.

4.1. Concept of BFOA

During the foraging period, real bacteria achieve their motion with the help of their tensile flagella. Using these tensile flagella, bacteria can perform two basic motion types called tumble and swim. In the classical BFOA, the bacteria undergo *chemotaxis*, where they like to move towards nutrient gradient while avoiding the noxious environments. When they get enough food, they increase their length and under suitable temperature, they break in the middle to form an exact replica of itself. This phenomenon is called the event of *reproduction* in BFOA. However, due to the occurrence of sudden environmental changes or attacks, the chemotaxis progress may be destroyed, and a group of bacteria may move to some other place or some other mutation may be introduced to the bacteria population. This phenomenon is called the *elimination dispersal event* in BFOA, where all the bacteria in the region are killed or a group is dispersed into a new part of the environment. Refs. [40,55–60] provide a comprehensive analysis of the classical BFOA in different optimization problems.

4.2. Primary steps of the proposed DBFOA

The proposed DBFOA improves upon the classical BFOA by modifying the principal mechanisms to specifically handle the PV re-phasing problem. The modified versions of the principal mechanisms of the algorithm were named as *D-Chemotaxis*, *D-Reproduction*, and *D-Elimination dispersal*. The following subsections discuss these three principal mechanisms which drive the proposed DBFOA. The mapping of the terms in the PV re-phasing problem and the classical BFOA problem are

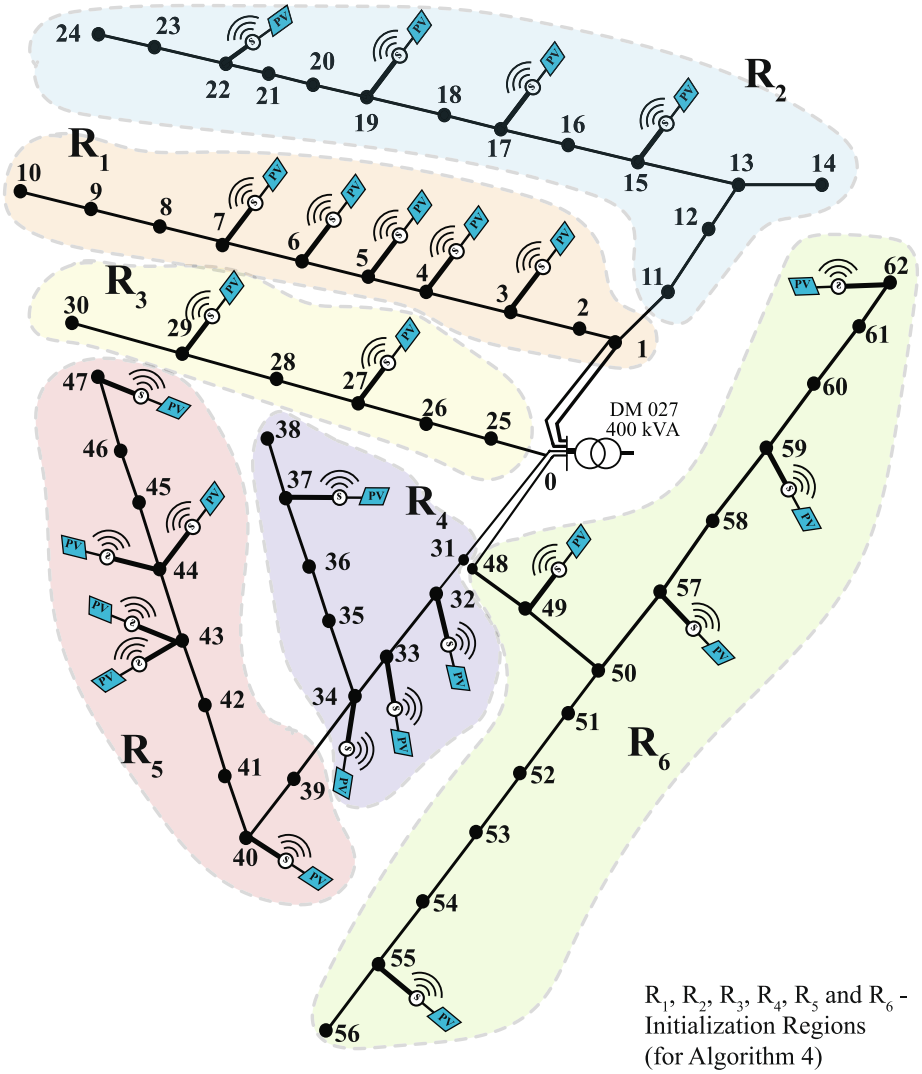

Fig. 8. Single line diagram of the test LVDG network (Lotus Grove, Sri Lanka) used for the simulations.

Table 4
Impedance matrix (Z^{abcn}) per km for the overhead cable (ABC 70) in the network.

	Phase a	Phase b	Phase c	neutral
Phase a	$0.4918 + 0.7888i$	$0.0486 + 0.6292i$	$0.0487 + 0.6701i$	$0.0486 + 0.7000i$
Phase b	$0.0486 + 0.6292i$	$0.4918 + 0.7888i$	$0.0487 + 0.6405i$	$0.0486 + 0.6490i$
Phase c	$0.0487 + 0.6701i$	$0.0487 + 0.6405i$	$0.4918 + 0.7888i$	$0.0487 + 0.7080i$
neutral	$0.0486 + 0.7000i$	$0.0486 + 0.6490i$	$0.0487 + 0.7080i$	$0.6790 + 0.7910i$

Table 5
The details of the grid-connected single-phase PV systems connected to the network.

PV No.	Connected busbar	Initial phase configuration (Fixed phase)	Capacity (P_{max})/ kW
PV1	**3**	a	2.40
PV2	**4**	b	7.20
PV3	**5**	a	4.80
PV4	**6**	c	2.40
PV5	**7**	a	6.00
PV6	**15**	a	5.04
PV7	**17**	b	5.04
PV8	**19**	a	2.40
PV9	**22**	c	8.20
PV10	**27**	a	4.80
PV11	**29**	c	6.48
PV12	**32**	a	6.00
PV13	**33**	b	3.96
PV14	**34**	a	6.00
PV15	**37**	b	3.12
PV16	**40**	c	4.20
PV17	**43**	c	6.00
PV18	**43**	b	8.2
PV19	**44**	c	6.36
PV20	**44**	b	5.76
PV21	**47**	a	8.28
PV22	**49**	a	5.16
PV23	**55**	c	8.40
PV23	**57**	b	2.20
PV25	**59**	a	4.80
PV26	**62**	c	7.20

shown in Table 2.

4.2.1. Discrete Chemotaxis (D-Chemotaxis)

The D-Chemotaxis step updates the phase combination of a PV configuration vector such that the new phase combination has a lower cost value compared to its previous phase combination. In other words, the D-Chemotaxis step updates the phase combination in a direction corresponding to a gradient of decreasing cost value.

Here, the present phase combination in i-th PV configuration vector is given by $x^i(j,k,l)$ and it's updated version is denoted by $x^i(j+1,k,l)$ where, j, k, and l are the index for D-Chemotaxis, D-Reproduction, and D-Elimination dispersal, respectively.

The proposed D-Chemotaxis step first identifies the highest unbalance region ($\mathbb{H}_{VU}{}^i$) in the network corresponding to the phase combination in the i-the PV configuration vector, $x^i(j,k,l)$. Here, the highest unbalance region is referred to the busbars within k_n number of busbars from the busbar with highest unbalance ($n_{VUF_{max}}$). Once the highest unbalance region $\mathbb{H}_{VU}{}^i$ is identified, only the phase combinations of grid-connected PV systems in the highest unbalance region, $\mathbb{H}_{VU}{}^i$, are randomly changed to generate the updated phase combination, $x^i(j+1,k,l)$. This reduces the number of possible phase configurations greatly, while mitigating the impact of re-phasing on the overall network. However, the random change in the phases of PV systems in the highest unbalance region $\mathbb{H}_{VU}{}^i$ does not guarantee that it finds a phase combination with a lower cost value compared to its present phase combination $x^i(j,k,l)$ at once. Therefore, in such a situation, the random phase changing is repeated until it finds a suitable phase combination with lower-cost value, within a maximum of N_r iterations. If D-Chemotaxis is unable to find a phase combination with lesser cost value within the maximum N_r cycles, then the present phase combination $x^i(j,k,l)$ is retained as its updated phase combination $x^i(j+1,k,l)$ as it is reasonable to assume that we have reached a low-cost point through random changes.

The pseudocode of the D-chemotaxis procedure is given in Algorithm 1 and the main steps are depicted in Fig. 5.

Algorithm 1: D-Chemotaxis	
Step 1:	Perform a load flow analysis for the phase combination in i-th PV configuration vector, $x^i(j,k,l)$.
Step 2:	Evaluate the cost function-$J(i,j,k,l)$ based on the load flow results, and set$J_{last} = J(i,j,k,l)$.
Step 3:	Identify the busbar with the highest voltage unbalance $n_{VUF_{max}}$ and, then identify the busbars within the radius of k_n busbars from the busbar with highest unbalance $n_{VUF_{max}}$ to form the highest unbalance region, $\mathbb{H}_{VU}$.
Step 4:	Randomly change the phase combination of PV systems in the highest unbalance region $\mathbb{H}_{VU}$ to find a phase combination with lower-cost value compared to J_{last}.
Step 5:	If a suitable phase combination is identified within N_r steps, then use that phase combination as the updated phase combination, $x^i(j+1,k,l)$.
Step 6:	Else, $x^i(j+1,k,l) = x^i(j,k,l)$.

4.2.2. Discrete reproduction (D-reproduction)

In D-Reproduction, the PV configuration vector having the highest cumulative cost (i.e. worst PV configuration) is eventually replaced by the PV configuration vector with the least cumulative cost (i.e. best PV configuration). The cumulative cost of the i-th PV configuration vector (J_C^i) for a given k and l was calculated from,

$$J_C^i = \sum_{j=1}^{N_c+1} J(i,j,k,l) \tag{10}$$

The pseudocode of the D-Reproduction step is given in Algorithm 2.

Algorithm 2: D-Reproduction	
Step 1:	Determine the cumulative cost J_C of all the PV configuration vectors for given k and l from Eq. (10).
Step 2:	Replace the phase combination of the PV configuration vector having the highest cumulative cost by the phase combination of the PV configuration vector having the least cumulative cost.

4.2.3. Discrete elimination dispersal (D-elimination dispersal)

In D-Elimination Dispersal, some PV configuration vectors are randomly liquidated (eliminated) with a very small probability P_{ed} while the new replacements are randomly initialized over the search space. The D-Elimination Dispersal operator helps PV combinations that are trapped in local minima to escape.

The pseudocode of the D-Elimination Dispersal step is given in Al-

Table 6
The capacity of loads and power factor values at each busbar.

Busbar	Active power/(kW)			pf	Busbar	Active power/(kW)			pf
	P^{a}_{max} (kW)	P^{b}_{max} (kW)	P^{ac}_{max} (kW)			P^{a}_{max} (kW)	P^{b}_{max} (kW)	P^{c}_{max} (kW)	
1	2.19	0.55	1.85	0.981	**35**	0.85	0.88	0.75	0.949
1	1.28	0.46	0.55	0.991	**36**	0.67	1.45	1.27	0.945
1	2.43	0.28	1.88	0.913	**37**	0.79	0.66	1.24	0.965
2	2.33	0.26	1.50	0.991	**37**	1.91	1.14	1.63	0.971
3	0.19	0.45	0.34	0.963	**38**	1.97	1.55	1.27	0.975
3	0.12	0.69	0.68	0.910	**41**	1.72	1.05	2.01	0.928
4	0.33	0.58	0.17	0.928	**41**	1.35	1.15	1.39	0.968
4	0.48	0.52	1.08	0.955	**42**	0.47	0.60	0.32	0.966
5	0.54	1.36	0.69	0.996	**42**	1.27	1.50	1.11	0.916
5	1.43	1.43	1.33	0.996	**43**	1.97	0.30	2.12	0.912
6	1.53	2.22	0.64	0.916	**43**	1.27	1.04	0.87	0.950
6	1.04	0.78	0.27	0.997	**44**	0.98	0.25	1.86	0.996
7	0.24	0.25	0.29	0.996	**44**	1.72	0.65	0.41	0.934
7	0.56	1.24	0.79	0.949	**45**	1.06	1.71	1.81	0.959
8	0.54	1.09	2.46	0.980	**45**	0.70	0.76	1.02	0.922
8	1.76	0.42	0.90	0.914	**45**	0.41	2.49	1.99	0.975
9	1.03	2.79	0.86	0.942	**45**	0.69	1.43	1.07	0.926
9	1.18	0.51	0.99	0.992	**46**	0.46	0.15	0.18	0.951
10	0.91	4.05	0.06	0.979	**46**	2.11	1.02	1.85	0.970
13	1.39	1.45	0.74	0.996	**46**	1.01	1.88	1.50	0.989
14	0.16	0.38	0.15	0.966	**47**	1.22	1.05	1.22	0.996
15	4.93	1.57	0.14	0.904	**47**	2.59	1.19	1.10	0.955
15	1.39	2.17	0.32	0.985	**47**	1.39	2.61	0.29	0.914
16	0.96	0.90	0.53	0.993	**50**	2.03	0.89	1.17	0.915
16	1.44	2.95	0.50	0.968	**51**	2.05	0.87	1.86	0.926
17	0.77	0.69	0.72	0.976	**51**	0.48	0.17	0.54	0.984
17	0.92	1.05	0.82	0.974	**52**	0.42	0.43	0.24	0.925
18	0.21	0.74	1.13	0.939	**52**	1.20	1.57	1.52	0.981
18	1.03	1.18	1.88	0.966	**53**	0.59	0.29	0.81	0.924
19	0.34	2.01	1.63	0.917	**53**	1.76	2.61	0.42	0.993
19	1.51	1.04	1.44	0.971	**54**	0.78	1.12	0.89	0.935
20	1.14	1.03	0.21	0.903	**54**	3.42	1.45	0.18	0.920
21	0.73	0.58	0.97	0.928	**55**	0.16	0.04	0.19	0.925
22	1.37	1.89	0.52	0.905	**55**	0.13	0.09	0.06	0.962
22	1.32	1.94	1.02	0.910	**56**	2.36	1.45	0.97	0.947
23	1.28	1.45	1.56	0.982	**57**	0.76	1.03	1.79	0.935
23	0.40	0.27	0.21	0.969	**57**	1.56	0.83	0.99	0.983
24	0.26	0.07	0.26	0.932	**58**	1.69	0.33	1.56	0.959
25	0.90	1.99	0.69	0.995	**58**	1.32	1.37	1.60	0.955
26	2.04	1.80	0.84	0.903	**59**	0.98	1.85	3.82	0.992
27	4.62	0.12	0.30	0.944	**59**	0.95	0.68	0.75	0.929
28	0.52	2.18	1.98	0.938	**60**	0.99	1.35	1.45	0.976
29	0.27	0.59	0.42	0.977	**60**	0.74	1.04	0.81	0.975
30	1.35	2.42	0.72	0.980	**61**	0.98	1.85	3.82	0.938
35	2.25	0.92	0.82	0.919	**62**	0.95	0.68	0.75	0.957

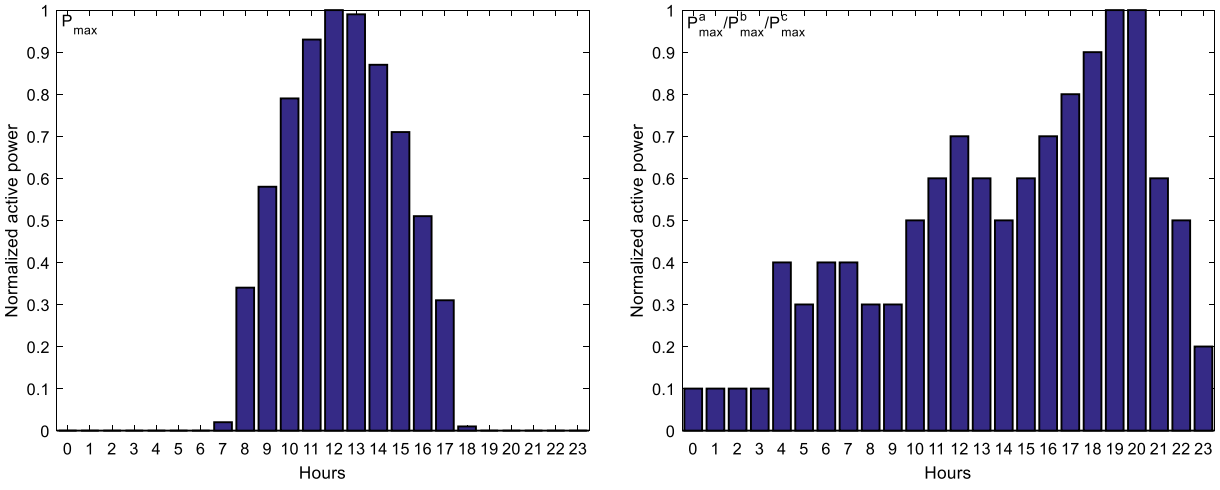

Fig. 9. (a) Hourly generation profile of PV systems (b) hourly load profile for single-phase/ three-phase loads.

gorithm 3.

Algorithm 3: D-Elimination Dispersal	
Step 1:	For all PV configuration vectors (i.e. for $i = 1, 2, 3, \cdots, S$) repeat the following steps to perform D-Elimination dispersal.v
Step 2:	Generate a Random Number between 0 and 1:$RN^i = rand(0, 1)$.
Step 3:	If $RN^i \leq P_{ed}$, Replace the phase combination in i-th PV configuration vector by a random phase combination.
Step 4:	Else, proceed to Step 2 for the next PV configuration vector $(i = i + 1)$.

4.3. Initialization of PV configuration vectors

The BFOA is a population-based optimization algorithm. Hence, the quality of the optimal solution and the time to convergence heavily depend on the initial population (in this paper the initial population is also referred to as the set of PV configuration initializers to add more contextual flavor). In most of the situations, the initial population is randomly selected from the solution space. However, it has been noted that random initialization is not an effective way to initialize the PV configuration initializers, especially when more contextual information is available to better optimize the selection of the initial points. Therefore, a novel initialization method was introduced to identify the suitable phase combinations for PV configuration initializers. A performance comparison is added in the results and discussion to highlight the effectiveness of the proposed initialization technique.

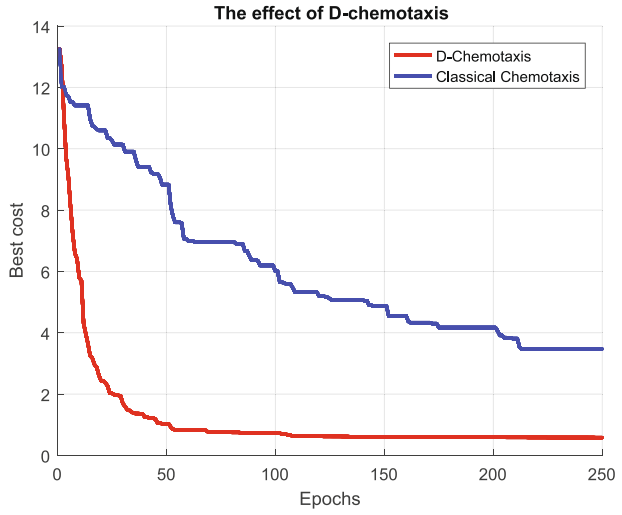

Fig. 10. The effect of D-chemotaxis on the convergence of DBFOA.

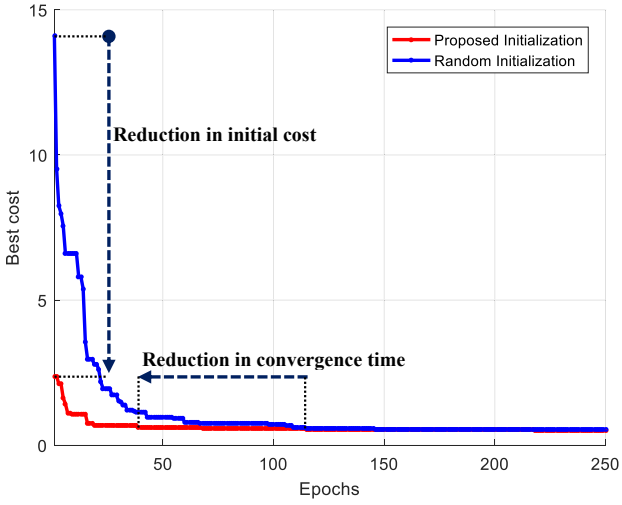

Fig. 11. Convergence of the DBFOA for proposed and random initialization methods.

The proposed initialization method determines the initial phase combinations for the PV configuration initializers in such a way that those initial phase combinations have a smaller active power mismatch (see algorithm 4, step 4) at the secondary side of the MV-LV transformer. The suitable phase combinations with smaller active power mismatch were selected from the brute force checking strategy where the active power mismatch for the whole solution space is computed to identify the phase combinations that have smaller active power mismatch.

However, it was observed that for an LVDG network having a large number of grid-connected PV systems, the brute force searching takes a longer time to find a set of suitable phase combinations with smaller active power mismatch because the algorithm needs to go through the entire solution space to identify the phase combinations that have smaller active power mismatch. For an example, let us consider the network used for the simulation (see Fig. 9) which has 26 number of grid-connected PV systems. For this network, the initialization algorithm should go through approximately $3^{26} \approx 2.54$trillion possible phase combinations (solutions) to identify the best phase combinations having smaller active power mismatch if the partitioning of the network is not considered. This not only leads to a longer execution time but also requires massive computer memory to execute the algorithm.

As a solution to the above problem, the network was partitioned into smaller zones/regions $(R_1, R_2, R_3, \cdots)$ which have about 2–6 nearby grid-connected PV systems, which are then utilized to identify phase combinations with smaller active power mismatch for each zone (see Fig. 9). In this way, the possible phase combinations (solutions) of each zone is in the order of hundreds $(3^6 = 729)$ and the initialization can be done very fast according to the algorithm outlined in Algorithm 4. In addition, this method does not require a large memory to execute and can also be executed in parallel for all the zones at the same time to make the initialization even faster. In other words, a regional minimization is performed to facilitate global optimization. The proposed initialization process is graphically illustrated in Fig. 6 and the pseudocode is given in Algorithm 4.

Algorithm 4: Initialization of PV configuration initializers	
Step 1:	Collect active power consumption of loads and the active power generation by PV systems through smart meters.
Step 2:	Partition the large network into smaller regions $(R_1, R_2, R_3, \cdots, R_r)$.
Step 3:	Identify the solution space (i.e. all possible phase combinations) for each region. Note: For a region having w number of grid-connected PV systems, there are 3^w possible phase combinations in the solution space.
Step 4:	***Execute in parallel for*** $R_1, R_2, R_3, \cdots, R_r$***:*** (1) Calculate the active power mismatch for each phase combination in the solution space. The active power mismatch is quantified by the standard deviation of the three-phase active power in that region. (2) Identify $k_R (= 4)$ phase combinations having a smallest active power mismatch among the all possible phase combinations.
Step 5:	Randomly combine the identified phase combinations for each region to form the initial phase combinations for PV configuration initializers.

4.4. Implementation of DBFOA

4.4.1. The complete structure of the proposed DBFOA

The complete structure of the proposed DBFOA is shown in Fig. 7.

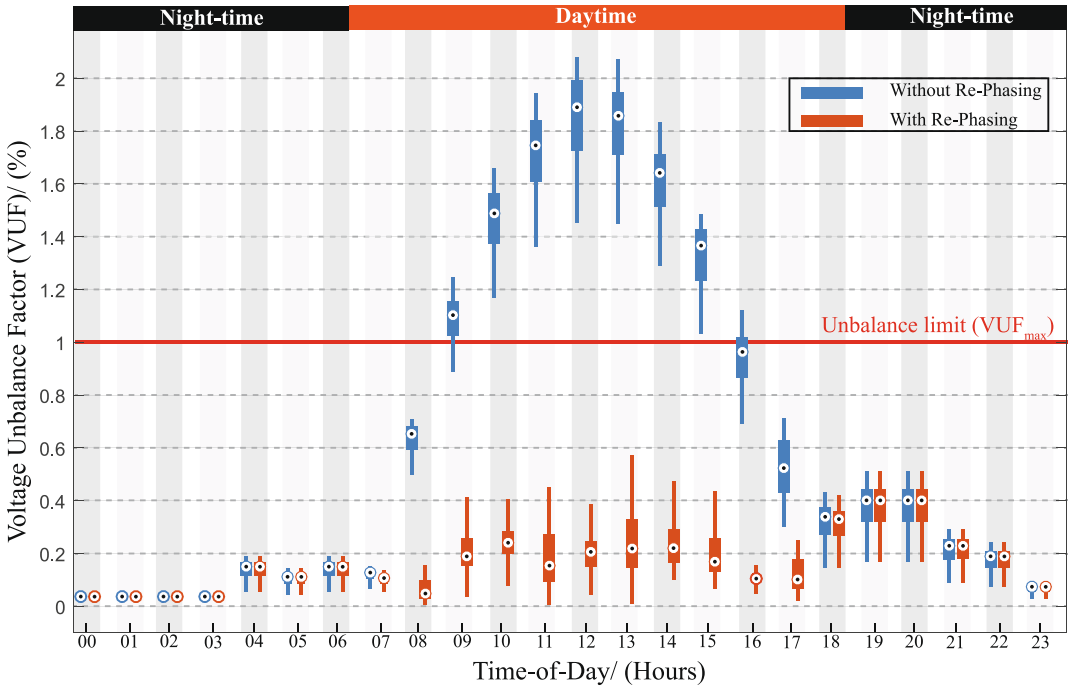

Fig. 12. Distribution of voltage unbalance values of the network throughout the day for 'with' and 'without' PV re-phasing.

4.4.2. Pseudocode of DBFOA

The pseudocode of the proposed DBFOA applied to reduce overall unbalance of a network is given in Algorithm 5.

Algorithm 5: The proposed DBFOA

Step 1: **Initialize all the PV configuration initializers - x^i (use Algorithm 4). Initialize of the following parameters:**

- S : The number of PV configuration initializers.
- N_c : The maximum number of D-Chemotaxis is performed.
- N_s : The Maximum number of times random phase changing is performed.
- N_{re} : The maximum number of times D-Reproduction is performed.
- P_{ed} : The probability that each *PV configuration vectors* are eliminated.

Set all loop counters to zero.

- Incremental counter for D-Elimination dispersal step $(l) = 0$.
- Incremental counter for D-Reproduction step $(k) = 0$.
- Incremental counter for D-Chemotaxis step $(j) = 0$.
- Index of the PV configuration vectors$(i) = 0$.

Step 2: D-Elimination Dispersal loop: $l = l + 1$.

Step 3: D-Reproduction loop: $k = k + 1$.

Step 4: **D-Chemotaxis loop**, $j = j + 1$. **[Algorithm 1]**

A. **For** $i = 1, 2, \cdots, S$, execute a D-Chemotaxis step for i-th PV configuration vector as follows.
B. Perform a load flow analysis for the phase combination in i-th PV configuration vector - $\boldsymbol{x}^i(j,k,l)$ to obtain three-phase voltages and voltage unbalance factors.
C. Evaluate the cost function $J(i,j,k,l)$.
D. Let $J_{last} = J(i,j,k,l)$ so that the PV configuration vector having a lower cost could be identified.
E. Identify the highest voltage unbalance region $\mathbb{H}^i_{VU}$ corresponding to phase combination $\boldsymbol{x}^i(j,k,l)$ from the voltage unbalance factors obtained in **Step 4B.**
F. Set: random phase changing loop counter to zero, $r = 0$.
G. **While** $r < N_r$,
   i. Increment the random phase changing loop counter: $r = r + 1$.
   ii. Randomly change the phase combination of the PV systems in the highest unbalance region to determine the new phase combination of i-th PV configuration vector $\boldsymbol{x}^i(j+1,k,l)$.

(*continued on next column*)

(*continued*)

Algorithm 5: The proposed DBFOA

   iii. Evaluate the cost function $J(i,j+1,k,l)$ corresponding to the phase combination $\boldsymbol{x}^i(j+1,k,l)$.
   iv. **If:** $J(i,j+1,k,l) < J_{last}$,
   v. Go to the next PV configuration vector $(i = i+1)$ (i.e. Go to **Step 4B.** to process the next PV configuration vector).
   vi. **Else:**
   vii. Go to **Step 4 G.**
H. **End of while.**
I. Couldn't find a phase combination better than $\boldsymbol{x}^i(j,k,l)$.
J. Set $\boldsymbol{x}^i(j+1,k,l) = \boldsymbol{x}^i(j,k,l)$.
K. Go to the next PV configuration vector $(i = i+1)$ (i.e. Go to **Step 4B.** to process the next PV configuration vector).

Step 5: **If,** $j < N_c$ go to **Step 4** $(j = j+1)$ In this case, continue D-Chemotaxis.**Else,** go to **Step 6.**

Step 6: **D-Reproduction** [Algorithm 2]:

A. For the given k and l, and for each $i = 1, 2, \cdots,$ Sevaluate the cumulative cost of i-th PV configuration vector as follows:

$$J^i_C = \sum_{j=1}^{N_c+1} J(i,j,k,l) \quad (11)$$

B. Replace the phase combination of the PV configuration vector having the highest cumulative cost by the phase combination of the PV configuration vector having the least cumulative cost.

Step 7: **If** $k < N_{re}$, go to **Step 3** $(k = k + 1)$. We have not reached the number of specified D-reproduction steps, so we start the next generation of the D-Chemotaxis loop.**Else,** go to **Step 8.**

Step 8: **D-Elimination Dispersal** [Algorithm 3]:

- **For** $i = 1, 2, \cdots, S$, eliminate PV configuration vectors with probability P_{ed} while the new replacements are randomly initialized over the search space.

Step 9: **If,** $l < N_{ed}$, go to *Step 2* $(l = l + 1)$;**Else,** End.

4.4.3. Parameters of DBFOA

The parameter values used in the proposed DBFOA are given in Table 3. The number of PV configuration initializers (S), and the values for N_c, N_r, N_{re}, and N_{ed} were selected by considering the convergence speed of the DBFOA and the values used in the previous studies [40,55,57]. The elimination-dispersal probability - P_{ed} and the radius of

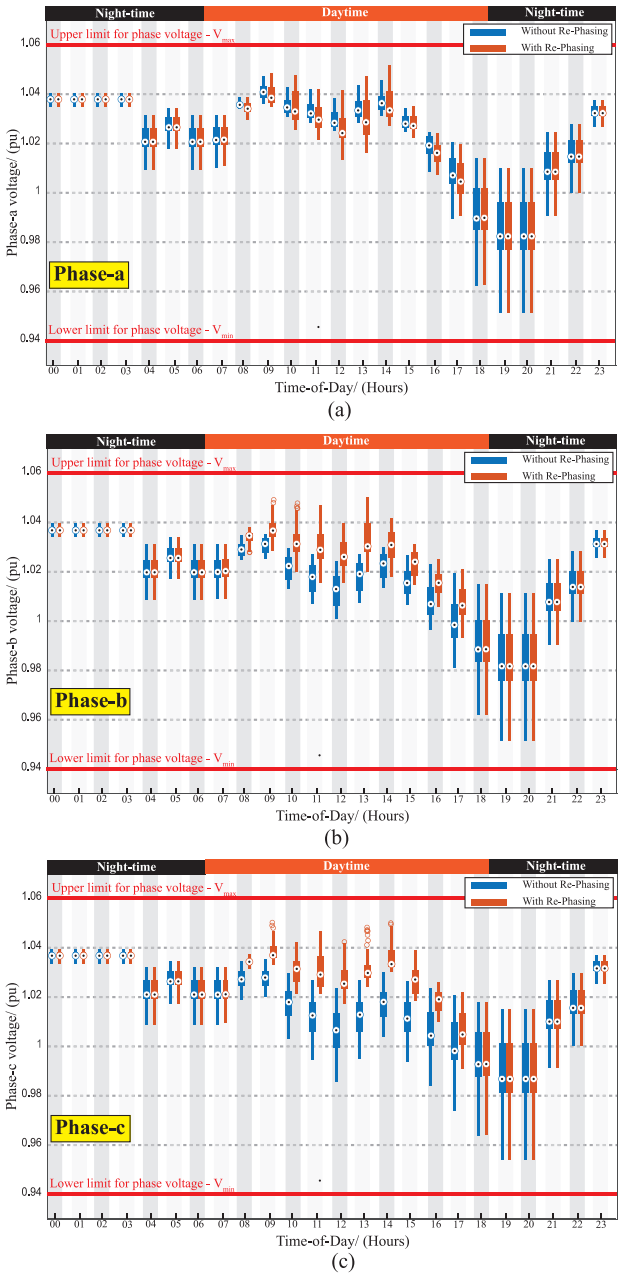

Fig. 13. Evolution of (a) phase-a, (b) phase-b, and (c) phase-c voltage of the network throughout the day for 'with' and 'without' PV re-phasing.

the highest unbalance region - k_n were selected to maximize the convergence speed of DBFOA by executing the algorithm for a possible range of values for P_{ed} and k_n.

5. Test network

The network topology with 63 busbars as shown in Fig. 8 was used for the simulations. The number 0 node is the root node and connected to the secondary side of the MV-LV transformer. The rated capacity of the transformer is 400 kVA and the input/output voltage rating is 11 kV/ 415 V. The solid lines in Fig. 8 represent the three-phase feeders with three-phase or single-phase loads and PV systems connected. The per length impedance matrix of the feeder line is given in Table 4.

There are 26 grid-connected single-phase PV systems and 92 single-phase or three-phase loads. The capacity of PV systems, their locations, and their default phase configuration are given in Table 5 and the daily operation curve (hourly generation profile) of PV systems is shown in Fig. 9(a).

Moreover, the network shown in Fig. 8 consists of 92 single-phase and three-phase loads. The maximum capacity of loads and their power factor values at each busbar are given in Table 6, and the hourly load profile of loads is shown in Fig. 9(b).

6. Results and discussion

6.1. Convergence characteristics of the proposed DBFOA

6.1.1. The effect of D-Chemotaxis

This section demonstrates the effectiveness of the D-Chemotaxis procedure utilized in DBFOA. The proposed D-Chemotaxis is specially designed for the PV re-phasing problem as opposed to merely directly adopting it from classical chemotaxis. The proposed D-Chemotaxis identifies the region around the busbar with the highest unbalance ($\mathbb{H}_{VU}$) and then, only the phase combination of grid-connected PV systems in that region are randomly changed to find the optimal solution iteratively. However, in classical chemotaxis, a fixed number of PV systems are randomly selected from the network and then, the phase configurations of those PV systems are randomly changed. This random selection of PV systems in classical chemotaxis may result in the formation of much higher unbalance levels in the network, thus, ultimately resulting in slower convergence.

Since the increase in voltage unbalance levels of a particular region of a network is mainly due to the mismatch of active and reactive power levels in the same region, the proposed D-chemotaxis step randomly changes the phase configuration of PV systems in the highest unbalance region iteratively. This could lead to a dramatic increase in the convergence speed of the DBFOA as shown in Fig. 10. According to the results, the proposed D-chemotaxis step in the DBFOA resulted in faster convergence of the algorithm when compared to the classical chemotaxis under the same conditions (same initial population, same values for parameters, etc.). Also, the proposed chemotaxis step causes the optimal solution to settle in a place with lower cost value as opposed to classical chemotaxis where final settling cost is much higher as Fig. 10 depicts.

6.1.2. Effect of the initialization of the PV configuration initializers

As described in Section 4.3, an active power balancing approach was introduced to find initial phase combinations for the PV configuration initializers as opposed to the random initialization of the classical technique. Fig. 11 depicts the convergence properties of the DBFOA under two cases: (1). The PV configuration initializers were initialized based on the active power balancing technique and (2). The PV configuration initializers were randomly initialized. According to the results, the starting cost of DBFOA under the proposed power balancing initialization is approximately 83% lower than the random initialization. This implies that the active power balancing technique was able to generate phase combinations that are closer to the optimal phase combination. Ultimately, the DBFOA with the proposed initialization technique converged to the optimal solution with fewer iterations compared to the random initialization.

6.2. Effects of PV re-phasing

This section demonstrates the effect of PV re-phasing on voltage unbalance and phase voltage magnitudes of residential distribution grid with high penetration of solar power. The proposed PV re-phasing algorithm was implemented on the real distribution network shown in Fig. 8. The variations of loads and PV power generation throughout the day were considered in the simulations by utilizing hourly load and PV generation profiles shown in Fig. 9.

The goal of PV re-phasing is to reduce overall voltage unbalance

Table 7
Hourly phase configurations of rooftop PV systems determined by the proposed DBFOA. The colored cells in the table represent the phase configuration of rooftop solar systems that are not changed in the subsequent hour.

Time	Hourly phase configuration of rooftop PV systems (a = Phase a, b = Phase b, and c= Phase c)																								
	1	2	3	4	5	6	7	8	9	10	11	12	13	14	15	16	17	18	19	20	21	22	23	24	25	26
6 - 7 am	b ↓	b ↓	a ↓	a ↓	c ↓	b ↓	c ↓	c ↓	b ↓	b ↓	a ↓	b ↓	c ↓	a ↓	a ↓	a ↓	a ↓	a ↓	a ↓	a ↓	a ↓	b ↓	a ↓	b ↓	b ↓	a ↓
7 - 8 am	a ↓	a ↓	a ↓	b ↓	a ↓	a ↓	b ↓	a ↓	a ↓	c ↓	a ↓	c ↓	a ↓	a ↓	c ↓	b ↓	a ↓	a ↓	a ↓	a ↓	a ↓	a ↓	b ↓	b ↓	a ↓	a ↓
8 - 9 am	a ↓	a ↓	a ↓	a ↓	a ↓	a ↓	a ↓	b ↓	b ↓	a ↓	a ↓	a ↓	b ↓	b ↓	a ↓	a ↓	a ↓	a ↓	a ↓	a ↓	b ↓	b ↓	b ↓	a ↓	a ↓	a ↓
9 - 10 am	a ↓	c ↓	a ↓	b ↓	b ↓	a ↓	a ↓	c ↓	b ↓	c ↓	c ↓	b ↓	b ↓	a ↓	b ↓	c ↓	a ↓	a ↓	a ↓	a ↓	a ↓	a ↓	a ↓	a ↓	b ↓	a ↓
10 - 11 am	c ↓	a ↓	c ↓	a ↓	a ↓	c ↓	a ↓	a ↓	b ↓	a ↓	b ↓	c ↓	a ↓	a ↓	c ↓	b ↓	b ↓	a ↓	b ↓	c ↓	b ↓	a ↓	a ↓	a ↓	a ↓	b ↓
11 - 12 am	a ↓	a ↓	a ↓	a ↓	b ↓	a ↓	a ↓	a ↓	a ↓	c ↓	c ↓	b ↓	c ↓	b ↓	b ↓	c ↓	a ↓	b ↓	a ↓	a ↓	a ↓	a ↓	a ↓	a ↓	a ↓	a ↓
12 - 1 pm	b ↓	a ↓	a ↓	a ↓	a ↓	a ↓	a ↓	c ↓	c ↓	a ↓	b ↓	a ↓	a ↓	a ↓	b ↓	a ↓	a ↓	a ↓	a ↓	b ↓	a ↓	b ↓	a ↓	a ↓	b ↓	b ↓
1 - 2 pm	a ↓	b ↓	a ↓	a ↓	a ↓	a ↓	a ↓	a ↓	b ↓	b ↓	c ↓	b ↓	b ↓	b ↓	a ↓	b ↓	a ↓	a ↓	b ↓	a ↓	c ↓	b ↓	a ↓	a ↓	a ↓	a ↓
2 - 3 pm	a ↓	a ↓	b ↓	a ↓	a ↓	a ↓	a ↓	a ↓	a ↓	c ↓	a ↓	c ↓	a ↓	a ↓	c ↓	a ↓	a ↓	a ↓	a ↓	a ↓	b ↓	a ↓	c ↓	b ↓	a ↓	a ↓
3 - 4 pm	a ↓	a ↓	a ↓	a ↓	a ↓	a ↓	a ↓	b ↓	b ↓	b ↓	a ↓	b ↓	b ↓	b ↓	b ↓	b ↓	a ↓	a ↓	a ↓	a ↓	b ↓	b ↓	a ↓	a ↓	a ↓	a ↓
4 - 5 pm	a ↓	a ↓	a ↓	a ↓	a ↓	a ↓	a ↓	c ↓	b ↓	b ↓	c ↓	b ↓	b ↓	b ↓	a ↓	c ↓	a ↓	a ↓	a ↓	a ↓	b ↓	b ↓	a ↓	a ↓	a ↓	a ↓
5 - 6 pm	a ↓	a ↓	a ↓	a ↓	b ↓	b ↓	a ↓	a ↓	a ↓	b ↓	a ↓	a ↓	c ↓	c ↓	b ↓	b ↓	a ↓	b ↓	a ↓	a ↓	b ↓	a ↓	a ↓	a ↓	a ↓	a ↓
6 - 7 pm	a ↓	a ↓	a ↓	a ↓	a ↓	a ↓	a ↓	a ↓	b ↓	a ↓	b ↓	b ↓	a ↓	b ↓	a ↓	a ↓	a ↓	a ↓	a ↓	a ↓	a ↓	b ↓	a ↓	a ↓	a ↓	a ↓
7 - 8 pm	a ↓	b ↓	a ↓	b ↓	a ↓	a ↓	b ↓	b ↓	c ↓	b ↓	b ↓	b ↓	c ↓	c ↓	c ↓	c ↓	a ↓	a ↓	b ↓	a ↓	c ↓	c ↓	a ↓	a ↓	b ↓	b ↓

$\left(\overline{\text{VUF}}\right)$ of the network by dynamically changing the phase configuration of rooftop solar systems in the network. Figs. 12 and 13 clearly illustrate the effect of PV re-phasing on the overall voltage unbalance and phase voltages, respectively. According to Fig. 12, significantly high voltage unbalances are observed during the daytime when PV systems have a fixed phase configuration. Whereas the dynamic PV re-phasing significantly reduces the overall voltage unbalance of the network (mean unbalance is below 1%) especially during the period from 8 am to 5 pm, where high PV penetration is present. In addition, Table 7 provides the optimal phase configuration of PV systems that are determined from the proposed DBFOA from 6 am to 7 pm. The colored cells in Table 7 belong to the phases of PV systems that are not changed in the subsequent hour.

Since not each rooftop PV system is subjected to PV re-phasing at each hour, SCADA needs to send the PV re-phasing commands only for the rooftop solar systems that are required to re-phase in the next PV-rephasing operation. Moreover, the proposed algorithm can be improved to minimize the number of PV re-phasing operations that each rooftop PV system undergoes throughout the day by modifying the cost function of the optimization algorithm. Finally, these results confirm that the proposed re-phasing strategy is successful in reducing the voltage unbalance levels of domestic distribution grids that have many grid-connected rooftop PV systems, while simultaneously maintaining the phase voltages within their acceptable limits.

Since the proposed PV re-phasing technique can maintain the voltage imbalances of the network well below the 1% threshold during the

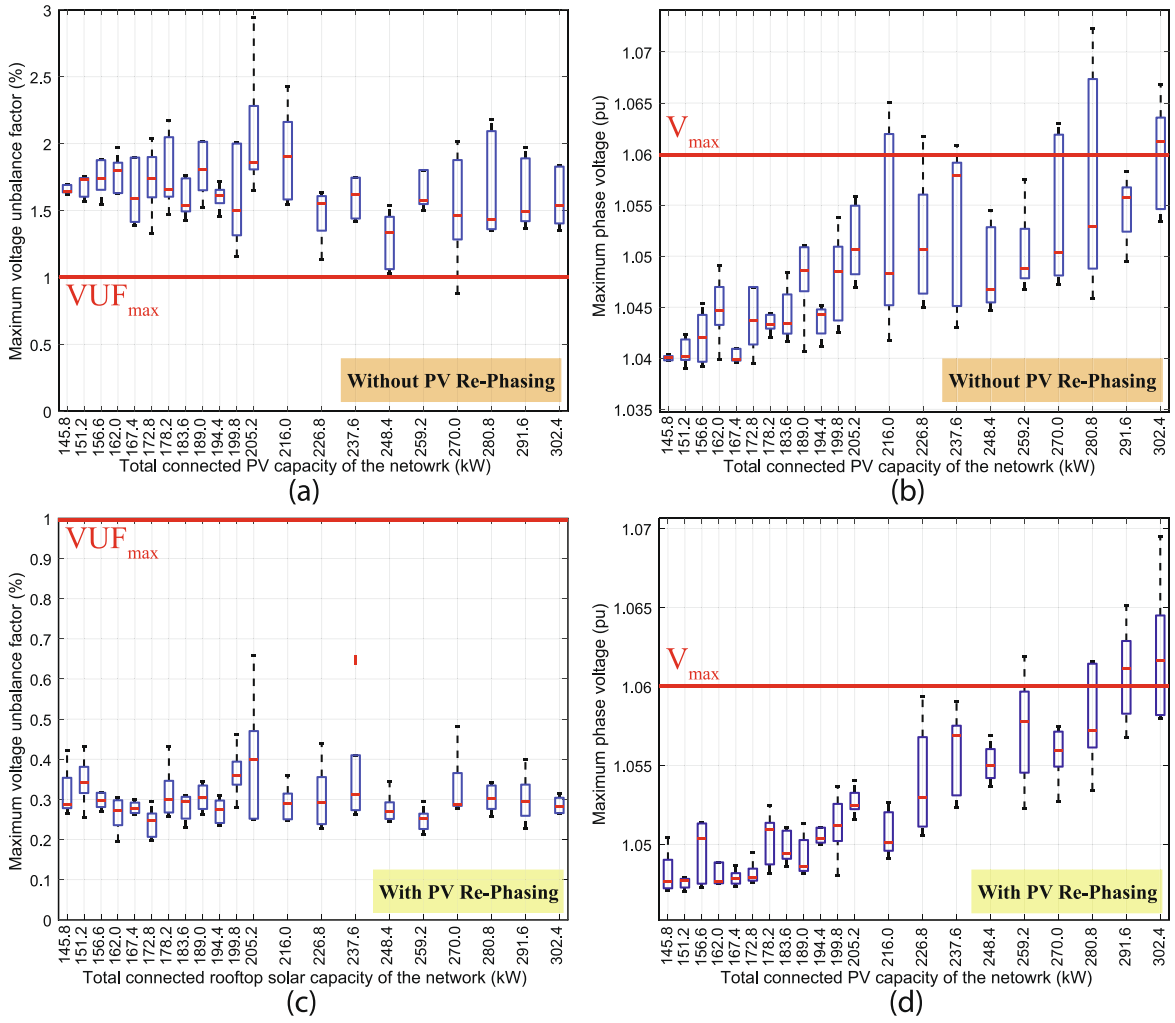

Fig. 14. Variation of (a) maximum voltage unbalance and (b) maximum voltage unbalance with the total connected PV capacity of the LVDG network for "without" re-phasing. Variation of (c) maximum voltage unbalance and (d) phase voltage magnitude with the total connected rooftop solar capacity for "with" re-phasing.

daytime while keeping the phase voltages within their acceptable voltage range, utility providers can allow additional rooftop solar systems into the network. In order to get a clear idea about the amount of additional renewable energy capacity facilitated by the PV re-phasing operation, simulations were performed by adding new rooftop solar systems (on top of existing 140.4 kW of solar PV as specified by Table 5) to the existing network. For each addition of a new rooftop solar system, 20 Monte-Carlo simulations were performed by randomly changing its connection point in the LV network to ensure an unbiased and fair simulation. For this study, the capacity of each new rooftop solar system to be connected to the existing LV network is considered to be 5.4 kW that corresponds to the average capacity of a rooftop PV system in the existing network. The maximum voltage unbalances and maximum phase voltage values of the network recorded for "with" and "without" re-phasing are depicted in Fig. 14.

According to Fig. 14(c), the maximum voltage unbalance of the network is well below the 1% threshold for the proposed PV re-phasing technique even under the integration of new rooftop solar systems up to a total capacity of 302.4 kW. In contrast, as can be seen from Fig. 14(a), the maximum voltage unbalance values of the network exceed the 1% threshold line for the fixed phase configuration. However, as depicted in Fig. 14(b) and (d), the maximum voltage of the network gradually increases with the addition of new rooftop solar systems to the network. Due to this reason, rooftop solar systems with a total capacity of 248.4 kW can be safely integrated into the LV network without violating the statutory limits of both voltage unbalance and phase voltage magnitudes. This is about a 77% increase in the rooftop solar capacity of the network compared to the originally installed solar capacity (140.4 kW). Therefore, it is apparent that the proposed PV re-phasing strategy can completely overcome the voltage unbalance issue due to the installation of distributed energy sources in the LV and facilitate to install additional rooftop solar systems into the network.

In addition, it should be pointed out that the above conclusions are made under the assumption that the voltage unbalance should be kept below 1%, and the phase voltage can vary between 0.94*pu* and 1.06*pu* (±6% tolerance level). However, some countries/regions allow the phase voltage to vary within a larger range, such as 0.9*pu* to 1.1*pu* (that is, a ±10% tolerance level). Under this new voltage limit, the proposed PV re-phasing approach can increase the usable PV capacity of the network to more than *thecapacity* obtained with a voltage tolerance of ±6%. It can be seen from Fig. 14(d) that if the maximum allowable voltage level is 1.1*pu*, solar PV totaling more than 302.4*kW* can be safely integrated into the original network. That is approximately a 115% increase compared to the originally installed solar capacity (140.4*kW*) of the network.

6.3. Comparison of different optimization techniques

In order to predict the superiority of the proposed DBFOA, the convergence characteristics of the proposed DBFOA for the test system is

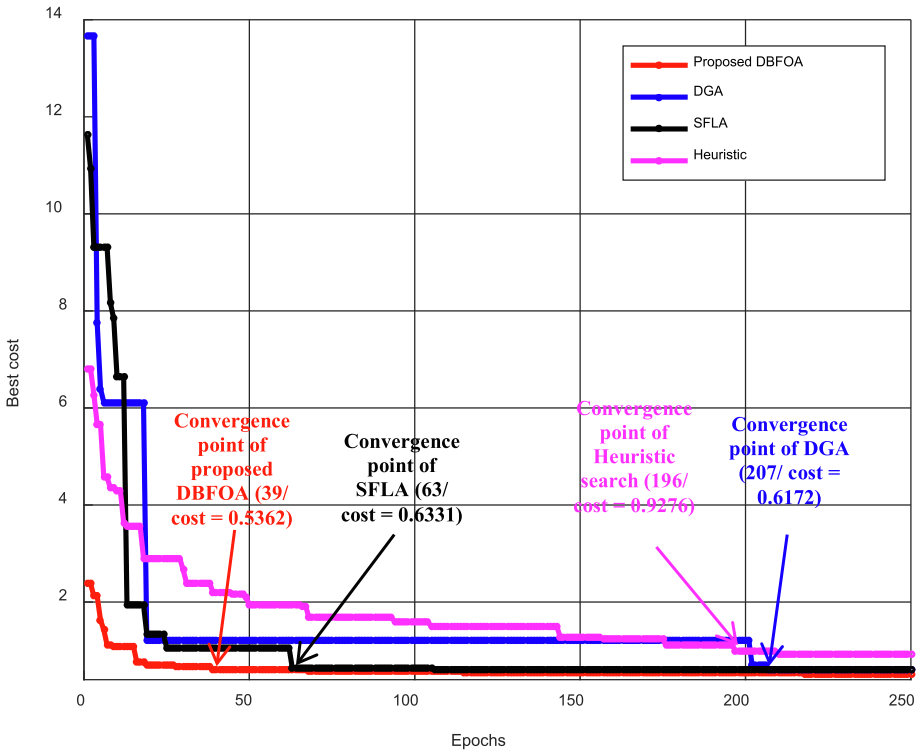

Fig. 15. Performance comparison of proposed DBFOA with DGA, SFLA, and Heuristic search.

Table 8
Computational efficiency of DBFOA, DGA, SFLA, and Heuristic search in terms of CPU time.

Algorithm	Execution time/Epoch (s)	Time to convergence/ (s)	Cost after 250 epochs
Proposed DBFOA	0.888	**33.744**	**0.5362**
DGA	0.846	175.122	0.6172
SFLA	0.897	56.511	0.6331
Heuristic search	0.622	121.912	0.9276

compared with three other widely used optimization algorithms in power systems, namely, Discrete Genetic Algorithm (DGA), Shuffled Frog-Leaping Algorithm (SFLA) and Heuristic Search (HS), and the results are shown in Fig. 15. The algorithms were written on Matlab® (version: R2016a) - Open DSS (version: 8.4.1.1) co-simulation environment and executed on a processor with Intel Core i7-7700HQ with 32 GB RAM running at 3.4 GHz. From the figure, it is clear that the DBFOA only takes 38 iterations to converge to the best solution. In addition to that, DBFOA shows a stable and quick convergence with a global searching capability to find the optimal phase configuration. Thereby, ensuring that the LVDG maintains strict power quality standards, even under heavy PV penetration in a near-real-time fashion.

Table 8 shows the computational performance of the four algorithms. The average execution time of a single epoch for the three algorithms is almost the same. However, the proposed DBFOA converges to the optimal solution very fast compared to DGA, SFLA, and Heuristic Search.

7. Conclusion

In this paper, a novel method was introduced to mitigate the voltage unbalance in LV distribution grids through coordinated re-phasing of grid-connected rooftop PV systems. The optimum phase combination of grid-connected rooftop PV systems is determined from the modified discrete bacterial foraging optimization algorithm (DBFOA) at fixed time intervals. The DBFOA takes smart meter measurements such as load demands and PV generations as the inputs to determine the optimum phase configuration such that the resulting phase combination minimizes the overall voltage unbalance in the network, subject to various operating and network parameters. In order to perform automatic PV re-phasing, a PV re-phasing switch is introduced. This can connect to the output of the single-phase PV inverters to enable the PV re-phasing. To nullify the transient time associated with the automatic re-phasing switch, a half-bridge inverter arrangement is also proposed.

In order to demonstrate the effectiveness of the proposed re-phasing strategy, the PV re-phasing algorithm was simulated on a real LV distribution network. The time-varying nature of loads and solar PV was considered using the hourly load and PV generation profiles. The results show that the proposed re-phasing strategy can significantly reduce the voltage unbalance well below the 1% threshold line as compared to the fixed phase configuration during the daytime where PV penetration is high. Thereby the proposed PV re-phasing strategy facilitates utility providers to allow more rooftop solar systems into LV networks. The proposed case studies demonstrate that PV re-phasing technique can increase the renewable energy penetration into the considered LV network by 77%.

The main advantage of the proposed PV re-phasing technique compared to existing load and feeder reconfiguration techniques is that this method only deals with single-phase PV systems. Hence, it will not create any impact on supply reliability. Furthermore, the initial cost for installation of PV re-phasing switches, and other indirect costs such as customer interruption cost and reliability cost are significantly minimal,

as compared to existing state-of-the-art DFR and phase balancing techniques. The initial cost for installing PV re-phasing switches can be recovered by the long-term economic benefits due to the improvement in usable PV capacity and due to the possibility of operating the system in a near balanced condition. Further, compared to the rephasing arrangements reported in the literature, i.e. introducing rephasing switches to all loads, the cost incurred due to the introduction of re-phasing switches, only to PV plants, makes the proposed method more cost-effective.

The main limitation of this work is that the proposed PV re-phasing method is only effective during the daytime and cannot make a significant reduction to the unbalance factor at night. However, the Volt-Var (Q-control) control can be used to reduce voltage unbalance and improve power quality during night-time, because PV inverters can supply reactive power (Q) to the grid up to their rated capacity at night. Therefore, combining the PV re-phasing technique with Volt-Var control would be an ideal solution and is considered as future research work. In addition, it should be noted that the unbalance reduction capability of the proposed PV re-phasing technique greatly depends on the number of grid-connected rooftop solar systems in the distribution network. Therefore, for distribution systems with a smaller number of grid-connected rooftop solar systems, the number of possible configurations is limited, thus, optimization via fine-tuning through re-phasing is not possible as the number of configurations to adjust is limited. Further, a communication protocol needs to be developed to ensure that the PV re-phasing command issued by the algorithm is actually performed by the switches, because if one/several re-phasing switch commands are not executed due to communication errors or other technical issues, the system can be at a worse state than before. Therefore, improvements should be made to address these, before implementing the proposed PV re-phasing technique in an actual network.

Even though the proposed re-phasing algorithm concentrates on mitigation of voltage unbalance, it is also possible to modify the objective function to minimize the number of PV re-phasings required for each PV re-phasing operation as well. Furthermore, additional research is required to determine the optimal timing for PV re-phasing operations and the effectiveness of a hybrid algorithm based on PV and load re-phasing techniques.

CRediT authorship contribution statement

W.G. Chaminda Bandara: Conceptualization, Methodology, Software, Validation, Writing - original draft, Visualization. **G.M.R.I. Godaliyadda:** Conceptualization, Methodology, Writing - review & editing, Supervision, Project administration, Funding acquisition. **M.P. B. Ekanayake:** Conceptualization, Methodology, Writing - review & editing, Supervision, Project administration, Funding acquisition. **J.B. Ekanayake:** Conceptualization, Methodology, Writing - review & editing, Supervision.

Declaration of Competing Interest

The authors declare that they have no known competing financial interests or personal relationships that could have appeared to influence the work reported in this paper.

Acknowledgment

We would like to acknowledge the financial support provided by the National Science Foundation (NSF), Sri Lanka (research grant no: RG/2018/EA & ICT/01).

References

[1] Jadeja K. Major Technical issues with increased PV penetration on the existing electrical grid. Murdoch University; 2012. https://core.ac.uk/download/pdf/11241964.pdf.
[2] Lu H, Zhao W. Effects of particle sizes and tilt angles on dust deposition characteristics of a ground-mounted solar photovoltaic system. Appl Energy 2018;220:514–26. https://doi.org/10.1016/j.apenergy.2018.03.095.
[3] Peters L, Madlener R. Economic evaluation of maintenance strategies for ground-mounted solar photovoltaic plants. Appl Energy 2017;199:264–80. https://doi.org/10.1016/j.apenergy.2017.04.060.
[4] Zhou Y, Chang F-J, Chang L-C, Lee W-D, Huang A, Xu C-Y, et al. An advanced complementary scheme of floating photovoltaic and hydropower generation flourishing water-food-energy nexus synergies. Appl Energy 2020;275:115389. https://doi.org/10.1016/j.apenergy.2020.115389.
[5] Wang Q, Zhu Z, Wu G, Zhang X, Zheng H. Energy analysis and experimental verification of a solar freshwater self-produced ecological film floating on the sea. Appl Energy 2018;224:510–26. https://doi.org/10.1016/j.apenergy.2018.05.010.
[6] Hong T, Lee M, Koo C, Jeong K, Kim J. Development of a method for estimating the rooftop solar photovoltaic (PV) potential by analyzing the available rooftop area using Hillshade analysis. Appl Energy 2017;194:320–32. https://doi.org/10.1016/j.apenergy.2016.07.001.
[7] Cole W, Lewis H, Sigrin B, Margolis R. Interactions of rooftop PV deployment with the capacity expansion of the bulk power system. Appl Energy 2016;168:473–81. https://doi.org/10.1016/j.apenergy.2016.02.004.
[8] Carpinelli G, Mottola F, Proto D, Varilone P. Minimizing unbalances in low-voltage microgrids: optimal scheduling of distributed resources. Appl Energy 2017;191:170–82. https://doi.org/10.1016/j.apenergy.2017.01.057.
[9] Zehir MA, Batman A, Sonmez MA, Font A, Tsiamitros D, Stimoniaris D, et al. Impacts of microgrids with renewables on secondary distribution networks. Appl Energy 2017;201:308–19. https://doi.org/10.1016/j.apenergy.2016.12.138.
[10] Wang L, Yan R, Saha TK. Voltage regulation challenges with unbalanced PV integration in low voltage distribution systems and the corresponding solution. Appl Energy 2019;256:113927. https://doi.org/10.1016/j.apenergy.2019.113927.
[11] Ma K, Li R, Hernando-Gil I, Li F. Quantification of additional reinforcement cost from severe three-phase imbalance. IEEE Trans Power Syst 2017;32:4143–4. https://doi.org/10.1109/TPWRS.2016.2635383.
[12] Yaghoobi J, Islam M, Mithulananthan N. Analytical approach to assess the loadability of unbalanced distribution grid with rooftop PV units. Appl Energy 2018;211:358–67. https://doi.org/10.1016/j.apenergy.2017.11.030.
[13] Islam MR, Lu H, Hossain MJ, Li L. Mitigating unbalance using distributed network reconfiguration techniques in distributed power generation grids with services for electric vehicles: a review. J Clean Prod 2019;239:117932. https://doi.org/10.1016/j.jclepro.2019.117932.
[14] Ramos-figueroa O, Quiroz-castellanos M, Mezura-montes E. Metaheuristics to solve grouping problems: a review and a case study. Swarm Evol Comput 2020;53:100643. https://doi.org/10.1016/j.swevo.2019.100643.
[15] Fukami T, Onchi T, Naoe N, Hanaoka R. Compensation for neutral current harmonics in a three-phase four-wire system by a synchronous machine. IEMDC 2001. In: IEEE int electr mach drives conf (Cat. No.01EX485), IEEE; n.d., p. 466–70. https://doi.org/10.1109/IEMDC.2001.939346.
[16] Jou H-L, Wu J-C, Wu K-D, Chiang W-J, Chen Y-H. Analysis of zig-zag transformer applying in the three-phase four-wire distribution power system. IEEE Trans Power Deliv 2005;20:1168–73. https://doi.org/10.1109/TPWRD.2005.844281.
[17] Enjeti P, Shireen W, Packebush P, Pitel I. Analysis and design of a new active power filter to cancel neutral current harmonics in three phase four wire electric distribution systems. In: Conf rec 1993 IEEE ind appl conf twenty-eighth IAS annu meet, IEEE; n.d., p. 939–46. https://doi.org/10.1109/IAS.1993.299011.
[18] Singh B, Jayaprakash P, Kothari DP. A T-connected transformer and three-leg VSC based DSTATCOM for power quality improvement. IEEE Trans Power Electron 2008;23:2710–8. https://doi.org/10.1109/TPEL.2008.2004273.
[19] Jayaprakash P, Singh B, Kothari DP. Three-phase 4-Wire DSTATCOM based on H-bridge VSC with a star/hexagon transformer for power quality improvement. In: 2008 IEEE reg 10 third int conf ind inf syst. IEEE; 2008. p. 1–6. https://doi.org/10.1109/ICIINFS.2008.4798378.
[20] Quinn CA, Mohan N. Active filtering of harmonic currents in three-phase, four-wire systems with three-phase and single-phase nonlinear loads. In: [Proceedings] APEC '92 seventh annu appl power electron conf expo., IEEE; n.d., p. 829–36. https://doi.org/10.1109/APEC.1992.228328.
[21] Jou H-L, Wu K-D, Wu J-C, Li C-H, Huang M-S. Novel power converter topology for three-phase four-wire hybrid power filter. IET Power Electron 2008;1:164. https://doi.org/10.1049/iet-pel:20070171.
[22] Sreenivasarao D, Agarwal P, Das B. Neutral current compensation in three-phase, four-wire systems: a review. Electr Power Syst Res 2012;86:170–80. https://doi.org/10.1016/j.epsr.2011.12.014.
[23] Omar AI, Abdel Aleem SHE, El-Zahab EEA, Algablawy M, Ali ZM. An improved approach for robust control of dynamic voltage restorer and power quality enhancement using grasshopper optimization algorithm. ISA Trans 2019;95:110–29. https://doi.org/10.1016/j.isatra.2019.05.001.
[24] Kashem MA, Ganapathy V, Jasmon GB. Network reconfiguration for load balancing in distribution networks. IEE Proc – Gener Transm Distrib 1999;146:563. https://doi.org/10.1049/ip-gtd:19990694.
[25] Babu PR, Kumar KA, Teja GC. New heuristic search approach to enhance the distribution system load balance. In: 2013 int conf power, energy control, IEEE; 2013, p. 159–64. https://doi.org/10.1109/ICPEC.2013.6527642.

[26] Babu PR, Shenoy R, Ramya N, Soujanya, Shetty S. Implementation of ACO technique for load balancing through reconfiguration in electrical distribution system. In 2014 annu int conf emerg res areas magn mach drives, IEEE; 2014, p. 1–5. https://doi.org/10.1109/AICERA.2014.6908233.
[27] Yuehao Y, Zhongqing Z, Wei B, Jun X, Limin Q, Yaoheng D. Optimal distribution network reconfiguration for load balancing. In: 2016 China int conf electr distrib, vol. 2016- Septe, IEEE; 2016, p. 1–4. https://doi.org/10.1109/CICED.2016.7576313.
[28] Taher SA, Karimi MH. Optimal reconfiguration and DG allocation in balanced and unbalanced distribution systems. Ain Shams Eng J 2014;5:735–49. https://doi.org/10.1016/j.asej.2014.03.009.
[29] Fu-Yuan Hsu, Men-Shen Tsai. A multi-objective evolution programming method for feeder reconfiguration of power distribution system. In: Proc 13th int conf on, intell syst appl to power syst, vol. 2005, IEEE; 2005, p. 55–60. https://doi.org/10.1109/ISAP.2005.1599241.
[30] Vitor TS, Vieira JCM. Optimal voltage regulation in distribution systems with unbalanced loads and distributed generation. In: 2016 IEEE innov smart grid technol – asia, IEEE; 2016, p. 942–7. https://doi.org/10.1109/ISGT-Asia.2016.7796512.
[31] Nara K, Mishima Y, Satoh T. Network reconfiguration for loss minimization and load balancing. In: 2003 IEEE power eng soc gen meet (IEEE Cat. No.03CH37491), vol. 4, IEEE; 2003, p. 2413–8. https://doi.org/10.1109/PES.2003.1271019.
[32] Zhou Qin, Shirmohammadi D, Liu W-HE. Distribution feeder reconfiguration for service restoration and load balancing. IEEE Trans Power Syst 1997;12:724–9. https://doi.org/10.1109/59.589664.
[33] Tolabi HB, Ali MH, Shahrin Bin Md, Ayob Rizwan M. Novel hybrid fuzzy-Bees algorithm for optimal feeder multi-objective reconfiguration by considering multiple-distributed generation. Energy 2014;71:507–15. https://doi.org/10.1016/j.energy.2014.04.099.
[34] Ke Y-L, Chen C-S, Kang M-S, Wu J-S, Lee T-E. Power distribution system switching operation scheduling for load balancing by using colored petri nets. IEEE Trans Power Syst 2004;19:629–35. https://doi.org/10.1109/TPWRS.2003.821433.
[35] Lin C-H. Distribution network reconfiguration for load balancing with a coloured Petri net algorithm. IEE Proc – Gener Transm Distrib 2003;150:317. https://doi.org/10.1049/ip-gtd:20030199.
[36] Ji H, Wang C, Li P, Zhao J, Song G, Ding F, et al. An enhanced SOCP-based method for feeder load balancing using the multi-terminal soft open point in active distribution networks. Appl Energy 2017;208:986–95. https://doi.org/10.1016/j.apenergy.2017.09.051.
[37] Diaaeldin I, Abdel Aleem S, El-Rafei A, Abdelaziz A, Zobaa AF. Optimal network reconfiguration in active distribution networks with soft open points and distributed generation. Energies 2019;12:4172. https://doi.org/10.3390/en12214172.
[38] Zhai HF, Yang M, Chen B, Kang N. Dynamic reconfiguration of three-phase unbalanced distribution networks. Int J Electr Power Energy Syst 2018;99:1–10. https://doi.org/10.1016/j.ijepes.2017.12.027.
[39] Santos SF, Fitiwi DZ, Cruz MRM, Cabrita CMP, Catalão JPS. Impacts of optimal energy storage deployment and network reconfiguration on renewable integration level in distribution systems. Appl Energy 2017;185:44–55. https://doi.org/10.1016/j.apenergy.2016.10.053.
[40] Kaveh MR, Hooshmand R-A, Madani SM. Simultaneous optimization of re-phasing, reconfiguration and DG placement in distribution networks using BF-SD algorithm. Appl Soft Comput 2018;62:1044–55. https://doi.org/10.1016/j.asoc.2017.09.041.
[41] Soltani SH, Rashidinejad M, Abdollahi A. Dynamic phase balancing in the smart distribution networks. Int J Electr Power Energy Syst 2017;93:374–83. https://doi.org/10.1016/j.ijepes.2017.06.016.
[42] Zhu Jinxiang, Chow Mo-Yuen, Zhang Fan. Phase balancing using mixed-integer programming [distribution feeders]. IEEE Trans Power Syst 1998;13:1487–92. https://doi.org/10.1109/59.736295.
[43] Zhu J, Bilbro G, Chow Mo-Yuen. Phase balancing using simulated annealing. IEEE Trans Power Syst 1999;14:1508–13. https://doi.org/10.1109/59.801943.
[44] Kuo C-C, Chao Y-T. Energy management based on AM/FM/GIS for phase balancing application on distribution systems. Energy Convers Manag 2010;51:485–92. https://doi.org/10.1016/j.enconman.2009.10.011.
[45] Chitra R, Neelaveni R. A realistic approach for reduction of energy losses in low voltage distribution network. Int J Electr Power Energy Syst 2011;33:377–84. https://doi.org/10.1016/j.ijepes.2010.08.033.
[46] Hooshmand RA, Soltani S. Fuzzy optimal phase balancing of radial and meshed distribution networks using BF-PSO algorithm. IEEE Trans Power Syst 2012;27:47–57. https://doi.org/10.1109/TPWRS.2011.2167991.
[47] Gray MK, Morsi WG. Economic assessment of phase reconfiguration to mitigate the unbalance due to plug-in electric vehicles charging. Electr Power Syst Res 2016;140:329–36. https://doi.org/10.1016/j.epsr.2016.06.008.
[48] Das CK, Bass O, Kothapalli G, Mahmoud TS, Habibi D. Optimal placement of distributed energy storage systems in distribution networks using artificial bee colony algorithm. Appl Energy 2018;232:212–28. https://doi.org/10.1016/j.apenergy.2018.07.100.
[49] BARRY WW. Power Electronics: devices, drives, applications and passive components; 1992.
[50] Dinesh C, Welikala S, Liyanage Y, Ekanayake MPB, Godaliyadda RI, Ekanayake J. Non-intrusive load monitoring under residential solar power influx. Appl Energy 2017;205:1068–80. https://doi.org/10.1016/j.apenergy.2017.08.094.
[51] Welikala S, Thelasingha N, Akram M, Ekanayake PB, Godaliyadda RI, Ekanayake JB. Implementation of a robust real-time non-intrusive load monitoring solution. Appl Energy 2019;238:1519–29. https://doi.org/10.1016/j.apenergy.2019.01.167.
[52] Andreadou N, Kotsakis E, Masera M. Smart meter traffic in a real LV distribution network. Energies 2018;11:1156. https://doi.org/10.3390/en11051156.
[53] Chaminda Bandara WG, Almeida D, Godaliyadda RI, Ekanayake MP, Ekanayake J. A complete state estimation algorithm for a three-phase four-wire low voltage distribution system with high penetration of solar PV. Int J Electr Power Energy Syst 2021;124:106332. https://doi.org/10.1016/j.ijepes.2020.106332.
[54] Wen H, Cheng D, Teng Z, Guo S, Li F. Approximate algorithm for fast calculating voltage unbalance factor of three-phase power system. IEEE Trans Ind Inform 2014;10:1799–805. https://doi.org/10.1109/TII.2014.2327485.
[55] Passino KM. Biomimicry of bacterial foraging for distributed optimization and control. IEEE Control Syst 2002;22:52–67. https://doi.org/10.1109/MCS.2002.1004010.
[56] Das S, Biswas A, Dasgupta S, Abraham A. Bacterial foraging optimization algorithm: theoretical foundations, analysis, and applications. In: Found comput intel, vol. 3. Stud. Comput. Intell., Berlin, Heidelberg: Springer-Verlag; 2009, p. 23–55. https://doi.org/10.1007/978-3-642-01085-9_2.
[57] Devi S, Geethanjali M. Application of Modified Bacterial Foraging Optimization algorithm for optimal placement and sizing of Distributed Generation. Expert Syst Appl 2014;41:2772–81. https://doi.org/10.1016/j.eswa.2013.10.010.
[58] Devabalaji KR, Ravi K, Kothari DP. Optimal location and sizing of capacitor placement in radial distribution system using Bacterial Foraging Optimization Algorithm. Int J Electr Power Energy Syst 2015;71:383–90. https://doi.org/10.1016/j.ijepes.2015.03.008.
[59] Sathish Kumar K, Jayabarathi T. Power system reconfiguration and loss minimization for an distribution systems using bacterial foraging optimization algorithm. Int J Electr Power Energy Syst 2012;36:13–7. https://doi.org/10.1016/j.ijepes.2011.10.016.
[60] Hooshmand R-A, Parastegari M, Morshed MJ. Emission, reserve and economic load dispatch problem with non-smooth and non-convex cost functions using the hybrid bacterial foraging-Nelder–Mead algorithm. Appl Energy 2012;89:443–53. https://doi.org/10.1016/j.apenergy.2011.08.010.

energies

MDPI

Article

A Sensitivity Matrix Approach Using Two-Stage Optimization for Voltage Regulation of LV Networks with High PV Penetration

A.S. Jameel Hassan [1,†], Umar Marikkar [1,†], G.W. Kasun Prabhath [1], Aranee Balachandran [1], W.G. Chaminda Bandara [1], Parakrama B. Ekanayake [1], Roshan I. Godaliyadda [1] and Janaka B. Ekanayake [1,2,*]

[1] Department of Electrical and Electronic Engineering, University of Peradeniya, Peradeniya 20400, Sri Lanka; jameel.hassan.2014@eng.pdn.ac.lk (A.S.J.H.); umar.m@eng.pdn.ac.lk (U.M.); gwkprabhath@eng.pdn.ac.lk (G.W.K.P.); aranee.balachandran@eng.pdn.ac.lk (A.B.); chaminda.bandara@eng.pdn.ac.lk (W.G.C.B.); mpb.ekanayake@ee.pdn.ac.lk (P.B.E.); roshangodd@ee.pdn.ac.lk (R.I.G.)

[2] School of Engineering, Cardiff University, The Parade, Cardiff CF24 3AA, UK

* Correspondence: ekanayakej@cardiff.ac.uk

† These authors contributed equally to this work.

Abstract: The occurrence of voltage violations is a major deterrent for absorbing more rooftop solar power into smart Low-Voltage Distribution Grids (LVDGs). Recent studies have focused on decentralized control methods to solve this problem due to the high computational time in performing load flows in centralized control techniques. To address this issue, a novel sensitivity matrix was developed to estimate the voltages of the network by replacing load flow simulations. In this paper, a Centralized Active, Reactive Power Management System (CARPMS) is proposed to optimally utilize the reactive power capability of smart Photovoltaic (PV) inverters with minimal active power curtailment to mitigate the voltage violation problem. The developed sensitivity matrix is able to reduce the time consumed by 55.1% compared to load flow simulations, enabling near-real-time control optimization. Given the large solution space of power systems, a novel two-stage optimization is proposed, where the solution space is narrowed down by a Feasible Region Search (FRS) step, followed by Particle Swarm Optimization (PSO). The failure of standalone PSO to converge to a feasible solution for 34% of the scenarios evaluated further validates the necessity of the two-stage optimization using FRS. The performance of the proposed methodology was analysed in comparison to the load flow method to demonstrate the accuracy and the capability of the optimization algorithm to mitigate voltage violations in near-real time. The deviations of the mean voltages of the proposed methodology from the load flow method were: 6.5×10^{-3} p.u for reactive power control using Q-injection, 1.02×10^{-2} p.u for reactive power control using Q-absorption, and 0 p.u for active power curtailment case.

Keywords: smart grid; renewable energy integration; rooftop solar PV; PV inverter control; voltage violation

Citation: Hassan, A.S.J.; Marikkar, U.; Prabhath, G.W.K.; Balachandran, A.; Bandara, W.G.C.; Ekanayake, P.B.; Godaliyadda, R.I.; Ekanayake, J.B. A Sensitivity Matrix Approach Using Two-Stage Optimization for Voltage Regulation of LV Networks with High PV Penetration. *Energies* **2021**, *14*, 6596. https://doi.org/10.3390/en14206596

Academic Editors: Saeed Golestan, José Matas and Helena Martin

Received: 23 August 2021
Accepted: 9 October 2021
Published: 13 October 2021

1. Introduction

Over the years, the integration of renewable Distributed Energy Resources (DERs) to Low-Voltage Distribution Grids (LVDGs) has gained high prominence due to technological advancements, increased demand in sustainable energy resources and the advent of decarbonisation programs by many countries [1–3]. In light of the increase in DERs, Photovoltaic (PV) generation systems are shown to be the most effective DER prospect for LVDGs [4]. However, since the conventional LVDG was designed based on the assumption that power flow would be from the primary substation to the loads [5], high PV penetration gives rise to unforeseen problems [6]. The high penetration of rooftop PV in LVDGs can result in reverse power flows [7] and an increase in the neutral current, leading to distribution

and transformer losses due to overheating of the conductor [5,8–11]. A major problem of reverse power flow is the occurrence of upper limit voltage violations, where the node voltage at specific points of LVDGs is greater than the specified limit [12]. Further, studies have revealed that voltage violations can occur at a penetration level as low as 2.5% due to the integration of rooftop PV panels at prosumers' will [13]. If such voltage violations occur over sustained periods of time, it will cause severe damages to loads connected to LVDGs. These detrimental effects of voltage violations compel the utility providers to limit the usable PV capacity for LVDGs. Therefore, there exists a crucial need for an effective solution to encourage the future integration of PV to LVDGs by attempting to mitigate the quality-of-supply ramifications. How to mitigate the voltage violations in LVDGs is a long-standing question to which much time and study have been devoted.

Multiple methods have been proposed in the literature to overcome this problem of voltage violations in LVDGs. Feeder enhancement is one such method based on changing the feeder cable with a larger cable or changing the characteristics of the feeder, such as changing the values of multigrounded resistances [14]. While this improves the voltage limits while decreasing neutral current, the approach is highly expensive. Moreover, given the future consumption and PV penetration possibilities, this is not the most economical solution. A more viable solution is the use of On-Load Tap Changing (OLTC) transformers to change the tap positions to control the voltage levels [15–18]. Furthermore, since frequent tap changes can increase the stress on the transformer, hence reducing its lifespan, a novel optimization algorithm was proposed for resource sharing in [19] to reduce the tap changing operations. However, the drawback of the slow response speed in OLTC switching persists. In order to remedy this issue, fast response devices such as Battery Energy Storage Systems (BESSs) and STATCOMs can be installed [20–24]. A piecewise droop control using a BESS for rapid changes in voltage profiles was presented in [25]. More recently, a reinforcement-learning-based management technique for BESSs was introduced in [26].

A more promising control method is the use of Active Power Curtailment (APC) during high PV penetration [27–30]. Due to the higher impact on voltage profiles by nodes at the farther end of the feeder, most APC operations are performed on distant customers. Since this is not equitable, a fair prosumer-based APC approach was proposed in [31]. A novel approach incorporating the Self-Consumption Ratio (SCR) of the customer to determine the allowable PV injection was developed in [32]. Despite the effectiveness, the spilling of solar power is not an economically attractive solution. Moreover, it is a waste and also detrimental to the whole purpose of renewable energy usage, which is to improve the energy mix such that the renewables receive a larger chunk. A more comprehensive solution to this problem is to utilize the capability of the PV inverters to the fullest to supply reactive power in order to mitigate voltage violations. Whilst this is a cost-effective method requiring no additional installations, mitigating voltage violations in the three-phase unbalanced system using only Reactive Power Control (RPC) is a challenging problem [33,34]. Due to the large R/X ratios of distribution networks, the effect of reactive power control is limited. Therefore, to completely remove the violations in the upper limit, APC is required.

Recent studies have vastly explored the APC and RPC mechanisms to minimize voltage violations. These studies can be categorized into two: local/decentralized control and centralized control methods. Control actions of decentralized control methods rely completely on local measurements [35–39]. A combined approach of RPC and APC as a droop control mechanism to mitigate the voltage violations was proposed in [34]. A Volt-VAR Control (VVC) using two methods to determine the reactive power equation slope was given in [40]. It presented a method with the robust minimization of absolute voltage deviation and a closed-form solution inspired by chance constraints. In [41], a rule-based decentralized RPC was performed taking into account the most sensitive nodes in the network. An optimization technique was developed in [42] to coordinate the fast dispatch of PV inverters with OLTCs in a decentralized manner due to computational burden in

centralized systems. Meanwhile, a two-level control algorithm incorporating OLTCs and BESSs with decentralized RPC was proposed in [43]. Multiple works in the literature have also developed control mechanisms based on droop control [44,45]. Nevertheless, the lack of information about the entire network status in decentralized control prevents the optimal use of reactive power capacity in controlling the voltage violations. Therefore, an uncoordinated management of PV inverters could result in violations shifting from one end of the feeder to another, or even an overkill of reactive power usage [46]. This gap in the lack of coordination among PV inverters has led to the use of optimization techniques based on a centralized system to address this [47]. Moreover, the prevalence of decentralized control has primarily hinged on the computational time burden in centralized systems [48]. However, this constraint is overcome by replacing the time-consuming load flow calculations by the introduced sensitivity matrix approximation in this paper.

However, provided that sufficient information about the network can be retained, centralized control is more efficient compared to decentralized control [46]. Such network state observability is achieved by means of solar predictions [49] and state estimation [50], enabling a control at the tertiary level of the control architecture, as shown in Figure 1. To overcome the lack of information about the network, a global solution is attained by the centralized control method, which determines the power injections/absorptions/curtailment by means of an Optimal Power Flow (OPF) problem [51]. In [52], a comprehensive PV control strategy was proposed to improve the operational performance of significantly unbalanced a three-phase four-wire LVDG with high residential PV penetration, by converting a multi-objective OPF problem into a single-objective OPF problem. A control algorithm was introduced for maintaining the average customer voltage profile obtained before introducing the PV into the circuit using the control of automatic devices, such as voltage regulation and switched capacitor banks along with PV inverter reactive power [53]. Here, the PV inverter control settings were determined by the circuit loading, time of day and PV location in the network. A combination of centralized and decentralized control strategies utilising OLTCs and Capacitor Banks (CBs) was also proposed in [47,54]. It further analysed the impact on the substation end and the effect of unbalance in phases in PV integration.

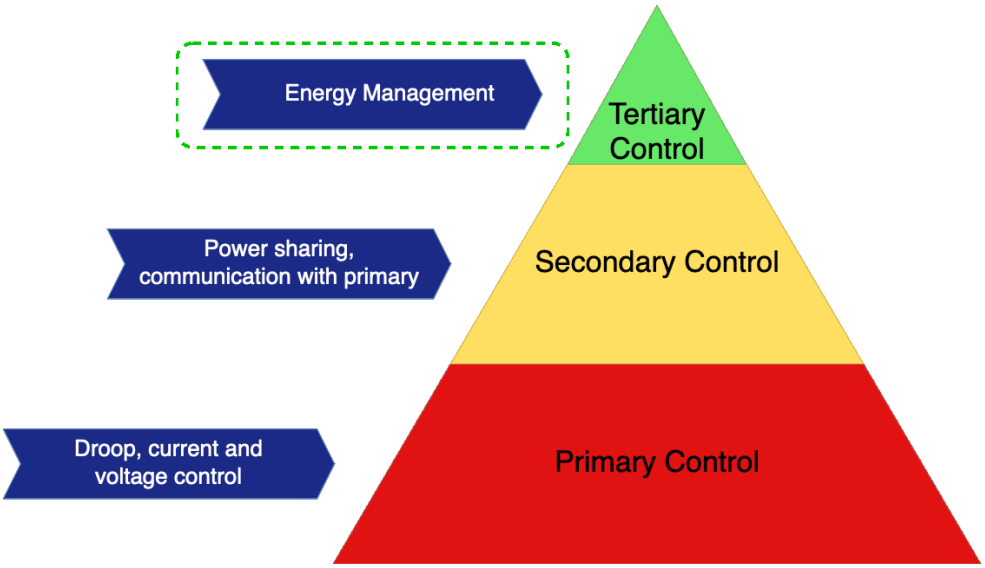

Figure 1. Hierarchical control architecture.

However, these methods suffer from a high computation time due to varying reasons such as the need to solve load flows within the optimization algorithm and the integration of VAR compensation equipment. Most of the referenced centralized methods related to power systems control use load flow analysis to calculate voltage variation [55–57]. Since these methods achieve accurate results at the expense of time, a voltage and PV power

sensitivity approach is used to calculate the voltage variations [27,58–61]. The different sensitivity matrices used in the literature are discussed in Table 1.

Table 1. Sensitivity matrices existing in the literature.

How the Sensitivity Matrix Was Developed	References	Disadvantages of the Method
Inverse from the Jacobian of Newton–Raphson power flow equations	[27,58]	Repetitive computation of the inverse of the Jacobian, which is computationally expensive with the increase in matrix size.
Surface fitting technique and using simulations of multiple load flow analysis	[59,60]	An extensive simulation needs to be run in case of a change in the network parameters to be able to develop a new sensitivity matrix that will fit the network.
Using the topological structure of the network	[61]	The derivation is performed for an MV distribution line assuming constant voltage for the slack bus. However, the secondary voltage of the LV network will fluctuate, which needs to be accounted for.

In order to find the optimum solution to the centralized control method in mitigating voltage violations, many optimization techniques have been researched. Among these, SQP [52], Nonlinear Programming (NLP) [62,63], the Evolutionary Algorithm [64], Lagrangian multipliers [65], the Multi-Objective Evolutionary Algorithm (MOEA) [66] and Particle Swarm Optimization (PSO) [55,67] have been widely used. In order to act as a viable near-real-time system, the accuracy and the computational time of the algorithm play a key role. Given the vast solution space of LVDG networks, i.e., high complexity of the network due to the number of PV connections in the power system, the computational time for convergence grows dramatically. Therefore, optimization techniques need to be tailored to LVDG power systems such that the computational time is minimal whilst maintaining robustness in terms of convergence to the optimal solution.

In this paper, we propose a Centralized Active, Reactive Power Management System (CARPMS), which uses the combination of both RPC and APC to mitigate the voltage violations in LVDGs at the tertiary control level. A sensitivity matrix derivation for the voltage with respect to the PV power changes and a modified two-stage optimization process with a Feasible Region Search (FRS) and PSO, to find the optimal power settings, were developed. The incorporation of the sensitivity matrix vastly reduced the computational time as compared to traditional load-flow-based optimization in centralized control. In addition, the FRS step in the two-stage optimization process was able to greatly reduce the search space for the solution by narrowing the solution towards the optimum and decreasing the time, thereby enabling a real-time application of the proposed solution. The PSO algorithm was used as the second step to drive the solution to its best solution to prevent frequent violations in the network.

The proposed CARPMS was simulated on a network belonging to an existing housing complex named "Lotus Grove", located in Colombo, Sri Lanka. The case study network was chosen from the same region of the authors whilst being similar to the IEEE European low-voltage test feeder [68,69] in network size and topology. Specifically, the following contributions were made in this paper:

- A novel PV-power to voltage Sensitivity Matrix (SM) for LVDGs was developed using line parameters accounting for the voltage variations in the secondary side;
- A Centralized Active, Reactive Power Management System (CARPMS) using this SM for voltage violations in LVDGs is proposed;
- A modified two-stage optimization process is proposed, with the Feasible Region Search (FRS) as an efficient space reduction algorithm to decrease the computational time and ensure convergence of the PSO optimizer that follows it.

2. Methodology

2.1. Centralized Active, Reactive Power Management System

In this section, the proposed CARPMS, which eliminates the voltage limit violations at each node, is described. Figure 2 shows the operating mechanism of the CARPMS. The CARPMS is equipped with smart meters at each PV panel in the network, ensuring the access to active, reactive power and voltage readings at each PV panel node. Due to delays incurred in communication and algorithm processing time [70], real-time data will not reach the CARPMS. Therefore, it acts as a real time management system with control actions relying on estimations of the network states predicted using historical data [50]. The proposed algorithm described in Section 4 is then used by the CARPMS to detect and correct any voltage violations in the nodes.

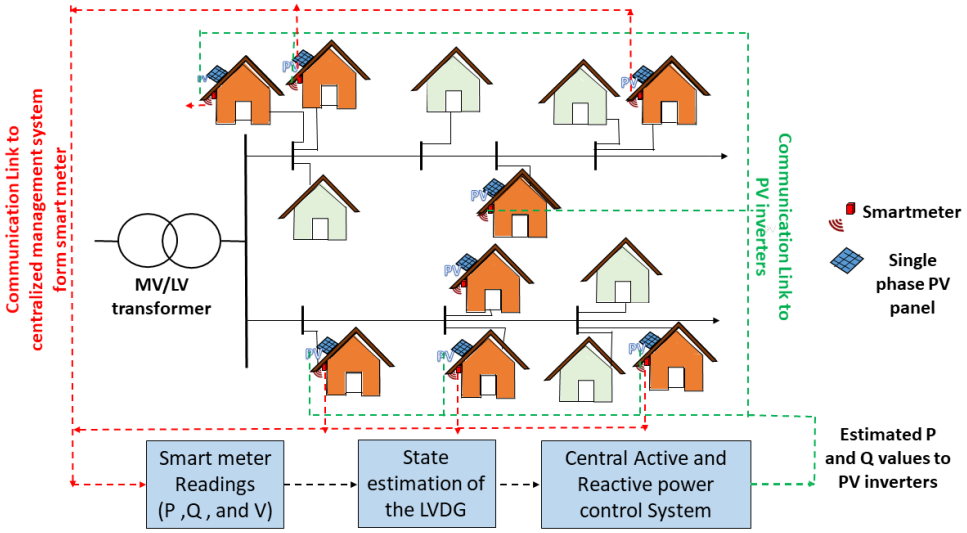

Figure 2. Schematic overview of the CARPMS information flow.

The proposed algorithm will encounter voltage violations of two types: upper limit and lower limit violations. Due to the low X/R ratio, the violations cannot be entirely removed by RPC alone. In this case, the algorithm utilizes an optimized combination of RPC and APC. A detailed flow of the algorithm steps is highlighted in Figure 3. The derivation of the SM used is given in Sections 2.2–2.4, and the two-stage optimization in the control algorithm is described in Sections 3 and 4.

2.2. Voltage Sensitivity Derivation for the Distribution Line

The SM is derived for a network without sparse line connections. This assumption was made for the ease of proof, which can be easily extended for a network with sparse line connections if necessary.

Consider a phase of a distribution line shown in Figure 4. Due to the negligible effect of the longitudinal component, by neglecting the power losses, the voltage drop between any kth and $(k+1)$th node is given by,

$$|V_k - V_{k+1}| \cong \frac{P_k R_k + Q_k X_k}{|V_k^*|} \tag{1}$$

where V_k, V_{k+1} are the complex voltages at the kth and $(k+1)$th nodes, respectively, R_k is the resistance of the line, X_k is the reactance of the line, P_k is the active power flow through the line and Q_k is the reactive power flow through the line.

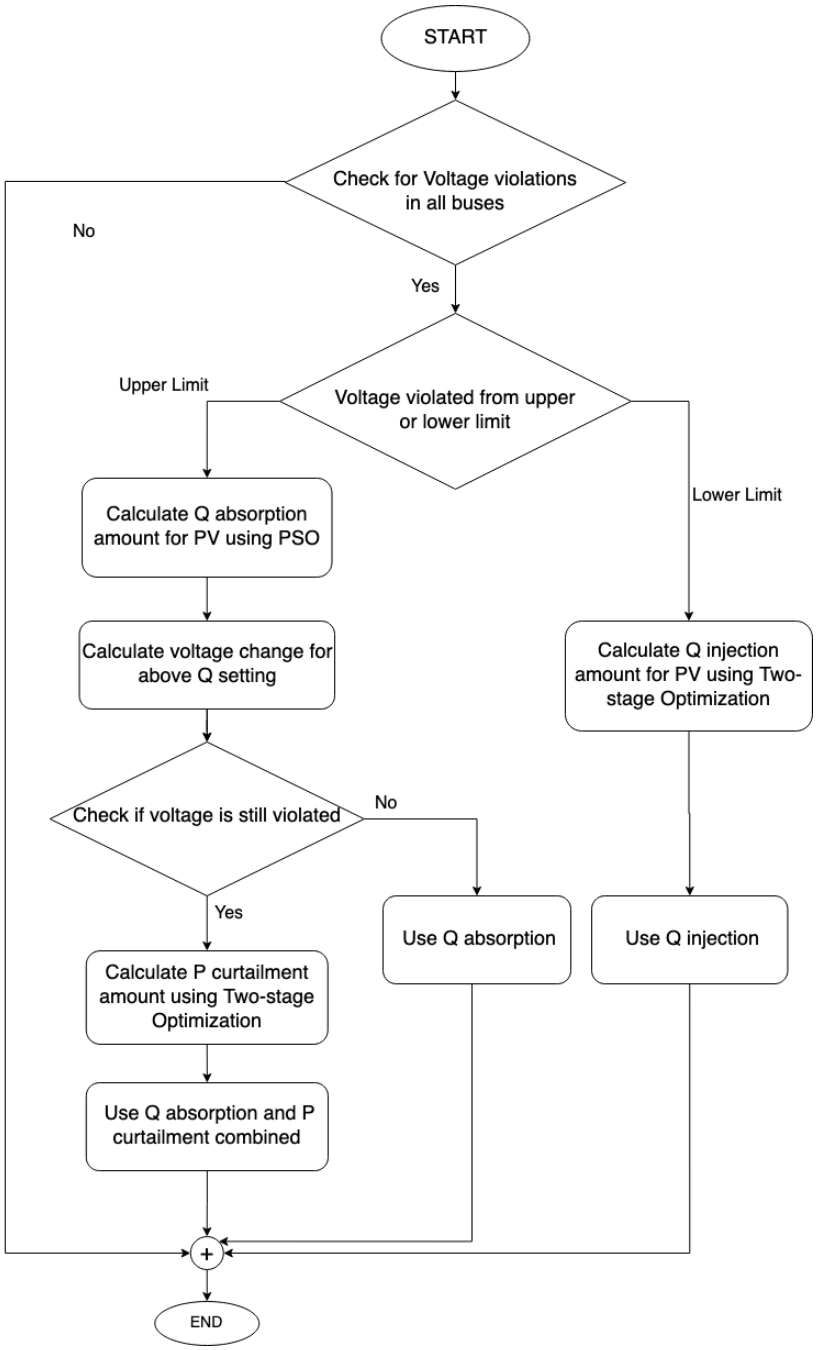

Figure 3. Proposed algorithm steps.

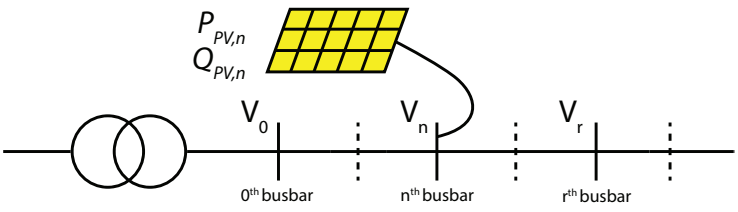

Figure 4. A schematic LVDG network.

The equation above expresses the difference in the magnitude of the voltage between two adjacent nodes. This equation was extended to calculate the voltages of all the nodes in the network. To generalize, a radial LVDG network with $(N + 1)$ number of nodes was considered. Considering the power flow from the LV transformer in the network as

positive power flow and using (1), the voltage drop up to the rth node from the transformer end is given by,

$$|V_0 - V_r| = \sum_{h=0}^{r-1} \frac{P_h R_h + Q_h X_h}{|V_h^*|} \tag{2}$$

where V_0 is the secondary voltage of the transformer for one of the three phases a, b or c, which is also the zeroth node of the network.

The power flow of the transmission line is a collective function of domestic loads, PV generations and power transmission losses. However, the power transmission losses are negligible compared to other variables. Thus, the power transmitted through the transmission line was derived as follows, which can be substituted in (2), yielding,

$$P_h + jQ_h = \sum_{m=h+1}^{N} ((P_{L_m} - P_{PV_m}) + j(Q_{L_m} - Q_{PV_m})) \tag{3}$$

$$|V_0 - V_r| = \sum_{h=0}^{r-1} \frac{\sum_{m=h+1}^{N} ((P_{L_m} - P_{PV_m})R_h + (Q_{L_m} - Q_{PV_m})X_h)}{|V_h^*|} \tag{4}$$

The network parameters X_h and R_h given in (4) are constant, unique and attainable for every LVDG network. Whilst the load power and PV power generation parameters are not easily obtainable in real time, the estimation of these parameters is possible [71–75]. The derivation of the voltage of the rth node with respect to the reactive power of the PV system in the nth node was derived as,

$$\frac{\partial V_r}{\partial Q_{PV_n}} = \frac{\partial V_0}{\partial Q_{PV_n}} + \sum_{h=0}^{n-1} \frac{X_h}{|V_h^*|} \qquad for(r \geq n) \tag{5}$$

$$\frac{\partial V_r}{\partial Q_{PV_n}} = \frac{\partial V_0}{\partial Q_{PV_n}} + \sum_{h=0}^{r-1} \frac{X_h}{|V_h^*|} \qquad for(r < n) \tag{6}$$

where $\frac{\partial V_r}{\partial Q_{PV_n}}$ is the voltage sensitivity of the rth node with respect to the reactive power variation of the PV panel at the nth node and V_0 is the voltage of the node connected at the secondary side of the transformer. A schematic LVDG network showing the node notations is shown in Figure 4.

Similarly, the voltage sensitivity of nodes with respect to the active power of the PV system in the nth node can be derived.

2.3. Voltage Sensitivity Derivation at the Transformer End

In order to calculate $\frac{\partial V_0}{\partial Q_{PV_n}}$ and similarly $\frac{\partial V_0}{\partial P_{PV_n}}$, the LV transformer of the residential network was modelled as shown in Figure 5.

Considering the secondary side of the transformer, the expression for current and power flow in the secondary side was derived in terms of voltages and impedances using the transformer model matrix in [76]. The power flow in the secondary side of the transformer was obtained as,

$$P_s^a - jQ_s^a = (V_{0_p}^a \cdot Y_1 - V_{0_p}^b \cdot Y_1 + V_{0_s}^N \cdot Y_2) * |V_{0_s}^a| \angle -\delta_k - |V_{0_s}^a|^2 \cdot Y_2 \tag{7}$$

where $V_{0_p}^a$, $V_{0_p}^b$ and $V_{0_p}^c$ are the primary side voltages of the LV transformer, $V_{0_s}^a$, $V_{0_s}^b$ and $V_{0_s}^c$ (generically denoted by V_0 in the previous section) are the secondary side voltages of the LV transformer and $I_{0_s}^a$, $I_{0_s}^b$ and $I_{0_s}^c$ are the secondary side currents of the LV transformer of the a, b and c phases, respectively. Y_1 and Y_2 are the primary and secondary side impedances of the LV transformer, and N is the secondary to primary transformer turn ratio. $Y_1 = \frac{Y_t}{N}$, and $Y_2 = Y_t$, $V_{0_s}^a = |V_{0_s}^a| \angle \delta_a$.

In order to calculate the voltage sensitivity of the transformer end with respect to reactive power changes, the derivative of the imaginary component of (7) with respect to $V_{0_s}{}^{a}$ was obtained as,

$$\frac{\partial Q_s^a}{\partial |V_{0_s}^a|} = 2|V_{0_s}^a| \cdot Im(Y_2) - Im((V_{0_p}^a \cdot Y_1 - V_{0_p}^b \cdot Y_1 + V_{0_s}^N \cdot Y_2)\angle -\delta_a) \tag{8}$$

Since the active and reactive power of loads can be assumed to be constant during a control sequence operation, using (3), the variation of reactive power for a given phase with respect to the transformer end voltage is only the variation of PV power in that phase.

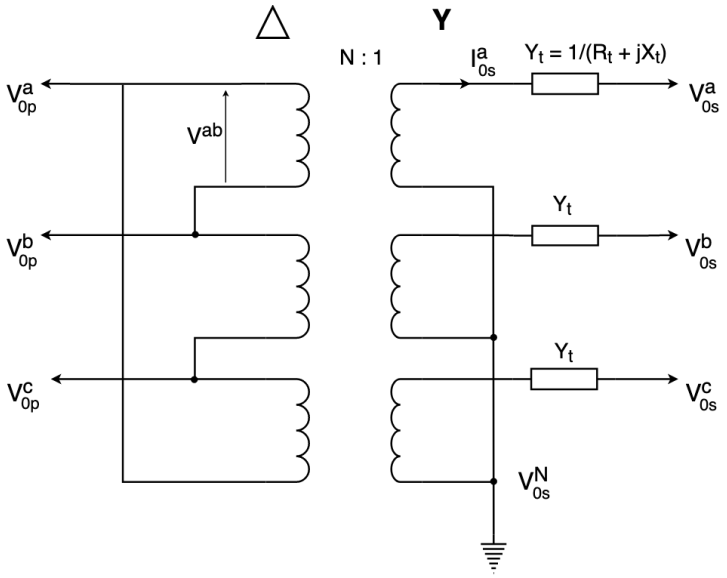

Figure 5. Equivalent circuit of the delta-wye transformer.

Then, by obtaining the reciprocals, the variation of the transformer end voltage with respect to the PV reactive power connected to the given phase was computed using Equation (8).

$$\frac{\partial |V_{0_s}^a|}{\partial Q_{PV}^a} = \frac{\partial |V_{0_s}^a|}{\partial Q_s^a} \tag{9}$$

Similarly, using the real part of (7), the variation of the transformer end voltage with respect to the PV active power can be obtained.

2.4. Combined Sensitivity Matrix Model

The combined sensitivity model was derived based on the results from Sections 2.2 and 2.3. Considering the number of PV panels in the system as M and the number of nodes in the system as N, using Equations (5), (6) and (9) and their analogous equations for active power, the combined SM model of the network with respect to the power generation of PV systems was derived as,

$$\begin{aligned} [\Delta V]_{N\times 1} &= \left[\frac{\partial V}{\partial Q_{PV}} \quad \frac{\partial V}{\partial P_{PV}}\right]_{N\times 2M} \begin{bmatrix}\Delta Q_{PV} \\ \Delta P_{PV}\end{bmatrix}_{2M\times 1} \\ &= \left[\sum_h \frac{X_h}{|V_h^*|} \quad \sum_h \frac{R_h}{|V_h^*|}\right]_{N\times 2M} \begin{bmatrix}\Delta Q_{PV} \\ \Delta P_{PV}\end{bmatrix}_{2M\times 1} + \Delta V_0 \begin{bmatrix}1 \\ 1 \\ \vdots \\ 1\end{bmatrix}_{N\times 1} \end{aligned} \tag{10}$$

where $[\Delta V_0]_{N\times 1}$ is the voltage change at the LV transformer end to be added to each node and $[\Delta V]_{N\times 1}$ is the combined voltage variation at each node due to the PV power variations (at each iteration). The system was linearized assuming that the variation in the PV system power within the control sequence algorithm is considerably small.

3. Problem Formulation

The aim of this work was to determine an optimum setting to prevent voltage violations in LV networks. An RPC mechanism followed by APC is carried out if RPC alone is unable to rectify the voltage violations. Thus, two optimization functions defined in Sections 3.1 and 3.2 were proposed to converge on the optimal operating point. The objective functions of the optimization algorithms intend to minimize the active and reactive power settings whilst satisfying the voltage limit constraints and the inverter constraints. The voltage limits pertain to the lower and upper limits of the acceptable voltages in LVDG networks, whereas the inverter constraints depend on the power ratings of the inverters.

The state of the PV inverter being varied by the algorithm depending on the three control methods Q-absorption, P-curtailment and Q-injection is depicted in Figure 6. The "X" mark shows an instance of an initial state of the inverter during the day. During RPC Q-absorption, the state moves vertically downwards to a given optimum point. If it reaches the inverter constraint/capability curve, this implies that Q-absorption cannot be performed under the given conditions. Then, P-curtailment is performed during which the state of the inverter moves along the capability curve, reducing the amount of active power injected to the network. It can also be noted that the maximum allowable value of Q-absorption, $Q_{abs,max}$, varies depending on the active power state of the inverter. The inverter state during night-time is marked "Y". Here, RPC (Q injection) is carried out, and the inverter state moves upwards along the Q-axis (injecting reactive power to the network) till it reaches an optimal point or its full Q injection capacity: $Q_{inj,max}$.

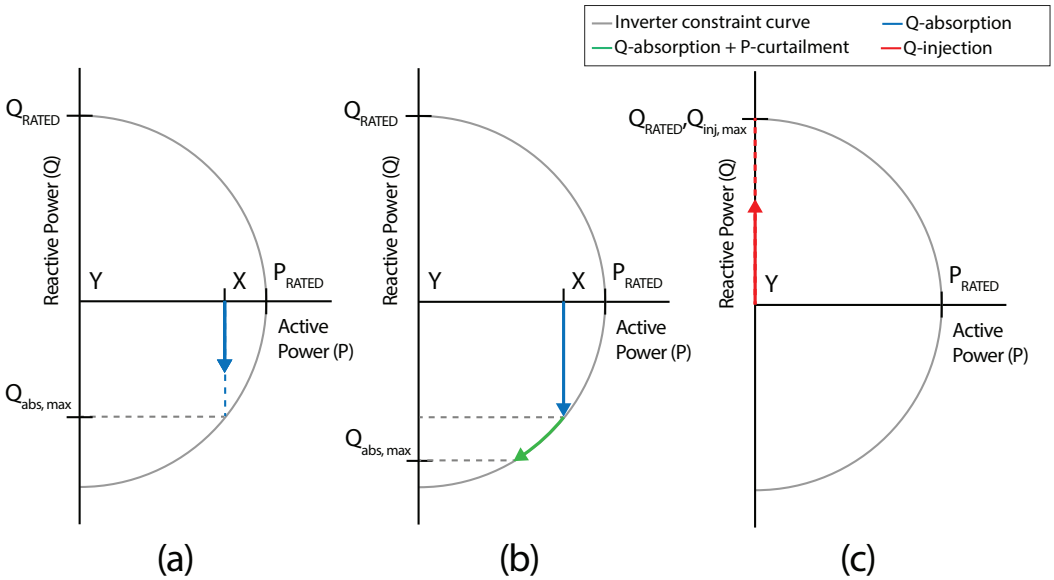

Figure 6. PV inverter status change for control using (**a**) Q-absorption, (**b**) Q-absorption and P-curtailment and (**c**) Q-injection.

3.1. Optimization of Reactive Power Control

The objective function of the optimization of RPC is expressed as a function of the total deviation of node voltages from 1 p.u and the neutral voltage as given by,

$$J_{RPC} = \min_{Q} \sum_{i=1}^{n} (c_d * V_{d,i} + c_{neut} * V_{neut,i}) \quad (11)$$

where $V_{d,i}$ is the total deviation of voltages of node i from 1 p.u, $V_{neut,i}$ is the neutral voltage of node i and c_d and c_{neut} are scaling constants. $V_{neut,i}$ is calculated by the vector addition of the three-phase voltages of node i.

Subject to the constraints:

1. The voltage of the node should be within the specified upper and lower limits given by,

$$V_{\text{lower limit}} \leq V_{\text{nodes}} + \Delta V \leq V_{\text{upper limit}} \tag{12}$$

   where $V_{\text{lower limit}}$ and $V_{\text{upper limit}}$ are the accepted lower (0.95 p.u) and upper limit (1.05 p.u) voltages in LVDG systems, respectively, V_{nodes} is the calculated voltage of the nodes using optimization variables and ΔV is the estimated voltage change due to changes in P and Q of the PV systems;
2. The inverter constraints given below should be satisfied,

$$S_{PV_i}^2 \geq P_{PV_i}^2 + Q_{PV_i}^2 \tag{13}$$

The variables of the optimization problem were the reactive power setting at each node with a PV panel in the network, which can be expressed as $Optim.\ Variable\ (OV)\ Q = \left[Q_{pv_1}, Q_{pv_2}, Q_{pv_3}, Q_{pv_4}, \ldots, Q_{pv_m}\right]$.

In order to formulate this optimization problem to minimize (11) whilst satisfying the above constraints, penalties were introduced to ensure that the optimal solution satisfies the constraint of voltage violations to the best case possible by penalising the cost function when constraints are violated. Hence, the optimization problem was reformulated as a minimisation of the penalized objective function J_1 given by (14).

$$J_1 = \min_{Q} \left(c_{vial} * e^{N_{vial}} * J_{RPC}\right) \tag{14}$$

where N_{vial} is the sum of the number of violations in each phase and c_{vial} is a scaling constant.

3.2. Optimization of Active Power Curtailment

The objective function of the optimization of APC included the amount of active power curtailed and is expressed as,

$$J_{APC} = \min_{P} \sum_{i=1}^{n} \left(\Delta P_{PV_i} + c_d * V_{d,i} + c_{neut} * V_{neut,i}\right) \tag{15}$$

where ΔP_{PV_i} is the amount of curtailed active power, $V_{d,i}$ is the total deviation of voltage of node i from 1 p.u, V_{neut} is the neutral voltage of node i and c_d and c_{neut} are scaling constants.

Subject to the constraints:

1. The voltage of the nodes should be within the specified upper and lower limits as in (12);
2. The inverter constraint given below should be satisfied,

$$S_{PV_i}^2 = P_{PV_i}^2 + Q_{PV_i}^2 \tag{16}$$

The variables of the optimization problem here were the active power setting at each node in the network, which can be expressed as $Optimization\ variable\ (OV)\ P = [P_{pv_1}, P_{pv_2}, P_{pv_3}, P_{pv_4}, \ldots, P_{pv_m}]$.

Similar to the RPC case, the optimization problem was reformulated by including the same penalties such that the penalty is applied when the constraint is violated. This ensures the optimal solution of the objective function satisfies all constraints.

4. Two-Stage Optimization

This section outlines the proposed modified optimization algorithm consisting of two processes in sequence:

- Feasible Region Search (FRS);
- Particle Swarm Optimization (PSO).

The aim of FRS is to drive the elements in the Optimization Variable (OV) towards the feasible region, where upper or lower limit voltage violations are nonexistent. This is followed by a PSO algorithm, where these variables in the feasible region are then optimized according to a predefined cost function, to find the best possible solution.

4.1. Feasible Region Search

The number of elements in the OV increases with the number of PV panels connected to a given network, which results in a large search space. At the initial violated conditions, the existence of the OV far away from the feasible region and the high dimensionality of the search space may result in the poor performance of a standard PSO algorithm. This is because the first step of the PSO is an initialisation procedure (discussed in Section 4.2), being a random scattering of OVs in the neighbourhood of the current OV.

Through FRS, we determine a new initial point for the PSO by moving the present OV towards the feasible region. The driving function of the OV is given by,

$$OV[i,j] = OV[1,j] + \alpha[i] * \Delta OV_{max}[j] \tag{17}$$

for all $j = 1, 2 \ldots m$ (total number of elements in $OV[i,:]$), where $OV[1,j]$ is the initial value of the jth element in the OV, driven towards the feasible region by $\alpha[i]$. Here, $\alpha[i]$ is the driving parameter, which is a monotonically increasing function from 0–1. $\Delta OV_{max}[j]$ is the maximum possible change of $OV[:,j]$. This results in $OV[i,j]$, the calculated position of the jth element of the OV at the ith iteration.

In a PV integrated network, the vector $OV[i,:]$ is the power settings of each inverter connected to the network at any given iteration i. $\Delta OV_{max}[j]$ is the maximum Q-absorption, Q-injection or P-curtailment capacity of the jth inverter. This also determines the driving direction of the elements of OV, as the sign of $\Delta OV_{max}[j]$ is dependent on the current nature of the voltage violation. In the instance of an upper limit violation, $\Delta OV_{max}[j]$ will be negative, as the P and Q setting of the jth inverter, which correspond to the maximum P-curtailment and Q-absorption capacity, are negative. $\Delta OV_{max}[j]$ will be positive for lower limit violations, as the inverter state travels in the direction of positive Q for Q-injection, as discussed in Section 3.

During each iteration, $OV[i,j]$ is computed such that it moves closer to the feasible region. As the sign of $\Delta OV_{max}[j]$ ensures the current $OV[i,:]$ moves towards the feasible region, the driving parameter α serves to gradually increase the change in $OV[:,j]$. If this change happens to be very large, there exists a possibility of OV overshooting towards unwarranted solutions, as illustrated in Figure 7. For example, lower limit violations may occur if Q-absorption takes place at its maximum capacity to mitigate an upper limit violation. This problem is overcome by the use of α, which gradually increases with each iteration i, allowing FRS to terminate as soon as $OV[i,j]$ reaches the feasible region.

For most instances, upon the termination of FRS, the system is devoid of any upper or lower limit violations. Although it is possible to complete the control process using only FRS, it does not fully optimize the network as it does not consider parameters relative to the cost function given by (14) and (15). Instead, it only accounts for the existence of violations in the system. Furthermore, FRS acts as a decoupled control algorithm, where the inverter power settings in the ith iteration are independent of each other, where each element in $OV[i,:]$ is modified by the same value of α. However, in the case that the FRS is unable to drive the OV to the feasible region, it is ensured that the OV is as close as possible to the feasible region. In the case of FRS on an upper limit violation, if a lower limit violation emerges, the FRS is terminated when the total number of violations is minimum.

Similarly, in the case of FRS on a lower limit violation, if an upper limit violation emerges, FRS is terminated when the total number of violations is again minimum. This establishes that the final *OV* from the FRS is as close to the feasible region and beyond adequate as an initialization for the PSO.

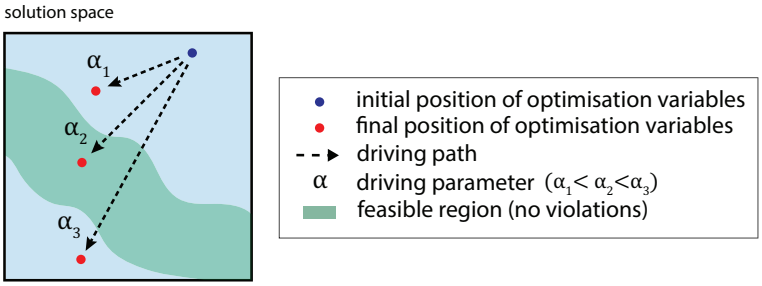

Figure 7. Effect of α on FRS.

Although slower than FRS, the PSO algorithm performs as a collective control algorithm. This implies that the factor α at which Q-absorption, Q-injection or P-curtailment is performed relative to the capacity of the inverter will be optimized. For instance, in the absence of solar power, PSO will ensure more Q is injected to the network by inverters furthest from the secondary transformer, where the cumulative voltage drop is high. Due to the properties of the cost function proposed in Section 3, PSO will further push the optimal point much more towards the centre of the feasible region. This allows for higher margins of errors in the state estimation of the PV integrated network, as a small deviation in the *OV* will not drift the solution towards unfeasible regions.

4.2. Particle Swarm Optimization

Particle Swarm Optimization (PSO) is a heuristic algorithm used in problems with high-dimensional search domains. It is a nature-inspired algorithm, which is based on the foraging technique of flocks of birds and schools of fish. There are six steps in standard PSO [67], as shown in Algorithm 1.

Algorithm 1: Steps of PSO.

1. Initialize the swarm of particles (i.e., population)
2. Compute the cost of each particle using the fitness function
3. Record the personal best of each particle and the global best of the entire population
4. Update the velocity of each particle using the personal and global best and other parameters
5. Calculate the new position of each particle
6. Repeat Steps 2–5 until each particle converges to its solution or the iteration count is completed, and extract the global best of the entire population as the optimal solution

Due to the large search space in this problem, standard PSO is unable to converge to a satisfactory solution. As discussed previously in Section 4.1, FRS is carried out, and the initial population is created by randomly scattering particles in the neighbourhood of the *OV*, which is now located in the feasible region.

4.3. Primary Steps of Particle Swarm Optimization

The steps involved in PSO are shown in Algorithm 1. The update equation for the position and velocity of the particles is given by,

$$x_i[j+1] = x_i[j] + V_i[j+1] \tag{18}$$

where $x_i[j]$ denotes the position of the ith particle at the jth iteration and $x_i[j+1]$ and $V_i[j+1]$ are the position and velocity of that particle for the next iteration. The velocity at which the particle travels is expressed by,

$$V_i[j+1] = V_i[j] + P_b * (p_i[j] - x_i[j]) + G_b * (g[j] - x_i[j]) \quad (19)$$

where $V_i[j]$ is the velocity of the particle at the jth iteration, $p_i[j]$ and $g[j]$ denote the current personal and global best of the jth particle and P_b and G_b are the confidence factors for the personal and global best, respectively.

The notion of the velocity is to set the direction of search and the extent of exploration by the particle. This depends on where in the search space the current particle exists, the recorded best position of that particle (personal best) and the recorded best position of all particles (global best) since the start of the algorithm. The dependency of the personal or global best on the velocity is governed by confidence factors, expressed by the two variables P_b and G_b.

To find the optimal values of the parameters P_b and G_b, an exhaustive search using the grid-search algorithm was carried out. Here, the ratio between P_b and G_b varied between 0.5 and 3 in steps of 0.5, and the number of iterations taken along with the final cost value was recorded. The magnitude of these parameters was set in the range of 0–1. It was found out that after FRS, as the particles were already scattered within the feasible region, each particle following its own local optima resulted in lower cost values for the final solution in most scenarios. Hence, more emphasis was given towards particles moving towards their own local optima rather than global optimum. Therefore, a 2:1 ratio between P_b and G_b was set during the optimization. This creates a wider net in the search space, thereby exploring many local minima. This increases the likelihood that the global minimum will be within this wide net.

To decrease the computational time whilst running the proposed two-stage optimization algorithm, the PSO population parameter needs to be optimized. Therefore, the convergence towards a feasible solution of the algorithm was recorded for initial populations varying from 5–50. Throughout the population search, it was observed that the optimization variable remained in the feasible region for all populations. Moreover, a population of 10 resulted in a significantly lower cost in comparison to an initial population of 5, whilst having a significantly lesser computational time compared to other population sizes. Hence, a population of 10 was chosen as the optimal population parameter for the PSO algorithm embedded in the proposed two-stage optimization.

5. Case Study

The network belonging to an existing housing complex "Lotus Grove" located in Colombo, Sri Lanka, was used as the case study. The network location also provides climatic variations of the tropical region. Its topology with 63 nodes is shown in Figure 8. The Number 0 node is the root node and connected to the secondary side of the MV-LV transformer. The rated capacity of the transformer is 400 kVA delta-wye, and the input/output voltage rating is 11 kV/415 V. The solid lines in Figure 8 represent the three-phase feeders where three-phase or single-phase loads and PV systems are connected. The overhead electricity distribution cable used is the aluminium aerial bundle cable (ABC-Al/XLPE of 3 × 70 + N54.6 + 1 × 16). There are 286 single-phase or three-phase customers and 50 PV panels connected to the network. The PV panel locations are uniformly distributed across the network with assigned ratings ranging from 2–7 kW and customer peak loads assigned in the range of 0.5–1 kW through a uniformly distributed assignment process. The daily operation curves for the PV systems and the daily load profile of customer loads used in the case study are shown in Figure 9. A few random load and PV profiles used in the case study are shown in Figure 10 to show the varying nature of the profiles evaluated. Images 1, 2 and 3 of Figure 10a represent sunny days that are randomly generated for a given PV panel, while Images 4 and 5 of Figure 10a represent cloudy days. Thus, these random generations encapsulate possible weather conditions that exist in a tropical environment.

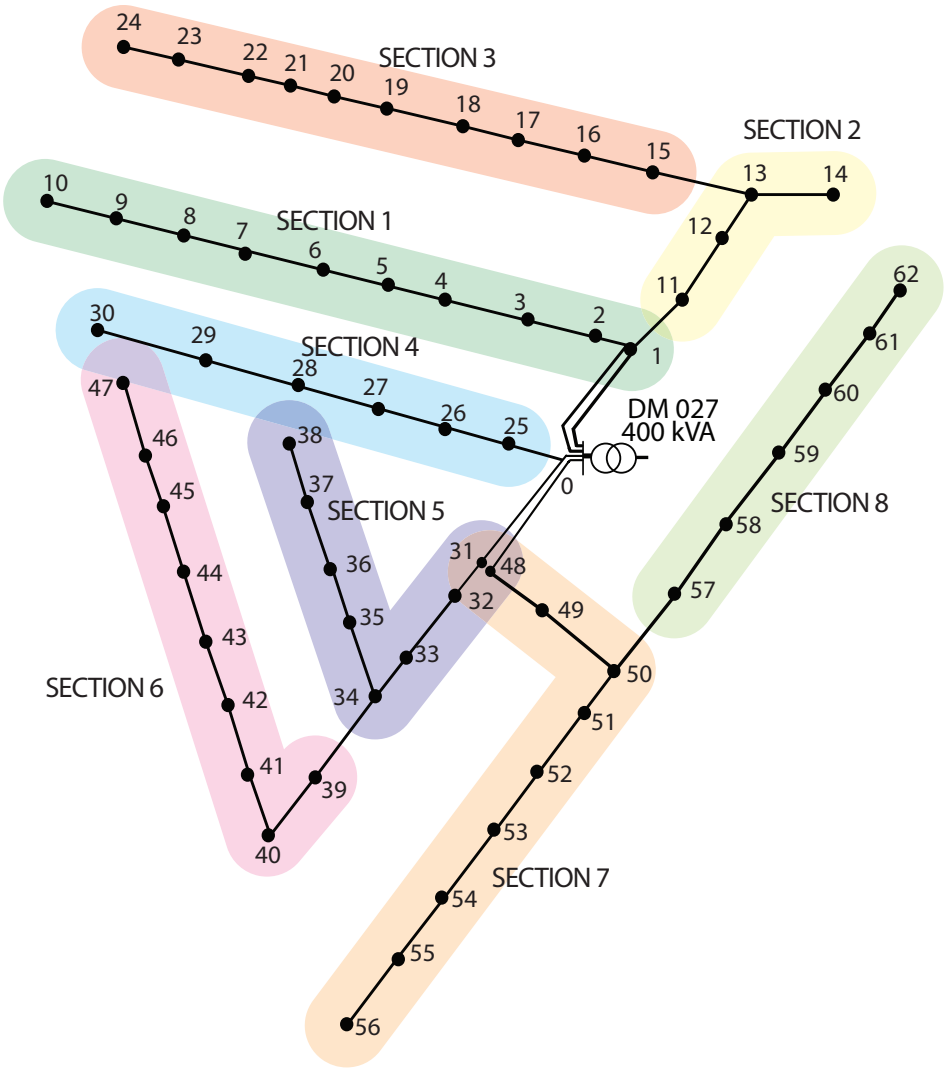

Figure 8. Single line diagram of the test LVDG network (Lotus Grove, Sri Lanka) used for the simulations.

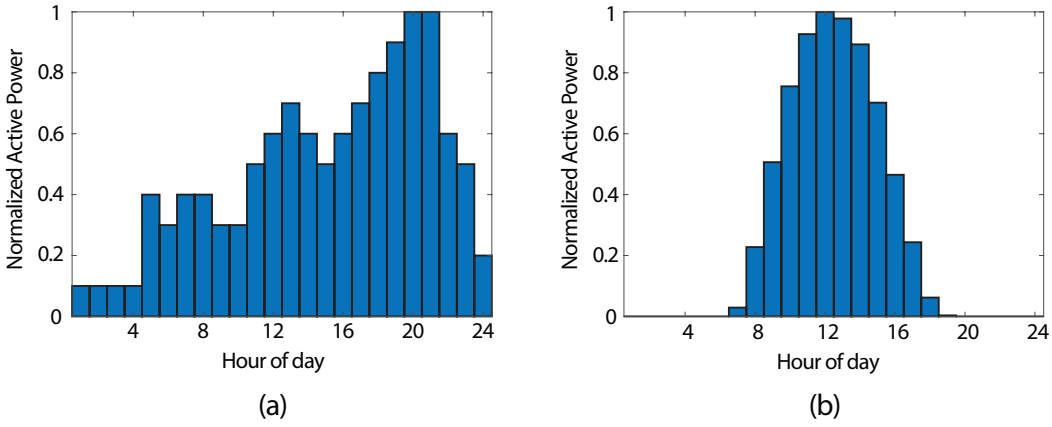

Figure 9. Daily (**a**) load profile and (**b**) PV profile.

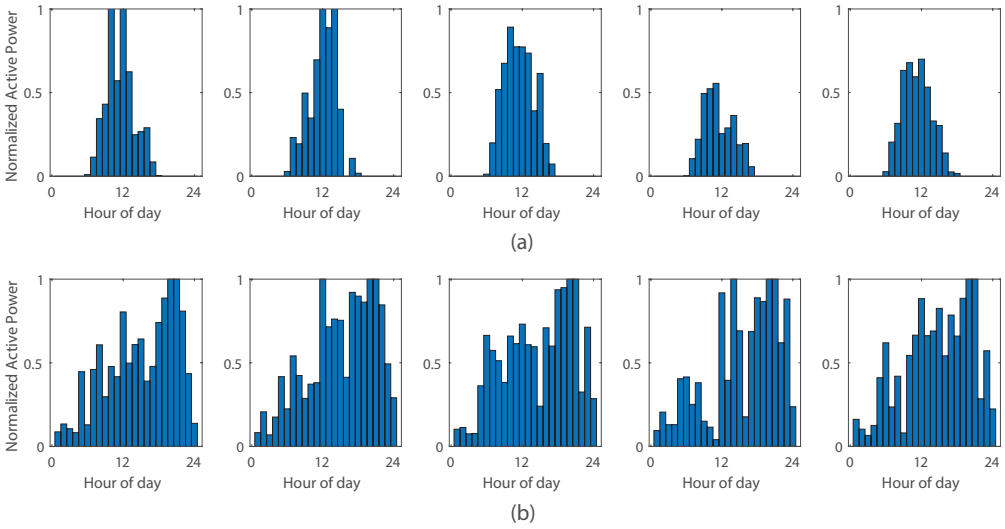

Figure 10. Random (**a**) PV profiles for a single PV panel and (**b**) load profiles for a single customer used in the case study.

6. Results and Discussion

To simulate the occurrences of upper and lower limit voltage violations, Monte Carlo (MC) simulations were run for three time instances. Since we intended to identify and mitigate voltage violations, the most prevalent cases for such violations were identified and Monte Carlo simulations were performed for these chosen times of the day: 10:00 h, 11:00 h and 21:00 h. This is due to the high PV power available between 10:00 h and 11:00 h, while the load is much less, leading to severe upper limit violations. Similarly, the load is maximum around 21:00 h while there is no PV power, leading to many lower limit violations. Since the violations occurring at other time instances were much less, they posed a much simpler problem to be solved. Therefore, showing the ability to solve the worst-case time instances confirmed the ability to handle the simpler violated cases. Table 2 describes the three instances in terms of the hour of simulation, the network settings (PV and load setting), the number of simulations and the number of control instances that employed reactive power control or active power control (RPC or APC) or both, to mitigate voltage violations.

Table 2. Monte Carlo simulations.

Time of Day	PV Source	Base Load	Number of Simulation Runs	Control Instances		
				RPC Q-abs	APC	RPC Q-inj
10:00	76%	30%	1000	403	7	0
11:00	93%	50%	2000	325	102	0
21:00	0%	100%	500	0	0	500

As observed in Table 2, voltages at simulations carried out at 10:00 violated more often, due to the low base loading. However, they tended to have a higher possibility of mitigating the upper limit violations using only RPC Q-absorption. Comparatively, at 11:00, when PV penetration increases, the rectification cannot be solely performed via Q-absorption, as shown in Table 2; hence, a higher number of APC rectifications (Q-absorption followed by APC) took place. For the simulation at 21:00 (night-time), every simulation contained lower limit violations only, which was caused by full base loading. With a large number of simulations using randomly generated individual base loads, PV sources and PV positions in the network for each simulation, the robustness of the control algorithm under extreme circumstances was ensured.

To maintain computational consistency within this study, all simulations were run on an Intel i7-8700k processor with 16GB of RAM. All scripts and functions were written using MATLAB R2020a. Load flow computations were carried out using the OpenDSS interface with MATLAB.

6.1. Validation of the Sensitivity Matrix

This section demonstrates the validity of the proposed sensitivity matrix for voltage sensitivity calculation for power injection/absorption/curtailment. The SM was analysed with respect to the load flow approach for the MC simulations discussed in Table 2 for the amount of power injected/absorbed/curtailed and the respective voltage change that was achieved. This is presented in Figure 11a for RPC and Figure 11b for APC, where each marker denotes the values after each MC simulation. The voltage change presented in this figure is for the worst violated node in each case where the deviation of the initial voltage is largest from 1 p.u. Therefore, the RPC Q-injection scenarios were analysed with respect to the node with the lowest voltage (less than 0.95 p.u) since it had lower limit violations, and the RPC Q-absorption scenarios were analysed with respect to the node with the highest voltage (greater than 1.05 p.u) since it had upper limit violations. APC was also analysed with respect to the node with the highest voltage, but in comparison to the active power used. The voltage profiles after the optimization using the load flow method and the SM method are further discussed in Section 6.3.

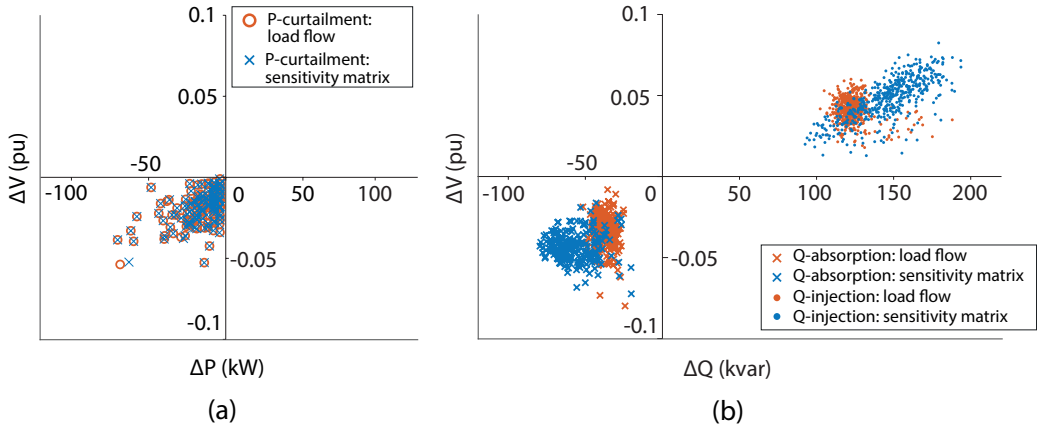

Figure 11. Change in reactive/active power and the corresponding voltage change in the most violated node for (**a**) reactive power control and (**b**) active power curtailment.

The amount of active power used in both methods was almost consistently the same in APC, as seen in Figure 11a. This is because the optimization was designed with a high penalty to the amount of active power curtailed. Therefore, it was FRS that greatly contributed to APC, as the FRS step drives the solution as close as possible to the feasible region and the PSO always ensures that the final solution has minimal active power curtailed, i.e., at the boundary of the feasible region.

Considering RPC, two distinct regions can be seen in Figure 11b. The RPC using Q-absorption reduced the voltage in the nodes by consuming reactive power, hence in the lower-left quadrant of the plane, whereas RPC using Q-injection lifted the voltage by supplying reactive power, hence on the top-right quadrant. It can be observed that the plots for both the SM and the load flow approach are very much overlapping. The SM can be seen to slightly overcompensate in reactive power usage in the range of 20–30 kVARs with a difference in the voltage change lying within 0.01 p.u.

While the SM overcompensates in reactive power usage, this difference is minimal in comparison to the computational time benefit of the SM over the load flow approach. The distribution of the computational times using the SM and the load flow for the MC simulations is shown in Figure 12. It can be observed that the SM approach converges to

the solution with a time benefit of 55.1% for the mean computational time, as shown in Table 3.

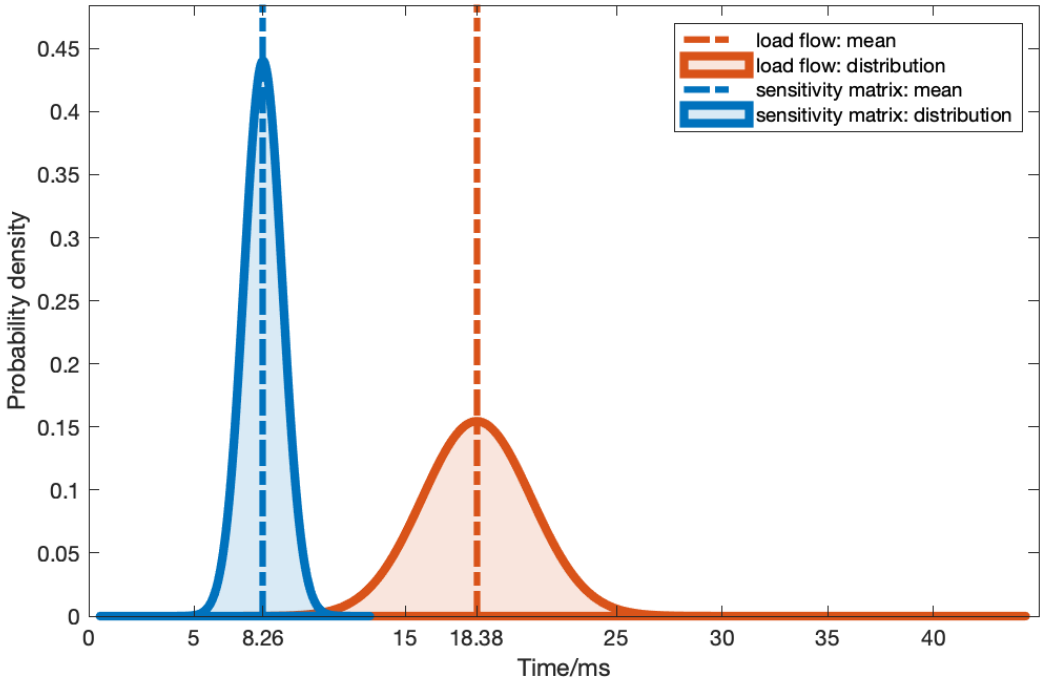

Figure 12. Comparison of computational time for the load flow and SM approaches.

Table 3. Elapsed computational time for sensitivity matrix and load flow calculation.

Calculation Method	Computational Time/s			
	Mean	**Std. Deviation**	**Minimum**	**Maximum**
Load Flow	18.38	2.58	14.75	44.38
Sensitivity Matrix	8.26	0.90	5.35	12.10

6.2. Feasible Region Search for Optimization

Out of the 3000 MC simulations conducted for the Q-absorption and APC scenarios (as in Table 2), FRS was able to drive the *OV* to the feasible region devoid of any voltage violations. Meanwhile, in the 500 MC simulations conducted for the Q-injection scenarios, except for 35 simulations, FRS was again able to drive the *OV* to the feasible region devoid of any violations. Considering the 35 rare instances out of all simulation runs, FRS ensured that the *OV* was driven to the closest possible setting to the feasible region, ensuring that the PSO was able to converge to the optimal solution.

To demonstrate the effectiveness and necessity of FRS in the proposed two-stage optimization algorithm, 100 separate MC simulations were run with and without FRS. Within each MC simulation, the two-stage optimization and the standalone PSO were carried out for varying population sizes and initialization parameters, and the solutions were analysed.

In this study, the initialization parameter used was the scatter variance, which determines the spread of the PSO particles that are initially populated in the neighbourhood at the starting point. Increasing the population and scatter variance together increases the probability of these particles being closer to the optimal solution, due to a large number of particles in the initial population being spread over a vast area in the solution space. However, given a large solution space as in this study, standalone PSO does not always guarantee a solution in the feasible region even under the aforementioned initial conditions. These results are summarized in Table 4. Here, it was observed that on average, 34% of

solutions obtained by standalone PSO did not fall under the feasible region. In contrast, when FRS was used with PSO, every scenario generated using the MC simulation resulted in the final solution being inside the feasible region, i.e., no violations. This shows the necessity of FRS in the optimization algorithm, where it effectively drives the optimization variable towards the solution, thus enabling PSO to carry out finer adjustments towards finding an optimal solution.

Table 4. Percentage of unfeasible solutions after standalone PSO for varying population size and scatter variance.

Population	Scatter Variance				
	0.1	**0.2**	**0.5**	**1.0**	**2.0**
5	41	41	45	45	46
10	38	38	38	40	41
20	33	30	30	33	33
30	30	30	29	29	30
50	28	27	27	28	28

It can be noted that increasing the population slightly reduces the overall number of instances where the solution is unfeasible. However, it was observed that the average computational time per iteration increased linearly with the size of the population. Hence, an increase in the population size for PSO in order to optimize its performance will lead to higher computational time in reaching the solution, which is unfavourable for the problem.

6.3. Two-Stage Optimization and Proposed Sensitivity Matrix

In order to create a considerable number of violations to emulate a possible worst-case scenario handling capability of the proposed SM method and to demonstrate its robustness, PV panel positions were randomly generated such that a relatively higher number of panels were connected to Phase 3, increasing the number of violations in that phase. Therefore, the initial and final voltages in the worst possible phase, Phase 3, after control using the SM approach and the load flow method, both using the two-stage optimization, are shown in Figure 13 for one particular simulation for each case at 10:00, 11:00 and 21:00.

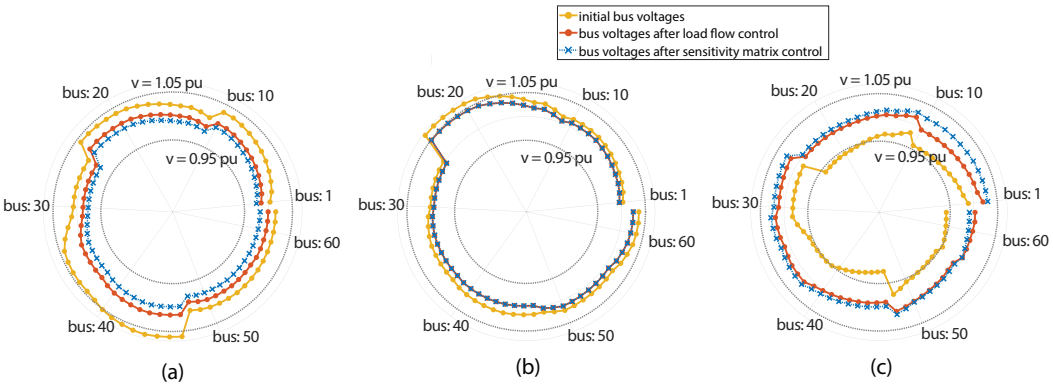

Figure 13. Voltage profiles of Phase 3 before and after control at (**a**) 10:00 using Q-absorption, (**b**) 11:00 using Q-absorption and P-curtailment and (**c**) 21:00 using Q-injection.

The distribution of the minimum voltage of the set of nodes after RPC using Q-injection obtained using the 500 MC simulations conducted at 21:00 as per Table 2 is shown in Figure 14. Similarly, the distribution of the maximum voltage after Q-absorption obtained using 410 MC simulations (violated simulations) out of the 1000 simulations conducted at 10:00 as per Table 2 is shown in Figure 15. It can be observed that the lower limit violations and upper limit violations were successfully eliminated by the control

sequences. There was a slight incremental shift of 6.5×10^{-3} p.u of the mean voltage in the minimum voltage distribution of the sensitivity matrix approach compared to the load flow approach after Q-injection (Figure 14). Similarly, the maximum voltage distribution of the sensitivity matrix method was slightly lower with a 1.02×10^{-2} p.u difference of the mean voltage compared to the load flow method (Figure 15). This was due to the overcompensation of power by sensitivity matrix due to its approximation, as described in Section 6.1. However, the optimization ensures that both methods successfully mitigate voltage violations while minimising the voltage deviations in each phase.

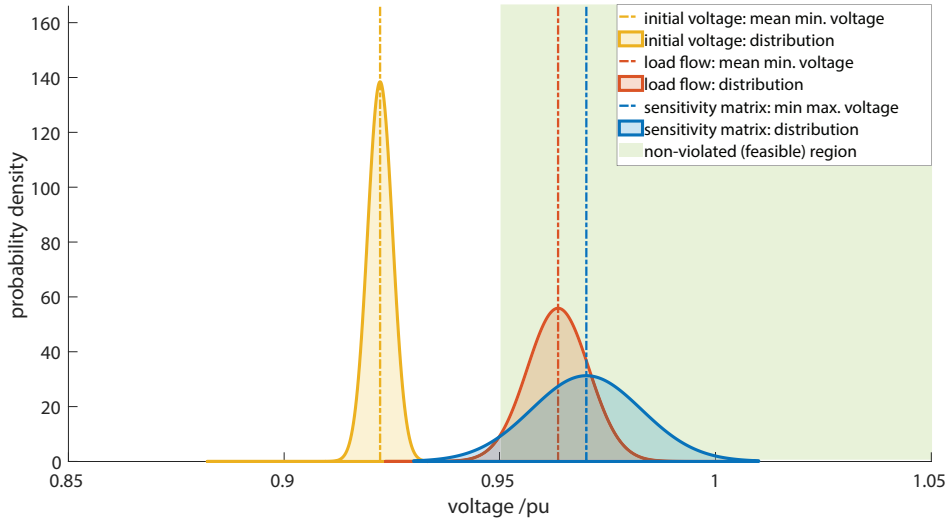

Figure 14. Distribution of minimum controlled voltages after Q injection obtained using MC simulations at 21:00.

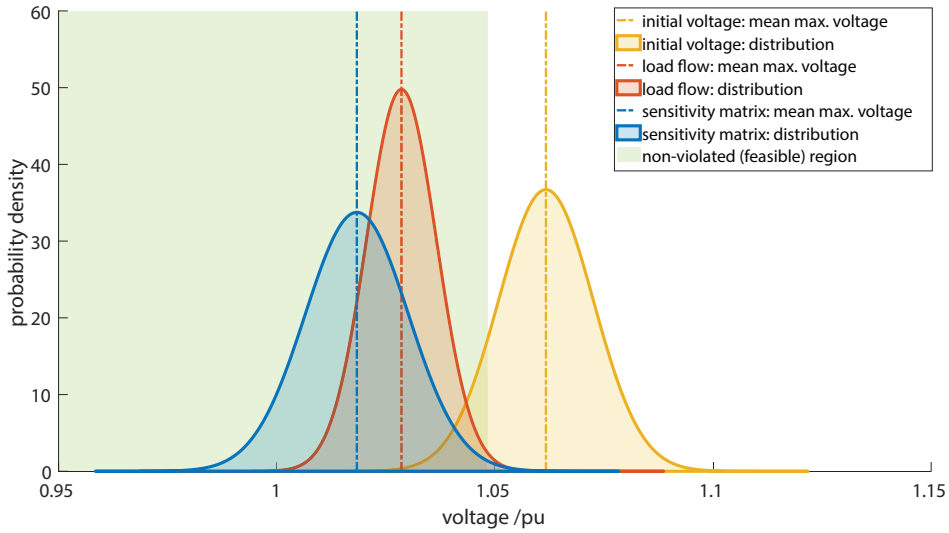

Figure 15. Distribution of maximum controlled voltages after Q absorption obtained using MC simulations at 10:00.

Finally, the APC algorithm is heavily dependent on the amount of active power curtailed rather than the voltage deviations in each phase. Hence, when the Q-absorption is not sufficient to remove the violations, APC is performed, which attempts to just remove the violation. Therefore, the maximum voltage of the set of nodes is always at 1.05 p.u (the upper limit). This is seen in Figure 16, which shows the distribution of the voltage profile obtained after APC, using the 102 MC simulations (violated simulations) out of 2000 simulations conducted at 11:00 as per Table 2. Hence, in the APC case, both the sensitivity matrix approach and the load flow approach yielded the exact same result.

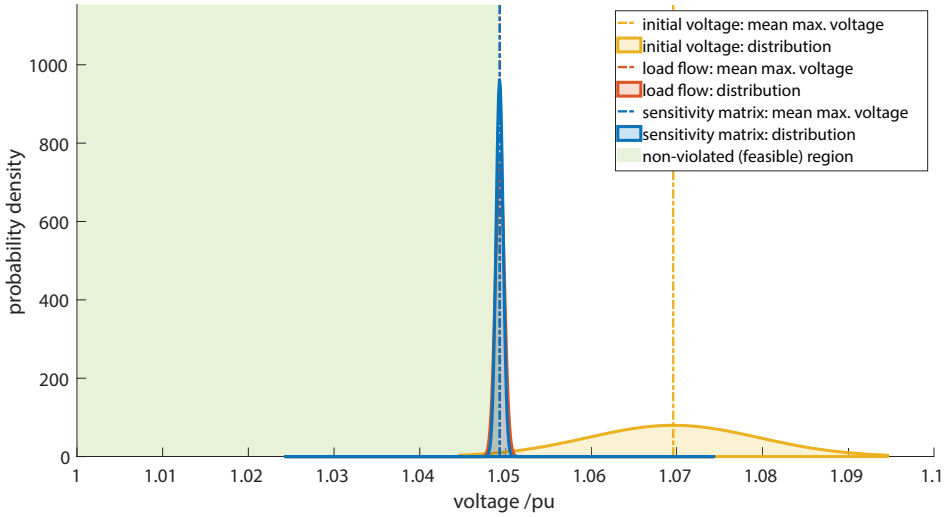

Figure 16. Distribution of maximum controlled voltages after P curtailment obtained using MC simulations at 11:00.

7. Conclusions

In this paper, a novel Sensitivity Matrix (SM) and a Centralized Active Reactive Power Management System (CARPMS) using inverter control to eliminate voltage limit violations were introduced. The optimum PV power settings for the control sequence were determined by a novel modified two-stage optimization algorithm. The two-stage optimization algorithm takes the predicted PV power and the estimated node voltages as inputs to determine the PV inverter active and reactive power settings to eliminate the voltage violations whilst minimising the unbalance in the network.

To demonstrate the effectiveness of the proposed SM approach and the two-stage optimization algorithm, a simulation study was performed on an existing LV network. The effectiveness and necessity of the FRS combination with PSO (two-stage optimization) was analysed by running 100 Monte Carlo simulations with FRS and without FRS (using only PSO). It was observed that nearly 34% of the simulation scenarios were not solved by the PSO-only optimization to remove the voltage violations. It was further observed that there was considerable overlap as to which cases had violations after optimization when using PSO only. This confirmed that the PSO algorithm is unable to handle specific voltage violation scenarios regardless of the parameters being tuned. However, with the combination of FRS (the two-stage optimization), all the simulations were able to find a solution removing all violations. Furthermore, the two-stage optimization was able to find solutions with a population of only 10, which further reduced the computational time.

The two-stage optimization algorithm performance was first implemented using load flows and then using the SM for the voltage profile generation. The results showed that the SM is able to successfully assimilate the performance of the state-of-the-art solution: the load flow, in all cases of reactive power injection, reactive power absorption and active power curtailment. The difference between the mean voltages of the proposed methodology and the load flow methods were 6.5×10^{-3} p.u for RPC using Q-injection, 1.02×10^{-2} p.u for RPC using Q-absorption. It is noteworthy that the voltage profiles obtained after APC were exactly the same for both methods (0 p.u mean voltage difference), which reaffirmed the SM approach. Furthermore, the SM reduced the time consumed for the voltage profile generation by 55% when compared to the load flow method. This faster inverter control will mitigate voltage violations in LVDGs, thereby allowing utility providers to accommodate more rooftop solar panels into LV networks.

The main advantage of the proposed two-stage optimization using the SM is the reduction in time to generate the voltage profiles during the control sequence. Since the SM approach is able to perform the network voltage estimation with a 55% reduction in time with negligible accuracy loss, this will speed up the control of voltage violations in

LVDGs. Furthermore, the CARPMS implementation' initial cost is minimal due to the use of existing PV inverters without the need for additional device installation for the control operation.

Author Contributions: Conceptualization, A.S.J.H., U.M., G.W.K.P., A.B., W.G.C.B., P.B.E., R.I.G. and J.B.E.; methodology, A.S.J.H., U.M., G.W.K.P., A.B., P.B.E., R.I.G. and J.B.E.; software, A.S.J.H., U.M., G.W.K.P. and A.B.; validation, A.S.J.H., U.M., W.G.C.B., P.B.E., R.I.G. and J.B.E.; formal analysis, A.S.J.H., U.M., P.B.E., R.I.G. and J.B.E.; investigation, A.S.J.H. and U.M.; resources, P.B.E., R.I.G. and J.B.E.; data curation, G.W.K.P., A.B. and W.G.C.B.; writing—original draft preparation, A.S.J.H., U.M., G.W.K.P. and A.B.; writing—review and editing, A.S.J.H., U.M., W.G.C.B., P.B.E., R.I.G. and J.B.E.; visualization, A.S.J.H. and U.M.; supervision, W.G.C.B., P.B.E., R.I.G. and J.B.E.; project administration, A.S.J.H., U.M., P.B.E., R.I.G. and J.B.E.; funding acquisition, P.B.E., R.I.G. and J.B.E. All authors have read and agreed to the published version of the manuscript.

Funding: This research was funded by the National Science Foundation (NSF), Sri Lanka, Research Grant Numbers RG/2018/EA and ICT/01, and the Peradeniya Engineering Faculty Alumni Association (PEFAA).

Institutional Review Board Statement: Not applicable.

Informed Consent Statement: Not applicable.

Conflicts of Interest: The authors declare no conflict of interest. The funders had no role in the design of the study; in the collection, analysis, or interpretation of data; in the writing of the manuscript; nor in the decision to publish the results.

References

1. U.S. Energy Information Administration. Annual Energy Outlook. Available online: https://www.eia.gov/outlooks/aeo/ (accessed on 6 November 2020).
2. Almeida, D.W.; Abeysinghe, A.H.M.S.M.S.; Ekanayake, J.B. Analysis of rooftop solar impacts on distribution networks. *Ceylon J. Sci.* **2019**, *48*, 103–112. [CrossRef]
3. Hamilton, J.; Negnevitsky, M.; Wang, X.; Lyden, S. High penetration renewable generation within Australian isolated and remote power systems. *Energy* **2019**, *168*, 684–692. [CrossRef]
4. Colantuono, G.; Kor, A.L.; Pattinson, C.; Gorse, C. PV with multiple storage as function of geolocation. *Sol. Energy* **2018**, *165*, 217–232. [CrossRef]
5. Walling, R.A.; Saint, R.; Dugan, R.C.; Burke, J.; Kojovic, L.A. Summary of Distributed Resources Impact on Power Delivery Systems. *IEEE Trans. Power Deliv.* **2008**, *23*, 1636–1644. [CrossRef]
6. Akeyo, O.M.; Patrick, A.; Ionel, D.M. Study of Renewable Energy Penetration on a Benchmark Generation and Transmission System. *Energies* **2021**, *14*, 169. [CrossRef]
7. Ma, C.; Dasenbrock, J.; Többermann, J.C.; Braun, M. A novel indicator for evaluation of the impact of distributed generations on the energy losses of low voltage distribution grids. *Appl. Energy* **2019**, *242*, 674–683. [CrossRef]
8. Tonkoski, R.; Turcotte, D.; EL-Fouly, T.H.M. Impact of High PV Penetration on Voltage Profiles in Residential Neighborhoods. *IEEE Trans. Sustain. Energy* **2012**, *3*, 518–527. [CrossRef]
9. Chaminda Bandara, W.; Godaliyadda, G.; Ekanayake, M.; Ekanayake, J. Coordinated photovoltaic re-phasing: A novel method to maximize renewable energy integration in low voltage networks by mitigating network unbalances. *Appl. Energy* **2020**, *280*, 116022. [CrossRef]
10. Ma, C.; Menke, J.H.; Dasenbrock, J.; Braun, M.; Haslbeck, M.; Schmid, K.H. Evaluation of energy losses in low voltage distribution grids with high penetration of distributed generation. *Appl. Energy* **2019**, *256*, 113907. [CrossRef]
11. Yaghoobi, J.; Islam, M.; Mithulananthan, N. Analytical approach to assess the loadability of unbalanced distribution grid with rooftop PV units. *Appl. Energy* **2018**, *211*, 358–367. [CrossRef]
12. Almeida, D.; Abeysinghe, S.; Ekanayake, M.P.; Godaliyadda, R.I.; Ekanayake, J.; Pasupuleti, J. Generalized approach to assess and characterise the impact of solar PV on LV networks. *Int. J. Electr. Power Energy Syst.* **2020**, *121*, 106058. [CrossRef]
13. Aziz, T.; Ketjoy, N. PV penetration limits in low voltage networks and voltage variations. *IEEE Access* **2017**, *5*, 16784–16792. [CrossRef]
14. Shahnia, F.; Majumder, R.; Ghosh, A.; Ledwich, G.; Zare, F. Voltage imbalance analysis in residential low voltage distribution networks with rooftop PVs. *Electr. Power Syst. Res.* **2011**, *81*, 1805–1814. [CrossRef]
15. Hashemi, S.; Østergaard, J.; Degner, T.; Brandl, R.; Heckmann, W. Efficient Control of Active Transformers for Increasing the PV Hosting Capacity of LV Grids. *IEEE Trans. Ind. Inform.* **2017**, *13*, 270–277. [CrossRef]
16. Yorino, N.; Zoka, Y.; Watanabe, M.; Kurushima, T. An Optimal Autonomous Decentralized Control Method for Voltage Control Devices by Using a Multi-Agent System. *IEEE Trans. Power Syst.* **2015**, *30*, 2225–2233. [CrossRef]

17. Christakou, K.; Paolone, M.; Abur, A. Voltage Control in Active Distribution Networks Under Uncertainty in the System Model: A Robust Optimization Approach. *IEEE Trans. Smart Grid* **2018**, *9*, 5631–5642. [CrossRef]
18. Payne, J.; Gu, F.; Razeghi, G.; Brouwer, J.; Samuelsen, S. Dynamics of high penetration photovoltaic systems in distribution circuits with legacy voltage regulation devices. *Int. J. Electr. Power Energy Syst.* **2021**, *124*, 106388. [CrossRef]
19. Xie, Q.; Shentu, X.; Wu, X.; Ding, Y.; Hua, Y.; Cui, J. Coordinated voltage regulation by on-load tap changer operation and demand response based on voltage ranking search algorithm. *Energies* **2019**, *12*, 1902. [CrossRef]
20. Chen, C.; Lin, C.; Hsieh, W.; Hsu, C.; Ku, T. Enhancement of PV Penetration With DSTATCOM in Taipower Distribution System. *IEEE Trans. Power Syst.* **2013**, *28*, 1560–1567. [CrossRef]
21. Arshad, A.; P′uvi, V.; Lehtonen, M. Monte Carlo-based comprehensive assessment of PV hosting capacity and energy storage impact in realistic finnish low-voltage networks. *Energies* **2018**, *11*, 1467. [CrossRef]
22. Zhao, B.; Ren, J.; Chen, J.; Lin, D.; Qin, R. Tri-level robust planning-operation co-optimization of distributed energy storage in distribution networks with high PV penetration. *Appl. Energy* **2020**, *279*, 115768. [CrossRef]
23. Ma, Y.; Azuatalam, D.; Power, T.; Chapman, A.C.; Verbič, G. A novel probabilistic framework to study the impact of photovoltaic-battery systems on low-voltage distribution networks. *Appl. Energy* **2019**, *254*, 113669. [CrossRef]
24. Alzahrani, A.; Alharthi, H.; Khalid, M. Minimization of power losses through optimal battery placement in a distributed network with high penetration of photovoltaics. *Energies* **2020**, *13*, 140. [CrossRef]
25. Mak, D.; Choi, D.H. Hierarchical look-ahead conservation voltage reduction framework considering distributed energy resources and demand reduction. *Energies* **2018**, *11*, 3250. [CrossRef]
26. Al-Saffar, M.; Musilek, P. Reinforcement Learning-Based Distributed BESS Management for Mitigating Overvoltage Issues in Systems With High PV Penetration. *IEEE Trans. Smart Grid* **2020**, *11*, 2980–2994. [CrossRef]
27. Tonkoski, R.; Lopes, L.A.C.; El-Fouly, T.H.M. Coordinated Active Power Curtailment of Grid Connected PV Inverters for Overvoltage Prevention. *IEEE Trans. Sustain. Energy* **2011**, *2*, 139–147. [CrossRef]
28. Tonkoski, R.; Lopes, L.A. Impact of active power curtailment on overvoltage prevention and energy production of PV inverters connected to low voltage residential feeders. *Renew. Energy* **2011**, *36*, 3566–3574. [CrossRef]
29. Alyami, S.; Wang, Y.; Wang, C.; Zhao, J.; Zhao, B. Adaptive Real Power Capping Method for Fair Overvoltage Regulation of Distribution Networks With High Penetration of PV Systems. *IEEE Trans. Smart Grid* **2014**, *5*, 2729–2738. [CrossRef]
30. Howlader, A.M.; Sadoyama, S.; Roose, L.R.; Chen, Y. Active power control to mitigate voltage and frequency deviations for the smart grid using smart PV inverters. *Appl. Energy* **2020**, *258*, 114000. [CrossRef]
31. Latif, A.; Gawlik, W.; Palensky, P. Quantification and mitigation of unfairness in active power curtailment of rooftop photovoltaic systems using sensitivity based coordinated control. *Energies* **2016**, *9*, 436. [CrossRef]
32. Nousdilis, A.I.; Christoforidis, G.C.; Papagiannis, G.K. Active power management in low voltage networks with high photovoltaics penetration based on prosumers' self-consumption. *Appl. Energy* **2018**, *229*, 614–624. [CrossRef]
33. Weckx, S.; Gonzalez, C.; Driesen, J. Combined Central and Local Active and Reactive Power Control of PV Inverters. *IEEE Trans. Sustain. Energy* **2014**, *5*, 776–784. [CrossRef]
34. Ghosh, S.; Rahman, S.; Pipattanasomporn, M. Local distribution voltage control by reactive power injection from PV inverters enhanced with active power curtailment. In Proceedings of the 2014 IEEE PES General Meeting | Conference & Exposition, Washington, DC, USA, 27–31 July 2014; IEEE: New York, NY, USA, 2014; pp. 1–5.
35. Calderaro, V.; Conio, G.; Galdi, V.; Massa, G.; Piccolo, A. Optimal Decentralized Voltage Control for Distribution Systems with Inverter-Based Distributed Generators. *IEEE Trans. Power Syst.* **2014**, *29*, 230–241. [CrossRef]
36. Zhu, H.; Liu, H.J. Fast Local Voltage Control Under Limited Reactive Power: Optimality and Stability Analysis. *IEEE Trans. Power Syst.* **2016**, *31*, 3794–3803. [CrossRef]
37. Wang, X.; Wang, C.; Xu, T.; Guo, L.; Li, P.; Yu, L.; Meng, H. Optimal voltage regulation for distribution networks with multi-microgrids. *Appl. Energy* **2018**, *210*, 1027–1036. [CrossRef]
38. Gandhi, O.; Zhang, W.; Rodríguez-Gallegos, C.D.; Verbois, H.; Sun, H.; Reindl, T.; Srinivasan, D. Local reactive power dispatch optimisation minimising global objectives. *Appl. Energy* **2020**, *262*, 114529. [CrossRef]
39. Tina, G.M.; Garozzo, D.; Siano, P. Scheduling of PV inverter reactive power set-point and battery charge/discharge profile for voltage regulation in low voltage networks. *Int. J. Electr. Power Energy Syst.* **2019**, *107*, 131–139. [CrossRef]
40. Jabr, R.A. Robust Volt/VAr Control With Photovoltaics. *IEEE Trans. Power Syst.* **2019**, *34*, 2401–2408. [CrossRef]
41. Zhang, Z.; Dou, C.; Yue, D.; Zhang, B.; Zhao, P. High-economic PV power compensation algorithm to mitigate voltage rise with minimal curtailment. *Int. J. Electr. Power Energy Syst.* **2021**, *125*, 106401. [CrossRef]
42. Zhang, Q.; Dehghanpour, K.; Wang, Z. Distributed CVR in Unbalanced Distribution Systems With PV Penetration. *IEEE Trans. Smart Grid* **2019**, *10*, 5308–5319. [CrossRef]
43. Emarati, M.; Barani, M.; Farahmand, H.; Aghaei, J. A two-level over-voltage control strategy in distribution networks with high PV penetration. *Int. J. Electr. Power Energy Syst.* **2021**, *130*, 106763. [CrossRef]
44. Cheng, Z.; Li, Z.; Liang, J.; Si, J.; Dong, L.; Gao, J. Distributed coordination control strategy for multiple residential solar PV systems in distribution networks. *Int. J. Electr. Power Energy Syst.* **2020**, *117*, 105660. [CrossRef]
45. Singh, S.; Pamshetti, V.B.; Thakur, A.K.; Singh, S. Multistage multiobjective volt/var control for smart grid-enabled CVR with solar PV penetration. *IEEE Syst. J.* **2020**, *15*, 2767–2778. [CrossRef]

46. Ilea, V.; Bovo, C.; Falabretti, D.; Merlo, M.; Arrigoni, C.; Bonera, R.; Rodolfi, M. Voltage control methodologies in active distribution networks. *Energies* **2020**, *13*, 3293. [CrossRef]
47. Wang, L.; Yan, R.; Saha, T.K. Voltage regulation challenges with unbalanced PV integration in low voltage distribution systems and the corresponding solution. *Appl. Energy* **2019**, *256*, 113927. [CrossRef]
48. Nguyen, H.M.; Torres, J.L.R.; Lekić, A.; Pham, H.V. MPC Based Centralized Voltage and Reactive Power Control for Active Distribution Networks. *IEEE Trans. Energy Convers.* **2021**, *36*, 1537–1547. [CrossRef]
49. Marikkar, U.; Hassan, A.S.J.; Maithripala, M.S.; Godaliyadda, R.I.; Ekanayake, P.B.; Ekanayake, J.B. Modified Auto Regressive Technique for Univariate Time Series Prediction of Solar Irradiance. In Proceedings of the 2020 IEEE 15th International Conference on Industrial and Information Systems (ICIIS), Rupnagar, India, 26–28 November 2020; IEEE: New York, NY, USA, 2020; pp. 22–27.
50. Chaminda Bandara, W.G.; Almeida, D.; Godaliyadda, R.I.; Ekanayake, M.P.; Ekanayake, J. A complete state estimation algorithm for a three-phase four-wire low voltage distribution system with high penetration of solar PV. *Int. J. Electr. Power Energy Syst.* **2021**, *124*, 106332. [CrossRef]
51. Degefa, M.; Lehtonen, M.; Millar, R.; Alahäivälä, A.; Saarijärvi, E. Optimal voltage control strategies for day-ahead active distribution network operation. *Electr. Power Syst. Res.* **2015**, *127*, 41–52. [CrossRef]
52. Su, X.; Masoum, M.A.S.; Wolfs, P.J. Optimal PV Inverter Reactive Power Control and Real Power Curtailment to Improve Performance of Unbalanced Four-Wire LV Distribution Networks. *IEEE Trans. Sustain. Energy* **2014**, *5*, 967–977. [CrossRef]
53. Jung, J.; Onen, A.; Arghandeh, R.; Broadwater, R.P. Coordinated control of automated devices and photovoltaic generators for voltage rise mitigation in power distribution circuits. *Renew. Energy* **2014**, *66*, 532–540. [CrossRef]
54. Ma, W.; Wang, W.; Chen, Z.; Wu, X.; Hu, R.; Tang, F.; Zhang, W. Voltage regulation methods for active distribution networks considering the reactive power optimization of substations. *Appl. Energy* **2021**, *284*, 116347. [CrossRef]
55. Yang, H.; Liao, J. MF-APSO-Based Multiobjective Optimization for PV System Reactive Power Regulation. *IEEE Trans. Sustain. Energy* **2015**, *6*, 1346–1355. [CrossRef]
56. Mahmoud, K.; Lehtonen, M. Three-level control strategy for minimizing voltage deviation and flicker in PV-rich distribution systems. *Int. J. Electr. Power Energy Syst.* **2020**, *120*, 105997. [CrossRef]
57. Su, X.; Masoum, M.A.S.; Wolfs, P. Comprehensive optimal photovoltaic inverter control strategy in unbalanced three-phase four-wire low voltage distribution networks. *IET Gener. Transm. Distrib.* **2014**, *8*, 1848–1859. [CrossRef]
58. Samadi, A.; Shayesteh, E.; Eriksson, R.; Rawn, B.; Söder, L. Multi-objective coordinated droop-based voltage regulation in distribution grids with PV systems. *Renew. Energy* **2014**, *71*, 315–323. [CrossRef]
59. Zhu, X.; Wang, J.; Mulcahy, D.; Lubkeman, D.L.; Lu, N.; Samaan, N.; Huang, R. Voltage-load sensitivity matrix based demand response for voltage control in high solar penetration distribution feeders. In Proceedings of the 2017 IEEE Power & Energy Society General Meeting, Chicago, IL, USA, 16–20 July 2017; IEEE: New York, NY, USA, 2017; pp. 1–5.
60. Zhang, Z.; Ochoa, L.F.; Valverde, G. A novel voltage sensitivity approach for the decentralized control of DG plants. *IEEE Trans. Power Syst.* **2017**, *33*, 1566–1576. [CrossRef]
61. Zad, B.B.; Hasanvand, H.; Lobry, J.; Vallée, F. Optimal reactive power control of DGs for voltage regulation of MV distribution systems using sensitivity analysis method and PSO algorithm. *Int. J. Electr. Power Energy Syst.* **2015**, *68*, 52–60.
62. Chen, Y.; Strothers, M.; Benigni, A. All-day coordinated optimal scheduling in distribution grids with PV penetration. *Electr. Power Syst. Res.* **2018**, *164*, 112–122. [CrossRef]
63. Ge, X.; Shen, L.; Zheng, C.; Li, P.; Dou, X. A Decoupling Rolling Multi-Period Power and Voltage Optimization Strategy in Active Distribution Networks. *Energies* **2020**, *13*, 5789. [CrossRef]
64. Alboaouh, K.; Mohagheghi, S. Voltage and power optimization in a distribution network with high PV penetration. In Proceedings of the 2018 IEEE/PES Transmission and Distribution Conference and Exposition (T&D), Denver, CO, USA, 16–19 April 2018; IEEE: New York, NY, USA, 2018; pp. 1–9.
65. De Din, E.; Pau, M.; Ponci, F.; Monti, A. A Coordinated Voltage Control for Overvoltage Mitigation in LV Distribution Grids. *Energies* **2020**, *13*, 2007. [CrossRef]
66. Ferreira, W.M.; Meneghini, I.R.; Brandao, D.I.; Guimarães, F.G. Preference cone based multi-objective evolutionary algorithm to optimal management of distribuited energy resources in microgrids. *Appl. Energy* **2020**, *274*, 115326. [CrossRef]
67. Jain, N.; Singh, S.; Srivastava, S. Particle Swarm Optimization Based Method for Optimal Siting and Sizing of Multiple Distributed Generators. In Proceedings of the 16th National Power Systems Conference, Hyderabad, India, 15–17 December 2010; pp. 669–674.
68. Resources. Available online: https://site.ieee.org/pes-testfeeders/resources/ (accessed on 1 August 2021).
69. Boglou, V.; Karavas, C.S.; Arvanitis, K.; Karlis, A. A fuzzy energy management strategy for the coordination of electric vehicle charging in low voltage distribution grids. *Energies* **2020**, *13*, 3709. [CrossRef]
70. Fu, C.; Wang, C.; Wang, L.; Zhao, B. Control of PV systems for distribution network voltage regulation with communication delays. *Electr. Power Syst. Res.* **2020**, *179*, 106071. [CrossRef]
71. Welikala, S.; Dinesh, C.; Ekanayake, M.P.B.; Godaliyadda, R.I.; Ekanayake, J. A real-time non-intrusive load monitoring system. In Proceedings of the 2016 11th International Conference on Industrial and Information Systems (ICIIS), Roorkee, India, 3–4 December 2016; pp. 850–855.
72. Welikala, S.; Thelasingha, N.; Akram, M.; Ekanayake, P.B.; Godaliyadda, R.I.; Ekanayake, J.B. Implementation of a robust real-time non-intrusive load monitoring solution. *Appl. Energy* **2019**, *238*, 1519–1529. [CrossRef]

73. Welikala, S.; Dinesh, C.; Ekanayake, M.P.B.; Godaliyadda, R.I.; Ekanayake, J. Incorporating Appliance Usage Patterns for Non-Intrusive Load Monitoring and Load Forecasting. *IEEE Trans. Smart Grid* **2019**, *10*, 448–461. [CrossRef]
74. Dinesh, C.; Welikala, S.; Liyanage, Y.; Ekanayake, M.P.B.; Godaliyadda, R.I.; Ekanayake, J. Non-intrusive load monitoring under residential solar power influx. *Appl. Energy* **2017**, *205*, 1068–1080. [CrossRef]
75. Fang, Z.; Lin, Y.; Song, S.; Song, C.; Lin, X.; Cheng, G. Active distribution system state estimation incorporating photovoltaic generation system model. *Electr. Power Syst. Res.* **2020**, *182*, 106247. [CrossRef]
76. Wang, C.; Wu, J.; Ekanayake, J.; Jenkins, N. *Smart Electricity Distribution Networks*; CRC Press: Boca Raton, FL, USA, 2017.

2019 IEEE 14th International Conference on Industrial and Information Systems (ICIIS), 18-20 Dec., Peradeniya, Sri Lanka

Reactive Power Compensation for Voltage Violations in Distribution Network

Aranee Balachandran, G. W. K. Prabhath, W. G. Chaminda Bandara,
G. M. R. I. Godaliyadda, M. P. B. Ekanayake, and J. B. Ekanayake

Department of Electrical and Electronic Engineering
University of Peradeniya
Peradeniya
Sri Lanka
{aranee.balachandran, gwkprabhath, chaminda.bandara}@eng.pdn.ac.lk
{roshangodd, mpb.ekanayake, jbe}@ee.pdn.ac.lk

***Abstract*—Due to high PV penetration, voltage violations are one of the major problems which occur in networks. Existing conventional voltage-var control techniques in such networks consider the voltages at their connection points, for maintaining the voltage profile within the limit. Though useful, this method is not an efficient method for voltage control in the network with rooftop PV panels which have voltage fluctuations throughout the feeder. The centralized reactive power control method is introduced in order to improve the effectiveness of the method. This paper addresses a technique for minimizing the voltage violations in the feeder by utilizing the unused capacity of PV inverters. The method is validated in three different type networks selected from a Sri Lankan distribution network. The obtained results demonstrate that this technique is able to reduce the voltage violations in the network.**

***Index Terms*—Voltage deviation, Voltage violation, Reactive power capacity, Reactive power compensation**

I. Introduction

In recent years, photovoltaic (PV) generation systems have grown rapidly due to the massive increase in demand and lack of other natural resources [1]. In addition, PV systems have the advantage of operating at both utilities and end-users (households). However, many utilities have identified problems with the installation of small-scale PV plants in the Low Voltage Distribution Grids (LVDGs) such as voltage violation, harmonics and dc injections [2]. Out of these problems, voltage violations are significant and many solutions to mitigate them are reported in the literature.

In [3], three types of voltage regulation methods based on the reactive power capability of the inverters have been proposed namely, voltage-var control, adjustable power factor control, and active power curtailment control. In voltage-var control, the inverter of the PV system injects reactive power by referring local voltage of the PV panel at the connection point to the feeder. Here the amount of reactive power provided by the inverter is determined by a droop controller. With adjustable power factor control, the PV systems reactive power output determines the amount of active power supplied by the PV inverter. Results from the above assessment indicate that depending on the states of the network, the effectiveness of the control method varies. Due to the high R/X ratio in LV networks, active power curtailment produces significant voltage drop compared to voltage-var method [4]. However, the cost of active power curtailment is much higher compared to reactive power management as the later can be freely obtained from the solar inverters.

The method depicted by [5], which is an extended version of voltage-var control method depicted by [3] is presented. The centralized reactive control method is introduced in this paper while minimizing power loss in the transmission line. Though this paper presents a centralized reactive power control method, the complexity of the algorithm is much higher compared to proposed algorithm.

Traditionally, voltage regulation in LV distribution networks is achieved by the use of manual offload tap changers. Typically, the tap positions are calibrated and changed only in case of network extension or modification [6]. Due to the random activities of both the load and generation and the obstacles in daily voltage trend forecasts, the traditional voltage control is expected to become inherently unreliable. But the use of On-Load Tap Changer (OLTC) is recently introduced to control voltage violations in LV network.

Reference [7] presents remote monitoring based control strategy. Each feeder endpoint, midpoint voltages and secondary side voltage of the transformer are used to determine the tap position. However, OLTC is unable to perform quick tap variations in real-time. Reference [8] presents a combination of two different local reactive power control methods to minimize energy losses in the network while regulating the voltage over feeders. A two-stage optimal approach to minimize the power losses and voltage deviations of the distribution system is presented in [9].

This paper presents a voltage control method to minimize the voltage violations of the network by utilizing the reactive power capability of the inverters. Without controlling the inverters separately, the centralized controlling method was used to maximize efficiency by utilizing their reactive power capacity while avoiding active power curtailment. After estimating the required reactive power change, the algorithm chooses the optimum location to inject reactive power within the boundaries of all constraints by using the minimum injection of reactive power. This method is much more efficient compared to methods presented in [9] and [8] because this method does not use any capacitors, Voltage Regulator(VR) or OLTC to regulate voltages as it uses the available reactive power capacities in PV panels. Case studies demonstrate the effectiveness of the proposed method through comparisons in voltage regulation and violation.

978-1-7281-3706-3/19/$31.00 ©2019 IEEE

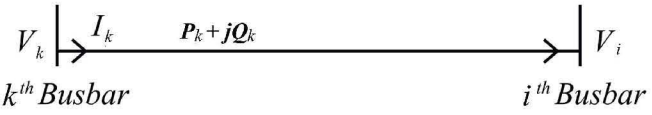

Fig. 1. Example of power flow in a busbar

II. Methodology

A. Equation of Power Flow Between Two Buses

Consider the k-th busbar connecting the nodes k and i in Figure 1. The equation for the power flow in the busbar can be expressed as,

$$S_k = P_k + jQ_k \tag{1}$$
$$S_k = V_k \cdot I_k{}^* \tag{2}$$

where, S_k is the power flow in the busbar, P_k is the active power component, Q_k is the reactive power component, V_k is the k-th bus voltage, I_k is the line current and $*$ is the complex conjugate operator. If the admittance of the busbar is Y_{ki} with a conductance of G_{ki} and susceptance of B_{ki}, then the power flow can be given by,

$$S_k = V_k.(Y_{ki}.V_i)^* \tag{3}$$
$$S_k = \mid V_k \mid \angle\delta_k(G_{ki} - jB_{ki}) \mid V_i \mid \angle -\delta_i \tag{4}$$

where, $\mid V_k \mid$ and $\mid V_i \mid$ denote the magnitude and δ_k, δ_i denote the angle of the bus voltages.

$$S_k = \mid V_k \mid\mid V_i \mid (G_{ki} - jB_{ki})(\cos(\delta_{ki}) + j\sin(\delta_{ki})) \tag{5}$$

where, $\delta_{ki} = \delta_k - \delta_i$

From (5), the active and the reactive power components were obtained as,

$$P_k = \mid V_k \mid\mid V_i \mid (G_{ki}\cos(\delta_{ki}) + B_{ki}\sin(\delta_{ki})) \tag{6}$$
$$Q_k = \mid V_k \mid\mid V_i \mid (G_{ki}\sin(\delta_{ki}) - B_{ki}\cos(\delta_{ki})) \tag{7}$$

B. Sensitivity Analysis

The changes that occurs in the bus voltages will let to deviations in the power flow in the busbar which can be given as,

$$\Delta P_k = \frac{\partial P_k}{\partial V}\Delta V + \frac{\partial P_k}{\partial \delta}\Delta\delta \tag{8}$$
$$\Delta Q_k = \frac{\partial Q_k}{\partial V}\Delta V + \frac{\partial Q_k}{\partial \delta}\Delta\delta \tag{9}$$

Therefore it is necessary to find the sensitivity of the power flow components with respect to bus voltages [10]. This was obtained by computing the Jacobian of the power flow equation as,

$$\begin{bmatrix}\Delta P_k \\ \Delta Q_k\end{bmatrix} = \begin{bmatrix}\frac{\partial P_k}{\partial \delta} & \frac{\partial P_k}{\partial V} \\ \frac{\partial Q_k}{\partial \delta} & \frac{\partial Q_k}{\partial V}\end{bmatrix}\begin{bmatrix}\Delta\delta \\ \Delta V\end{bmatrix} \tag{10}$$

$$J = \begin{bmatrix}\frac{\partial P_k}{\partial \delta} & \frac{\partial P_k}{\partial V} \\ \frac{\partial Q_k}{\partial \delta} & \frac{\partial Q_k}{\partial V}\end{bmatrix} = \begin{bmatrix}J_A & J_B \\ J_C & J_D\end{bmatrix} \tag{11}$$

where , J denotes the Jacobian matrix, J_A, J_B, J_C and J_D denotes the sensitivity of power flow component with respect to bus voltages. For the k-th busbar the sensitivity matrix was written as,

$$J = \begin{bmatrix}\frac{\partial P_k}{\partial \delta_k} & \frac{\partial P_k}{\partial \delta_i} & \frac{\partial P_k}{\partial V_k} & \frac{\partial P_k}{\partial V_i} \\ \frac{\partial Q_k}{\partial \delta_k} & \frac{\partial Q_k}{\partial \delta_i} & \frac{\partial Q_k}{\partial V_k} & \frac{\partial Q_k}{\partial V_i}\end{bmatrix} \tag{12}$$

TABLE I
JACOBIN MATRIX VALUES

J	$i \neq k$	$i = k$
J_A	$\mid V_k \mid\mid V_i \mid (G_{ki}sin(\delta_{ki}) - B_{ki}cos(\delta_{ki}))$	0
J_B	$\mid V_k \mid (G_{ki}cos(\delta_{ki}) + B_{ki}sin(\delta_{ki}))$	$2 \mid V_k \mid G_{kk}$
J_C	$\mid V_k \mid\mid V_i \mid (G_{ki}cos(\delta_{ki}) + B_{ki}sin(\delta_{ki}))$	0
J_D	$\mid V_k \mid (G_{ki}\sin(\delta_{ki}) - B_{ki}\cos(\delta_{ki}))$	$2 \mid V_k \mid B_{kk}$

and their values are illustrated in the Table I.

Lets consider the elements related with the reactive power component from the J matrix. It can be assumed that there are no considerable changes in the angles δ_k and δ_i. Therefore the deviation of the reactive part is mainly due to the change in the voltage magnitude. For a unbalanced 4-wire LV side network, the incremental change of the reactive power term with respect to the incremental change in voltage were written as ,

$$\begin{bmatrix}\Delta Q_{k,1} \\ \Delta Q_{k,2} \\ \Delta Q_{k,3} \\ \Delta Q_{k,N}\end{bmatrix} = [J_D]\begin{bmatrix}\Delta V_{k,1} \\ \Delta V_{k,2} \\ \Delta V_{k,3} \\ \Delta V_{k,N} \\ \Delta V_{i,1} \\ \Delta V_{i,2} \\ \Delta V_{i,3} \\ \Delta V_{i,N}\end{bmatrix} \tag{13}$$

where,

$$[J_D] = \begin{bmatrix}J_{Dk,1} & 0 & 0 & 0 \\ 0 & J_{Dk,2} & 0 & 0 \\ 0 & 0 & J_{Dk,3} & 0 \\ 0 & 0 & 0 & J_{Dk,N} \\ J_{Di,1} & 0 & 0 & 0 \\ 0 & J_{Di,2} & 0 & 0 \\ 0 & 0 & J_{Di,3} & 0 \\ 0 & 0 & 0 & J_{Di,N}\end{bmatrix}^T \tag{14}$$

$\Delta Q_{k,m}$ is the change in Q, $\Delta V_{k,m}$ and $\Delta V_{i,m}$ are changes in bus voltages at wire m. Here $m = 1, 2, 3, N$.

The maximum violated bus is identified and the voltage deviation of this bus is calculated by considering the acceptable voltage limit as 0.06pu,

$$\Delta V_{bus} = V_{MaxViolated} - V_{limit} \tag{15}$$

For a radial network, the injection/absorption of reactive power using the PV panels will let to similar voltage deviation throughout the feeder [8]. Therefore it was assumed that, the all the bus voltage in the network is going to have the same amount of voltage change as ΔV_{bus}.

Using equation (13) the required Q by each busbar to have the ΔV_{bus} shift in the bus voltages was found.

But during stimulation it was observed that in most cases, the violated busbars could be brought within the limits, by only supplying/absorbing the Q required by these violated segments. The total required Q was calculated by adding the ΔQ in the violated busbars. The total Q is absorbed/injected using the PV panels starting from the end of the network till it meets the Q requirement or till all PV inverter reach their available reactive power limit which is denoted by,

$$Q_{PV\ avalible} = \sqrt{S^2_{Rating} - P^2_{PV}} \tag{16}$$

TABLE II
CASE 1 DAY TIME : 3 ITERATIONS

Phase no:	3			
PV panel No	1	2	3	4
Q avaliable | kVAr	3.92	3.92	10.25	7.48
Q used | kVAr	0	0	5.06	0
Total no of violations	0			

TABLE III
CASE 1 NIGHT TIME : PHASE 1 AND 2 ARE VIOLATED NO OF ITERATION

Phase no:	1		2	
PV panel No	1	2	1	2
Q avaliable | kVAr	6.68	4.68	5.57	4.68
Q used | kVAr	5.37	4.68	4.34	4.6
Total no of violations	0		0	

where,
$Q_{PV\ avalible}$ is the maximum available Q injection/absorption
S_{Rating} is the PV panel inverter rating
P_{PV} is the active power of operating PV panel

If voltage violations are still present in the system and if reactive power is available in the PV inverters, then the above process in (15) can be iteratively applied until there are no voltage violations or no available reactive power in the violated phase. The flow of the above algorithm is represented in the Figure 2.

As Q injection/absorption effect all the bus voltage in the specific feeder, if there are more than one link connecting to a bus bar, then the maximum violated link is identified first and attempted to bring it within the limit.

III. CASE STUDIES FOR SELECTED NETWORKS

Three different types of networks were selected from the Figure 16 and for each network, day-time and night-time cases are considered. Few more PV panels were added to the network and network parameters are given in appendix.

A dead-zone function as depicted in Figure 3 was used to calculate the amount of voltage violation. For each case, the amount of violation before and after reactive power compensation are illustrated using stem plot and the details about the violated phases, total no of iterations made and the details about PV panels used for Q compensation are described by tables.

A. Case study 1 : Single-feeder Network

Transformer with first feeder of the network is selected for the case study 1.

1) Day time data: Phase 3 of feeder 1 is violated and the details about this case is illustrated using Table II, Figure 4 and 5.

2) Night time data: The Table III, Figure 6 and 7 illustrates the details about the violated phase 1 and 2 before and after injection of reactive power.

B. Case study 2 : Two-feeder network

Transformer with first, second and third feeders of the network is selected for the case study 2.

TABLE IV
CASE 2 DAY TIME : PHASE 2 AND 3 ARE VIOLATED - NO OF ITERATION IS 1

Phase no:	2						
PV panel No	1	2	3	4	5	6	7
Q available | kVAr	5.9	7.4	5.1	7.4	4.9	4.9	5.9
Q used | kVAr	5.9	7.4	5.1	0	0	0	0
Total no of violations	0						
Phase no:	3						
PV panel No	1	2	3	4	5	6	-
Q available | kVAr	4.9	4.2	3.7	4.4	5.8	5.8	-
Q used | kVAr	4.9	4.2	3.7	4.4	5.8	5.9	-
Total no of violations	0						-

TABLE V
CASE 2 NIGHT TIME : PHASE 1 AND 3 ARE VIOLATED - NO OF ITERATION IS 1

Phase no:	1		3			
PV panel No	1	2	1	2	3	4
Q available | kVAr	4.7	8.9	4.7	3.7	11.1	13.4
Q used | kVAr	4.7	8.9	0	0	0	3.5
Total no of violations	6		4			
Maximum violation | pu	0.0064		0.0015			

TABLE VI
CASE 3 DAY TIME : PHASE 1 AND 3 ARE VIOLATED - NO OF ITERATION IS 3

Phase no:	1		3	
PV panel No	1	2	1	2
Q available | kVAr	8.5	12	5.8	8.9
Q used | kVAr	8.5	12	0	3.8
Total no of violations	7		7	
Maximum violation | pu	0.007		0.008	

1) Day time data: Phase 2 and 3 have subjected to voltage violation in feeder 3 and 1 respectively. The details about this case is described by Table IV, Figure 8 and 9.

2) Night time data: Although feeder 1 and 3 of phase 1 have voltage violation,feeder 3 violation is considered first as it is having maximum violation. But it is unable to bring it into limit as its not having enough PV panels for compensation. Although after feeder 3 compensation, it is observed that the feeder 1 also brought into the voltage limit. Feeder 3 of phase 3 is violated and details about this case is described in Table V, Figure 10 and 11.

C. Case study 3 : whole network

The whole network is selected for the Case study 3.

1) Day time data: Phase 3 of feeder 6 and phase 1 of feeder 1 and 6 are violated in this case. In phase 3 by compensating the feeder 6 violation feeder 1 also brought into its limit. The Table VI, Figure 12 and 13 illustrates the details about this case.

2) Night time data: Phase 2 and 3 of feeder 6 and 8 are violated respectively. The details about this case is described by Table VII, Figure 14 and 15.

IV. CONCLUSION

This work outlines a reactive power compensation technique to reduce the amount of voltage violations in an unbalanced distribution network using single phase rooftop

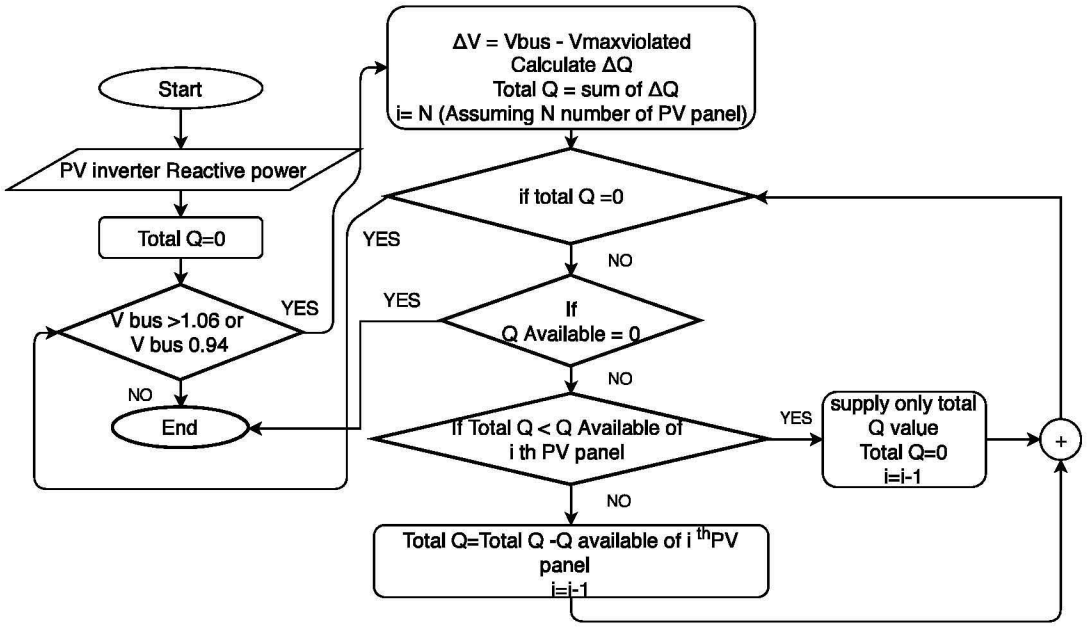

Fig. 2. Flow Diagram of the algorithm

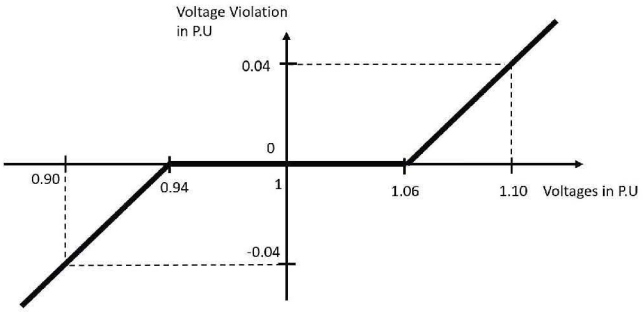

Fig. 3. Function of voltage violation

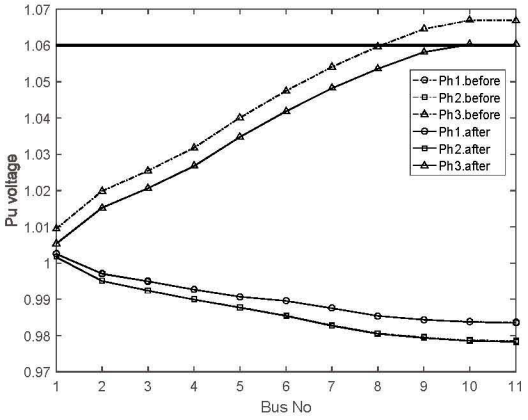

Fig. 4. p.u voltages of busbars before and after applying Q in case 1 day time

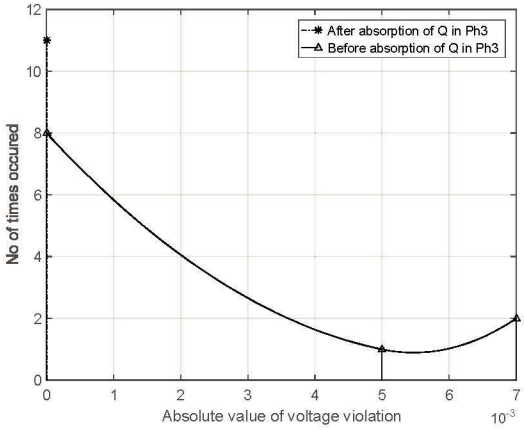

Fig. 5. Stem plot of voltage violation of the case 1 network day time

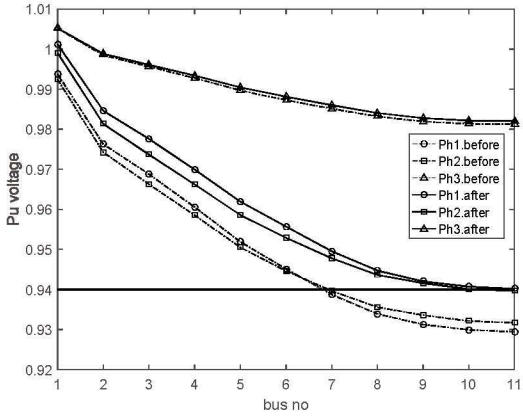

Fig. 6. p.u voltages of busbars before and after applying Q in case 1 night time

PV panels. The proposed algorithm has been based on a basic power flow equation and considered the violated busbars for the voltage compensation. This algorithm has been validated on a hybrid environment for three different networks for two different time scenarios, namely day time and night time. Results of these case studies reveals that, the proposed algorithm was able to completely reduce the voltage violations in the distribution network if there are enough single phase PV inverters to supply the required reactive power for the violates busbars.

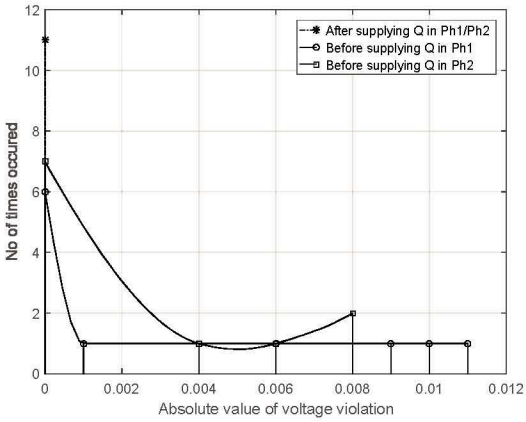

Fig. 7. Stem plot of voltage violation of the case 1 night time network

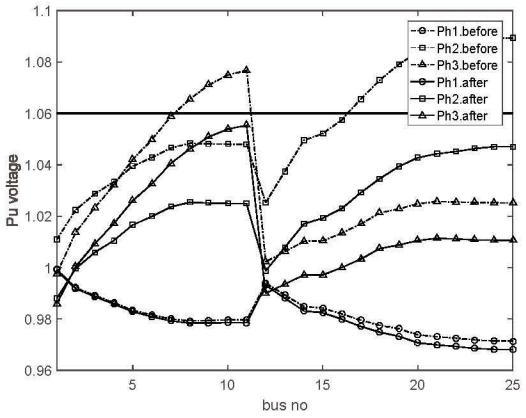

Fig. 8. p.u voltages of busbars before and after applying Q in case 2 day time

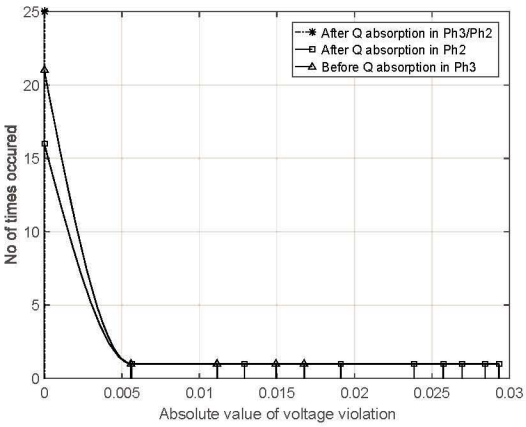

Fig. 9. Stem plot of voltage violation of the case 2 day time network phase 2 and phase 3

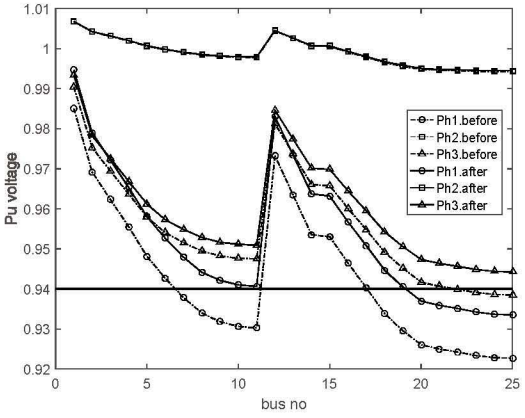

Fig. 10. p.u voltages of busbars before and after applying Q in case 2 night time

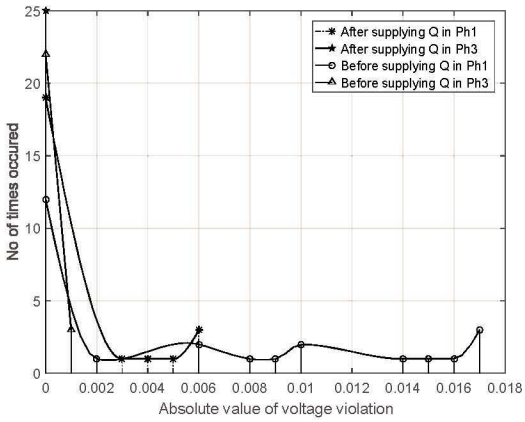

Fig. 11. Stem plot of voltage violation of the case 2 night time network phase 1 and phase 3

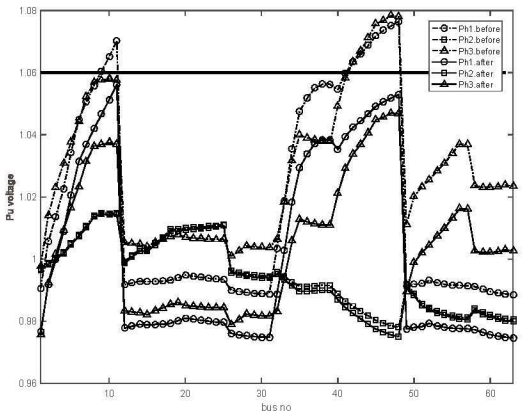

Fig. 12. p.u voltages of busbars before and after applying Q in case 3 day time

APPENDIX

The network in Figure 16 is a three-phase 4 wire LV side network with the following parameters

- $11kV/415kV$ transformer of $400kVA$ with Dyn11.
- The total length of the network is $1.6km$ and Aluminium Aerial Bundle Cable (ABC-Al/XLPE of 3x70+N 54.6 +1x16).
- 43 single-phase PV panels are connected throughout the network with the rating of 22.5kVA to 2kVA.
- Load power 5kW to 0.1kW.
- Total of 276 customers/loads.
- Day loading is 50% of night loading.

ACKNOWLEDGMENT

We would like to acknowledge the financial support provided by the National Science Foundation (NSF), Sri Lanka under the Research Grant No: RG/2018/EA & ICT/01.

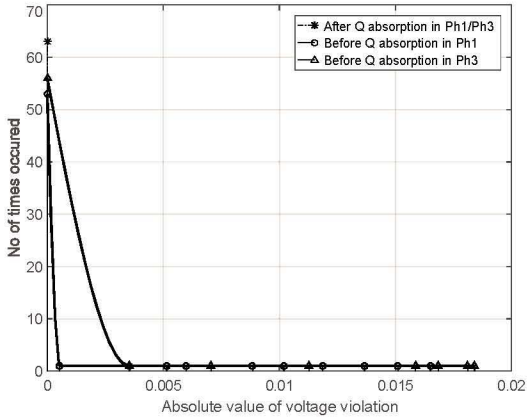

Fig. 13. Stem plot of voltage violation of the case 3 day time network phase 1 and phase 3

TABLE VII
CASE 3 NIGHT TIME : PHASE 2 AND 3 ARE VIOLATED - NO OF ITERATION IS 1

Phase no:	2				
PV panel No	1	2	3	4	5
Q available | kVAr	4.1	2.7	2.1	4.3	4.3
Q used | kVAr	4.1	2.7	2.1	4.3	4.3
Total no of violations	0				
Phase no:	**3**				
PV panel No	1	2	3	4	-
Q available | kVAr	5.3	9.8	6.1	12.0	-
Q used | kVAr	5.3	9.8	6.1	12.0	-
Total no of violations	1				-
Maximum violation | pu	0.0005				-

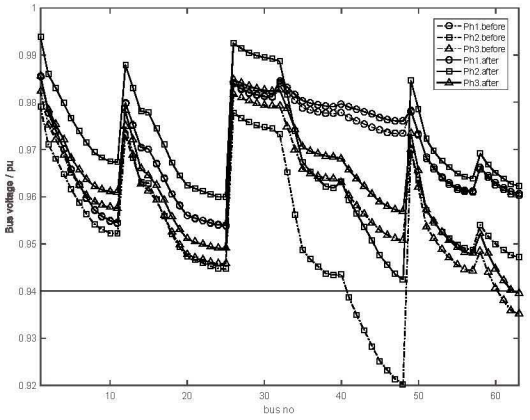

Fig. 14. p.u voltages of busbars before and after applying Q in case 3 night time

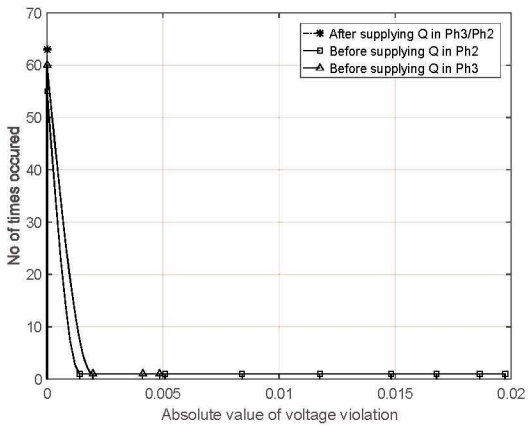

Fig. 15. Stem plot of voltage violation of the case 3 night time network phase 2 and phase 3

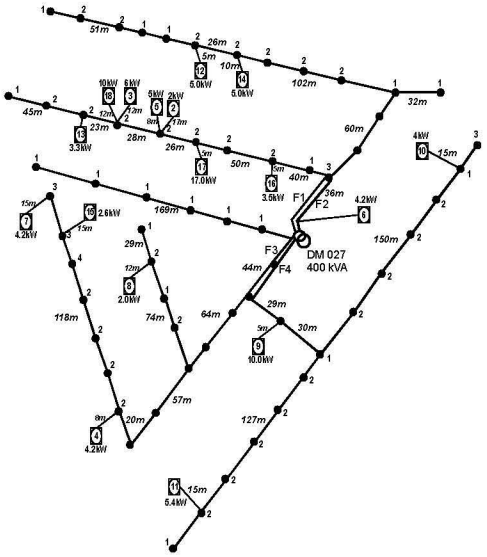

Fig. 16. Diagram of Residential Network

REFERENCES

[1] Solar Energy Industries Association "Solar Market Insight Report 2017 Year in Review" [Online] https://www.seia.org/research-resources/solar-market-insight-report-2017-year-review access date-18-08-2019

[2] Turitsyn, K., Sulc, P., Backhaus, S., & Chertkov, M. (2011). Options for control of reactive power by distributed photovoltaic generators. Proceedings of the IEEE, 99(6), 1063-1073. [5768094]. https://doi.org/10.1109/JPROC.2011.2116750

[3] H. Sun et al., "Review of Challenges and Research Opportunities for Voltage Control in Smart Grids," in IEEE Transactions on Power Systems, vol. 34, no. 4, pp. 2790-2801, July 2019. doi: 10.1109/TPWRS.2019.2897948

[4] S. Hashemi, J. stergaard, T. Degner, R. Brandl and W. Heckmann, "Efficient Control of Active Transformers for Increasing the PV Hosting Capacity of LV Grids," in IEEE Transactions on Industrial Informatics, vol. 13, no. 1, pp. 270-277, Feb. 2017.

[5] A. Cagnano, E. De Tuglie, M. Liserre and R. A. Mastromauro, "Online Optimal Reactive Power Control Strategy of PV Inverters," in IEEE Transactions on Industrial Electronics, vol. 58, no. 10, pp. 4549-4558, Oct. 2011. doi: 10.1109/TIE.2011.2116757

[6] T. Aziz and N. Ketjoy, "Enhancing PV Penetration in LV Networks Using Reactive Power Control and On Load Tap Changer With Existing Transformers," in IEEE Access, vol. 6, pp. 2683-2691, 2018. doi: 10.1109/ACCESS.2017.2784840

[7] C. Long, A. T. Procopiou, L. F. Ochoa, G. Bryson and D. Randles, "Performance of OLTC-based control strategies for LV networks with photovoltaics," 2015 IEEE Power & Energy Society General Meeting, Denver, CO, 2015, pp. 1-5. doi: 10.1109/PESGM.2015.7285618

[8] A. R. Malekpour and A. Pahwa, "Reactive power and voltage control in distribution systems with photovoltaic generation," 2012 North American Power Symposium (NAPS), Champaign, IL, 2012, pp. 1-6. doi: 10.1109/NAPS.2012.6336354

[9] Y. Chen, B. Luckey, J. Wigmore, M. Davidson and A. Benigni, "Real-time volt/var optimization for distribution systems with photovoltaic integration," IECON 2017 - 43rd Annual Conference of the IEEE Industrial Electronics Society, Beijing, 2017, pp. 2658-2663. doi: 10.1109/IECON.2017.8216447

[10] R. Aghatehrani and R. Kavasseri, "Reactive Power Management of a DFIG Wind System in Microgrids Based on Voltage Sensitivity Analysis," in IEEE Transactions on Sustainable Energy, vol. 2, no. 4, pp. 451-458, Oct. 2011. doi: 10.1109/TSTE.2011.2159745

[11] Almeida, D. W., Abeysinghe, A. H. M. S. M. S., & Ekanayake, J. B. (2019). Analysis of rooftop solar impacts on distribution networks. Ceylon Journal of Science, 48(2), 103112. DOI: http://doi.org/10.4038/cjs.v48i2.7614

Appendix 1

Gantt Chart Proposed in the Original Grant Proposal

Gantt Chart

	Activity	Months																							
		0	1	2	3	4	5	6	7	8	9	10	11	12	13	14	15	16	17	18	19	20	21	22	23	24
1	Literature review and project initialization																									
2	Implementation of the system for load monitoring under voltage fluctuation																									
3	Impact analysis of PV influx on the load monitoring and prediction system																									
4	Identification and analysis of anomalies and unknown loads using load monitoring																									
5	Developing a predictive type state estimator for the distribution network																									
6	Incorporating the smart transformer and smart inverter to control the load side																									
7	Optimizing the energy management with the presence of PV influx and fluctuations																									
8	Developing the S-DSM incorporating the above tasks																									
9	Verification of functionalities of S-DSM on real appliances																									

Milestones and Performance Indicators

	Milestone (M) / Performance Indicator (P)	Months																							
		0	1	2	3	4	5	6	7	8	9	10	11	12	13	14	15	16	17	18	19	20	21	22	23	24
M1	Literature review																									
M2	Problem formulation																									
M3	Reliable basic NILM algorithm																									
M4	Reliable robust NILM algorithm (SS, MS, CV, MS/L load handling)																									
M5	Energy disaggregation and mode estimation algorithm																									
M6	Smart meter interface																									
M7	Reliable measurement nodes																									
P1	Submit conference paper																									

Appendix 2

Requests for the Extensions

ජාතික විද්‍යා පදනම
தேசிய விஞ்ஞான மன்றம்
National Science Foundation
(Ministry of Higher Education, Technology & Innovation)

NATIONAL SCIENCE FOUNDATION

මගේ අංකය, எனது இல., **My No.-**

ඔබේ අංකය, உமது இல., **Your No.-** NSF/RD/07/RG/2018/EA&ICT/01

24.03.2021

Dr M.P.B. Ekanayake
Department of Electornical & Electronic Engineering
Faculty of Engineering
University of Peradeniya
Peradeniya

Dear Dr Ekanayake,

Request for an extension

Grant No : RG/2018/EA&ICT/01

Title : Development of a novel predictive based Smart Distribution Management System (S-DMS) to maximize the rooftop PV absorption capacity of last mile network

This has reference to your letter dated 08th March 2021, on the above subject.

In view of the justifications given, the NSF approved three months extension of the grant period up to 09th June 2021, without additional funds.

Thank you.

Yours sincerely,

Chris

Ms. Christine Dasanayake
Head /Research Division (Covering)

cc: Dr G.M.R.I. Godaliyadda, Dept. of Electornical & Electronic Engineering, Univ. of Peradeniya
Prof J.B. Ekanayake, Dept. of Electornical & Electronic Engineering, Univ. of Peradeniya
Bursar, University of Peradeniya
Accountant, NSF

RD/SW/mw

ජාතික විද්‍යා පදනම
தேசிய விஞ்ஞான மன்றம்
National Science Foundation
(Ministry of Higher Education, Technology & Innovation)

මගේ අංකය, எனது இல., **My No.-**
ඔබේ අංකය, உமது இல., **Your No.-**

NSF/RD/07/RG/2018/EA&ICT/01

12.07.2021

Dr M.P.B. Ekanayake
Department of Electrical & Electronic Engineering
Faculty of Engineering
University of Peradeniya
Peradeniya

Dear Dr Ekanayake,

Request for an extension

Grant No : RG/2018/EA&ICT/01

Title : Development of a novel predictive based Smart Distribution Management System (S-DMS) to maximize the rooftop PV absorption capacity of last mile network

This has reference to your letter dated 07h June 2021, on the above subject.

In view of the justifications provided and considering prevailing Covid-19 pandemic situation of the country, NSF approved five months extension of the grant period up to **09th November 2021**, without additional funds.

Thank you.

Yours sincerely,

Eng. Mahesh Dissanayake
Head /Research Division

cc: Dr G.M.R.I. Godaliyadda, Dept. of Electrical & Electronic Engineering, Univ. of Peradeniya
Prof J.B. Ekanayake, Dept. of Electrical & Electronic Engineering, University of Peradeniya
Bursar, University of Peradeniya
Accountant, NSF

RD/SW

Outcomes of the Research Proposed Under the Grant

This grant has been highly successful in producing two high-impact journal papers and one conference paper published along with one patent application pending and one high-impact journal paper being finalized for submission at the moment.

Journal Papers

(1) Wele Gedara Chaminda Bandara, Dilini Almeida, Roshan Indika Godaliyadda, Mervyn Parakrama Ekanayake, Janaka Ekanayake, "A complete state estimation algorithm for a three-phase four-wire low voltage distribution system with high penetration of solar PV", International Journal of Electrical Power & Energy Systems, Volume 124, 2021, 106332, ISSN 0142-0615
https://doi.org/10.1016/j.ijepes.2020.106332.
https://www.sciencedirect.com/science/article/pii/S0142061519336518
Science Citation Index Expanded Impact Factor 3.588
[NOTE: This paper was accepted for publication after submitting the December 2020 report]

(2) W.G. Chaminda Bandara, G.M.R.I. Godaliyadda, M.P.B. Ekanayake, J.B. Ekanayake, "Coordinated photovoltaic re-phasing: A novel method to maximize renewable energy integration in low voltage networks by mitigating network unbalances", Applied Energy, Volume 280, 2020, 116022, ISSN 0306-2619,
https://doi.org/10.1016/j.apenergy.2020.116022.
https://www.sciencedirect.com/science/article/pii/S0306261920314641
Science Citation Index Expanded Impact Factor 8.848

Conference Paper

(1) A. Balachandran, G. W. K. Prabhath, W. G. C. Bandara, G. M. R. I. Godaliyadda, M. P. B. Ekanayake and J. B. Ekanayake, "Reactive Power Compensation for Voltage Violations in Distribution Network," 2019 14th Conference on Industrial and Information Systems (ICIIS), Kandy, Sri Lanka, 2019, pp. 245-250, doi: 10.1109/ICIIS47346.2019.9063332.

Timeline of Key Events

- Date of Award – December 2018
- Fist installment of funds received – April 2019
- Commencement of the grant – 09th March 2019 (Backdated with the permission of the NSF)
- Closing of Universities and other institutes due to the Easter Attack – late April 2019 to late May 2019
- Frequent stoppage of academic activities due to other issue (in particular union actions, holidays etc.) July to December 2019
- Stoppage/major restrictions of academic activities due to containment measures of COVID-19 pandemic – March 16th to date
- Second (last) installment of funds received – January 2021
    - The funds available in the consumables / equipment were utilized to pay the salary of the Research Assistant until the funds were received
- Scheduled date of completion of the grant (two years from the date of commencement) – 09th March 2021
- Scheduled date for settling the finances and closing the account – 09th April 2021
- Final report due – 09th June 2021

Justification for the Request

Due to the continued turbulent circumstances and frequent stoppage of work, most of the work pertaining to the project were carried out without the luxury of having direct laboratory access. Due to these reasons and the delays in the receipt of funds, the procurements under this grant could not be completed as expected. Now that the NSF has kindly disbursed the funds and the operations of the university has converged to a steady rhythm after all the calamities, we are in a position to do the required procurements.

These equipment and consumables will enable a great value addition to the project funded by this grant and would enable the future development activities targeting possible practical deployment and/or commercialization. In addition, the hardware implementation will most surely enable us to achieve yet another application oriented high-impact publication.

Therefore, authorization to utilize the funds up until the final report is due (i.e., 09th June 2021) will be much beneficial from the grant's point of view as well as in realizing the objectives of the NSF in such funding.

The plan for the utilization of the funds and the progress of work over the extended period of time is shown in the Gantt Chart attached.

Gantt Chart for the Extended Funding Utilization

			Starting 09th											Ending 09th July
		Task	**Week 1**	**Week 2**	**Week 3**	**Week 4**	**Week 5**	**Week 6**	**Week 7**	**Week 8**	**Week 9**	**Week 10**	**Week 11**	**Week 12**
Procurement Processes	P1.	Send out purchase orders / calling for quotations												
	P2.	Receiving bids from suppliers (all local suppliers)												
	P3.	Evaluation of quotations, inspections and TEC procedures, purchasing												
	P4.	Receiving of goods												
Technical Activities	T1.	Implement the control algorithms in the dedicated processor												
	T2.	Emulation studies												
	T3.	Implementing the system on newly purchased hardware												
	T4.	Final assessment of the system performance												
Reporting	R1.	Writing the final report												
	R2.	Closing the financial accounts and final reporting												
	R3.	Submission of the final report												

Dr. M. P. B. Ekanayake,
Department of Electrical and Electronic Engineering,
Faculty of Engineering,
University of Peradeniya,
Peradeniya.
07th June 2021.

Through:
The Head of Department,
Department of Electrical and Electronic Engineering,
Faculty of Engineering,
University of Peradeniya,
Peradeniya.

To:
The Director,
The National Science Foundation
No. 47/5, Maitland Place,
Vidya Mawatha,
Colombo 07.

Dear Sir/Madam,

Requesting an Extension for the Completion of Research Grant Number RG/2018/EA&ICT/01

With reference to the letter by me on the same title, dated 08th March, 2021:

The grant period of the above grant number was scheduled to terminate on 09th March 2021 and I am grateful that the NSF provided me an extension till the 09th of July 2021 to complete the grant considering the numerous hindrances and stoppage of work due to a multitude of reasons over the past two years.

Thanks to the extension, and reopening of the country concurrently, we were able to initialize the final hardware implementation component promised by the grant. Unfortunately, a few weeks after this, soon after the new year break, the country was again put under strict restrictions due to the raging COVID pandemic and the work was brought to an abrupt stop. As the universities are not considered "essential services", the operation of university offices, including laboratories, is at a minimal level. Therefore, it was not possible to proceed with any hardware implementation activities or any financial transactions. Furthermore, the quotations that were called for have already expired due to the delays due to the closing of facilities.

Considering the present epidemiological predictions, the month of July may be quite critical for Sri Lanka in terms of COVID. It is quite likely that the universities may be closed until this wave is over. Therefore, it is quite unlikely that any work which requires access to laboratory facilities at the university could be executed at least until early August. Once the universities are open, we will require an additional three months to complete the final stages of the grant proposal.

Therefore, considering the successful outcomes of the grant and the stoppage of work due to the COVID pandemic, I would be most grateful if you would be kind to grant us an extension until 09th of November (three months from August – when it is anticipated to restore normalcy) to complete the grant.

Thank You,

Yours Sincerely,
Dr. M. P. B. Ekanayake – Principal Investigator

Outcomes of the Research Proposed Under the Grant

This grant has been highly successful in producing two high-impact journal papers and one conference paper published along with one patent application pending and one high-impact journal paper being finalized for submission at the moment.

Journal Papers

(1) Wele Gedara Chaminda Bandara, Dilini Almeida, Roshan Indika Godaliyadda, Mervyn Parakrama Ekanayake, Janaka Ekanayake, "A complete state estimation algorithm for a three-phase four-wirelow voltage distribution system with high penetration of solar PV", International Journal of Electrical Power & Energy Systems, Volume 124, 2021, 106332, ISSN 0142-0615 htt ps://do i.or g/10.1016/j.ijepes.2020.106332.
htt ps://www.sc ie ncedirec t.com/science/article/pii/SO142061519336518Science Citation Index Expanded Impact Factor 3.588
[NOTE: This paper was accepted for publication after submitting the December 2020 report]

(2) W.G. Chaminda Bandara, G.M.R.I. Godaliyadda, M.P.B. Ekanayake, J.B. Ekanayake, "Coordinated photovoltaic re-phasing: A novel method to maximize renewable energy integration in low voltage networks by mitigating network unbalances", Applied Energy, Volume 280, 2020, 116022, ISSN 0306-2619,
https: //doi.org /10.1016/j.apenergy.2020.116022.
https: //www.scienced irect.co m/science /article / pii /S0306261920314641 Science Citation Index Expanded Impact Factor 8.848

Conference Paper

(1) A. Balachandran, G. W. K. Prabhath, W. G. C. Bandara, G. M. R. I. Godaliyadda, M. P. B. Ekanayake and J. B. Ekanayake, "Reactive Power Compensation for Voltage Violations in Distribution Network," 2019 14th Conference on Industrial and Information Systems (ICIIS), Kandy, Sri Lanka, 2019, pp. 245-250 , doi: 10.1109/ICIIS47346.2019.9063332.

Timeline of Key Events

- Date of Award-December 2018
- First installment of funds received-April 2019
- Commencement of the grant- 09th March 2019 (Backdated with the permission of the NSF)
- Closing of Universities and other institutes due to the Easter Attack- late April 2019 to late May 2019
- Frequent stoppage of academic activities due to other issue (in particular union actions,holidays etc.) July to December 2019
- Stoppage/major restrictions of academic activities due to containment measures of COVID-19pandemic - March 16th to date
- Second (last) installment of funds received - January 2021
    - The funds available in the consumables / equipment were utilized to pay the salary ofthe Research Assistant until the funds were received
- Scheduled date of completion of the grant (two years from the date of commencement) - 09thMarch 2021
- Original scheduled date for settling the finances and closing the account - 09th April 2021
- Original scheduled date for the final report due - 09th June 2021
- ***Extension granted to complete the grant and settle finances until 09th June 2021***
- ***New Year break 11th to 17th April 2021***
- ***Closing of the University to students and curtailment of staff presence due to rising COVID cases – from 18th April 2021***

Justification for the Request

Due to the continued turbulent circumstances and frequent stoppage of work, most of the work pertaining to the project were carried out without the luxury of having direct laboratory access. Due to these reasons and the delays in the receipt of funds, the procurements under this grant could not be completed as expected. Even with all these constraints beyond our control, this grant has produced several high impact publications.

Due to the apparently clam situation early March this year, we anticipated that we would be able to finalize all the procurements and complete the hardware implementation at our laboratories. With this expectation, we made a request to the NSF and it was kindly honored and granted us an extension of three months according to the time plan given by us.

However, just one month (four weeks) of work according to the plan, all laboratory work had to be suspended due to the sudden closing of facilities in view of the rapidly rising COVID cases and several reported cases from the University. Furthermore, the entire country was put under severe travel restrictions with “non-essential” operations being suspended. As a result, on one side, we were barred access to laboratory facilities. On the other side, the quotations called were expired. Whatever responses received to that extent could not be processed due to the minimal work and staff allocation at the University. Therefore, we are now required to call in for fresh quotations as they have expired. For all this to happen, the universities should be re-opened.

According to experts of epidemiology the number of COVID cases are expected to rise through July. Therefore, it is only safe to assume that strict containment strategies may be enforced at least up until August. Therefore, it is quite unlikely that laboratory access will be entertained until then. Therefore, the actual physical hardware implementation of the platform cannot be started until after that.

In the view of the quotation will have to be re-called for, the procurement process will at lease take six weeks to complete. During that time, the initial designs testing may be carried out. After the required equipment and consumables are procured, the final work can be completed within another one and a half months. Therefore, the total work alone will require three months to complete, from the time the laboratory facilities at the university are re-opened.

The plan for the utilization of the funds and the progress of work over the extended period of time is shown in the Gantt Chart attached.

Gantt Chart for the Grant Extension

			Week Number from Recommencement of Activities											
		Task	**1**	**2**	**3**	**4**	**5**	**6**	**7**	**8**	**9**	**10**	**11**	**12**
Procurement Processes	P1	Send out purchase orders / Calling for quotations												
	P2	Receiving bids / quotations from local suppliers												
	P3	Evaluation of quotations, inspections and TECs												
	P4	Purchasing and receiving of goods												
Technical Activities	T1	Implement the control algorithms in the dedicated processor												
	T2	Hardware emulation studies												
	T3	Implementing the system on the hardware												
	T4	Final assessment of system performance												
Reporting	R1	Finalizing the final report												
	R2	Closing the financial account and fund transfer												
	R3	Submission of the final report												